TRIBOLOGICAL AND MECHANICAL BEHAVIOR OF RARE EARTH DOPED COMPOSITE COATING BY THERMAL SPRAYING

A Thesis Submitted
In Partial Fulfilment of the Requirements
for the Degree of

DOCTOR OF PHILOSOPHY

in

Mechanical Engineering

by

Mohit Vishnoi
(2K18/PhD/ME/517)

Under the Supervision of

Prof. Qasim Murtaza
(Professor, DTU, Delhi)

Dr. Paras Kumar
(Associate Professor, DTU, Delhi)

Department of Mechanical Engineering

DELHI TECHNOLOGICAL UNIVERSITY
(Formerly Delhi College of Engineering)
Shahbad Daulatpur, Main Bawana Road, Delhi-110042, India

October, 2024

CERTIFICATE

This is to certify that the thesis entitled **"Tribological and Mechanical Behavior of Rare Earth Doped Composite Coating by Thermal Spraying"** being submitted by **MOHIT VISHNOI**, Roll No.2K18/PhD/ME/517 to the Delhi Technological University, Delhi for the award of the degree of **Doctor of Philosophy** is a bonafide record of original research work carried out by him. He has worked under our guidance and supervision and has fulfilled the requirements for the submission of this thesis, which has reached the requisite standard. The results contained in this thesis have not been submitted, in part or full, to any other University or Institute for the award of any degree or diploma.

Prof. Qasim Murtaza
Department of Mechanical Engineering
(Professor, DTU, Delhi)

Dr. Paras Kumar
Department of Mechanical Engineering
(Associate Professor, DTU, Delhi)

ACKNOWLEDGEMENTS

I express my deep gratitude to my supervisors Prof. Qasim Murtaza and Dr. Paras Kumar, for assisting me in identifying and formulating the research problem. Their valuable comments and advice gave me the confidence to overcome the challenges in the formulation of this research work.

I express my special thanks to Prof. B. B. Arora, Head of Mechanical Engineering Department, DTU, for his continuation inspiration and support during research work.

I sincerely express my profound gratitude to His Holiness Jagadguru Sri Shivaratri Deshikendra Mahaswamiji and the leadership at JSS Mahavidhyapeetha for granting me the opportunity to pursue my Ph.D.

I would like to thank Dr. Mamatha T. G., Professor (MED) and Vice-Principal, JSS Academy of Technical Education, Noida, for her valuable moral support, constant motivation, valuable feedback during my experimental and thesis work.

I would like to thank Prof. R. C. Singh, Head of Department of Design, DTU, Prof. Suresh Kumar Garg, Professor (MED), DTU and Dr. Amar Patnaik, Professor (MED), MNIT Jaipur, for his valuable feedback during my experimental and thesis work.

I would also like to thank all those who directly and indirectly supported me in carrying out this thesis work successfully. Furthermore, I would like to express my sincere gratitude to my parents, my wife and to all members of my family for their endless inspiration, support and guidance throughout my whole life. Last but not least, I express my sincere gratitude to the Almighty for everything.

Mohit Vishnoi
(Roll No. 2K18/PhD/ME/517)

DELHI TECHNOLOGICAL UNIVERSITY
(Formerly Delhi College of Engineering)
Shahbad Daulatpur, Main Bawana Road, Delhi-42

CANDIDATE'S DECLARATION

I _____**Mohit Vishnoi**_____hereby certify that the work which is being presented in the thesis entitled _____"**Tribological and Mechanical Behavior of Rare Earth Doped Composite Coating by Thermal Spraying"**_____ in partial fulfillment of the requirements for the award of the Degree of Doctor of Philosophy, submitted in the Department of _____**Mechanical Engineering**_____, Delhi Technological University is an authentic record of my own work carried out during the period from ___**31-December-2018**__ to __**21-October-2024**__ under the supervision of _____**Prof. Qasim Murtaza** and **Dr. Paras Kumar**_____**.**

The matter presented in the thesis has not been submitted by me for the award of any other degree of this or any other Institute.

Candidate's Signature

This is to certify that the student has incorporated all the corrections suggested by the examiners in the thesis and the statement made by the candidate is correct to the best of our knowledge.

Signature of Supervisor (s) **Signature of External Examiner**

DELHI TECHNOLOGICAL UNIVERSITY
(Formerly Delhi College of Engineering)
Shahbad Daulatpur, Main Bawana Road, Delhi-42

CERTIFICATE BY THE SUPERVISOR(s)

Certified that **Mohit Vishnoi** (2K18/PHD/ME/517) has carried out their research work presented in this thesis entitled **"Tribological and Mechanical Behavior of Rare Earth Doped Composite Coating by Thermal Spraying"** for the award of **Doctor of Philosophy** from Department of Mechanical Engineering, Delhi Technological University, Delhi, under our supervision. The thesis embodies results of original work, and studies are carried out by the student himself and the contents of the thesis do not form the basis for the award of any other degree to the candidate or to anybody else from this or any other University/Institution.

Signature
(**Prof. Qasim Murtaza**)
(Professor)
(DTU, Delhi)

Signature
(**Dr. Paras Kumar**)
(Associate Professor)
(DTU, Delhi)

Date: **21-10-2024**

ABSTRACT

Rare earth elements (REEs) are known as the “vitamins or nutrients” of metals. The addition of rare earth elements in a limited quantity can enhance the properties of materials. The high pressure-high velocity oxy liquid fuel (HP-HVOLF) also called as high pressure-high velocity oxy fuel (HP-HVOF) process is well-known industry-adopted thermal spraying process for developing high melting point powder coatings over various surfaces. This study is mainly focused on effect of adding various rare earth oxides such as erbium oxide (Er_2O_3)/lanthanum oxide (La_2O_3) /cerium oxide (CeO_2) with a limited quantity in tungsten carbide (WC-10Co-4Cr) powder on surface, mechanical and tribological characterization of coated samples. Each rare earth oxides was added in equal proportions as 0.2, 0.3 and 0.4 wt.% mixed with tungsten carbide powder and deposited on stainless steel using HP-HVOF process. The thickness of deposited coatings varies from 270µm -320µm. The study consists of four sets of experiments as without rare earth oxides as 0 wt.% (Cp1000 - Exp.1) and with each rare earth oxides as 0.2 wt.% ((CpLCE-2) - Exp. 2), 0.3 wt.% ((CpLCE-3) - Exp. 3), 0.4 wt.% ((CpLCE-4) - Exp. 4). All the sets of experiments were characterized using tribological test such as slurry jet erosion test, surface characterization using energy spectroscopy analysis (EDS) scanning electron microscope (SEM), porosity, X-ray diffraction (XRD) analysis, surface roughness, wettability test and mechanical test includes tensile, flexural and hardness test to support the results. Apart from carbide coated samples, the same characterization methods were used for the substrate as SS410. The slurry jet erosion test at different impingement angles was performed on the substrate as well as on all the coated samples. The minimum weight loss has observed as 20.273 mg, 16.658 mg, 19.002 mg, 13.011 mg and 15.183 mg at 15º impingement angle for uncoated (substrate), Cp1000 –Exp.1, (CpLCE-2) - Exp. 2, (CpLCE-3) - Exp. 3, and (CpLCE-4) - Exp. 4 respectively. The eroded surface micrographs were observed using Scanning Electron Microscope at higher magnification. The examined micrographs demonstrated the presence of several wear mechanisms, including micro cutting, micro indentation, ploughing, and crater wear. By the addition of each rare earth

oxides up to 0.3 wt.% in (CpLCE-3) - Exp. 3 showed the least weight loss due to its high hardness value among all sets of experiments. The EDS (Energy Dispersive Spectroscopy) has recognized the occurrence of different elements on the surface together with rare earth. Moreover, its compounds such as cobalt-tungsten bimetallic carbide (Co_3W_3C) and tungsten semi-carbide (W_2C) are identified using X-ray diffraction (XRD) analysis on coated samples. The porosity level of all the coated samples except (CpLCE-2) - Exp. 2 is less than 1%. Moreover the porosity level of (CpLCE-2) - Exp. 2 is ≥1 to ≤ 2%. This leads to higher value of surface roughness. The value of surface roughness is found to be comparable and less for the (CpLCE-3) - Exp. 3, and (CpLCE-4) - Exp. 4 due to grain refinement.

The value of static water contact angle for all the coated samples is obtained to be greater than 90º. This causes the coated surface to exhibit hydrophobic properties as evaluated by wettability analysis. The wettability characteristics are influenced by the level of surface roughness. It is well known that in general the higher the value of surface roughness turns the higher contact angle from Wenzel and Cassie Baxter's model, The highest average static water contact angle i.e. 134.4º value has observed for (CpLCE-2) - Exp. 2 due to its highest surface roughness value of 7.02 μm. The mechanical tests have conducted to support the results as well as to explore the possible fields of applications. All the mechanical properties obtained from mechanical test are the highest for (CpLCE-4) - Exp. 4 except hardness. The Vickers hardness values of the coatings obtain from (CpLCE-3) - Exp. 3 showed the highest value i.e. HV (0.3) ≈ 1123. The aim of the current study is to minimize the slurry erosion of the hydro turbine blades. The study reveals that the coatings obtain from (CpLCE-3) - Exp. 3 shows higher erosion resistance. Moreover; the mechanical tests explored the different other fields of applications such as tiller blades for agricultural purposes and to support results of tribological tests.

TABLE OF CONTENTS

LIST OF TABLES

LIST OF FIGURES

LIST OF SYMBOLS, ABBREVIATIONS AND NOMENCLATURE

TSP	Thermal Spraying Process
PVD	Physical Vapor Deposition
CVD	Chemical Vapor Deposition
PEO	Plasma Electrolytic Oxidation
MAO	Micro Arc Oxidation
HP-HVOF	High Pressure- High Velocity Oxy Fuel
HP-HVOLF	High Pressure- High Velocity Oxy Liquid Fuel
SLPM	Standard Litres Per Minute
ASTM	American Society for Testing and Materials
SS	Stainless Steel
WC–Co-Cr	Tungsten Carbide Cobalt Chromium
REOs	Rare Earth Oxides
REEs	Rare Earth Elements
La_2O_3	Lanthanum Oxide
CeO_2	Cerium Oxide
Er_2O_3	Erbium Oxide
WC	Tungsten Carbide
Co_3W_3C	Cobalt-Tungsten Bimetallic Carbide
W_2C	Tungsten Semi Carbide
EDS/EDX	Energy Dispersive X-ray Spectroscopy
XRD	X-ray Diffraction
JCPDS	Joint Committee on Powder Diffraction Standards
SEM	Scanning Electron Microscope
BSE	Back Scattered Electron
FIB	Focus Ion Beam
FE-SEM	Field Emission-Scanning Electron Microscope
SR	Surface Roughness

WCA	Water Contact Angle
CA	Contact Angle
HV	Vickers Hardness
μ-Hardness	Micro Hardness
MPa	Mega Pascal
GPa	Giga Pascal
A.U.	Arbitrary Unit
SLPM	Standard Litre Per Minute
Cp-1000	Without Rare Earth doped Tungsten Carbide Coating
CpLCE-2	Doping of REOs (La_2O_3/ CeO_2/ Er_2O_3)- 0.2wt.% each in Tungsten Carbide Powder
CpLCE-3	Doping of REOs (La_2O_3/ CeO_2/ Er_2O_3)- 0.3wt.% each in Tungsten Carbide Powder
CpLCE-4	Doping of REOs (La_2O_3/ CeO_2/ Er_2O_3)- 0.4wt.% each in Tungsten Carbide Powder

CHAPTER 1

Introduction

This chapter provides an overview of the background and motivation, about existing hydro-turbine blade materials, issue and challenges associated with hydro-turbine blade materials and various types of coating techniques and their comparisons.

1.1. Back Ground and Motivation:

Hydropower is a highly developed non-conventional technique for power generation with great versatility over a century ago. Hydroelectric power facilities are typically closed during the rainy season as a result of the elevated concentration of slurry. One of the main reasons for erosion on turbine blades is the different sizes of slurry particles in the water. This leads to decrease in the turbine efficiency and the anticipated lifespan of the turbine blades. The difficulties associated with materials used in turbine blades have intensified the need to tackle the requirement for coatings. The goal of developing new materials for coating turbine blades is to improve their resistance to erosion, abrasive wear, and cavitation, therefore extending their effective lifespan. On the other hand, abrasive erosion on parts like runners and guide vanes can increase dramatically in settings with sediments rich in hard minerals like quartz. This increased erosion presents a significant risk, which could lead to a rapid decrease in efficiency or a complete failure of the turbine in a short amount of time [1].

Novel approaches include the creation of coatings for steel surfaces using highly durable ceramic materials, which offer erosion resistance and retard the degradation process. Erosion generally refers to a broad range of phenomena, including the progressive wearing of the terrain by glaciers, rain, windblown dust, meteorites, and the amputation of material by cavitation in fluids. Furthermore, it includes the adverse impacts of intense precipitation, hail, and airborne dust on several modes of air transportation, as well as the depletion of materials occurring in different industrial facilities where solid particles are transported in a liquid stream [2]. Erosion on turbine blades is impacted by a variety of parameters, including the size, shape, quantity, hardness, concentration, and velocity of silt, as well as the intrinsic base material qualities. The debates have mostly

focused on two types of erosion: slit and slurry erosion. Slurry attrition of hydro turbine parts is a major concern that can affect the efficiency of hydropower projects. During rainy seasons, high amounts of unsettled silt particles pass through the turbines, causing wear and tear on the turbine components. This issue is especially obvious in run-of-river power plants [3].

Slurry erosion is a type of erosion that occurs on turbine blades when a mixture of suspended solid particles in liquid (slurry) collides with the blade and wears it down. This kind of erosion is especially relevant to industrial processes like mining, oil and gas extraction, and power generating that use slurries containing abrasive particles. The HVOF-coated steel demonstrated a substantially improved performance in comparison to plasma nitriding of 12Cr and 13Cr–4Ni steels under specific conditions of erosion and abrasion testing. Upon examination of the coated WC microstructures, a few holes were found to be flaws. These defects may cause the quality of the HVOF sprayed coating to deteriorate if exposed to higher particle impingement enthalpies. In contrast, the microstructures of 12Cr and 13Cr–4Ni plasma nitrides steels show no signs of these flaws. Researchers found that plasma nitrides 12Cr steel had a higher micro-hardness value (>1100) than plasma nitrides 13Cr–4Ni steels, indicating greater resistance to abrasion and erosion. Its ability to capture more nitrogen in the same experimental conditions is thought to be the source of this ability [4].

The researcher stated that the HVOF coatings had an effect on the CF8M steel in terms of slurry erosion ratings, providing critical fundamental data for material and coating selection that is useful for coating applications. The researchers made many conclusions after analyzing experimental results and inspecting the microstructures of steel samples [with or without coating] both before and after erosion. They found that the coated WC-10Co-4Cr greatly improved its erosive resistance, mostly due to its increased strength [hardness]. On the other hand, the HVOF-sprayed Al_2O_3+TiO_2 coating was less efficient against slurry erosion. This was attributed to the Al_2O_3 particles' higher melting temperature and relative lack of hardness, which left a lot of unmelted particulates on the coated surface.

The presence of these unmelted and partially melted particles would have hindered the adhesion to the substratum, resulting in higher rates of erosion. Furthermore, it was established that the rotational velocity had the greatest impact on the erosion rate in all cases that were analyzed. Nevertheless, the average particle size had a more distinct impact on the Al_2O_3+TiO_2 coating sprayed with HVOF, as compared to the coating with WC-10C0-4Cr and the blank CF8M steel without any coating. Significantly, the uncoated one exhibited enhanced ductility during slurry erosion. In contrast, the 86WC–10Co–4Cr coated with HVOF mostly exhibited ductile properties with a mixed response, while the Al_2O_3+TiO_2 coating sprayed with HVOF mostly presented brittle behavior throughout the same tests [5].

Sand erosion and cavitation may have a combined effect on hydraulic turbine components. Even if the geometry is free of cavitation, high velocity surface roughness caused by sand erosion can still cause cavitation-induced erosion. The combined effect of these two elements is greater than any factor acting alone. The revolving disc equipment can be used in a laboratory to simulate sand erosion and cavitation. Cavitation alone is unlikely to have a significant impact on HVOF coating, but combined, they can provide observable results. Using the spinning disc apparatus's accelerated testing, various turbine and coating materials can be ranked for their resistance to sand erosion and cavitation combined [6].

A potential effect on hydraulic turbine equipment may arise from a combination of sand attrition and cavitation. Even in the absence of cavitation, sand erosion in high-speed regions can initiate cavitation erosion. The concurrent presence of sand erosion and cavitation results in more pronounced impacts compared to each phenomenon when considered alone. The revolving disc system is capable of simulating both impacts within a controlled laboratory environment. The individual effect of cavitation on HVOF coating is not substantial; yet, the combined influence of both cavitation and sand erosion is clearly apparent. A comprehensive evaluation of the impact of this combination on various turbine materials and coatings should be carried out using an accelerated test using the rotating disc apparatus.

In order to achieve the precise balance of hardness, toughness, and ductility necessary for enhanced resistance against cavitation, it is imperative to carefully enhance the composition of the coating. Prior to putting the coating on real components, it is imperative to carry out a comprehensive research. The application of commercially available thermal spraying methods, such as HVOF, to coat hydro turbine components results in the observation of problems such as micro-cracking, disbonding, and the release of implanted ceramic particles.

An alternative coating technique worth investigating is laser cladding, which generates metallurgically bonded coatings that may offer enhanced durability when subjected to loading impacts. Potential future research should give priority to investigating novel composite coatings, such as nano-composites consisting of ternary and quaternary phases that offer a combination of enhanced hardness, strength, toughness, and adhesion. The integration of both soft and hard stages can help in fulfilling intricate requirements [7].

In order to reduce the negative effects of cavitation on hydro turbine blades, technical coatings are applied to enhance their durability and overall efficiency. Among the viable coating options are polymer coatings, often based on epoxy, which provide a smooth and durable surface on the blades, therefore reducing the risk of cavitation erosion. Ceramic coatings, such as chromium oxide or tungsten carbide, are employed on account of their exceptional hardness and erosion resistance, which offer a protective layer that greatly minimizes cavitation damage.

Thermal spray coatings of tungsten carbide, achieved by high-speed flame or plasma spray techniques, offer excellent wear resistance and are particularly effective in reducing cavitation. An alternative method involves the use of durable chrome plating, where a layer of chromium is applied to the turbine blades, resulting in a durable and polished surface that can endure the impact of cavitation.

More tactics used to reduce degradation caused by cavitation include hybrid coatings, which combine unique coating types, and surface end optimization for smoother surfaces. These steps, which include routine maintenance and monitoring, add up to

make the hydro turbine blade system more robust for green energy. Because surface modification of the substrate is 50% less expensive than its spare cost, it should be chosen over the substrate material replacement in order to improve mechanical and tribological properties at a reduced cost.

1.2. Coated Hydro-Turbine Blade Materials:

Various researchers have employed a variety of hydro turbine materials for the purpose of investigation, as illustrated in Table 1.1.

Table 1.1: Previous studies on hard coatings on various hydro turbine blade materials with their observations

Sr. No.	Blade Material	Coating Material	Studies	Observations	Ref.
1.	13Cr4Ni steel	WC-12Co	Micro-structural evolution	The coating exhibiting the highest hardness at 40 bars and 800 °C is well-suited for use in anti-wear applications for hydraulic turbine blades.	[8]
2.	13Cr-4Ni-(Mo)	WC–Co	Corrosion failures, fatigue failure, cavitation wear	WC–Co coatings, particularly those incorporating nano-sized WC particles, have proven effective in applications involving wear-resistant equipment	[9]
3.	SS-316L	Cryogenic heat treatment	Slurry erosion issues	The transformation of steel from austenite to martensite enhances slurry erosion resistance.	[10]
4.	13Cr–4Ni	Stellite 6	Grievous corrosion, abrasion and erosion	A Stellite 6 layer was applied onto 13Cr–4Ni by laser surface alloying (LSA) and subsequently assessed for its slurry erosion wear characteristics, revealing increased hardness and improved resistance to erosion.	[11]
5.	1Cr18Ni9Ti	Cr_3C_2–NiCr and WC-CoCr	Cavitation erosion	Two coated ceramic-metals, specifically Cr_3C_2–NiCr and WC-Co-Cr, were deployed onto SS (1Cr18Ni9Ti) using HVOF, aiming to bolster its resilience against cavitation erosion.	[12]

6.	SS316	Cr_3C_2–NiCr	Erosion and corrosion	Coatings containing Cr_3C_2–NiCr have been widely employed to mitigate erosion in turbine blades.	[13]
7.	16Cr5Ni	Nano TiO_2 and Al_2O_3	Slit erosion	The coating increase erosion and wear resistance and corrosion protection.	[14]
8.	AISI 410	WC-10Co-4Cr	Cavitation, erosion and corrosion	Improve the erosive resistance of blade material.	[15]
9.	Cobalt	WC–10Co–4Cr	Abrasive wear, slurry and cavitation erosion	WC-based coatings exhibited improved resistance to erosive wear when cobalt was employed as the binding metal.	[16]
10.	13Cr-4Ni	Boride	Slurry erosion	The increased wear resistance observed in pack boronized 13-4 MSS is ascribed to the significantly increased hardness of the boride coated material, which measures 2300 VHN, in contrast to the base 13-4 MSS hardness of 345 VHN.	[17]
11.	16Cr5Ni	WC-Co-Cr	Slurry erosion	The HVAF coated (WC–Co-Cr) samples at higher velocity exhibited superior erosion resistance.	[18]
12.	Martensitic stainless steel	$Fe_3Al)_{30}Ti_{35}BN_{35}$, WC–Co-Cr, Cr_3C_2–NiCr	Cavitation erosion	HVOF-applied coatings from commercially available powders such as WC–Co-Cr and Cr_3C_2–NiCr show marginally reduction in erosion rates when compared to martensitic stainless steel.	[19]
13.	CA6NM	50%, WC-Co-Cr and 50%, Ni-Cr-B-Si	Slurry erosion	Materials with coatings exhibit superior performance compared to untreated steel	[20]

Based on the literature review presented in Table 1.1, several researchers examined the mechanical, surface, and tribological (particularly slurry erosion) behavior of hydro turbine blade materials such as 13Cr4Ni, 16Cr5Ni, 21Cr4Ni-N, and 28/8N, as well as different steels [17, 18, 21-23]. Erosion is causing damage to many applications, including hydro turbines. However, the upkeep and restoration of 13/4 steel continue to

be the key concern in its application. Nitrogen (N) alloying has attracted a lot of attention as a means of strengthening austenitic stainless steel. This is due to the fact that nitrogen (N) has a strong solid solution hardening effect and is highly soluble in austenite, improving corrosion resistance. Nitrogen (N) also has a role in the hardening of grain size [24].

1.3. Issue and Challenges Associated with Hydro-Turbine Blade Materials:

The rapid escalation of erosion in the river water of the Himalayan area, caused by high silt concentration, is having a detrimental effect on the availability of essential hydropower energy in India. Numerous researchers have looked into various methods to reduce erosion on pumps, seats, runners, valves, directing vanes, turbine blades, and other parts. Although some have succeeded, others have not. The phenomenon of sediment erosion becomes more prominent during seasons of high-flow monsoons. Several approaches have been developed to enhance suitable coatings, such as chemical vapour deposition (CVD), thermal spray procedures, and electroplating coating protocols. Hence, the feasibility of applying micro and nano-composite coatings by the HVOF deposition process has been demonstrated to address the problem of sediment erosion in hydropower plants [14].

The coating can greatly extend the life of submerged turbine parts, such as nozzles, lances, and buckets for Pelton turbines and guide vanes, cheek plates, and runners for Francis turbines. There are several different types of abrasion-resistant coatings that range from ceramic coatings to hard metal coatings. The longer they are exposed to silt, the less effective they usually are. Co and WC have recently shown to perform better in terms of binding in a few Indian projects. Penstock, spiral casing, and draft tubes are examples of less abrasion-prone components that could be made of functional steel and protected with flexible, long-lasting coatings like epoxy or polyurethane-based plastics.

Thermal sprayed coating techniques are becoming increasingly popular because of their adaptability, which allows for the application of a diverse array of particles (such as ceramic, polymeric, metallic, or composite) onto different surfaces. Despite its intrinsic characteristics, thermal spray coating systems result in reduced environmental impact compared to other existing methods such as PVD, electroplating procedures, and CVD. Researchers have extensively investigated many coating combinations for different tribological purposes. Diverse coating combinations have been proposed as a means to enhance surface characteristics [3]. The scanning electron microscope (SEM) images of the Al_2O_3+13TiO_2 coating on CF8M steel, obtained by the hot-water immersion technique (HVOF), are shown in Figures 1.1a and 1.1b.

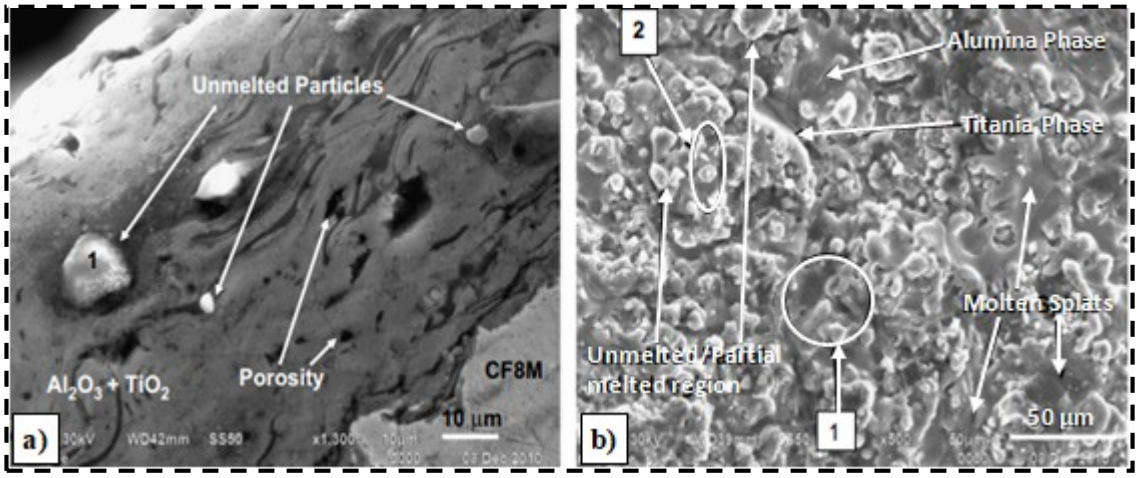

Figure 1.1: Analysis of a) Cross-section and b) Surface SEM micrographs HVOF-coated Al_2O_3 +13TiO_2 on CF8M steel [5]

The scanning electron micrographs clearly show that the coating has a lamellar microstructure, with liquefied splat lamellae that are completely melted and some trapped unmelted particles inside the splats. First, as shown by 1, there is an intermixing of partially melted and fully melted areas without apparent boundaries; second, there are partially molten sections with a spherical structure surrounded by entirely molten parts. Other researchers have also recorded similar annotations for Al_2O_3+13TiO_2 coatings that were applied using plasma spray techniques.

In general, the coating exhibits a microstructure that closely resembles a solid solution supplemented with aggregate particles. Moreover, it was observed that some powder particles, indicated as 2 in Figure 1.1b, may have experienced partial melting on their outside sections while the inside half remained unmelted. The outer surface exhibited a nearly spherical region of un-melted material, despite the attempted flattening induced by the liquid region. The presence of partially melted and un-melted particles in the Al_2O_3+13TiO_2 coating produced by the HVOF process can be ascribed to the comparatively lower temperatures associated with this thermal treatment. The cross-sectional scanning electron microscope (SEM) image is used to measure the coating thickness, which is ≈130 μm [5].

The erosion rate is influenced by several elements, including flow dynamics and material properties, irrespective of whether it is in liquid or solid form inside slurry. These parameters determine the manner in which sand particles engage with pipe walls and are influenced by material characteristics such as hardness, fracture strength, surface polish, elasticity, and the coefficient of restitution. Santa et al. [25] found that thermal spray coated steel exhibited a threefold increase in erosion resistance. According to their findings, thermal spray coated steel exhibits a sixteen fold increase in resistance to erosion induced by slurry in comparison to bare steel. The main modes of material removal, when examined for all the various coatings exposed to slurry erosion, revealed mass removal processes such as micro-cutting, micro-plowing, and the separation of hard particles. Figure 1.2 displays a snapshot of the deteriorated spear of a Pelton turbine at Bhaba hydropower generating station.

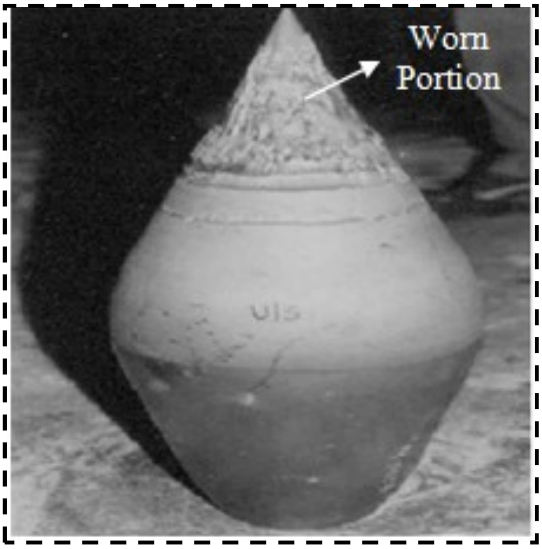

Figure 1.2: Worn spear of Pelton turbine [4]

Cermet materials have the best resistance to abrasive wear when the proportion of reserved WC is greater than the consistent dispersion of carbide particles in the matrix. Under low-speed conditions, the carbide demonstrates enough hardness to withstand direct impact of the fine particles. The material loss mechanism for WC-M coated samples is mostly determined by the structural behavior of the matrix, which experiences substantial wear leading to the progressive degradation of carbides. Conversely, at greater speeds, the carbides undergo little abrasion and separate from the surrounding matrix phase.

The shape, microstructure, and dispersion of tungsten carbide within the matrix have a significant impact on the hydro-abrasive resistance of the coated material. Due to their heterogeneous microstructure, metallic glazes have an erosive mechanism that differs greatly from bulk materials [26]. Slurry jet impingement erosion tests were performed on various cermet-HVOF sprayed coatings that were considered by various researchers. They postulated a mechanism for ductile erosive behavior after scanning electron microscopy revealed plastic deformities and platelet formation.

Furthermore, several researchers have proposed that cermet coatings exhibit enhanced resistance to erosion when the proportion of carbide is increased inside the matrix. Moreover, the Cobalt-based matrix, as compared to the Nickel-based ones, exhibited superior carbide binding, thereby improving the erosion rating of the coating [27, 28].

The phenomenon of abrasion wear occurs when hard particles, upon contact, remove material chips from a surface. In contrast, erosive wear is triggered by the collision of particles with a solid surface. Effluent particles can induce erosion but do not induce friction. The practical consequences of these differences are relevant for the choice of materials in wear resistance, since several microscopic wear processes are involved in abrasion, erosion, and cavitation. Especially, the abrasive and erosive processes are fast and could lead to substantial maintenance expenses if not controlled. The abrasive wear is also affected by the properties of the abrasive particles.

For instance, an abrasive with a fractured outer layer composed of many micro-edges causes substantially more material erosion compared to un-fractured pyramidal or spherical abrasives. The repetitive forces exerted by abrasives that indent the outer layer of a sample may result in the development of internal metallic fatigue. Artificial materials such as silicon carbide (SiC) with a hardness value of 3000HV, and natural minerals like quartz with a hardness value of 1100HV, along with other harder minerals, are recognized as the main causes of abrasion in demanding industrial processes, which usually have a maximum hardness value of 800HV [29].

The process of cavity creation is initiated when a liquid undergoes abrupt pressure fluctuations, leading to the emergence and quickly decreasing number of tiny bubbles or voids in the fluid near a surface. The collapse of these bubbles produces high-velocity shockwaves that can directly cause the material to erode. Wear arises from the consecutive formation of pits or holes on the surface subjected to this cavitation action, which can result in significant damage to the whole machinery component. Cavitation-induced resistance can often impede the functioning of machinery components such as runners by generating higher vibrations. Cavitation-induced acceleration of solid particles coming into contact with the surface can lead to fatigue damage.

Multiple investigations have documented that cavitation arises as a result of fluctuations in velocity or pressure in the course of fluid flow across bluff bodies. Cavity investigations utilize many forms of bluff bodies, including Triangular, cylindrical, rectangular, and circular bluff bodies. These bluff bodies are equipped with slurry particles in water (H_2O) that serve as extra sites for the formation of cavities and the resulting erosion caused by cavitation [30].

Thermal spraying is a technique that produces coatings that are resistant to wear and tear. Its unique properties include mass, intensity, and energy transmission. Material characteristics related to cavitation erosion resistance are different from those related to slurry wear resistance. Among the different grades of WC that are used, the thermal spray (86WC-10Co-4Cr) carbide coating is one that is particularly effective. Enhancements in the HVOF 86WC-10Co-4Cr coatings' deposition limitations have shown a 1.5-fold increase in wear ratings over conventional Detonation-gun-induced coatings with the same minimum composition. It has been noted that the HVOF technique yields coatings with noticeably lower values for phase changes and carbide degradation. Tribological properties of thermal spray coatings, such as their resistance to cavitation, erosion, and abrasion, depend on a number of variables, including coating composition, phase integrity, distribution, microstructural features, porosity, and residual stresses. When cobalt was utilized as the coating material, it was found that WC-based coatings showed better resistance to erosive wear [16].

1.4. Thermal Spraying Processes:

There are several coating deposition processes, including PVD, CVD, TSP, and PEO. Additional categorizations of TSP are illustrated in Figure 1.3. Thermal spraying is the application of coatings onto various materials to improve their characteristics or shield them against corrosion, wear, or heat. The procedure entails subjecting the selected coating to elevated temperatures until it reaches the point of melting, and thereafter directing it onto the surface of the substrate, where it solidifies under contact. There exist several significant categories of thermal spraying techniques, each operating on certain fundamental principles as outlined below:

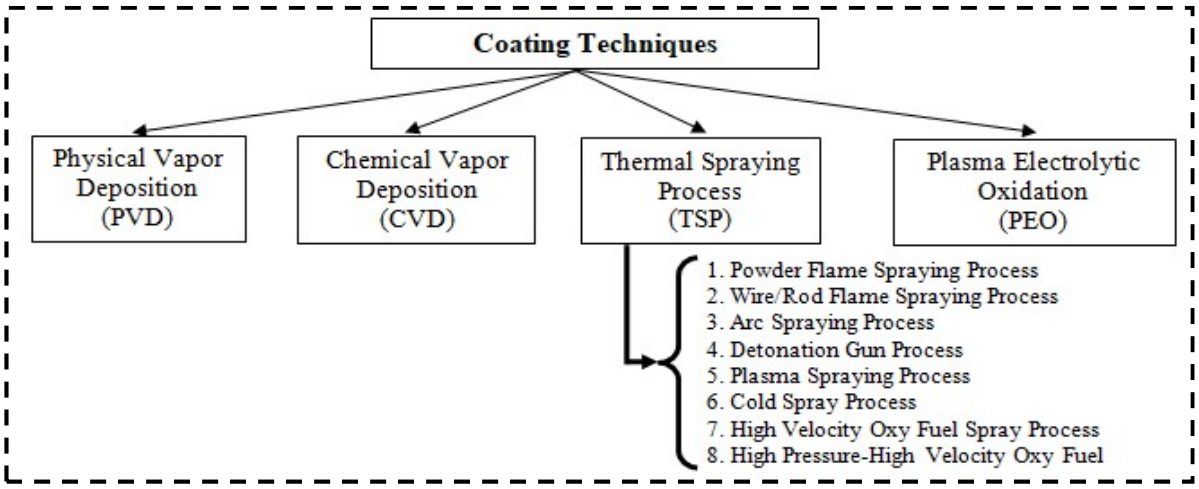

Figure 1.3: Various coating techniques with its classification [31]

1.4.1. Powder Flame Spraying:

Initially, this method was primarily employed for low-melting metals like tin or lead, but over time, its application expanded to encompass more heat-resistant metals and even ceramics as depicted in Figure 1.4 [32].

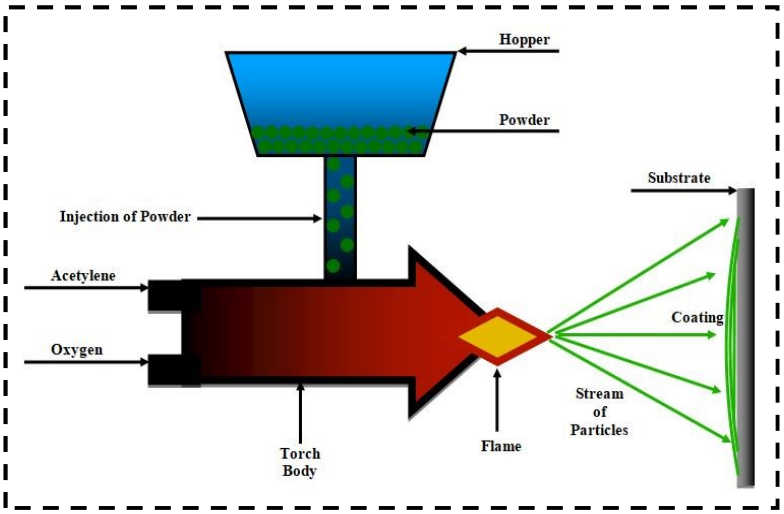

Figure 1.4: Schematic of flame spraying of a powder (adapted from [32])

The working principle of powder flame spraying also referred to as thermal spraying, entails applying a coating onto the substrate through the utilization of a high-temperature flame.

Advantages and limitations:

This method could be introduced to various different metals, ceramics, and combinations of ceramic materials. An issue frequently encountered in the powder spraying process is the challenge of sustaining a consistent powder feed and capacity of deposition of powder is limited [33].

1.4.2. Wire/Rod Flame Spraying:

The Figure 1.5 displays the schematic representation of flame spraying of wire/rod process. In this operation, a rod or a metallic wire is heated and pushed through the nozzle directly upon the substrate in order to obtain a coating.

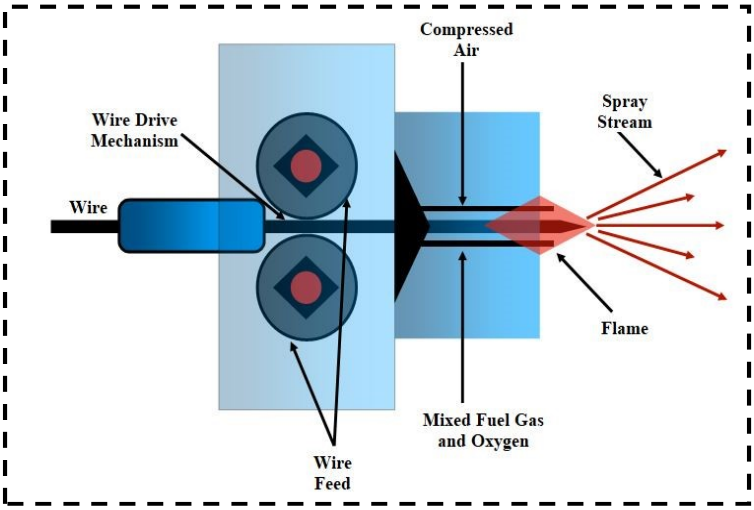

Figure 1.5: Schematic of flame spraying of wires/rods (adapted from [34])

Advantages and limitations:

The wire or rod spraying process ensures a steady and uninterrupted feed of the wire or rod with high deposition efficiency. The composition of the coating is determined by the material of the wire or rod used. It is typically limited to one material at a time.

1.4.3. Arc Spraying:

This is a thermal spraying method that involves melting and propelling metal wires to create protective coatings or functional layers on various surfaces. Figure 1.6 displays an illustration depicting the setup of arc spraying (AS).

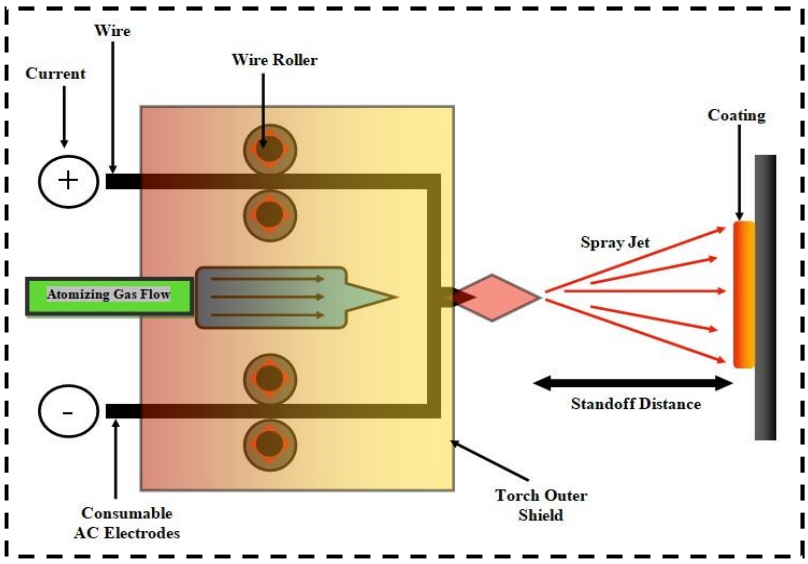

Figure 1.6: Schematic of an arc-spraying installation (adapted from [35, 36])

In this setup, there are two wires, which serve as consumable arc electrodes. When these wires are exposed to arc heating, they melt and form liquid droplets. These droplets are then propelled by an atomizing gas. The atomizing gas plays a key function in breaking down the molten droplets into fine particles, which are directed upon the sample. Interestingly, this process could create a 'pseudo-alloy' coating if the wires have multi-metallic composition [37, 38].

Advantages and limitations:

This process involves melting of only the wire feedstock. It typically generates less heat in contrast to other thermal spray methods, reducing the risk of distortion of the substrate material. Although arc spraying is versatile, it may not be suitable for all materials, especially those with extremely high melting points or non-conductive materials.

1.4.4. Detonation Gun Spray:

The detonation gun process operates based on the principles of combustion, shockwave propagation, and particle acceleration. The detonation gun process, illustrated in Figure 1.7, involves introducing assortment acetylene taken in the presence of oxygen which is paired along a burst of powdered material, straight in to a storage barrel. This mixture is then ignited using a spark. As a result, a high temperature and pressure ignition wave travels down the length of the barrel.

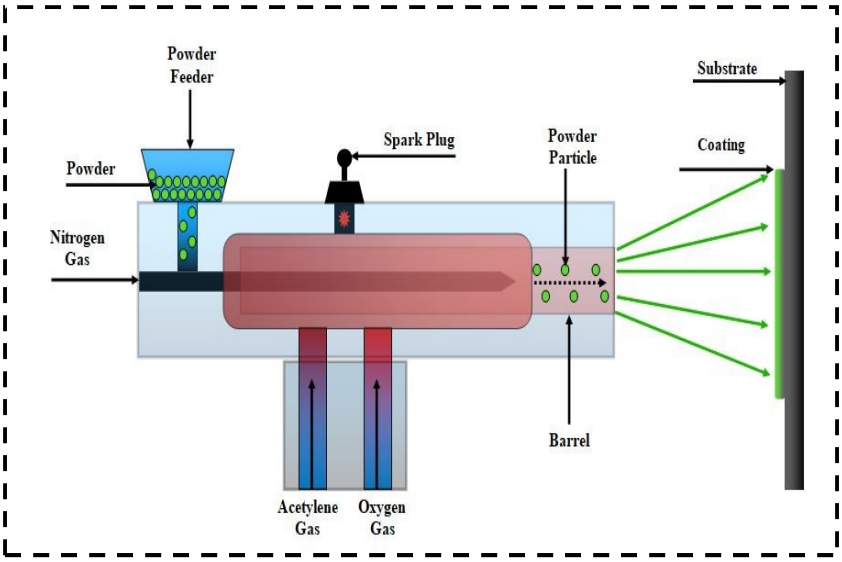

Figure 1.7: Schematic of the D-gun (adapted from [39-42])

By modifying factors such as the choice of fuel and other pertinent properties, this process can attain even greater velocities, reaching around 1000 meters per second. This allows for the repetition of the process at a rapid pace, often achieving a frequency of up to about 10 times per second [35].

Advantages and limitations:

The cyclic nature of this process along with the ability to repeat detonations at a high frequency, allows for rapid deposition of coatings. This can be advantageous for production environments where efficiency and throughput are essential. The process may have limitations in terms of fine control over coating properties. Achieving precise

thickness and porosity control can be more challenging compared to other thermal spray methods.

1.4.5. Plasma Spraying:

This technique is used to deposit a wide variety of materials onto various different surfaces. The Figure 1.8 displays an illustration depicting the setup of the same.

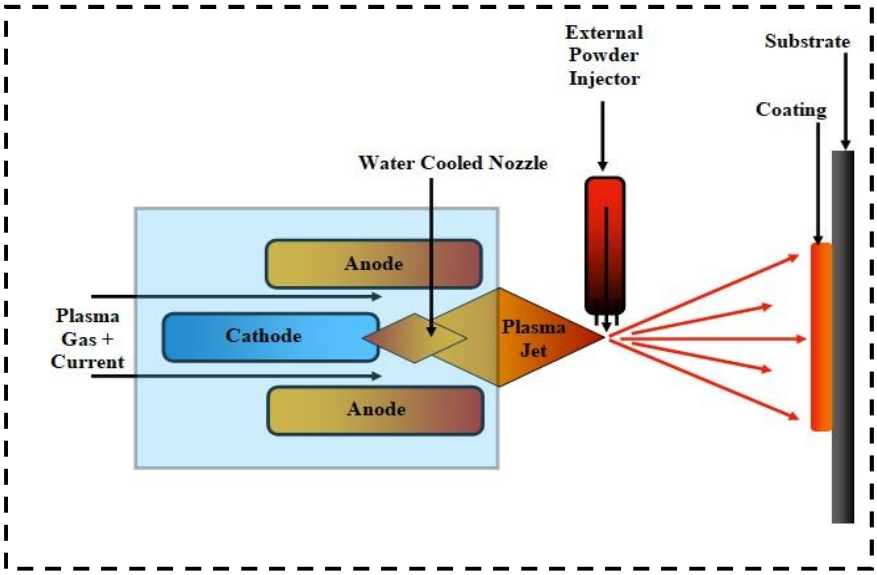

Figure 1.8: Schematic of the plasma spraying process (adapted from [43, 44])

The process begins with the generation of a high-temperature plasma arc when an inert gas, typically argon, is passed through a plasma torch. The process is repeated with successive layers of molten droplets until the desired coating thickness is achieved. Many parameters could be controlled with plasma spraying, such the torch and the substrate distance; powder feed rates, torch power, and plasma gas flow rates. These adjustments enable the coating's composition, porosity, and thickness to be fine-tuned [45].

Advantages and limitations:

This technique can generate a plasma jet operating at temperatures above 10,000 degrees Celsius. Materials with high melting points can readily melt and exhibit enhanced

spraying behavior at elevated temperatures. An vital stage in the procedure is the application of heat to the substrate, and it is imperative to comprehend that this will unavoidably result in certain alterations in the microstructure. Furthermore, the use of this method is limited to substrates that have electrical conductivity and can withstand a certain level of melting [35].

1.4.6. Cold Spray:

The cold spray employs supersonic streams of pressurized gas to propel powder particles at ambient temperature onto the substrate of a component at extremely high speeds. This method yields high-density coatings with minimal oxygen content, and it offers rapid deposition rates, making it exceptionally well-suited for the refurbishment of worn components. The Figure 1.9 illustrates the cold spray process.

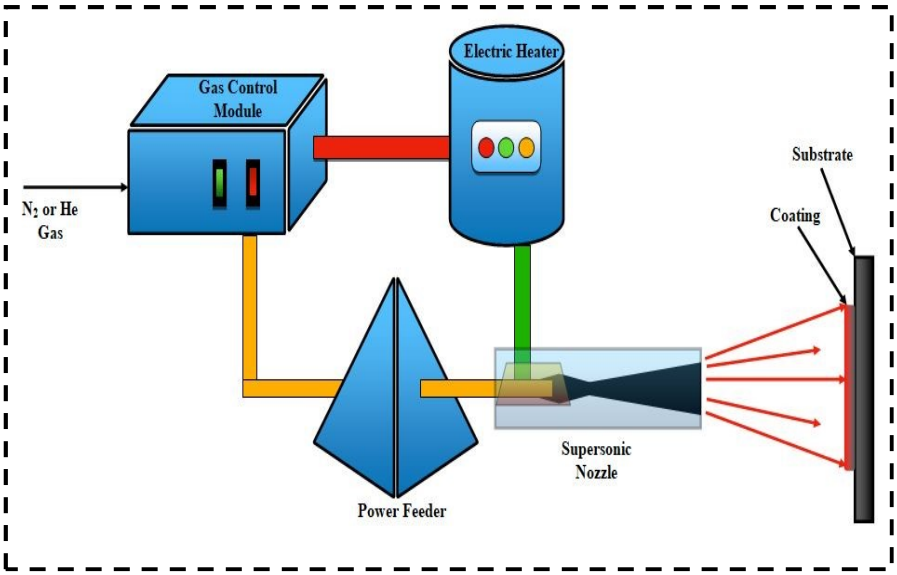

Figure 1.9: Systematic diagram of cold spray process (adapted from [46])

It is the deposition technique in which helium gas is utilised as a transporting agent to feed powder from feedstock to combustion chamber. It is in which powder particle of sizes ranging from 1 to 50 micrometres at 300-1200 m/s speed through de Laval nozzle.

Advantages and limitations:

The cold spray process operates at or near room temperature, minimizing the risk of thermal distortion or material degradation. This is a significant advantage when working with temperature-sensitive materials. Cold spray is typically used for relatively small components due to limitations in the size and manoeuvrability of cold spray equipment.

1.4.7. High Velocity Oxy Fuel Spray:

This coating method involves the spraying of fully or half-molten particulates onto a surface in order to create a protective or functional coat. The Figure 1.10 illustrates the systematic diagram of the HVOF process.

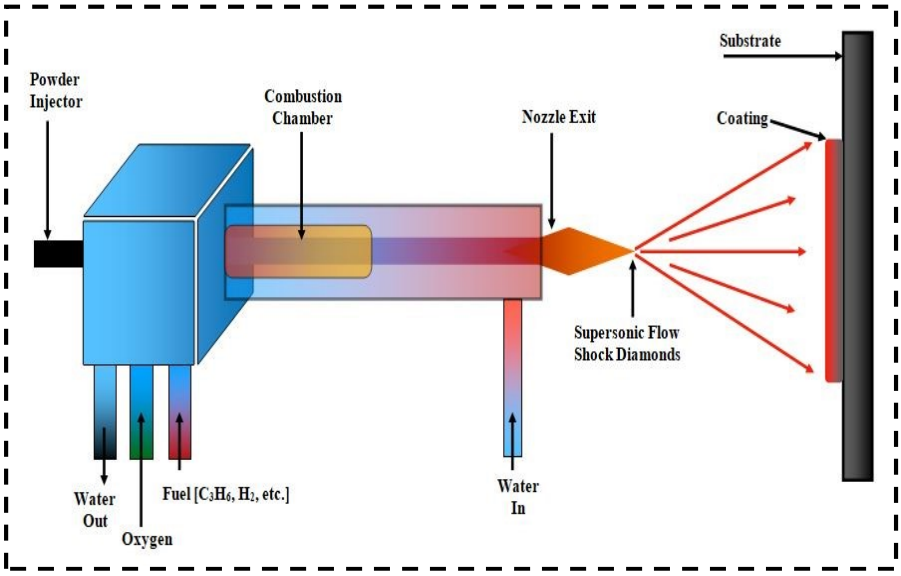

Figure 1.10: Schematic of HVOF (adapted from [47, 48])

The combustion chamber is packed with fuel (Kerosene, Hydrogen, Propane, and Propylene) and oxygen at pressures between 7 and 20 bars. The combustion process is started by ignition, and the exhaust gas that results is then discharged into the atmosphere by way of a barrel. The powder is added to the gas jet either axially or radially. Water or air is used for effective cooling of the combustion chamber, nozzle, and barrel to avoid overheating. The flame temperature typically ranges from 2300 to 3000 ˚C, propelling particles out of the gun nozzle at supersonic speeds exceeding 400 to 800 m/sec toward the substrate [32].

Advantages and limitations:

Porosity level is very less (approx. 1-2%). Setting up HVOF apparatus and optimizing the process parameters for definite applications can be time-consuming and may require specialized expertise.

1.4.8. High Pressure-High Velocity Oxy Fuel Spray:

This procedure is a variation of the traditional HVOF coating method. It involves the use of high-pressure combustion to produce a supersonic jet of gas and particles for coating substrates. The Figure 1.11 illustrates the systematic diagram of the HP-HVOF process.

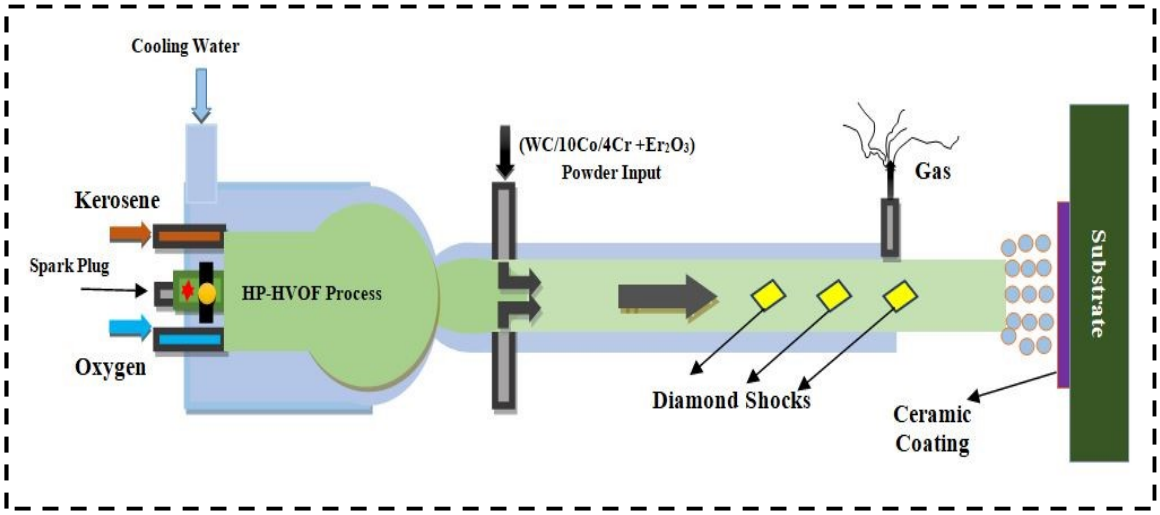

Figure 1.11: Illustration of HP-HVOF (adapted from [49])

The development of this spraying procedure aimed to address the constraints associated with the well-known existing method famous as HVOF. The Figure 1.12 depicts the methodology of HP-HVOF process.

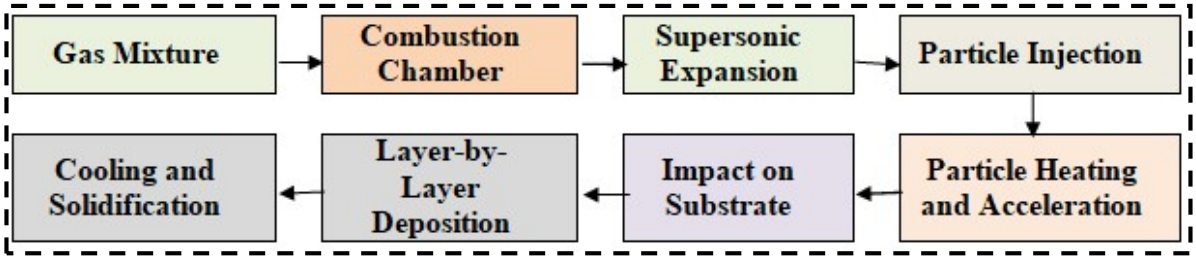

Figure 1.12: Steps of HP-HVOF Process

Similar to the HVOF, the HP-HVOF process begins with a composition of a fuel as kerosene along with oxygen. However, in HP-HVOF, this gas mixture is delivered at higher pressures, often exceeding those used in conventional HVOF. The high-pressure gas mixture is ignited within a combustion chamber. The increased pressure results in a more intense combustion process and higher temperatures. As the combustion occurs, the high-pressure gas is rapidly expanded through a specially designed nozzle. The increased pressure and temperature lead to supersonic velocities in the gas stream. Powdered coating material is introduced into the high-speed gas jet.

The high speed of gaseous stream accelerates the powder particles to extremely high speeds. The powder particles travel within the supersonic gas stream, and as they pass through the high-temperature region, they heat up and may partially melt or reach a semi-molten state. They are accelerated to extremely high velocities simultaneously. The heated or semi-molten particles are pollinated and directed towards the sample via the medium of high speed gaseous stream. The particles generate a covering upon the sample's surface when they collide, flattening, and deforming. Repeating the process builds up the coating layer by layer. A small layer of material is deposited with each pass, giving exact control over the coat's thickness as well as quality. Throughout the process, the substrate may be preheated or chilled to guarantee correct adherence and coating quality. Cooling may be necessary to promote the solidification of particles upon impact.

Advantages and limitations:

Porosity level is very less (< 1%). The HP-HVOF equipment can be expensive to purchase and maintain, which may pose a cost barrier for some businesses [49].

1.5. Differences among the available Thermal Spraying Processes:

Table 1.2: Comparison of various parameters of available thermal spraying techniques with their properties such as bond strength, coating thickness, hardness, and porosity for carbide coatings [50].

Thermal Spray Process	Principle	Pressure (Bar)	Particle Velocity (m/sec)	Coating Quality	Applications
High Velocity Oxy-Fuel	Combustion-based	7-20	500-800	High-quality, wear-resistant, corrosion-resistant coatings	Aerospace, automotive, industrial, marine
High-Pressure High-Velocity Oxy Fuel	Enhanced HVOF	>20	>800	Superior coating quality, exceptional wear resistance	High-performance components, critical applications
Plasma Spray	Plasma arc-based	<100	1000-1500	Versatile, wide material compatibility, excellent for ceramics	Aerospace, thermal barrier coatings, electronics
Flame Spray (Wire/ Powder)	Combustion-based	<10	100-300	Good coatings for corrosion protection and dimensional restoration	General industry, repair, anti-corrosion coatings
Electric Arc Spray	Electric arc-based	<10	50-250	Economical, good for large-area coatings	Structural steel, bridges, industrial components
Cold Spray	Kinetic energy-based	>50	400-1200	High-quality coatings without melting, minimal heat impact	Aerospace, repair, additive manufacturing

The HP-HVOF procedure is highly recommended due to its remarkable combination of high pressure and velocity, as shown in Table 1.2, which compares different thermal spraying processes. Plasma spray, on the other hand, has the fastest particles and the highest chamber pressure of any of these methods. However, plasma spray is not as popular as other methods because the high plasma temperature causes coatings to develop more oxides and carbides.

CHAPTER 2
Literature Review

This chapter comprises the review of surface preparation techniques with their advantages and constraints, surface texturing on various grade of steel, tungsten carbide coatings applied using HVOF and survey on impact of rare earth oxides with current trends on thermal spray coatings and its influence.

The surface preparation is mandatory before thermal sprayed coatings for following reasons:

a) Thermal sprayed coatings adhere mechanically rather than chemically, so the substrate must have a roughened surface to allow the coating to "anchor" itself. Proper surface preparation ensures strong adhesion between the substrate and the coating.

b) The substrate surface often contains contaminants such as oils, greases, oxides, and dirt. These contaminants can act as barriers between the substrate and the coating, leading to poor adhesion, weak spots, and corrosion issues. Surface preparation removes these contaminants, ensuring a clean bonding surface.

c) The appropriate level of surface roughness, usually achieved through methods like grit blasting, provides the necessary texture for the coating to adhere properly.

d) Surface preparation methods, particularly those involving abrasive techniques, can introduce beneficial compressive residual stresses in the substrate. These stresses can enhance the fatigue resistance and durability of the coated component.

e) In some cases, surface preparation might involve cleaning and applying a protective layer to prevent oxidation before coating, as oxidation can lead to poor coating quality and reduced service life.

f) A well-prepared surface ensures that the thermal sprayed coating performs as expected, in terms of both mechanical properties and resistance to wear, corrosion, and thermal cycling.

A comprehensive literature review has been conducted on various surface preparation techniques, materials employed in hydro turbine blades, and thermal sprayed coatings.

2.1. Review on Texturing Methods of Surface Preparation:

The Table 2.1 shows the few surface modification techniques with its benefits and limitations.

Table 2.1: Illustrate the benefits and limitations of each texturing methods

S No.	Method of Surface Texturing	Benefits	Limitations	Ref.
1.	Laser Surface Texturing	• High precision. • Applied at ambient temperature. • Demonstrating high efficiency in its operation. • Fast and environmentally sustainable. • Ability to finely manipulate the dimensions and contours of micro-dimples.	• Heat affected zone. • Machining speed is sluggish. • Residual stresses form during the process. • Pileups occur during machining.	[51-54]
2.	Abrasive Jet Machining / Shot blasting	• This jet nozzle machining process reduces costs and simplifies masking procedures. • The specimen's surface is automatically cleaned.	• Random texturing results from variations in impact velocity of abrasive particulates, their size, geometry, texture and hardness as well. • Implementing AJM with masking incurs high costs.	[55]
3.	Chemical Etching	• Eradication of stress or other kinds of distortions. • There is no such requirement of mechanical work • Free from Burr. • Complex geometries could be computed efficiently.	• Not environmentally friendly. • Slow processing. • Very low Material Removal Rate (MRR) • Corrosive and potentially toxic chemicals are used. • Results in poor surface finish.	[56-59]

4.	Ultrasonic Assisted Grinding [UAG]	• Decrease in average cutting force. • Reduced wheel wear rate. • Diminished grinding heat.	• Reduction in workpiece surface finish. • Minimal spindle vibration. • Decreased subsurface damage.	[60-63]
5.	Metal Injection Moulding	• High Precision. • Enhanced Controllability. • Cost-Effective.	• High requirements for raw materials. • Manufactured parts should be small.	[64]
6.	Micro Milling	• Fabrication of hard materials is possible. • Enhanced surface treatments are achievable. • Directional textures can be fabricated.	• Milling cutter maintenance cost is high.	[65]
7.	Electro Spark Process	• Better Controllability.	• Only conductive materials can be machined.	[66]
8.	IPVD	• Highly stable coatings.	• Complex process control.	[67, 68]
9.	CA-SAG	• Complex shape with a high-level finish.	• Grinding of thin wall surface leads to complication in SAG tools.	[69]
10.	TP & ALD	• It can be used for miniaturized parts.	• The substrate material purity should be high.	[68, 70]
11.	FDUAM	• High Precision • Can manufacture fragile materials.	• Minor adjustments to milling or vibration parameters can result in substantial alterations to the tool path.	[71, 72]
12.	EVC	• It can be used for the intricate pattern.	• Not a continuous cutting.	[73]
13.	Plasma Nano-Texturing	• Isotropic contribution.	• The substrate being utilized plays a significant role in this. • The pristine nano-textured surface got contaminated by inorganic species.	[74]

The first stage in applying any kind of powder to base materials via a thermal spray technique is surface preparation. In order for the coating powder to bind with the substrate, the surface could be prepared using a variety of texturing techniques in addition to conventional approaches. However, laser surface texturing is the most widely used method because to its many advantages and accessibility.

.

2.1.1. Review on Surface Texturing on different Grades of Steel:

The sand blasting process is the standard practice for surface modification prior to deposition of coating using thermal spray process. The shape on the surfaces generated is different irregular shapes. Because an irregular surface shape is generally better for supporting the adhesion of thermal spray coatings compared to a regular, smooth surface. An irregular surface is better for supporting the adhesion of thermal spray coatings because it enhances mechanical interlocking, increases surface area, improves stress distribution, and allows for better penetration of the coating material. These factors collectively lead to stronger, more durable coatings that are less likely to fail during service.

In the present study, the substrate underwent pressure blasting using specialized pressure blasting equipment. The surface blasting was conducted using brown alumina particles of 20 mesh fineness. The irregular surface was formed by taking into account the blasting characteristics, including air pressure (5 bars), blasting distance (4.5"), and blasting angle

The Table 2.2 has shown the literatures review on surface texturing on various steels with texturing methods, shapes of texturing methods, materials, various texturing parameters with its critical observations.

Table 2.2: The different shapes of textures with process parameters and observations by various researchers

Texturing Method	Texturing Shape	Materials	Texturing Parameters	Observations	Ref.
Laser	Circular and Bi-triangular dimples	100Cr6 Bearing steel	• Power: 80, 40, and 30% • Speed: 200, 1000, and 1000	**1.** Dimples with a bi-triangular shape at a higher density (20%) exhibited lower	[75]

			mm/sec • Frequency: 40, 55, and 65 kHz • Density: 7 and 20% • Average depth: 8 µm • Distance in the array: 714, 1137, 681 µm	coefficients of friction (COF) and wear. **2.** Increasing the dimple density has resulted in a reduction in wear.	
CO_2 laser	Triangle Circular and Square	HSS	• Average power: 21.1 W • Frequency: 20 kHz • Wavelength: 950 nm • Dimple area size: 0.01, 0.03 and 0.09 mm^2 • Dimple area density: 7.5, 10, and 15% • Dimple depth :10-15 µm	**1.** Circular-shaped dimples with an area density of 7.5% and a dimple area of 0.09 mm^2 demonstrated greater efficiency for wet lubrication compared to triangular shapes. **2.** Dry lubricated, triangularly-shaped dimples along with the same dimple area and density, provided optimal wear resistance. Despite that, when it comes to machining without lubricating agent, the texture-less surface exhibited lower wear parameter ratings.	[76]
Nano-second pulsed Nd: YAG laser Ultra short pulsed femto second Ti:Sa.	Circular	SAE 1035 steel	• Dimple diameter: 25, 30, and 100 µm • Dimple depth :4, 5 and 10 µm	**1.** Reducing the diameter of dimples decreases the coefficient of friction considerably. **2.** The most favorable dimple (diameter of 100 microns and depth of 10 microns) has identified. Textured with small, shallow dimples exhibit	[77]

				reduced friction and high wear resistance, especially in lubricated contact with materials like ceramics.	
Pico-second Nd-YAG	(Circular dimple, Elliptical dimple, and Groove)	40 Cr steel and Cast iron	• Dimple diameter: 100, 200, and (80/120) µm • Dimple depth :10 µm • Column space : 0.2, 0.4 and 0.5 mm • Line Space: 0.4 and 0.6 mm	According to the study, grooves, elliptical dimples, and circular dimples all performed better in terms of wear resistance, friction stabilization, and friction reduction, respectively.	[78]

Various researchers [91-94] have effectively achieved various forms of texturing on steels using diverse techniques. However, laser surface texturing (LST) has been the predominant approach for texturing due to its numerous advantages, as illustrated in Table 2.1. The analysis of Table 2.2 has determined that the circular form of texturing is the most beneficial since it reduces sliding wear most effectively. b). Texturing significantly improves the characteristics of materials for which adequate lubrication is required. Absence of lubrication renders the impact of texturing on material performance insignificant.

2.2. Review on Tungsten Carbide Coatings Deployed using HVOF:

Following the completion of the surface preparation stage of the substrate, the subsequent phase involves the selection of the coating powder. The literature review has led to the identification of the research gaps such as the thermal spray method as high pressure-high velocity oxy fuel (HP-HVOF) has not yet been thoroughly investigated previously. There exists a paucity of research on martensitic steel (SS 410), which has been suggested as the substrate material.

The literatures survey has done on the coating deposited harnessing thermal spray procedure especially HVOF. The Table 2.3 shows the coating powder, the substrate material used by the different researchers, Moreover test conducted on coated samples with their observation.

Table 2.3: Thermal sprayed coatings with coating powder, the substrate, and test conducted to analyze the coating with observations

Coating Powder	**Substrate**	**Test Conducted**	**Coating Thickness**	**Observations**	**Ref.**
WC-10Co4Cr	35CrMo steel	• SEM • XRD • μ-Hardness • Silt Erosion • Porosity and, • Roughness	$(Thickness)_{Avg.}$: 325 microns.	The bimodal coating has superior erosion protection.	[79]

WC-10Co-4Cr	AISI-4140	• SEM • XRD • EDS • μ-Hardness • Roughness and, • Abrasive Wear.	Pre Grinding: Hardened Chromium: 203±16 microns. Tungsten Carbide: 218±23 microns. Post Grinding: Hardened Chromium: 135 microns. Tungsten Carbide: 138 microns.	**1.** The wear resistance values for WC-10Co-4Cr coat turned out to be 500 folds more than that of SAE 4140 steel. **2.** The principal wear mechanisms identified were abrasion and adhesion resulting from plastic deformation.	[80]
WC-17Co	Steel	• SEM • BSE • FIB • EDS • XRD	Area (μm^2): 13.	Greater degree of flaws and porosity in the starting composition of the powder which develops when the fine particulates are sprayed (Less than five micrometers). This is validated in considerable plastic deformation during impact.	[81]

WC-Co reinforced with carbon nanotube	Ti-6Al-4V	• FE-SEM • XRD • μ-Hardness • Roughness • Super abrasive grinding • Cohesive Strength • Residual Strength and, • Ball on disc	There is an increase in diameter up to 28nm.	**1.** The elastic modulus, cohesion, and hardness values were enhanced up by 10%, 33%, and 30% in the case of the strengthened coating. **2.** CNT improves the coat's characteristics, such as hardness, fracture toughness, elastic modulus, and wear resistance.	[82]
1.(Cr_3C_2 25Ni Cr) **2.** (WC 10Co 4Cr)	Tool steel (H13)	• SEM. • XRD • μ-Hardness • Roughness and, • Abrasive Wear	118.3 and 122 microns respectively as in coatings	A variety of wear events were encountered by both punches, with abrasion and thermal fatigue being the most common.	[83]
WC-17Co	AISI 1045 steel	• SEM • XRD • EDS • μ-Hardness • Sliding Wear (Ball on disc)	$(Thickness)_{Avg.}$: 300 microns.	Cermet exhibited the highest levels of hardness values as well as the transverse rupture strength (TRS).	[84]

1. Ni-Cr_2O_3 **2.**NiBCrSi-WC(Co)	SS 316L	• SEM • XRD • EDS • Micro Hardness • Roughness • Silt Erosive Wear	**1.** 261±95 microns. **2.** 265±35 microns respectively as in coatings	**1.** The erosion wear rating order was established as NiBCrSi-WC (Co) > Ni-Cr-O > SS316L at angles of 45°, 30°, and 0°. **2.** However, at an impingement angle of 60°, the sequence shifted to Ni-Cr-O > NiBCrSi-WC (Co) > SS316L.	[85]

WC-Co-Cr and WC-Co-Cr/Mo	Ti6Al4V	• SEM • XRD • μ-Hardness • Bond Strength • Scratch Test • Erosion Test	Average thickness: 255 ± 20 μm.	For the WC-Co-Cr and WC-Co-Cr/Mo coatings **1.** Average micro hardness (1173 ± 25 and 1020 ± 32 HV0.3) respectively **2.** Porosity: (1.14 ± 0.10 and 1.30 ± 0.14) respectively 3. Bond strength: (58.32 and 54.51 MPa) respectively **4.** Scratch resistance: (65.36 and 52.76 N) **5.** Density: (9.4061 and 7.0213 g/cc g/cc) **6.** The WC-Co-Cr coating, when sprayed, demonstrated superior erosion resistance compared to WC-Co-Cr/Mo across all tested temperatures.	[86]

The thorough literature research [79-86] on tungsten carbide (WC-10Co-4Cr, also known as WOKA-3653) coatings created by thermal spraying, particularly high velocity oxy fuel, has led to the following important conclusions. Hard metal-based coatings typically use two main constituents: Cr_2C_3/NiCr and Co, respectively, mixed with tungsten (WC) carbides. For wear-related applications, tungsten carbide particle coatings

are generally advised in settings where the service temperature is less than 500 ºC. Not only does chromium increase impact resistance but it also improves corrosion resistance; substantial amounts of cobalt are added to boost toughness.

Typically, chromium carbide is utilized at temperatures higher than those appropriate for tungsten carbide, with a functional temperature range of 540 ºC to 815 ºC. Nickel (Ni) and chromium (Cr) are included as additional alloying elements into chromium carbide to prevent its degradation during spraying (carbon loss) and enhance its targeted physical and mechanical characteristics. Composite coatings based on TiC-Ni are designed to narrow the gap between WC and Cr_3C_2 coatings by exhibiting quite high resistance to corrosion and abrasion.

2.3. Literature Survey on the Effect of Rare Earth Oxides on HVOF Coatings:

To enhance the carbide coating's erosion performance, the scientific development moves with the addition of the rare earth oxides (REOs) in the carbide coatings. In this section, a review of the literature has been done on the impact of doping rare earth oxides on coats deposited using thermal spray techniques, specifically HVOF. The substrate material and rare earth oxides employed by the various researchers, as well as the effect of rare earth oxides on different attributes with observations, are displayed in Table 2.4.

Table 2.4: Rare earth oxides, the substrate, and its effect with its observations

Rare-earth oxides	Substrate	Effect of rare-earth oxides	Observations and results	Ref.
CeO_2	**1.** AA 1050, **2.** AISI 304, and; **3.** Nickel Alloy (NIMONIC C263).	**1.** Thin Iridium coating (5–15 nm) exhibited an enhancement comparable to its superior surfaces which comprises a progressive structure. **2.** The hydrophobic nature of the coated substrate was touchy to O/Ce proportion. **3.** The 'delayed' hydrophobicity observed in CeO_2 coatings was attributed to the gradual reduction from Ce^{4+} to Ce^{3+} over time. This incomplete reduction process eventually resulted in a gradual transition from hydrophilic to hydrophobic behavior.	**1.** The coating behavior is closed to super-hydrophobicity with an increase in contact angle by 30-40% in contrast to a smooth surface. **2.** The greatest interaction angle, smoothest surface and the most vital surface texture has been achieved on SS, which showed the best among the three.	[87]

1 wt% CeO_2 + WC-12CO powders	Q345 steel	**1.** When the temperature was below 550ºC, WC–12Co coating modified with CeO_2 showed good oxidation resistance. **2.** The coatings rapidly shedded and failed over 750ºC. **3.** By preventing the development of the W_2C phase and the creation of WC crystals, the introduction of Rare Earth enhanced the quality of the coating. **4.** The high micro-hardness, low porosity, and surface roughness have been achieved by rare-earth modified coatings than those of the nano-modified coatings.	**1.** Oxidation results of the altered coating were mainly comprised of WO_3 and $CoWO_4$ with the temperature ranging between 450–750ºC.	[88]
NiCrAlY powder + additive CeO_2 (0.4 wt-%)	Ni and Fe based super alloys	**1.** Coatings showed murky and splat-like stacked morphology with porosity under 1.5%. **2.** Due to the presence of ceria in a tiny percentage in the coatings exhibited higher hardness.	**1.** Using X-ray diffraction patterns, a conclusion has been made that the c-nickel structure, along with chromium, was the dominant phase.	[89]

NiCrAlY–0.4 wt-%CeO_2	Super alloys	**1.** The HVOF technique was successfully employed to sediment NiCrAlY–0.4 wt-%CeO_2 on the surface, using LPG as fuel. **2.** The coating resulted in a decrement in areal density by approximately 1/20 for Superni 76, 1/50 for Superni 750 and 1/100 for Superfer 800, respectively.	**1.** The NiCrAlY with cerium oxide coatings deposited by the HVOF process over Superni 76 alloy showed a grey scale along with a bit of light green marks. **2.** When bare super alloys exposed at 900ºC in the given environment showed a considerable enhancement in the weight followed by cracking and splintering the oxide scale.	[90]
Ni–20Cr + 1%Zr	Boiler steel with and without 1%Zr addition (ASTM-SA213-T22)	**1.** The coating hardness enhanced greatly by Zr. **2.** The oxidation resistance and hardness of the Ni–20Cr coating were observed to elevate upon the incorporation of 1% Zr. **3.** Zirconium-rich oxide stringers contribute to the improved bonding of the oxide scale in HC_2 coating, enhancing its aversion to oxidation. **4.** Spallation was noted to decrease in compositions containing base coating subsequent to the addition of 1% Zr.	**1.** The HC_2 coating had a dark grey tint, whereas the HVOF-sprayed HCl coating looked brilliant grey. **2.** A marginal rise in the hardness ratings of the steels was noted. **3.** Elemental mapping revealed that the scale primarily comprised nickel and chromium. **4.** Zirconium contributed to a reduction in oxide scale development and enhanced bonding of the oxide scales during hot corrosive wear.	[91]

1% CeO_2-doped WC-12CO	Carbon steel	**1.** Introduction of RE induced a betterment in mechanical characteristics of coating. **2.** The mechanical characteristics of CeO_2-doped traditional WC-12Co coating were near to the nano-structured WC-12Co coating. **3.** By adding CeO_2, a reduction in porosity and hardness of the RE coating was observed and 15% higher than C coating.	**1.** The microstructure of nano-structured WC-12Co coatings exhibited the highest density, minimal porosity, and no signs of decarburization. **2.** Nano-structured WC-12Co coatings demonstrated the greatest values of micro-hardness, elastic modulus, as well as fracture toughness.	[92]
1 wt.% CeO_2-modified WC-12CO	Carbon steel	**1.** CeO_2-modified WC-12Co coating possessed the best wear resistance. **2.** CeO_2- altered WC-12Co coating possessed the densest microstructure with the lowest porosity.	**1.** The lowest erosion-corrosion resistance has been observed for conventional WC- 12Co coating. **2.** The erosion-corrosion process for all coatings showed a dominated erosion mechanism due to enhancement in corrosion. **3.** Nano-structured WC-12Co coatings have demonstrated the greatest levels of micro-hardness, elastic modulus and fracture toughness also. **4.** The roughness of the conventional WC-12Co coating was more significant as compared to nano-structured WC-12Co coating.	[93]

CeO_2 + WC-12Co	Carbon steel	**1.** Better high-temperature sliding wear resistance has been shown by CeO_2-altered WC-12Co to traditional WC-12Co coating. **2.** Dense oxides of $CoWO_4$ were formed in CeO_2-modified WC-12Co coatings.	**1.** The hardness of the worn surface first increased and decreased with an increment in the test temperature. **2.** At 550°C, the CeO_2-altered WC-12Co coating achieved the maximum micro-hardness value of 1333 ± 25 HV 0.5.	[94]
NiCrAlY Powders plus cerium rich, rare earth metal	Stainless steel	**1.** By the addition of RE, adhesive strength firstly increased up to 0.6 wt. % RE and then decreased further. **2.** The morphological characteristics of the oxide in the case of thermal shock cycles has been improved by RE's addition.	**1.** Fabrication of NiCrAlY powders with rare earth metals by ultrasonic gas atomization showed a shiny and murky surface. **2.** The particle size was distributed uniformly, refinement of powder, and improved cross-sectional micro-hardness.	[95]
0.8 wt.% CeO_2	Carbon steel	**1.** The hardness of the altered 1006-0.8 wt. % coating has been improved by the CeO_2 addition as compared to the unaltered 1006 coating. **2.** Altered 1006-0.8 wt. % coating showed higher Erosion resistance than the unaltered 1006 coating.	**1.** RSM was used to develop an empirical relation to understand and predicate erosive wear behavior. **2.** The increment of hardness was observed because of the refinement and development of new phases. **3.** The main mechanisms of MRR in the unaltered 1006 and altered 1006-0.8 wt. % coatings were cutting craters and platelets.	[96]

CeO_2	-	**1.** The improvement in the quality of Cr_3C_2–the addition of CeO_2 took Ni-Cr composite coating and refinement in the microstructure. **2.** Extreme adhesive wear prevailed in HVOF-spray coats, which were responsible for hot oxidation.	**1.** The frictional coefficient of Cr_3C_2–NiCr coating at 800º C decreased with CeO_2 but was not significant at 20 and 400ºC. **2.** The refinement in microstructure and improved hardness has been achieved in Cr_3C_2–NiCr/CeO_2 coatings.	[97]
WC-10Co-4Cr + Erbium oxide (0.9 wt.% Er_2O_3)	Martensitic stainless steel (SS410)	**1.** The improvement in the mechanical properties of the coated samples has observed. **2.** There is an improvement the slurry erosion resistance behavior.	**1.** All the coatings sprayed using HP-HVOF show the hydrophobic behavior with contact angle (≈125˚) due to presence of surface roughness.	[49]
WC-10Co-4Cr + (La_2O_3/CeO_2/Er_2O_3-0.4 wt%. each)	Martensitic stainless steel (SS410)	**1.** The betterment in the hardness ratings of coat up to HV (0.3) ≈ 931. **2.** When compared to the substrate, the slurry's erosion resistance behavior has improved.	**1.** All the coatings sprayed using HP-HVOF show the hydrophobic behavior with contact angle (≈130˚) due to presence of surface roughness.	[98]
WC-10Co-4Cr + (La_2O_3/CeO_2/Er_2O_3-0.2 wt%. each)	Martensitic stainless steel (SS410)	**1.** The betterment in the hardness ratings of the coat up to HV (0.3) ≈ 791. **2.** The slurry erosion resistance behavior has been enhanced.	**1.** All the coatings sprayed using HP-HVOF show the hydrophobic behavior with contact angle (≈134˚) due to presence of surface roughness.	[99]

The mixing of rare earth oxides in the carbide coating and effect of doping on erosion performance is a relatively unexplored field. In the present study a range of REOs (%) doping in carbide coating and synergistic effect on erosion performance has investigated. This combination of unmet research needs result in unique experimental designs. The following important findings have been derived from the comprehensive literature research on the effects of rare earth elements on coatings applied by the thermal spray technique.

a) Rare earth oxides (REO) enhance the mechanical characteristics such as hardness, strength, and elastic modulus.

b) In addition to refining the microstructure, rare earth elements have facilitated the reduction in porosity and cracks.

c) Rare earth oxides have a vital function in improving tribological characteristics, such as strengthening the adhesion of coatings to the substrate and increasing resistance to erosion, corrosion, and wear.

d) The incorporation of rare earth elements improves the resistance of coatings to thermal shock during cyclic temperature shock occurrences.

e) The incorporation of rare earth metals enhances the design of the oxide, therefore inhibiting the formation of spinel-like structures on the underlying surface.

Furthermore, it facilitates the formation of spherical agglomerates and decreases the rate of chromium expenditure.

2.4. Recent Trends on Thermal Sprayed Coatings:

Significant advancements in the field of Materials Science and Engineering have been documented in recent years. Furthermore, even within that field, our primary target has been on enhancing diverse material characteristics. Given the wide range of applications for mechanical components in sectors such aerospace, manufacturing, and vehicles, enhancing the quality of materials has always been imperative. The thermal spray coating technique was developed in the 1900s for this specific purpose. Thermal spraying is a widely used industrial method for surface and the resurfacing of engineered

components [33, 100]. Functional coatings, which are deposited via high-velocity oxygen fuel spraying, are widely used in many industries to enhance performance, extend lifespan, and reduce service costs. notable instances are the use of wear-resistant coatings based on WC-Co in drilling equipment, thermal barrier depositions based on yttria-stabilized zirconia (YSZ) applied to turbine blades, and nickel-based anti-corrosive coatings used in chemical reactors.

Prior research has extensively recorded a diverse range of uses, including heat insulation, conduction, oxidation resistance, hot corrosion prevention, abradable coatings, decorative applications, corrosion protection, repair and restoration, mitigation of different types of wear such as abrasion, erosion, and scuffing, among others.

The term "tribology" is derived from the Greek word "tribos," which means rubbing. It is a field that investigates the process of friction, wear, and lubrication in elements that interact. Mechanical components are utilized in a variety of industries, frequently operating in challenging environments such as high loads, extreme temperatures, and toxic chemical environments. Wear continues to be a common issue in virtually all industries that utilize moving parts, despite their adaptability. It is essential to promptly address deterioration in order to prevent increased costs and a shorter lifespan of components, thereby preserving operational efficiency. Surface coatings are frequently employed to establish a protective barrier between the metal surface and severe environmental conditions, thereby extending the service life of components and assemblies [101].

Thermal spray technology is a collection of coating processes and techniques that are intended to improve the performance of components by incorporating functionality into the surface. The thermal spray technique aims to either extend the lifecycle of a material beyond its inherent structure-based limitations or to impart specific properties, such as optical or electrical characteristics. It is possible to apply thermal spray to nearly any component and find applications in a variety of industries due to its high versatility. A thriving global business valued at several billion dollars has been established as a result of the widespread use of coatings since their invention in the early 20^{th} century. It is

capable of repairing and restoring components, as well as combating corrosion, wear, and severe heat, as a result of its adaptability.

The most significant advancement in thermal spray technology occurred post-World War II. The first decades of the twentieth century witnessed numerous innovations focused on methods of metalizing that employed either combustion or electric (arc) processes. This development was propelled by the requirements and advancements of the space and aviation sectors. During this period, there was a pressing want for methods that could create flames at elevated temperatures in order to manufacture coatings from materials with high melting points, such as ceramics and refractory metals. The period under consideration witnessed significant progress in thermal spray technology with regards to the development of tools and materials [102].

Recent advancements in equipment and material quality have significantly enhanced the technical reliability of thermal spraying operations. Consequently, there has been a significant growth into more specialized sectors including biomedical, dielectric, and electronic coatings. Consequently, spray coating suppliers now offer a broad range of options for thermal spraying equipment, coating materials, and gas selection. However, the available options are typically contingent upon the particular environmental conditions to which the coating will be subjected [103].

The thermal spray process is now well recognized as a crucial and ecologically sound technique for shaping and altering surface properties and component characteristics [104]. The process of thermal spray involves the continuous and concentrated melting and propulsion of particles, usually ranging from 1 to 50 micrometers in diameter, of almost any material, at high velocities. In order to accomplish this, either a combustion flame or a non-transferred thermal-plasma arc using direct current (DC) or radio frequency (RF) is employed. The liquid or partially molten droplets rapidly solidify upon contact with the substrate, generating a thin layer referred to as a "splat." Successive impingements and inter-bonding among these splats result in the accumulation of further layers. Ultimately, a strongly adherent layer, typically around 10

micrometers in thickness, is created. When applying ceramic coatings, it is necessary to employ either a thermal-plasma arc or a combustion flame to melt the particles.

The microstructure and characteristics of the resultant deposit are not only affected by the sprayed material but also are greatly influenced by a range of complex processing parameters. These criteria include a broad spectrum of variables and intricacies. The composition of materials used in thermal spray ranges from metals and alloys with varying melting points, ceramics, to polymers. Coating deposition integrity and quality are evaluated based on three key parameters: oxide concentration, porosity, and bond strength. The relevance of each attribute may differ based on the type of thermal-spray technique used and the intended result [33].

Thermal spray technology comprises a wide array of methods, each providing distinct benefits and tailored to particular uses. Gaining a thorough understanding of the mechanical and tribological characteristics of coatings requires a substantial knowledge of these methodologies. The two most commonly used thermal spray techniques are:

a) Flame Spray (Oxy-Fuel): In flame spraying, a combustible gas is mixed with oxygen to create a high-temperature flame, into which powdered or wire feedstock materials are introduced. The heat from the flame melts the material, which is then propelled onto the substrate to form the coating. Flame spray is known for its simplicity, cost-effectiveness, and versatility in coating a wide range of materials [105].

b) Plasma Spray: Plasma spray involves the use of a plasma torch, which generates temperatures exceeding 10,000°C by ionizing a gas (typically argon) and passing it through an electric arc. The extreme heat melts feedstock materials, which are then accelerated and deposited onto the substrate. Plasma spray is renowned for its ability to produce coatings with exceptional adhesion, density, and wear resistance, making it suitable for demanding aerospace and industrial applications [106]. Beyond flame and plasma spraying, other thermal spray techniques such as high-velocity oxy-fuel (HVOF), detonation gun spraying, and cold spraying offer distinct advantages in terms of coating properties and application versatility. The choice of technique depends on factors like

material requirements, coating thickness, and the specific demands of the application [107-109].

There are many useful methods in thermal spraying but we will only focus on one specific method as we have found it is more precise and provides a better finish to the materials and that method is HVOF. HVOF is a thermal spraying technique pioneered in the 1980s. It involves propelling and heating micro-sized particles of metals, alloys, or cermets within a high-speed, combusting gas stream, depositing them onto the substrate to create a coating layer. Combustion flame spraying, vacuum plasma spraying, plasma spraying, and two-wire electric arc spraying are more examples of such techniques. In compare to plasma spraying, coatings applied through HVOF exhibit superior traits such as increased density, bond strength, and toughness. This is attributed to a notably higher impact speed and comparatively lower temperature of the particulates [110].

Fuels like hydrogen, acetylene, propylene, or propane are used in conjunction with pressurized air or oxygen to achieve combustion flame spraying. It is best to avoid this technique when a dense, strongly bonded coat is required, as it usually produces coatings with lower performance. The relatively sluggish flame speed (50 m/s approx.) and the attainment of limited temperatures are the causes of these deficiencies. The HVOF technique uses special torch designs that allow a compressed flame to expand freely when it leaves the torch nozzle, which accelerates the gas significantly—possibly more than Mach 4—. Using a flame that is orientated in a concentrically fashion, the powder feedstock is introduced at the rear of the torch. Particulate matter thus experiences speeds that approach supersonic levels. Thus, the particle thins out upon impact with the substrate and binds firmly to it and any nearby splats. Three important factors that define the quality and integrity of the coated deposition are its oxide content, porosity, and binding strength [33].

The coatings produced by HVOF spraying procedure possess increased bond strength as well as less porosity than those produced by other techniques such as plasma, flame, and electric arc spraying due to a greater impact force and velocity of sprayed powder particulates. HVOF is a continuous process, which is advantageous over air or vacuum

plasma spraying [111]. The mechanical components are exposed to demanding operating conditions encompassing high loads, speeds, temperatures, and aggressive chemical environments. These components are discovered in a diverse variety of applications, which includes exhaust manifolds/ headers, pump shafts; wear sleeves, crankshaft bearings, and more. To safeguard these components from different forms of deterioration, surface modification methods, such as protective coatings, prove highly effective [112].

The well-known thermal spray coating method creates surface coatings by continuously impacting fast-moving droplets and particles that are molten or semi-molten, and by hasty cooling, solidification, and flattening [113]. The fundamental basis of a thermal spray coating is created by quick solidification followed by accumulation of molten metal or ceramic particles, which is accomplished by repeatedly torching various materials such as metals, polymers, ceramics and specially blended combinations of these [114, 115]. The following parts are usually included in the thermal spray process: the substrate, powder/wire feeder, spray torch, gas supply, power supply, control panel and etc. Oxyacetylene flames are used in flame spraying to melt the target materials. This method was the initial development in thermal spraying and involved modifications to oxy-acetylene torches.

The materials that are going to be coated can be wires, rods, or powders. Powders can be gravity-fed from a canister that is directly installed on the spray cannon, or they can be delivered via a central tube utilizing carrier gases like argon or nitrogen. The powders are then introduced into the combustion flame, where they are carried towards the prepared the substrate surface by a mixture of gases. It's worth noting that this process tends to introduce high levels of oxide inclusions in metals. In flame spraying, coating materials typically consist of metals or metal alloys, with flame temperatures typically ranging from 2,800°C to 3,200°C [116].

Accelerated droplets or particles can form a coating when they do the following: (i) stick to the surface, (ii) experience plastic deformation or rapid cooling upon impact to build thin layers, and (iii) overlap and interlock throughout the solidification phase to

form a cohesive coating. Depending on the required thickness, the coating is usually created through a series of passes, ranging from five to hundred [117]. The microstructure and properties of the resulting coat are affected by factors such as particle's characteristics (size, distribution, velocity, and temperature) and the interactions that occur when the particle impacts the substrate.

This process could be divided in to five primary processes: (i) HVOF; (ii) Plasma arc spraying; (iv) Detonation Gun; and (iii) Flame arc spraying [104]. In any thermal spray process, two critical variables, namely the flame jet temperature and the particle speed, are combined to form what is referred to as the 'TV relationship.' This term describes the immediate spatial relations among three distinct physical distributions: the characteristics of feedstock, the high-energy temperature environment, and the speed distribution of gas jet [117]. The particle speed represents speed just before the particles make contact with the sample surface which is influenced by both of inert carrier gas as well as the jet induced velocity field. It's worth emphasizing that in the contemporary context (post-2000), the understanding of TV relationships encompasses factors related to the properties of particles in flight, including details about their size distribution. The flame jet temperature serves as a valuable reference for the operator, offering insights into how thoroughly the sprayed material has melted [118].

Almost 60% of global thermal spray market, which comprises supplies of chemicals, tools, consumables, and coating services, is accounted for by applications involving industrial gas turbines (IGTs) and aerospace. The remaining forty percent is split up among other industries, such as electronics, pulp and paper, biomedical, and oil and gas [115]. Thermal spray coatings find their primary application in high-temperature scenarios, where they provide resistance to oxidation or the corrosive effects of fused salts. Typically, these coatings incorporate rare earth elements to effectively counteract oxidative degradation processes [119].

Nano-structured materials with adjustable properties are gaining significance in various fields, including tribology. Industries such as automotive, heavy machinery, and cutting tools require specialized materials to operate efficiently with minimal energy wastage.

The utilization of nano-structured coatings in tribology, especially under challenging contact conditions, has been a well-established research focus. The exceptional mechanical characteristics exhibited by nano-structured coatings render them ideal for tribological applications, offering reduced friction and minimal wear [120].

Alumina-titania coats are typically produced using atmospheric plasma spraying method. This process, conducted at elevated temperatures, allows for the creation of coatings that exhibit strong adhesion to the substrate and possess controlled porosity levels. Extensive researches have been dedicated to investigating how the projection parameters affect characteristics like porosity, hardness and Young's modulus within the alumina-titania system [121].

Plasma-sprayed alumina-titania coatings find extensive utility across various applications due to their exceptional attributes. Increased wear, heat shock, thermal shock, hot corrosion and oxidation resistance, and electrical insulating qualities could be few of these. Moreover, these coatings are highly desirable because they form strong metallic bonded coats, demonstrate resilience against solid particle erosion, exhibit high hardness, as well as maintain chemical stability even at elevated temperatures [122].

Another option worth considering is NiCr coatings. Generally, this coating functions as a bonding layer for ceramic or cermet coatings in order to enhance the attachment of the deposited material to the surface of the sample. Furthermore, the NiCr 80/20 alloy is employed as a metallic framework to fabricate composite coatings that are strengthened with carbides [119]. Precise monitoring of the velocity and temperature of particles throughout the HVOF spraying process is crucial for maximizing the ultimate structure of the coatings. The Spray Watch system, an online monitoring system, offers valuable insights into the behavior of molten particles during their flight and enables comparisons between the same activities under different situations. The main objective of this comparison study is to examine various compositions produced using different combustion gases and circumstances. The primary focus of this study is to examine the oxidation and porosity characteristics of coatings, as these parameters have the greatest influence on corrosion resistance [123].

Ceramic coatings are primarily applied to components expected to endure extreme conditions. Although when the ceramic material possesses a very high level of hardness, it tends to be brittle. To harness the benefits of hardness while mitigating the drawbacks of brittleness, innovative materials like shape-memory alloys have been engineered. An example of such a material is NIINOL, a nickel-titanium alloy with a chemical composition of Ni50Ti50 [124].

Numerous thermal spray techniques are available for depositing metallic coatings. However, for applications requiring higher temperatures, techniques like flame spraying, arc spraying, plasma spraying, D-Gun, and HVOF spraying are commonly employed [125]. Of all the thermal spraying methods, HVOF has become a powerful and advanced tool for surface engineering. It can provide thick coatings with superior resistance to erosion, corrosion, and wear, as well as high μ-hardness and adhesion characteristics [126]. Detonation spray and HVOF spray stand out as the top choices among commercially available thermal spray coating techniques for obtaining hard, dense, and wear-resistant coatings [127]. HVOF coatings exhibit homogeneity and density superior to other types of thermal-sprayed coatings. However, residual oxides and porosity persist at the boundaries of splats [128].

HVOF spraying has a number of disadvantages, including high costs and the requirement for skilled labor to ensure safety and maintain consistent coating quality; limitations in powder sizes, which typically range from 5 to 60μm and require precise size distributions; and complexity, as properties and microstructure depend on multiple processing variables. Moreover, the need for a line-of-sight and a spray distance of 150–300 mm might make deposition onto the inside surfaces of tiny cylindrical components or other regions with restricted access difficult or impossible [126]. Furthermore, compared to electroplating techniques, HVOF is quicker to apply, less disruptive to the surroundings, and requires less downtime. It also provides less holes and cracks and more density [129].

In many applications, including seals, valves, drilling tools, wire drawing equipment, actuators, impellers, rams, pistons, bearings, shafts, wear and corrosion protection, wear

rings, and valve plugs, HVOF coating is preferred over environmentally hazardous hard chrome. Its versatility allows it to be applied to give high-grade, wear-resistant coatings for satellites and carbides [130]. The industries that now make substantial use of thermal spray technology include aerospace, industrial gas turbine, automotive, biomedical, oil and gas, maritime, processing, textile, paper, and metal processing. This broad use is driven by the potential of thermal spray to create coatings for a variety of purposes, including wear prevention, dimensional restoration and repair, thermal insulation, corrosion and oxidation resistance, lubricity, and biocompatibility.

The potential of thermal spraying for new applications and entry into expanding markets is further expanded by ongoing developments in feedstock materials and thermal spray processes [116]. In an era defined by technological progress and the constant pursuit of innovation, the field of materials science has emerged as a cornerstone of modern engineering. The ability to design, engineer, and optimize materials with specific properties has ushered in a new age of possibilities, enabling the development of cutting-edge technologies and enhancing the performance of existing ones. Among the myriad techniques employed in materials science, thermal spray technology has emerged as a pivotal method for enhancing the properties of surfaces and materials, particularly in the context of coatings.

The mechanical and tribological characterization of thermal spray-developed coatings represents a pivotal area of research, as it not only underpins the viability of these coatings in diverse applications but also unlocks novel possibilities in fields ranging from aerospace to automotive, and beyond. Thermal spraying, a versatile and highly effective materials processing technique, has been utilized for several decades to apply coatings with a wide array of desired characteristics. This method involves the deposition of a molten or semi-molten material onto the substrate, creating a dense, adherent coating that can significantly enhance the performance, durability, and wear resistance of the substrate material [131, 132].

Thermal spray coatings have demonstrated their value in numerous applications, such as prolonging the lifespan of turbine blades in a jet engine, safeguarding vital components

in industrial machinery, and enhancing the corrosion resistance of automobile parts [133, 134]. In order to effectively use the capabilities of thermal spray technology, it is essential to thoroughly investigate the mechanical and tribological characteristics of these coatings. The study of mechanical characteristics, including hardness, adhesion, and tensile strength, is essential for assessing the coating's capacity to resist external forces and wear [135]. Conversely, tribological characterization is concerned with the examination of friction, wear, and lubrication, which are of utmost importance in environments where two surfaces make contact, such as in sliding components and bearings [136].

This extensive investigation of the mechanical and tribological behavior of coatings produced by thermal spray not only answers basic scientific queries but also has significant real-world consequences. We will explore the different thermal spray techniques, the importance of mechanical and tribological characterization, and some notable applications where these coatings have made a significant impact in this introductory discussion. Coatings produced by thermal spray must be mechanically and tribologically characterized as part of materials engineering and science. Coatings tailored to the unique needs of various sectors can be better designed and optimized with its help, since it acts as a link between theory and practice. It is crucial to know the coating's hardness and adhesion strength, among other mechanical qualities, in order to evaluate its resistance to impact, wear, and mechanical stresses [137, 138].

Similarly, tribological properties, including friction and wear resistance, are pivotal in determining the coating's performance in dynamic applications, where the interaction between surfaces can result in wear, friction-induced heating, and even material transfer between surfaces [139]. The significance of mechanical and tribological characterization extends across a multitude of industries. In the aerospace sector, thermal spray coatings have revolutionized the longevity and performance of components subjected to extreme conditions, such as turbine blades and engine parts. The automotive industry relies on these coatings to enhance the wear resistance and corrosion protection of critical components, including engine cylinders and brake components [140, 141].

Thermal spray coatings are crucial in enhancing the longevity and effectiveness of wind turbine components in the renewable energy sector. In the medical domain, they are employed in orthopedic implants to enhance biocompatibility and minimize wear during operation [142]. The objective of this study was to analyze the effects of laser modified HVOF on corrosion and wear resistance in AISI 4140 carbon steel being used as the substrate [143]. Moreover, in the pursuit of sustainability and cost-efficiency, a more profound comprehension of the mechanical and tribological characteristics of thermal spray coatings might result in refinement of coating designs, so reducing material consumption and waste. Therefore, the investigation of this subject area not only enhances technical progress but also corresponds with the wider worldwide objectives of sustainability and resource efficiency.

2.5. Applications and Impact of Thermal Sprayed Coatings:

The impact of thermal spray-developed coatings on various industries can't be overstated. In the aerospace sector, these coatings have enabled the development of more fuel-efficient and environmentally friendly aircraft, reducing maintenance costs and downtime. In automotive manufacturing, thermal spray coatings have improved the performance and lifespan of engine components, contributing to enhanced fuel efficiency and reduced emissions. In the energy sector, wind turbine blades coated with thermal spray materials have demonstrated increased durability, ultimately advancing the adoption of renewable energy sources.

Furthermore, the medical sector has witnessed significant progress in orthopedic implants by the application of biocompatible thermal spray coatings, which guarantee the sustained effectiveness of joint replacements. Within the oil and gas sector, thermal spray coatings serve to safeguard vital components against corrosion and wear in challenging conditions, therefore extending the lifespan of equipment and decreasing maintenance expenses [144]. These applications underscore the multifaceted impact of thermal spray technology, and the mechanical and tribological characterization of coatings remains integral to their continued success in these fields. In conclusion, the

mechanical and tribological characterization of thermal spray-developed coatings is a topic of immense importance with far-reaching implications.

Moreover, combining various reinforcing elements and their oxides is in line with the direction of current research. Through bridging the gap between scientific knowledge and practical applications, researchers and engineers can produce coatings enhancing the sustainability, performance, and durability of materials in many different sectors. As researchers embark on this journey of discovery learning about the ideas, techniques, and advancements driving this field ahead, they will delve deeper into the mechanical and tribological aspects of thermal spray coatings. The researchers will get a greater understanding of the revolutionary potential of thermal spray technology and its critical role in influencing the direction of materials science and engineering via this endeavor.

CHAPTER 3

Problem Formulation

In this chapter, after reviewing the literature critically, brainstorming the research gap and setting out the objectives of the present study have been formulated.

3.1. Research Gaps:

The literature review has led to the identification of the following research gaps:

- The thermal spray method as high pressure-high velocity oxy fuel (HP-HVOF) has not yet been thoroughly investigated in many uncharted research areas.
- There is very little research conducted on martensitic steel (SS 410), which has been considered as the substrate material.
- There is a limited work available on the doping of rare earth elements in WC-Co-Cr coatings.

3.2. Research Objectives:

In light of the above-mentioned gaps, the present investigation aims to complete the following objectives:

- To develop the rare earth doped tungsten carbide composite coating by HP-HVOF thermal spray on stainless steel as the substrate.
- To characterize the rare earth doped tungsten carbide composite coating.
- To test and analyze the mechanical characteristics of the rare earth doped composite coating.
- To test and analyze the tribological characteristics of the rare earth doped composite coating.

CHAPTER 4

Materials and Methods

This chapter includes materials and methods include the information about the substrate, coating materials and process of coating deposition along with equipment specifications to characterize the coated and uncoated samples.

4.1. The Substrate Material:

The base metal used was annealed and pickled Martensitic stainless steel of grade SS410, with dimensions (305×254×5) mm^3. It was received from Bhagirath Steel and Alloys, Delhi. The specification of the received material (SS410) is listed in Table 4.1.

Table 4.1: Chemical composition of the substrate (SS410)

Element	**C**	**Si**	**Mn**	**P**	**S**	**Cr**	**Ni**
Wt.%	0.13	0.53	0.65	0.03	0.004	12.45	0.18

In this research work, Stainless Steel (SS410) has been selected as the base material for applying high pressure-High Velocity Oxy Fuel (HP-HVOF) sprayed coatings. SS410 is a martensitic stainless steel known for its excellent mechanical properties, corrosion resistance, and heat treatability, making it a suitable choice for hydromachinery components that operate under harsh conditions. After procuring the SS410 material, a comprehensive elemental analysis was performed using spectroscopy techniques to determine its exact chemical composition. The spectroscopy results revealed the presence of the following elements: Chromium (Cr) at 12.45%, Manganese (Mn) at 0.65%, Silicon (Si) at 0.004%, Carbon (C) at 0.13%, Phosphorus (P) at 0.03%, Sulfur (S) at 0.53%, Nickel (Ni) at 0.18%, and rest as Iron (Fe). All the elements are found to be in good accordance with the ASTM standards. These elements contribute to the unique properties of SS410, with chromium providing corrosion resistance, manganese and silicon enhancing strength and hardness, and carbon allowing for heat treatment and increased wear resistance.

4.2. Coating Powder:

4.2.1. Tungsten Carbide (WC-10Co-4Cr):

The Metallizing Equipment Company (MEC) Pvt. Ltd. Jodhpur provided the cermet powder (WC-10Co-4Cr) for coating, with specifications is depicted in Table 4.2.

Table 4.2: Detail of carbide coating powder (WOKA-3653)

Powder	Particle shape	Morphology	Particle size	Supplier
WC-Co-Cr (86/10/4)	Spheroidal	Agglomerated Sintered	15-45 µm	MEC Pvt. Ltd.

The closely clustered sintered spheroidal shaped carbide (86WC-10Co-4Cr) powder with a particles range of 15-45 microns were used for coating purpose, as listed in Table 4.2. The Scanning Electron Micrograph (SEM) and Energy Dispersive X-ray Diffraction (EDS) of powder have shown in Figure 4.1a.

4.2.2. Rare Earth Oxides (REOs):

The rare earth oxides powder for doping was available commercially at Nano Research Lab. The specifications of the rare earth oxides have been depicted in the Table 4.3. The doping element used was rare earth (99% purity) oxides such as Cerium oxides, Lanthanum oxides and Erbium oxides powder with a particles range of 5-10 microns.

Table 4.3: Detail of rare earth oxides powder

Powder	Particle shape	Purity	Particle size	Supplier
Cerium Oxides (CeO_2)	-	99%	5-10 µm	Nano Research Lab
Lanthanum Oxides (La_2O_3)				
Erbium Oxides (Er_2O_3)				

The coating powders utilized in this study were subjected to thorough characterization using Field Emission Scanning Electron Microscope (FESEM) equipped with an INCAx-act attachment for Energy Dispersive X-ray Spectroscopy (EDS). This analysis aimed to authenticate the morphology and elemental composition of the WC-10Co-4Cr powder, as

well as the rare earth materials (La_2O_3, CeO_2, and Er_2O_3) incorporated into the coating formulations. The FESEM imaging revealed distinct morphological features of each coating powder. The WC-10Co-4Cr powder exhibited agglomeration and sintering processes, resulting in an elongated spherical morphology. The particle size distribution ranged from 15 to 45 µm, as depicted in Figure 4.1(a).

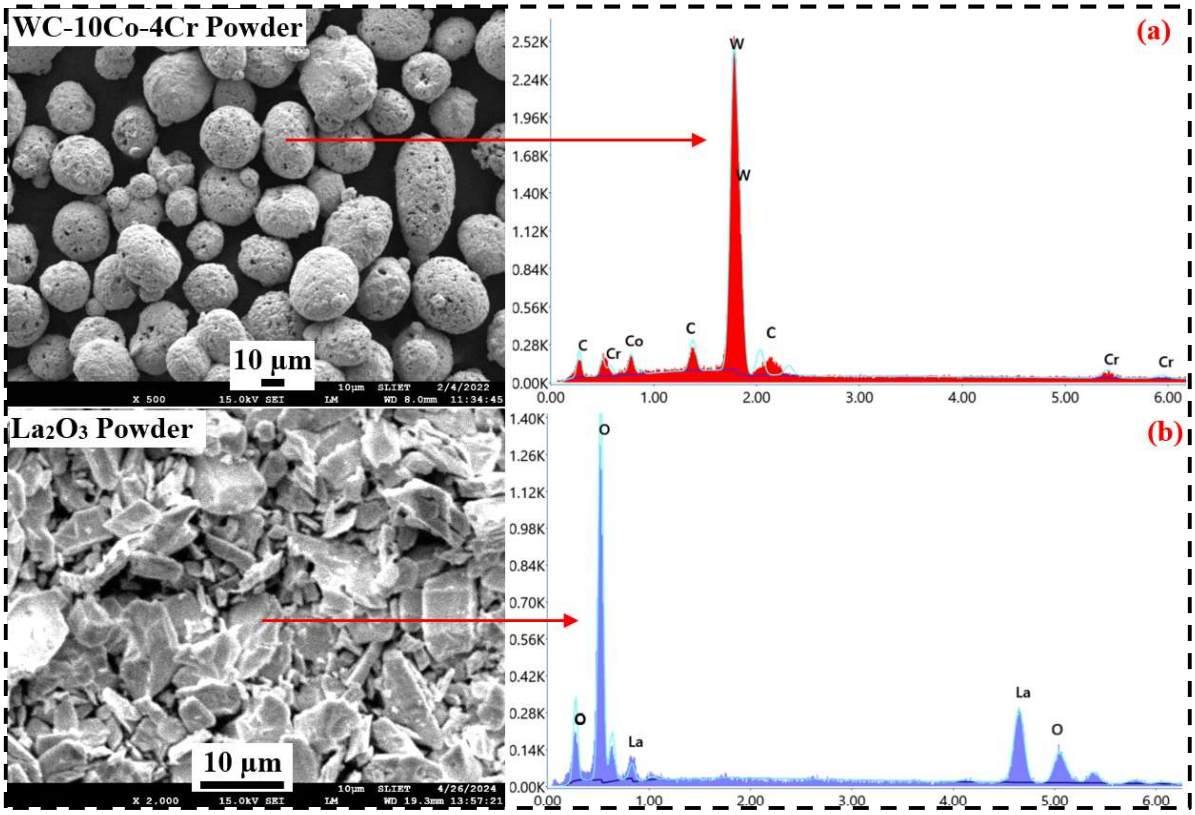

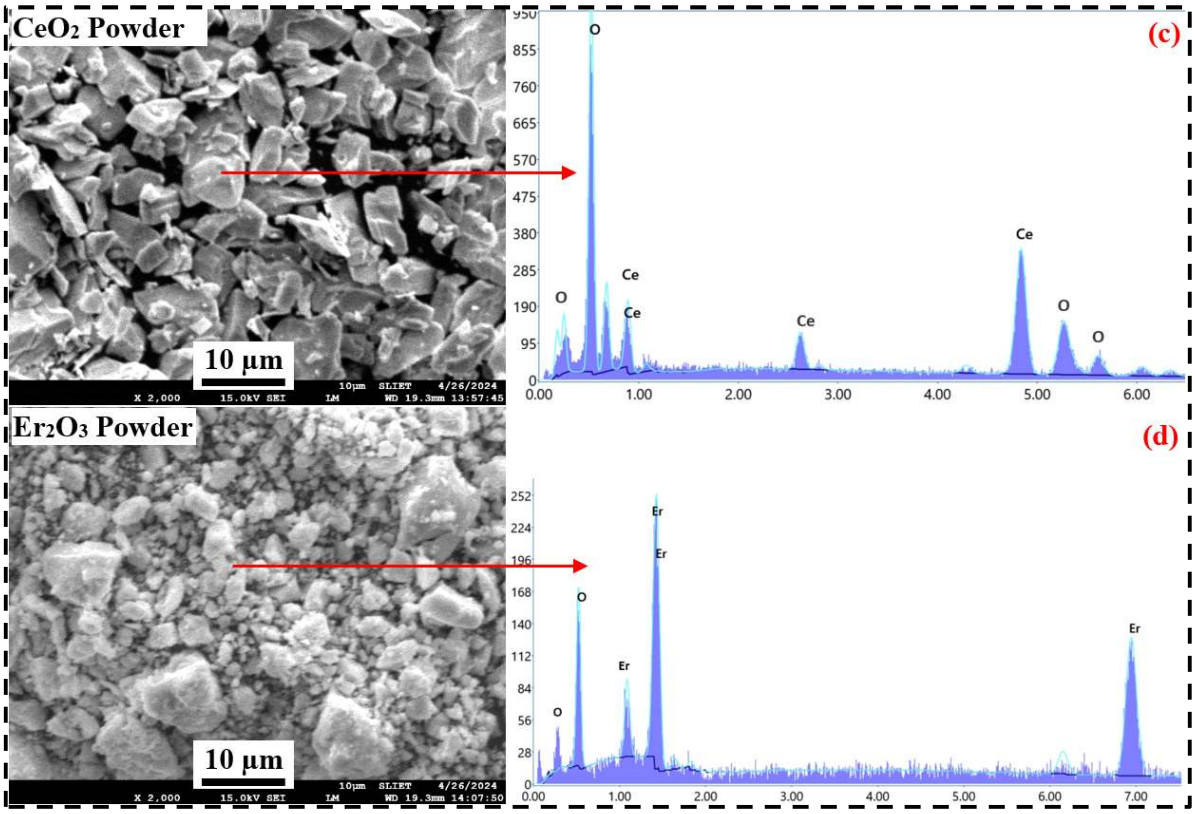

Figure 4.1: SEM and EDS analysis of (a) WC-10Co-4Cr, (b) La_2O_3, (c) CeO_2, and (d) Er_2O_3 coating powder

This morphology is characteristic of thermal spray powders and is conducive to achieving uniform coating deposition with enhanced mechanical properties. Further examination of the rare earth materials, La_2O_3 and CeO_2, revealed a mixed type of morphology, with particles exhibiting an irregular shape and an average size ranging from 5 to 10 µm, as illustrated in Figure 4.1(b) and Figure 4.1(c), respectively. These morphologies are conducive to homogeneous dispersion within the coating matrix, thereby facilitating the desired enhancements in mechanical and protective properties. In contrast, Er_2O_3 material exhibited relatively smaller particle sizes, ranging from 2 to 5 µm, as shown in Figure 4.1(d). This finer particle size distribution may contribute to improved dispersion and homogeneity within the coating, potentially leading to enhanced performance characteristics. Moreover, EDS analysis was conducted to verify the elemental composition of the coating powders. The results confirmed the presence of tungsten (W), cobalt (Co),

chromium (Cr), and carbon (C) in the WC-10Co-4Cr powder, as well as the rare earth elements (lanthanum, cerium, and erbium) in the respective rare earth materials. The good content and uniform distribution of these elements within the coating powders were indicative of their suitability for use in the HP-HVOF spraying process.

4.3. The Substrate Surface Preparation:

Before applying a coating to the surfaces, the substrate (SS410) was subjected to pressure blasting utilizing pressure blasting equipment. The surface blasting was carried out using brown alumina with 20 mesh particle sizes. The blasting parameters, such as air pressure (5 bars), blasting distance (4.5”), and blasting angle were considered to create the rough surface. The rough texture on the surface can enhance the mechanical bonding between the coating and the substrate. To produce the coating, a WC-10Co-4Cr composition of agglomerated sintered carbide powder with a particle size ranges from 15 µm to 45 µm was used. The doping material was rare earth oxides of spherical in shape and particle sizes ranging from 5 µm to 10 µm. Moreover; various concentrations of CeO_2, La_2O_3, and Er_2O_3 were blended with carbide powder to ensure proper dispersion.

4.4. High Pressure - High Velocity Oxy Fuel (HP-HVOF) Method:

This currently industrial opted HP-HVOF process, illustrated in Figure 4.2 was developed to overcome the limitations of the existing high-velocity oxy-fuel (HVOF) process. The coating on martensitic steel (SS410) has been developed using the HP-HVOF system of model XPOJET-5000. The chosen blend of powders has been developed on martensitic steel as the substrate at Metallizing Equipment Company Pvt. Ltd. at Jodhpur, utilizing a commercially available thermal spray (HP-HVOF) coating machine. The coating thickness ranged from 250 to 320 µm.

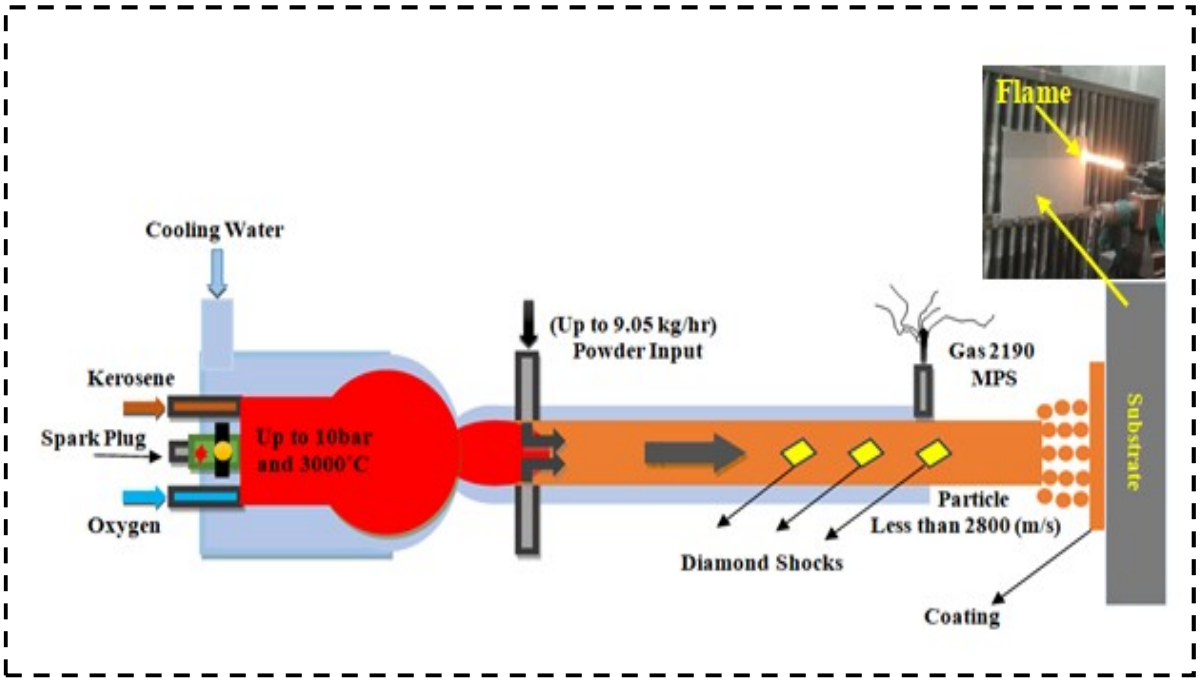

Figure 4.2: Schematic of thermal spray (HP-HVOF) process

The High Pressure-High Velocity Oxy Fuel (HP-HVOF) spraying system has been employed in this research to apply protective coatings onto the SS410 base material. HP-HVOF spraying has been chosen due to its ability to produce coatings with high density, excellent adhesion, and superior wear resistance. The process involves the combustion of a fuel gas, typically hydrogen or kerosene, with oxygen in a high-pressure combustion chamber. The resulting high-temperature flame is then directed through a nozzle, where coating powder is injected into the flame.

The coating powder particles have been accelerated to supersonic velocities and partially melted by the high-temperature flame. Upon impact with the substrate, these particles have flattened and bonded to the surface, forming a dense and cohesive coating layer. The rapid cooling associated with this process has minimized oxidation and thermal degradation of the coating material, thereby preserving its desirable properties. A schematic representation of the HP-HVOF process has been included to illustrate the key components and stages of the spraying system (refer Figure 4.2).

Table 4.4: Process parameters of HP-HVOF spraying system

Gun	MJP-5000
Oxygen flow (SLPM)	850
Fuel flow (ml/min)	380
Chamber pressure (Bar)	6.9
Powder feed rate (gm/min)	75
Spray distance (mm)	330
Particle velocity (m/sec)	785
Flame temperature (˚C)	2630
Spray gun angle (Degree)	90˚

Through the use of the HP-HVOF spraying system, WC-10Co-4Cr coatings were applied to the SS410 substrates in both their pure form and with the addition of rare earth oxides (mixture of La_2O_3, CeO_2, and Er_2O_3 with equal proportions). This specific concentration has been selected based on previous research, indicating that overall 0.9% & 1.2% are optimal for achieving improvements in hardness, toughness, and erosion resistance while maintaining the excellent adhesion and density characteristics provided by the HP-HVOF process.

Further, the parameters for the High Pressure-High Velocity Oxy Fuel (HP-HVOF) spraying process were selected based on existing literature and with the assistance of industry experts to ensure optimal coating deposition and performance. Table 4.4 presents a comprehensive overview of the parameters involved in the HP-HVOF spraying process for applying WC-10Co-4Cr coatings, both in their pure form and with the addition of rare earth materials (La_2O_3, CeO_2, and Er_2O_3), onto the SS410 substrates. The coatings produced by this method were characterized by their high density and strong adhesion to the substrate, which are critical factors in enhancing the resistance of hydromachinery components to slurry erosion.

4.5. Surface Characterization Tests:

The following tests were conducted to recognize the surface behavior of the material at Indian Institute of Technology (IITK) Kanpur.

4.5.1. Energy Dispersive X-ray Spectroscopy (EDS):

The energy dispersive X-ray spectroscopy (EDS), also known as energy dispersive X-ray analysis (EDXA) or energy dispersive X-ray fluorescence (EDXRF), is presented in Figure 4.3. This is a useful analytical technique for determining the elemental composition of a material. EDS is widely used in transmission electron microscopes (TEM) and scanning electron microscopes (SEM) to provide detailed information about the elemental composition of materials at the micro or nano-scale level.

Figure 4.3: Scanning Electron Microscope attached with EDS detector

The μ-compositional analysis were conducted using a W-SEM (JSM-6010 LA) attached with Energy Dispersive X-ray (EDX) detector. EDS has some limitations, including the inability to detect light elements (e.g., hydrogen and helium) and difficulties in distinguishing elements with similar atomic numbers. Quantitative analysis can be challenging, especially in complex or mixed materials. In addition, EDS is a surface analysis technique and may not provide information about the bulk composition.

4.5.2. X-ray Diffraction (XRD) Analysis:

This is a potent analytical procedure employed for discriminating the crystallographic structure of materials. It operates on Bragg's Law, establishing a relationship between the angles of X-ray diffraction by a crystal lattice, the lattice spacing, and the wavelength of the X-rays. The X-ray diffraction analysis was conducted using a machine, such as the Panalytical X-Pert, capable of ultra-fast X-ray diffraction on both bulk and powder samples utilizing a line detector as shown in Figure 4.4.

Figure 4.4: Panalytical XRD machine

The different phases were recognized using respective JCPDS files. XRD has some limitations, such as the requirement for crystalline samples and the need for a monochromatic X-ray source. Amorphous materials, liquids, and gases do not produce X-ray diffraction patterns. Additionally, XRD provides information about the atomic arrangement in a crystal but does not provide detailed structural information about non-crystalline regions in a material.

4.5.3. Scanning Electron Microscope (SEM):

This is a highly effective microscopy method employing a focused beam of high-energy electrons to scrutinize the surface and topography of specimens at exceptional resolution.

Widely embraced across scientific and industrial domains, SEM offers detailed imaging and analysis of material microstructure and morphology. The surface morphologies were evaluated using a scanning electron microscope (model/supplier: JSM-6010 LA, JEOL) (W-SEM) as shown in Figure 4.3. SEM has limitations, such as the need for samples to be vacuum-compatible, which can affect the analysis of some materials. Additionally, because it is a surface imaging technique, SEM may not provide information about the internal structure or bulk properties of a sample.

4.5.4. Surface Roughness Measurement:

Surface roughness measurement involves the quantification and evaluation of the irregularities, or "roughness," present on the surface of a material. The test has been conducted as per ASTM D7127 standard. The surface roughness was measured by means of a surface roughness tester with Mitutoyo Surtest SJ301 as shown in Figure 4.5.

Figure 4.5: Surface roughness tester

A profilometer, or stylus profiler, uses a sharp stylus or diamond-tipped probe to trace along the surface profile of the material. The vertical movement of the stylus is measured, and this data is used to calculate parameters such as Ra (average roughness) and Rz (average maximum height).

4.5.5. Porosity Measurement:

The metallurgical microscope with model: Axiovert A1, Make- Carl Zeiss with a mmagnification range of 100-1000X has been used to test the porosity on coated surface as shown in Figure 4.6.

Figure 4.6: Axiovert A1 Metallurgical Microscope

This test was conducted to determine the total volume of pores to the total volume of the coating. It was also used to determine the overall compactness and rigidity of the coating. The level of porosity has been measured as per ASTM E2109-01(reapproved 2007), Method A.

4.5.6. Contact Angle Measurement:

It is a technique used to evaluate the wettability of a solid surface by a liquid. It provides important information about how a liquid droplet interacts with the solid substrate. Contact angle (CA) measurements are typically performed using a goniometer, a specialized instrument equipped with a camera and lighting to capture the shape of a liquid droplet on a solid surface. The contact angle has been measured using the sessile droplet method as per ASTM D7334-08, using the Contact angle meter (DMe-211 plus, Make: Kyowa Interface, Japan) as shown in Figure 4.7. It characterizes the degree of wetting. Contact angles can vary between 0 degrees (complete wetting) and 180 degrees (complete non-wetting).

Figure 4.7: DMe-211 plus Contact Angle Meter

Common contact angle (θ) measurement values include:

θ < 90°: Indicates a "hydrophilic" surface (favorable wetting).

θ > 90°: Indicates a "hydrophobic" surface (poor wetting).

θ = 0°: Indicates complete wetting, where the liquid completely spreads on the surface.

θ = 180°: Indicates a non-wetting or super-hydrophobic surface.

Contact angle measurements provide valuable information about wettability but may not consider other factors, such as surface roughness, which can influence wetting behavior. The interpretation of contact angles also depends on the nature of the liquid used and its surface tension.

4.6. Mechanical Characterization Tests:

The following tests were carried out to know the mechanical properties of the material at Indian Institute of Technology (IITK) Kanpur.

4.6.1. Tensile Test:

The mechanical properties were determined through a tensile test using an Instron-1195 Universal Testing Machine. The machine has a maximum capacity of 100kN, with a crosshead speed ranging from 0.005 to 40 mm/min and a maximum crosshead displacement

of 700mm, as depicted in the Figure 4.8.

Figure 4.8: Instron-1195 Tensile Test Machine

The tensile test, sometimes referred to as the tension test, is a fundamental mechanical analysis that evaluates a material's mechanical characteristics under axial load. Its primary objective is to determine a material's strength, ductility, and various other mechanical properties when subjected to pulling or tensile forces. The samples were prepared in accordance with the standard of ASTM-E8.

4.6.2. Flexural Test:

The flexural test, alternatively called the three-point bend test or simply the bending test, is a mechanical examination employed to assess the flexural or bending characteristics of materials. This test is particularly useful in assessing the strength, stiffness, and deformation behavior of materials, especially when subjected to a bending load. The flexural test is commonly applied to materials like metals, ceramics, composites, and polymers. The mechanical properties were assessed through a flexural (3-point bend test) conducted on the Instron-1195 Universal Testing Machine. The machine's specifications include a crosshead speed ranging from 0.005 to 40 mm/min, a maximum capacity of 100 kN, and a maximum crosshead displacement of 700 mm, as depicted in Figure 4.8. The samples were prepared in accordance with standards of ASTM- D790.

4.6.3. Hardness Test:

The Vickers hardness test is commonly used to assess the hardness of metals, ceramics, composites, and other materials. The Vickers micro hardness tester, such as the Matrix DVS 1AT8 model, is utilized to determine the hardness value of samples. This tester has a maximum hardness capability of 1600HV and can apply a maximum load of 1 kg as shown in Figure 4.9.

Figure 4.9: Matrix DVS 1AT8 micro Vickers Hardness Machine

The Vickers hardness test is a widely used method for determining the hardness of materials. It measures the ability of a material to resist plastic deformation by an indenter in the form of a diamond pyramid. The following steps were involved for the preparation of hardness test i) To cut the sample of 10mm *10mm dimension ii) Spectro polisher for polishing rubbing uneven surface, iii) Moulding machine for making the mould of hardness samples iv) To polish the surface of mould using double disc polishing. The Vickers hardness test (HV0.3) was conducted in accordance with ASTM-A270 standards with 300g load for 10 seconds of dwell time.

4.7. Tribological Characterization Test:

The applications of the rare earth doped ceramics coating is in the field of marine environment such as hydro turbine blades, impellers and piston cylinder in automobile etc. The silt erosion test has considered analyzing the slurry erosion wear behavior especially for the hydro turbine blade materials application.

4.7.1. Slurry Jet Erosion Test:

In the present study, a slurry jet erosion test rig (TR41 by Ducom, India) has been utilized (shown in Figure 4.10a) to examine the effects of various impingement angles over the slurry erosion of coated and uncoated samples. Also, the triplicate of all the testing has been taken with an aim to get the repeatability of the results and their mean value has been taken into consideration for the mass loss values.

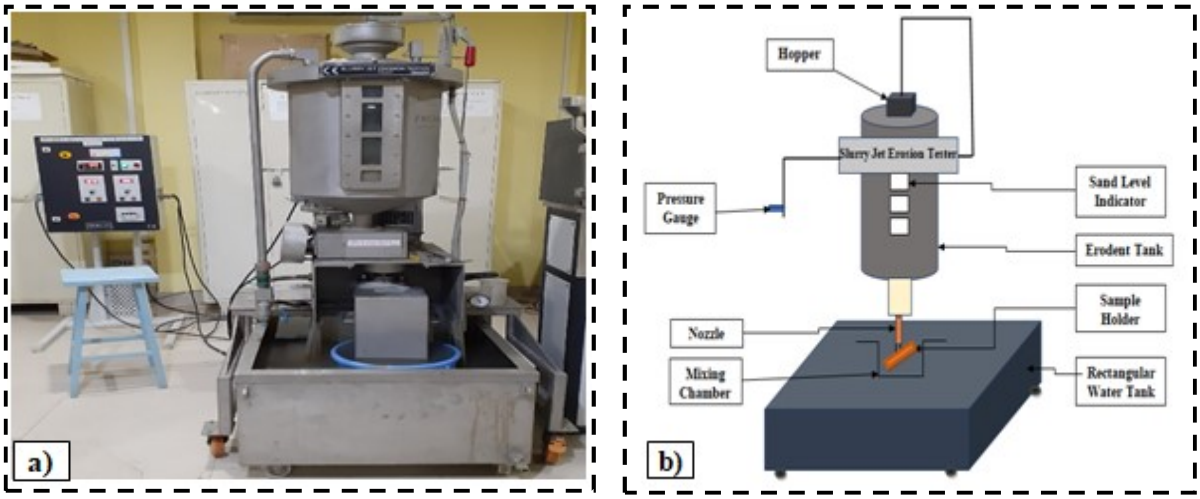

Figure 4.10: a) Slurry Jet Erosion Tester (TR-41), b) Schematic of Slurry Jet Erosion Rig

A detailed schematic of the test rig's configuration has shown in Figure 4.10b. The setup includes a sand hopper designed to contain up to 60 kg of slurry with specified particle sizes. A 1.5 kW single-phase motor is used to pump clean water from a tank positioned at the rig's base for delivering the slurry. Equipped with a 10-mm water filter, the tank ensures the water's cleanliness. Fresh erodent particles are introduced for each test via a spiral mechanism connected to the sand hopper. The flow rate is regulated by adjusting the motor's RPM to guarantee a consistent blend of erodent and high-pressure water within the

mixing chamber. The resulting slurry is sprayed onto secured samples within the specimen holder through a bottom-positioned nozzle under high pressure. In all experiments, the jet velocity and slurry concentration are standardized at 30 m/s and 40,000 ppm, respectively, as previous literature has identified this combination to yield maximum mass loss [30].

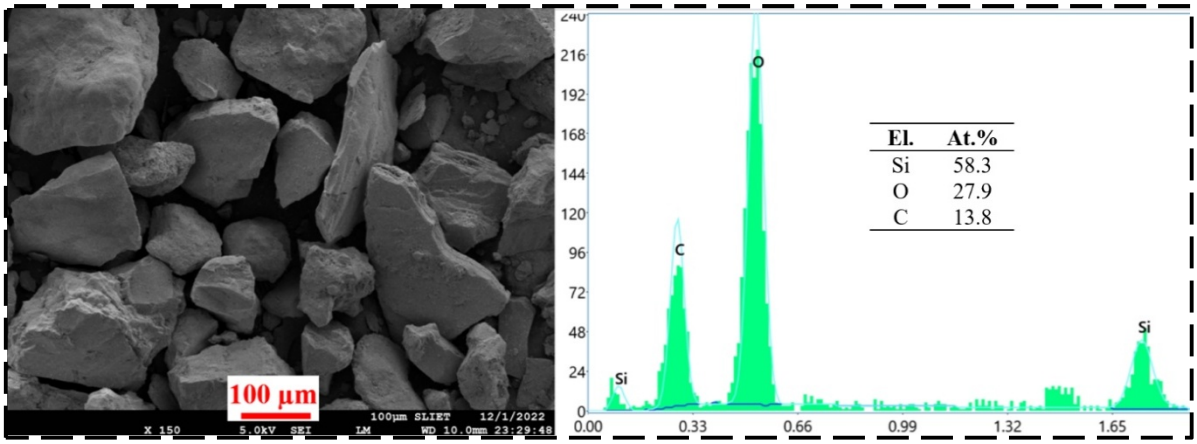

Figure 4.11: SEM and EDS analysis of erodent (sand) used for slurry erosion testing

However, the impact of impingement angle remains inadequately investigated; thus, various angles (ranging from 15° to 90°) are considered in the current study for comprehensive exploration. Also, in Pilot study, 120-minute time had significantly affected stainless steel (SS410). So, the 120 minute-time is considered in current study. Additionally, for precise determination of mass loss, a precision weighing balance with a minimum sensitivity of 0.1 mg is employed prior to and post each erosion trial. These measurements yield crucial data for the experimental analyses. The erosion testing protocols conform strictly to the directives outlined in ASTM G-73 Standard. Furthermore, Figure 4.11 displays a scanning electron microscopy (SEM) image of the sand employed in the slurry erosion tests, accompanied by the corresponding energy-dispersive X-ray spectroscopy (EDS) examination.

CHAPTER 5

Results and Discussion

This chapter presents the details of the results and discussion on all the experimentation including the substrate. Moreover; mechanical, surface and slurry erosion behavior tests of samples have been performed to determine the different properties and characteristics of the coated samples.

PART 1

5.1. Surface Characterization of the Substrate (SS410):

The surface characterizations of the substrate (base material) were investigated using different techniques as follows:

5.1.1. Energy Dispersive X-ray Spectroscopy (EDS):

The identification and mapping of various elements have done using EDS as shown in Figure 5.49.

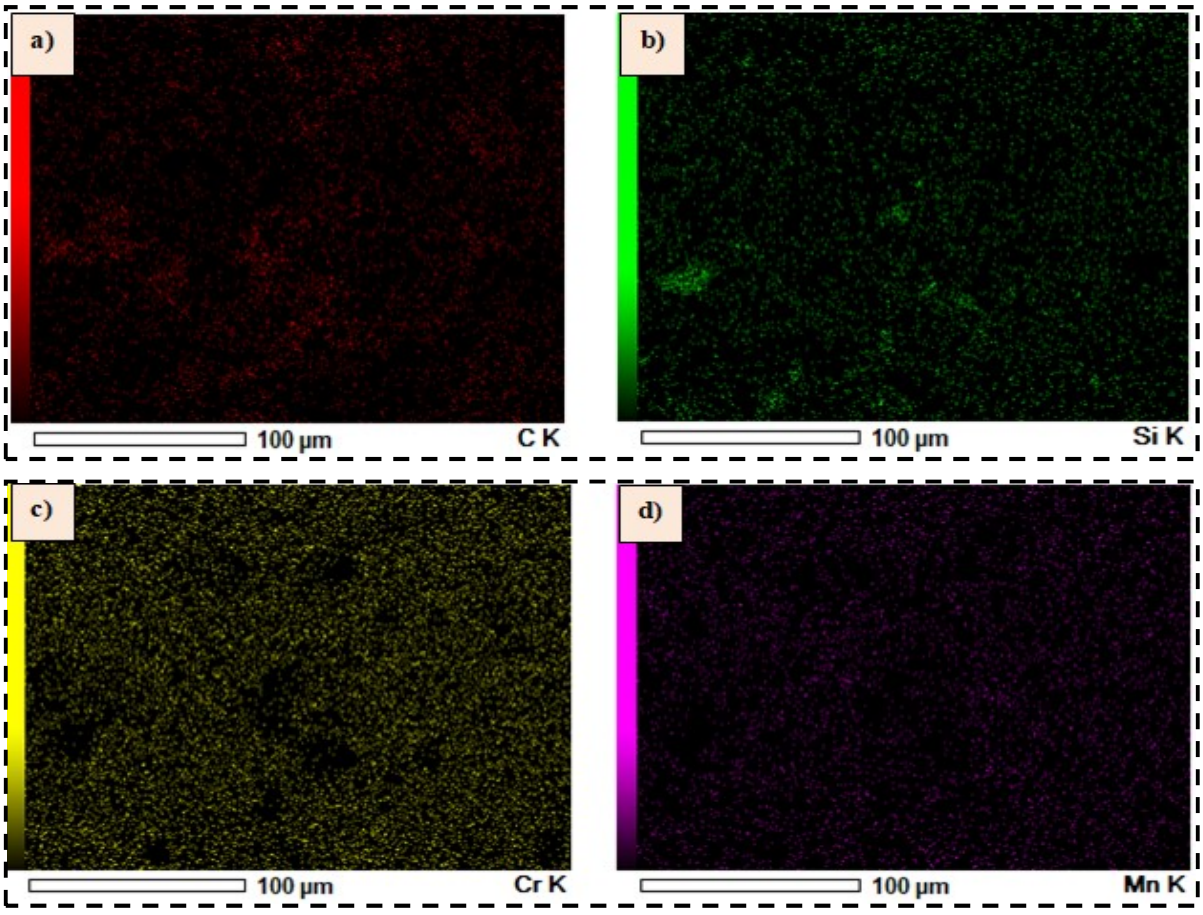

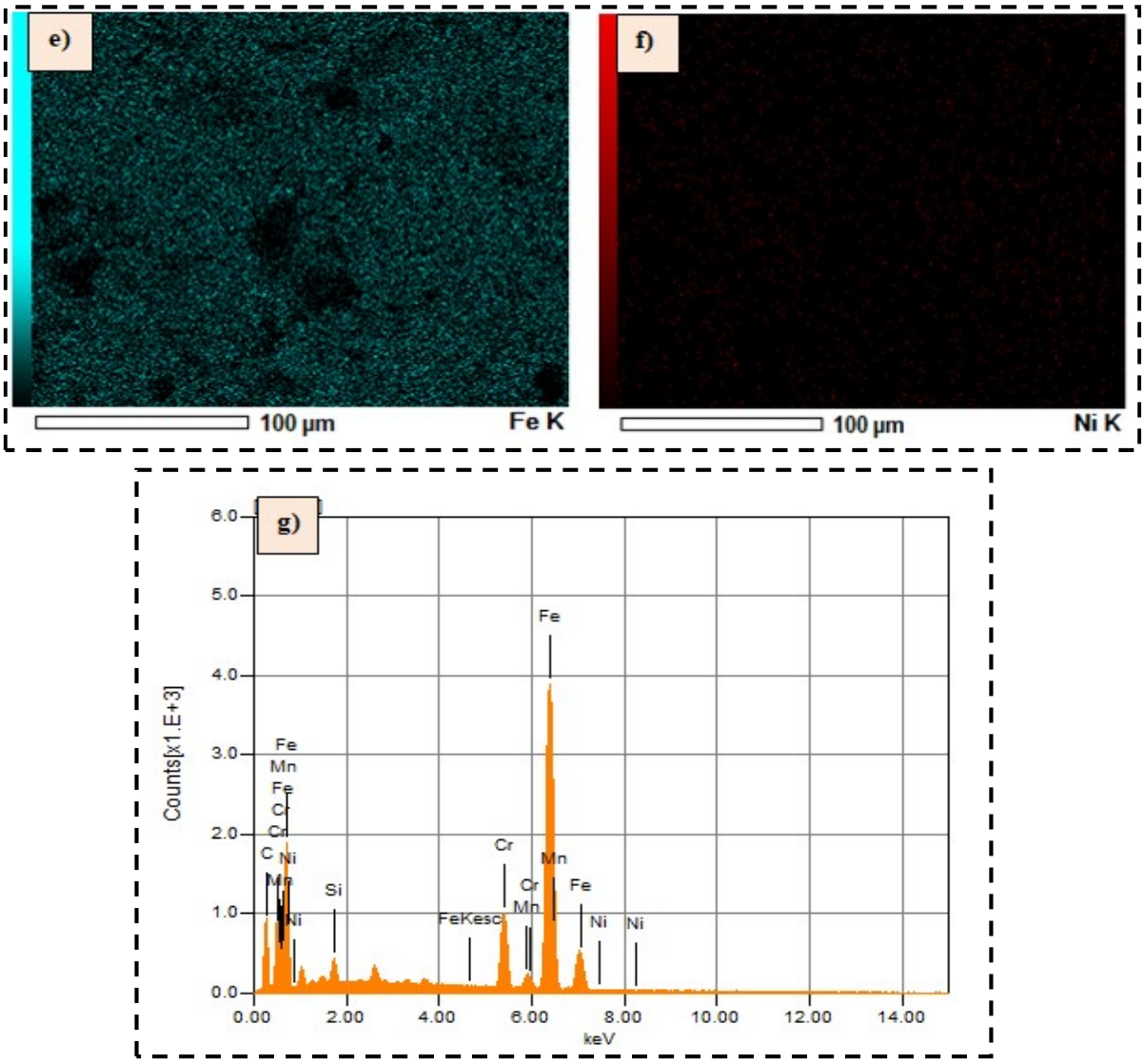

Figure 5.1: The elements identification using energy dispersive X-ray analysis a) Carbon (C), b) Silicon (Si) c) Chromium (Cr), d) Manganese (Mn), e) Iron (Fe), f) Nickel (Ni) and g) EDX peaks of elements for substrate (SS410)

The identification of elements was conducted using EDX, as depicted in Figure 5.1g through peaks of elements. The Figures 5.1a to 5.1f showcase the distinct identification of individual elements, including carbon (C), silicon (Si), chromium (Cr), manganese (Mn), Iron (Fe), and nickel (Ni), with each element represented by a unique color. Prior to the coating deposition on the substrate, the presence of various elements were identified via energy dispersive spectroscopy analysis. The working parameters of EDS have given in Table 5.1 in which live time indicates that the actual time spent collecting useful data, dead

time is the time when the detector is inactive and unable to record new events, and real time is the total duration from the start to the end of the data acquisition, including both live and dead times.

Table 5.1: Working parameters

Acquisition Condition of EDS	
Volt	20.00kV
Live Time	196.60 sec.
Real Time	202.27 sec.
Dead Time	4.00%
Count Rate	1754.00 CPS

5.1.2. X-ray Diffraction (XRD) Analysis:

The XRD analysis was performed on martensitic stainless steel (SS410) samples, depicted in Figure 5.2.

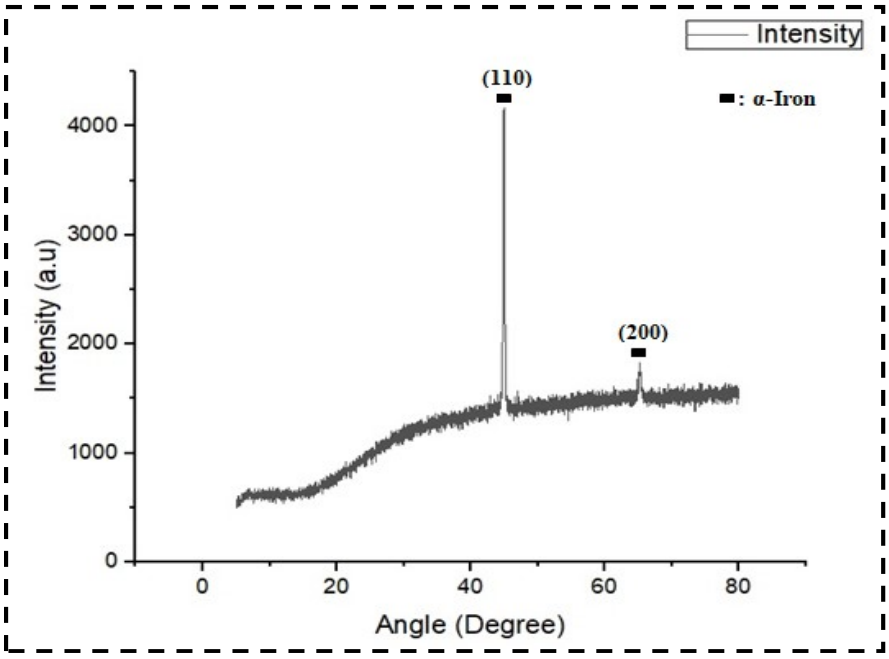

Figure 5.2: X-ray diffraction spectra of the substrate (SS410)

The X-ray diffraction analysis reveals that the different phases available with crystallographic planes. Among various allotropes of iron, the α-phases of iron at different crystallographic planes were identified using JCPDS files. The crystallographic planes (110) and (200) of α- iron were observed as depicted in Figure 5.2.

5.1.3. Surface Morphology of Bare Samples:

The micrographs of the substrate (SS410) using scanning electron microscope at 1000X magnification have shown in Figure 5.3.

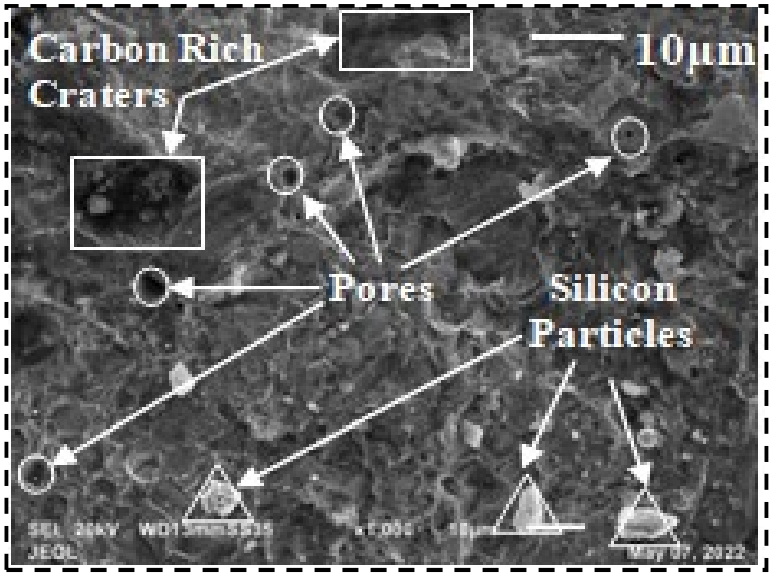

Figure 5.3: SEM micrographs of the substrate (SS410)

The substrate (SS410) has large and deep carbon-rich craters with few silicon particles (identified using EDX). There are limited literatures available on SS410 that includes experimental studies [145, 146].

5.1.4. Surface Roughness (SR) Measurement:

Using a surface roughness tester in accordance with ASTM-D7127 standard, the surface roughness of the substrate (SS410) was measured. The average roughness value of the substrate was 4.38 µm as calculated in Table 5.2.

Table 5.2: Roughness values of the substrate (SS410)

Experiment	Surface Roughness (SR) Values (µm)				Average SR (µm)
The substrate	4.27	4.35	4.65	4.25	4.38

5.1.5. Contact Angle (CA) Measurement:

The static water contact angle (WCA) has been measured on the substrate using the sessile drop method as per ASTM-D7334-08 standard. The average value of static water contact angle has shown in Figure 5.4.

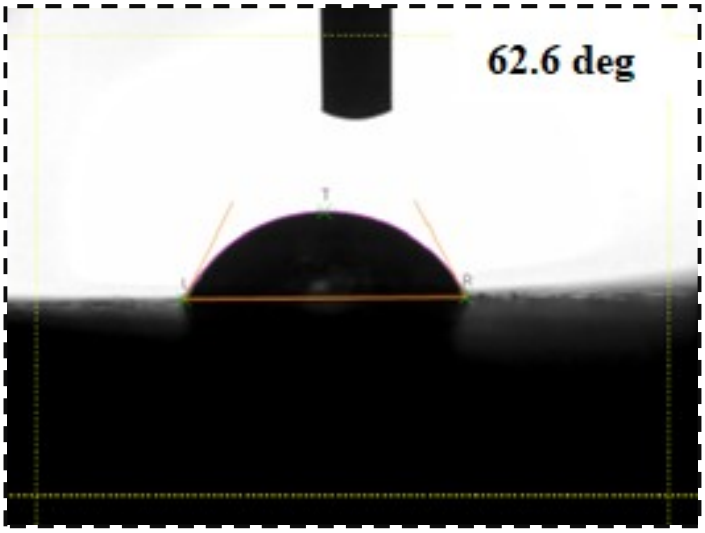

Figure 5.4: Average contact angle of the substrate (SS410)

The average value of WCA for uncoated surfaces was 62.6 degree, which turns out the surface to be hydrophilic as shown in Table 5.3.

Table 5.3: Static water contact angle values of the substrate (SS410)

Experiment	Contact Angle (CA-deg.)			Average CA (deg.)
The substrate (SS410)	60.9	64.2	62.7	62.6

5.2. Mechanical Characterization of the substrate (SS410):

5.2.1. Tensile Test:

The samples were ready using standard (ASTM-E8) as shown in Figure 5.5a. The digital microscope (model: AM7115MT at 150X) was used to investigate the fractured sample's cross-sectional area as shown in Figure 5.5b.

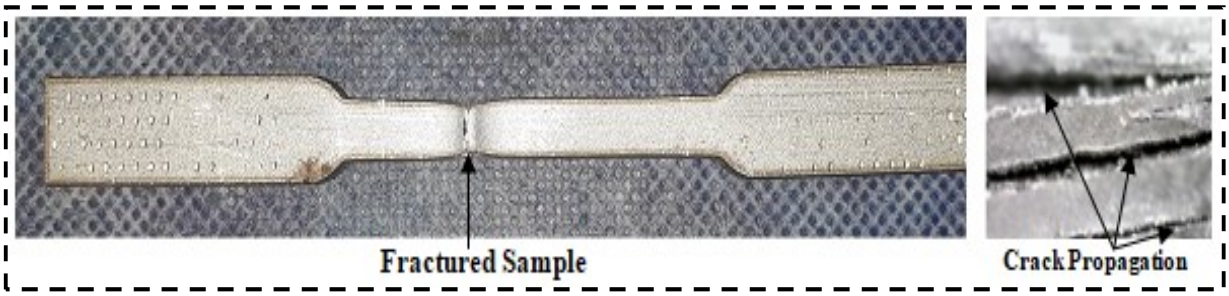

Figure 5.5: Sample of tensile test, a) after fracture and; b) fractography of the substrate (SS410)

The large size cracks propagation was observed at the fractured area as shown in Figure 5.5b. The stress-strain diagram for the substrate was generated through a tensile test conducted employing the universal tensile testing (UTM) machine.

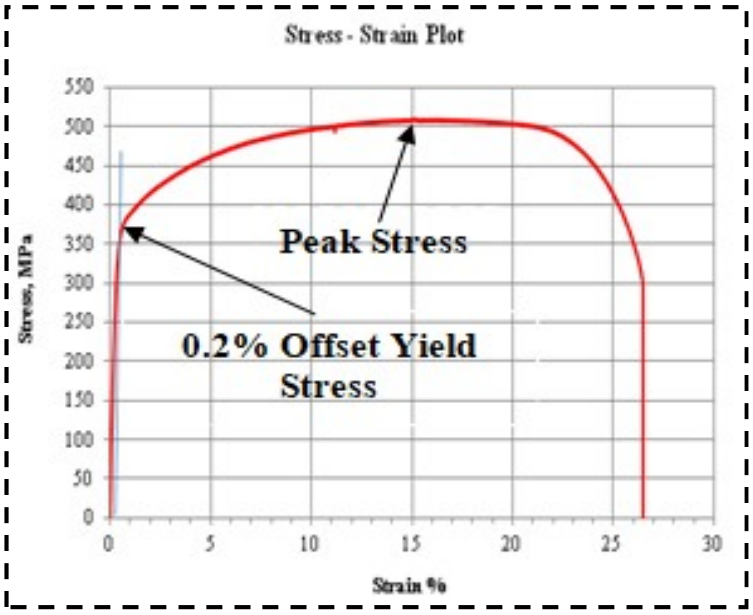

Figure 5.6: Stress-strain curve of the substrate (SS410) generated from tension test

The stress-strain data is computed in order to derive the different values of mechanical properties, as illustrated in Figure 5.6 and average values have been illustrated in Table 5.4.

Table 5.4: Different values of mechanical properties of the substrate (SS410)

Properties	Average Values
Peak Stress (MPa)	508.7
0.2% Offset Yield Stress (MPa)	355
Yield Strain (%)	0.47
0.02% Offset Yield Stress (MPa)	251
Modulus (GPa)	117
Elongation at Break (Using Strain) (%)	26.48

5.2.2. Flexural Test:

The specimen was prepared as per the ASTM-D790 standard. The substrate (SS410) sample after the bend test has been shown in Figure 5.7.

Figure 5.7: Samples of flexural test of the substrate (SS410) after bend test

To know the flexural strength of bare sample, three point bend test has been carried out.

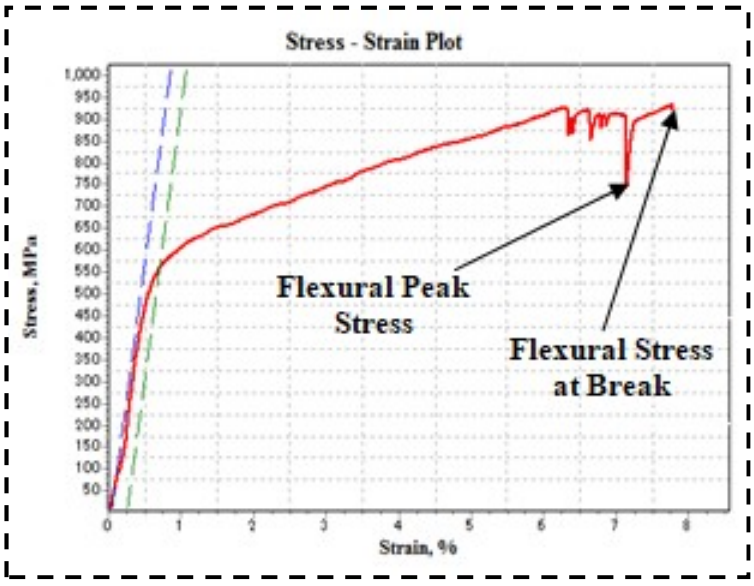

Figure 5.8: Stress-strain curve of the substrate (SS410)

The flexural stress v/s strain diagram as shown in Figure 5.8 is for the substrate, made up of stainless steel.

Table 5.5: Flexural (3-point bend) test results of the substrate (SS410)

Properties	Average values (MPa)
Flexural Peak Stress	781.82
Offset Flexural Yield Stress	0.72
Flexural Stress at Break	921.67

.

The flexural peak stress value shows the capability to resist bending before yield. The values of different mechanical properties obtained from flexural test were premeditated from stress-strain plot as depicted in Figure 5.8 and average values have shown in Table 5.5.

5.2.3. Hardness Test:

This test has been conducted on the substrate in accordance with ASTM-A270 standards with 300g load for 10 seconds of dwell time.

Table 5.6: Vickers hardness test values of the substrate

Experiment	Hardness Value (HV0.3)			Average Value
The substrate (SS410)	194.2	192.5	193.7	193.47

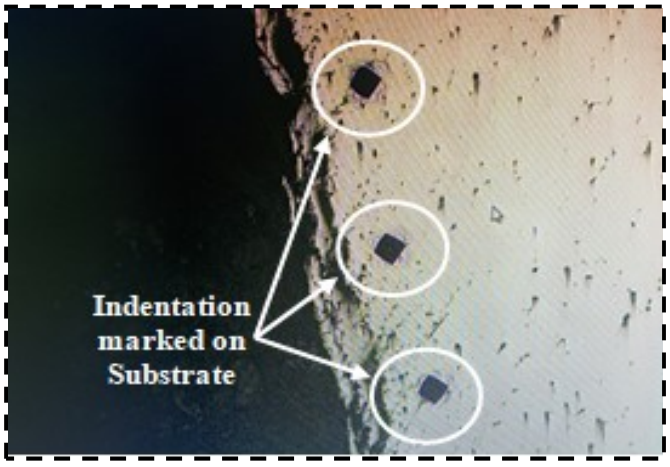

Figure 5.9: Indentation marked on the substrate (SS410)

The average Vickers hardness value has shown in Table 5.6 and the obtained indentations marked using indenter on the substrate has shown in Figure 5.9.

5.3. Tribological Characterization of the Substrate (SS410):

To know the tribological behavior, the slurry erosion test has performed on the substrate (SS410) at varied impingement angle.

5.3.1. Slurry Jet Erosion Test:

Figure 5.10 depicts the impact of impingement angle on weight loss for the substrate. The silt erosion test is done in accordance with ASTM G-136 standards.

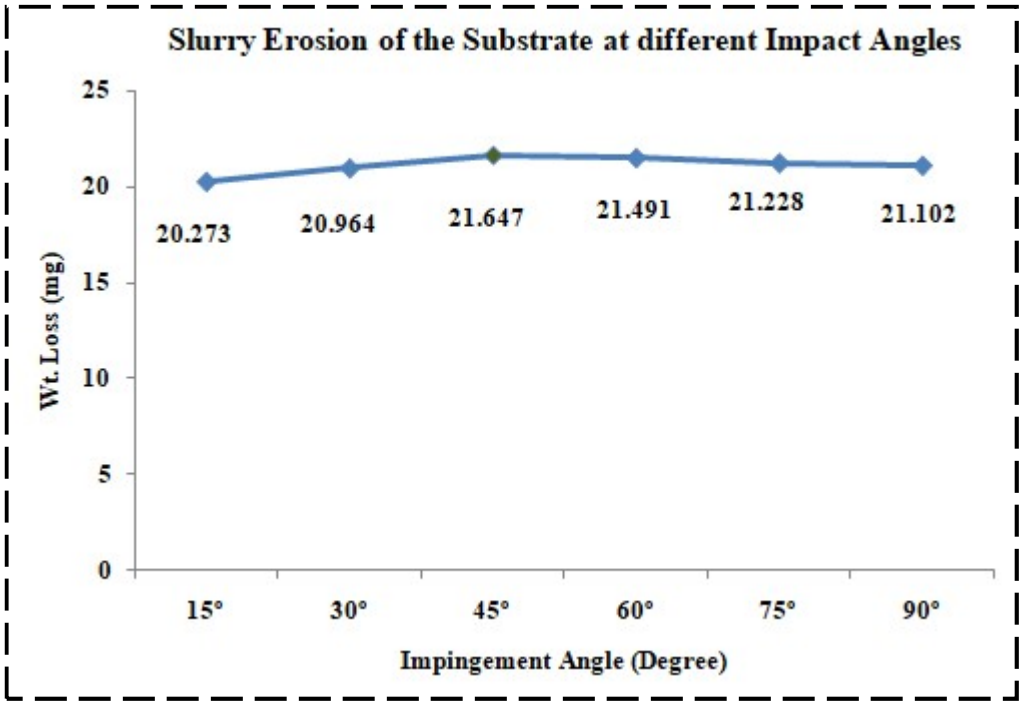

Figure 5.10: Plot of weight loss v/s impingement angle of the substrate (SS410)

The optimal parametric factors including the impact velocity, erodent size, and time duration as 30 m/sec, 300 µm and 120 minutes respectively were considered for the test from the various available literatures [147-149]. Three experiments were conducted at a specific angle, and the average values of weight loss are presented in Figure 5.10. The loss of weight of the substrate was calculated at different impingement angles such as 15º, 30º, 45º, 60º, 75º and 90º. The weight loss of the substrate increased by increasing the impact angle, the maximum value of weight loss was 21.467mg at an angle 45º than it slowly decreasing by increasing the impact angle. The Figure 5.11 shows the micrographs of eroded surface at 500X magnification.

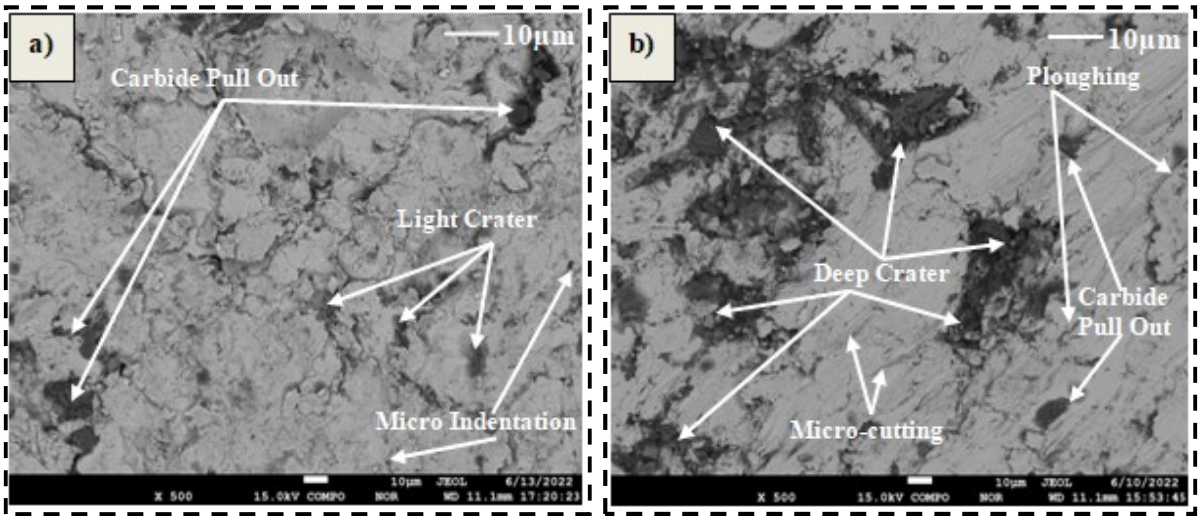

Figure 5.11: SEM micrographs of slurry jet eroded surfaces a) minimum erosion (at an angle 15º) and b) maximum erosion (at an angle 45º) for substrate at 500X

Figures 5.11a and 5.11b show the micrographs of slurry jet eroded samples of the substrate. During the analysis of micrographs, various types of wear mechanisms were observed, including crater wear, ploughing, micro-cutting, micro-indentation, and carbide particle pull-out. Through topographic analysis of silt jet eroded samples, it was noted that micro-cutting and ploughing wear mechanisms were predominant on the eroded surface at a 45º impact angle of the slurry.

PART 2

5.4. Different Types of Deployed Coatings:

The experiment consists of the following combinations of coatings as shown in Table 5.7. The experiment 1 consists of only tungsten carbide powder without addition of any rare earth oxides and denoted as Cp-1000 indicated coating powder only. The experiment 2 consists of tungsten carbide powder with the doping of rare earth oxides and denoted as CpLCE-2 indicated coating powder with mixture of rare earth oxides such as Lanthanum, Cerium, Erbium oxides with 0.2 wt.% each. The experiment 3 consists of tungsten carbide powder with the doping of rare earth oxides and denoted as CpLCE-3 indicated coating powder with mixture of rare earth oxides such as Lanthanum, Cerium, Erbium oxides with 0.3 wt.% each. Similarly experiment 4 consists of tungsten carbide powder with the doping of rare earth oxides and denoted as CpLCE-4 indicated coating powder with mixture of rare earth oxides such as Lanthanum, Cerium, Erbium oxides with 0.4 wt.% each.

Table 5.7: Various types of coatings with their compositions

Experiment No.	Coating powder (WC-10Co-4Cr-wt.%)	Lanthanum oxide (La_2O_3 - wt.%)	Cerium oxide (CeO_2 - wt.%)	Erbium oxide (Er_2O_3 - wt.%)	Total rare earth oxides (wt.%)
(Cp-1000) - Exp. 1.	100	-	-	-	0
(CpLCE-2) - Exp. 2.	99.4	0.2	0.2	0.2	0.6
(CpLCE-3) - Exp. 3.	99.1	0.3	0.3	0.3	0.9
(CpLCE-4) - Exp. 4.	98.8	0.4	0.4	0.4	1.2

The doping of rare earth oxides were done in carbide powder as shown in Table 5.7. From the previous published papers, the values of different rare earth addition were considered during experimentation. With the insertion of rare earth oxides up to 0.9 and 1.2 wt. % elements in carbide coatings, there was an enhancement in most of the coating properties beyond this percentage the deterioration in coating properties was claimed by various researchers [88, 92, 93, 150, 151].

5.5. Characterization of Different Types of Deployed Coatings:

The characterizations of the substrate and different types of developed coatings were investigated using various testing as shown in Figure 5.12.

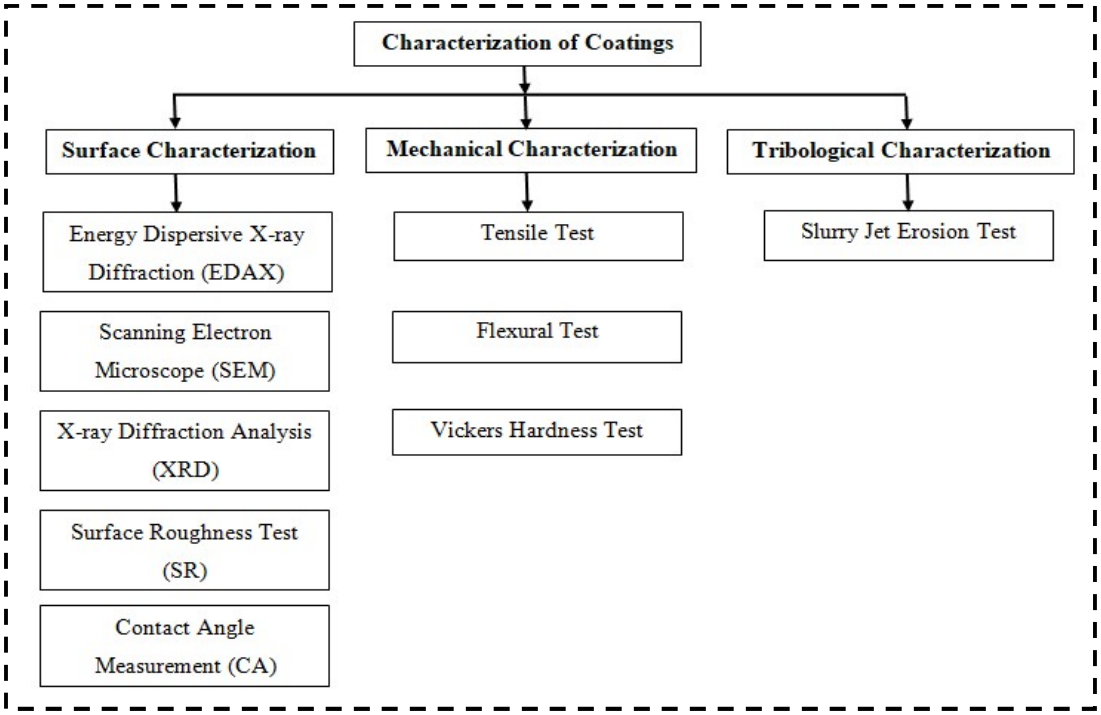

Figure 5.12: Test performed to characterize the coatings

The synthesis of coatings has been done using surface characterization, mechanical characterization and tribological characterization as explained in the Figure 5.12.

Experiment 1 (Cp-1000)

5.6. Surface Characterization of Deposited Coating- Experiment 1 (Cp-1000):

In experiment 1, there was no addition of rare earth oxides in WC-10Co-4Cr powder as shown in Table 5.8.

Table 5.8: Composition of without rare earth oxides doped coating

Experiment No.	Coating powder	Lanthanum oxide (La_2O_3 - wt.%)	Cerium oxide (CeO_2 - wt.%)	Erbium oxide (Er_2O_3 - wt.%)	Total rare earth oxides (wt.%)
(Cp-1000) - Exp. 1.	WC-10Co-4Cr	-	-	-	0

5.6.1. Energy Dispersive X-ray Spectroscopy (EDS):

The identification and mapping of various elements have done using EDS as shown in Figure 5.13.

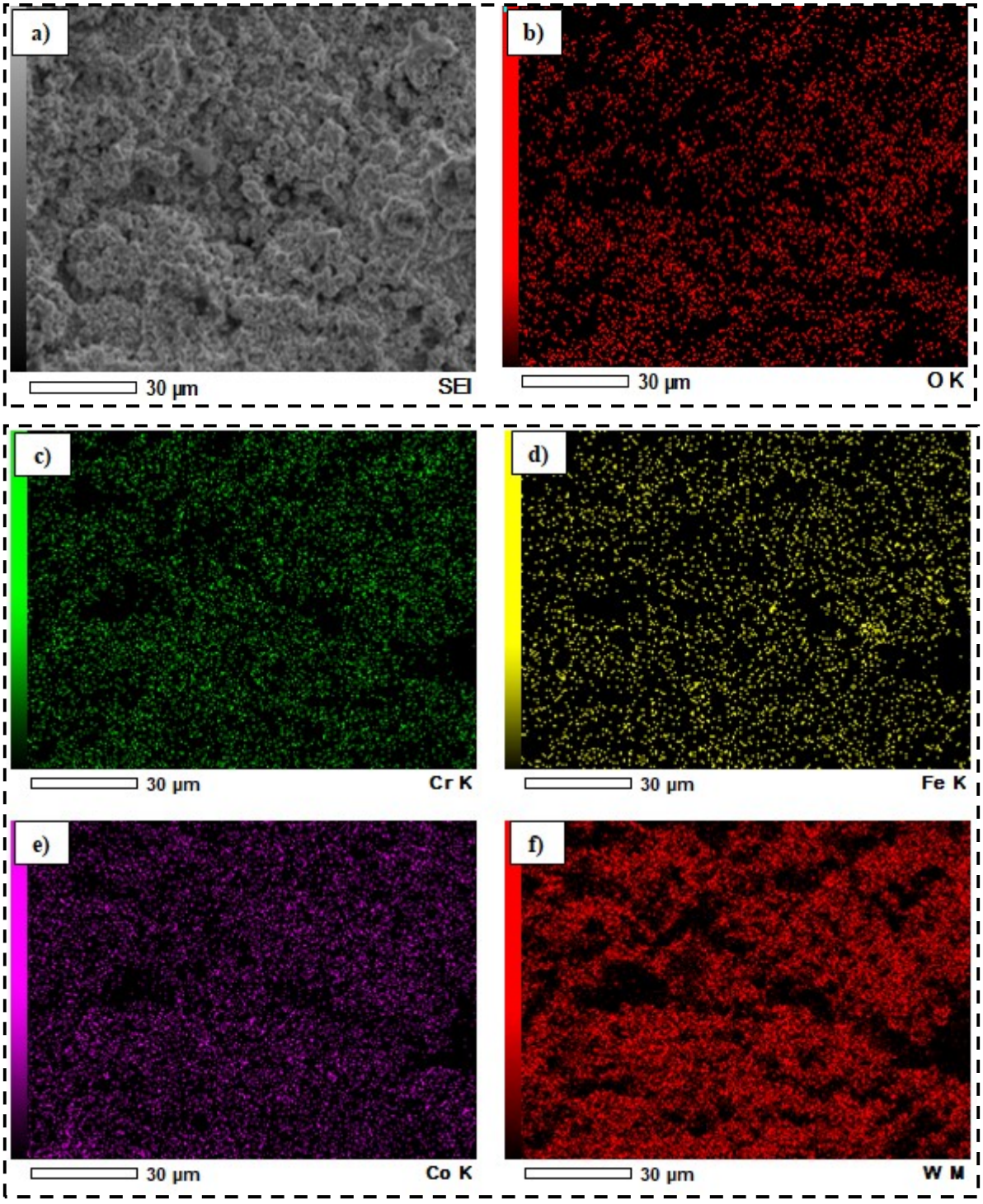

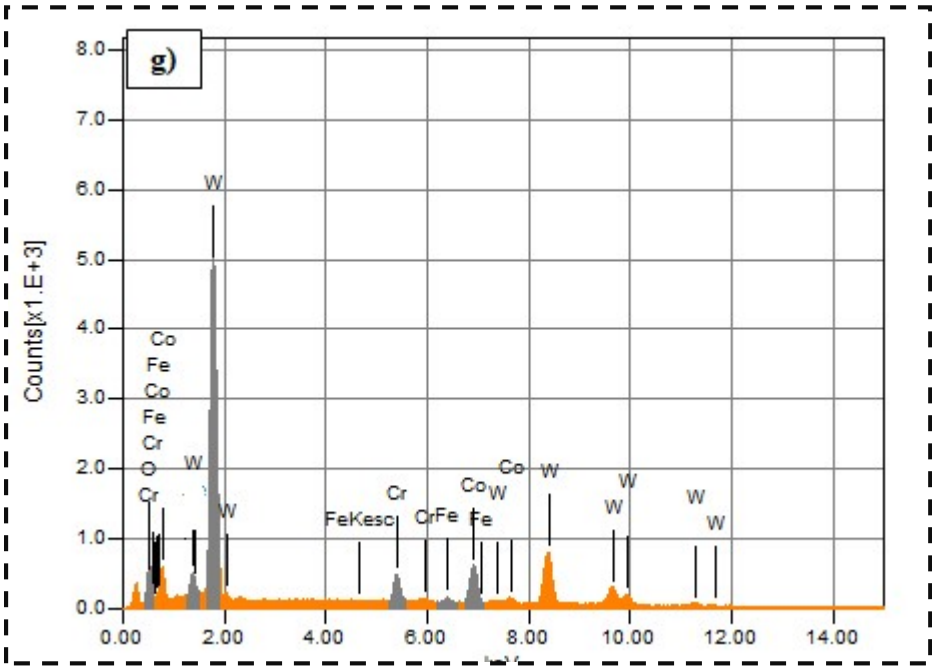

Figure 5.13: Identification of various elements using energy dispersive spectroscopy analysis a) mapped area, b) Oxygen (O), c) Chromium (Cr), d) Iron (Fe), e) Cobalt (Co), f) Tungsten (W) and, g) EDS peaks of elements for coated sample

The process parameters for the energy dispersive spectroscopy (EDS) test have shown in Table 5.9. The Figure 5.13a shows the micrograph of the mapped area. The detection of available elements (like Oxygen (O), Chromium (Cr), iron (Fe), Cobalt (Co), and Tungsten (W)), as shown in Figures 5.13b to 5.13f with different colors, Moreover the peaks of different elements with various intensity has shown in Figure 5.13g.

Table 5.9: Process parameters of EDS

Acquisition condition of EDS	
Volt (kV)	20.00
Live time (sec)	245.76
Real time (sec)	248.41
Dead time (%)	1.00
Count rate (CPS)	1300.00

5.6.2. X-ray Diffraction Analysis (XRD):

The various phases present on coatings surface was obtained using X-ray diffraction as shown in Figure 5.14.

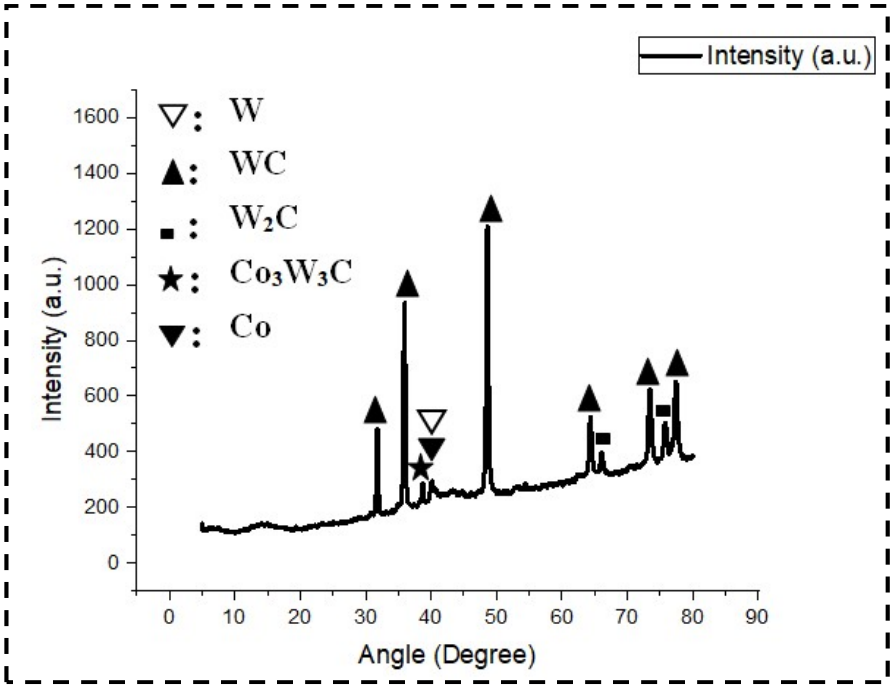

Figure 5.14: XRD analysis of without rare earth oxide doped coating

The formation of compounds such as Cobalt-Tungsten Bimetallic Carbide (Co_3W_3C, (JCPDS 27-1125)) and Tungsten Carbide (WC, (JCPDS 51-0939)) were recognized as shown in Figure 5.14. The decarburization of (WC) tungsten carbide into Tungsten Semi-Carbide (W_2C) was taken place according to the reactions (5.1) and (5.2) [152, 153].

$$2WC \rightarrow W_2C + C \quad (5.1)$$

$$W_2C \rightarrow 2W + C \quad (5.2)$$

The X-ray diffraction (XRD) of the coated samples revealed the existence of Cobalt (Co, JCPDS 05-0727) tungsten carbide (WC) and the decarburized brittle W_2C (JCPDS 35-776) phase after deposition.

5.6.3. Surface Morphology of Deposited Coating:

The micrograph of without rare earth doping carbide coating is obtained using scanning electron microscope (SEM) at 1000X as shown in Figure 5.15.

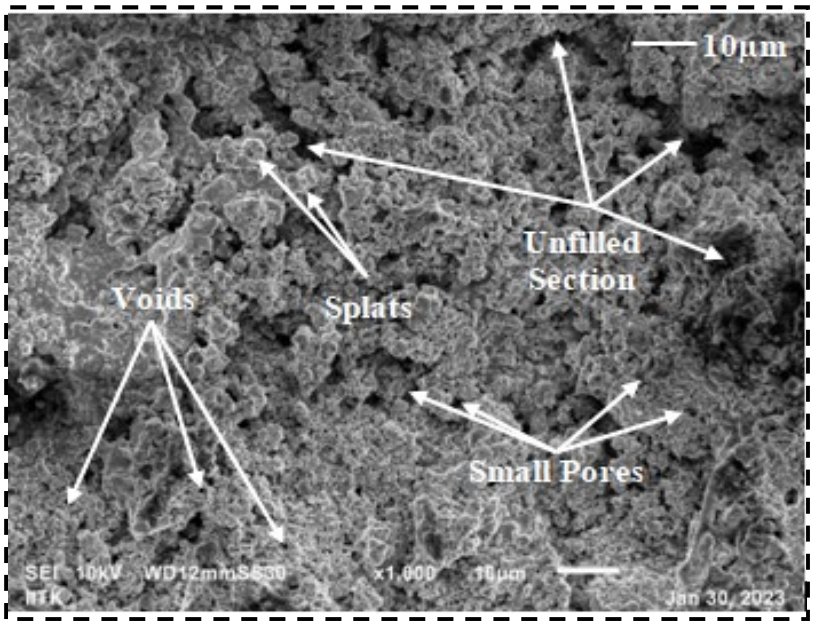

Figure 5.15: SEM micrographs of coating without rare earth oxides at 1000X

There were large numbers of splats and small pores available on the coating surface. Moreover unfilled section is also observed in the micrographs as shown in Figure 5.15.

5.6.4. Surface Roughness (SR) and Porosity Measurement:

A surface roughness tester was used to assess the coated samples' surface roughness in accordance with ASTM D7127. Table 5.10 yielded an average roughness value of 5.96 µm for the coating.

Table 5.10: Surface roughness value of coated sample

	Roughness Value (µm)	Average Roughness (µm)
Without rare earth oxide doped carbide coating (Experiment 1 (Cp-1000))	5.93	5.96
	5.98	
	5.97	

The porosity test was conducted on a cross-section of the coating with ASTM-E-2L09-01(2007, method A) [154]. The level of porosity was in the range of ≥1 to ≤ 2% in the 24 mm of coating length without RE carbide coatings.

5.6.5. Coating Thickness and Contact Angle Measurement:

As shown in Figure 5.16, the thickness of the coating was in the range of 301.12 µm - 327.23 µm. The static water contact angle (WCA) has been measured on the substrate using the sessile drop method as per ASTM D7334-08 standard.

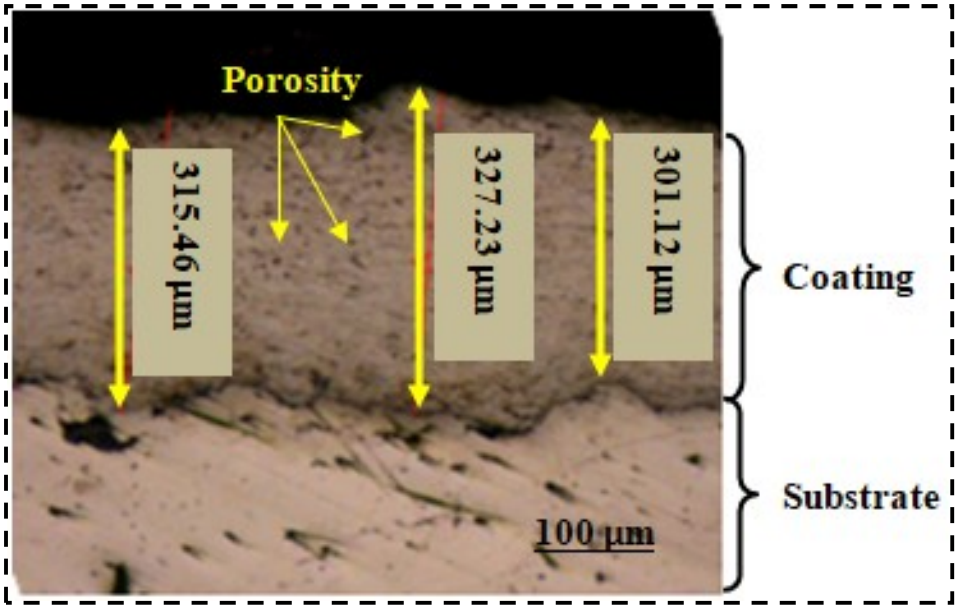

Figure 5.16: Coating thickness measurement of un-doped coating

Due to the presence of porosity, the value of surface roughness is higher for un-doped coating. The above statement validation could be done with the help of SEM micrographs, which showed that the unfilled section for un-doped coating was more which leads to the higher roughness. The porosity leads to a rough surface and the effect of surface roughness on wettability behavior, which has been analyzed using contact angle measurement. The static water contact angle is as shown in Figure 5.17.

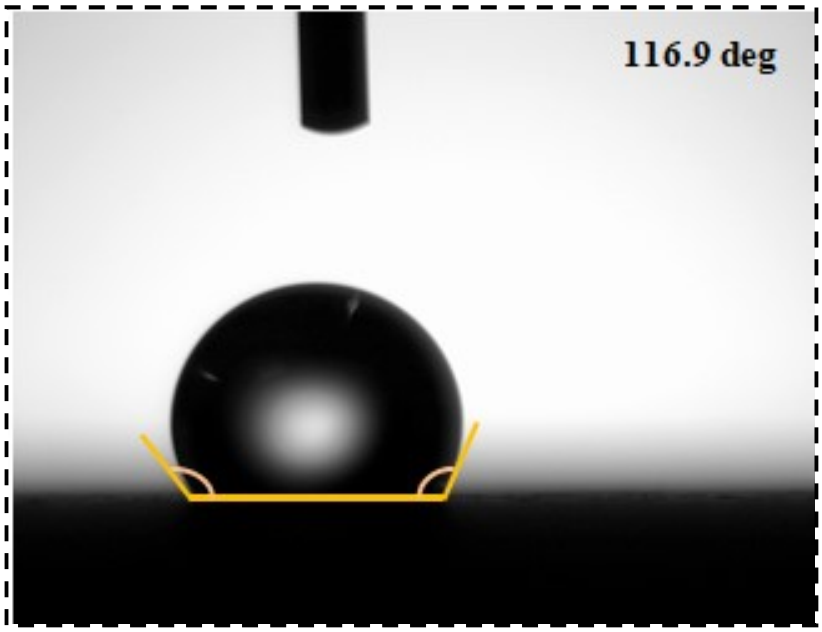

Figure 5.17: Contact angle of un-doped coating

The static water contact angle (WCA) is a commonly used parameter to describe the hydrophobic or hydrophilic nature of a surface. If the WCA is less than 90 degrees, then the surface is considered hydrophilic, meaning it has an affinity for water and tends to be wetted by it. In contrast, if the WCA is greater than 90 degrees, then the surface is considered hydrophobic, meaning it tends to repel water and is difficult to wet. It is important to note, however, that the WCA alone does not provide a complete description of a surface's hydrophobicity or hydrophilicity. Other factors, such as surface roughness, chemical composition, and surface energy, can also play important roles in determining how a surface interacts with water [155, 156]. The Table 5.11 shows the static water contact angle values and average value in degree.

Table 5.11: Static water contact angle values of un-doped coating

Experiment	**Contact Angle (CA-Deg.)**			**Average CA (deg.)**
Without rare earth oxide doped carbide coating (Experiment 1 (Cp-1000))	115.8	118.1	116.8	116.9

Based on the experimentation, it appears that the un-doped cermet coated samples have an

average contact angle value of 116.9 degree as shown in Figure 5.17, indicating a hydrophobic surface. This means that droplets of water will tend to bead up and roll off the surface, rather than spreading out and wetting it.

5.7. Mechanical Characterization of Deposited Coating - Experiment 1 (Cp-1000):

5.7.1. Tensile Test:

The samples were ready according to standard (ASTM- E8). One of the un-doped coated sample after the test have depicted in Figure 5.18.

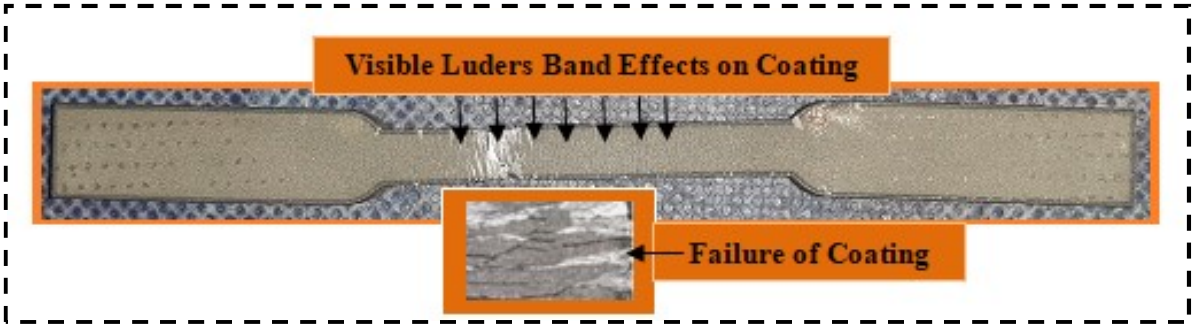

Figure 5.18: Fractured tensile test sample of without doped coating

There are stretcher-strain marks over the coated surface has been observed. Moreover the Luders band effects have also been observed on the coated surface as shown in Figure 5.18.

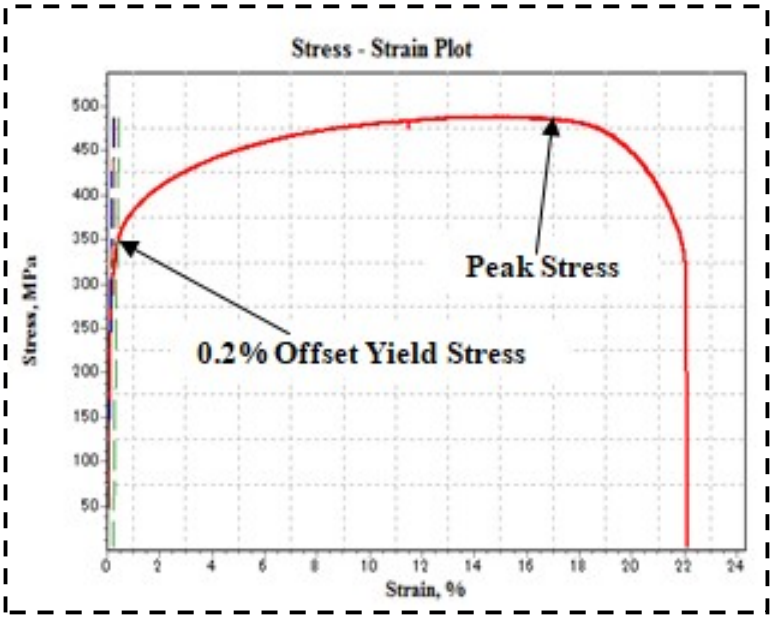

Figure 5.19: Stress-strain plot of un-doped coated sample

Figure 5.19 shows the stress-strain curve for without RE doped coated sample. The different mechanical property values were calculated with the help of stress-strain curve as shown in Figure 5.19 and depicted in Table 5.12.

. Table 5.12: Tensile test results of up-doped coated sample

Properties	Average Values
Peak Stress (MPa)	476.692
0.2% Offset Yield Stress (MPa)	344.218
Yield Strain (%)	0.493
Modulus (GPa)	115.117
Elongation at Break (Using Strain) (%)	33.54

5.7.2. Flexural Test:

The specimen was prepared as per the ASTM- D790 standard. The un-doped coated sample after the bend test has been shown in Figure 5.20.

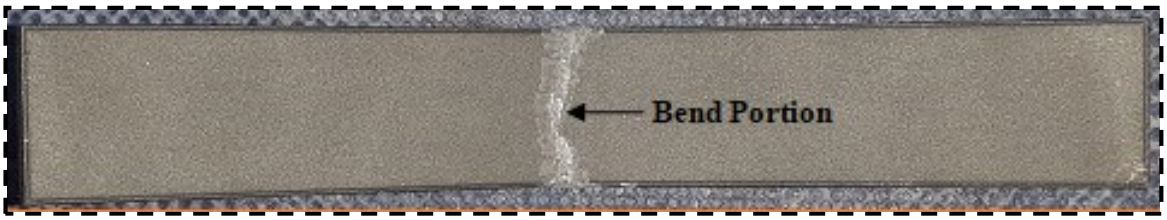

Figure 5.20: Sample of flexural test after bend test of un-doped coating

To know the flexural strength of un-doped carbide coating, three point bend test has been carried out. The flexural stress v/s strain diagram as shown in Figure 5.21 is for the un-doped carbide coated sample.

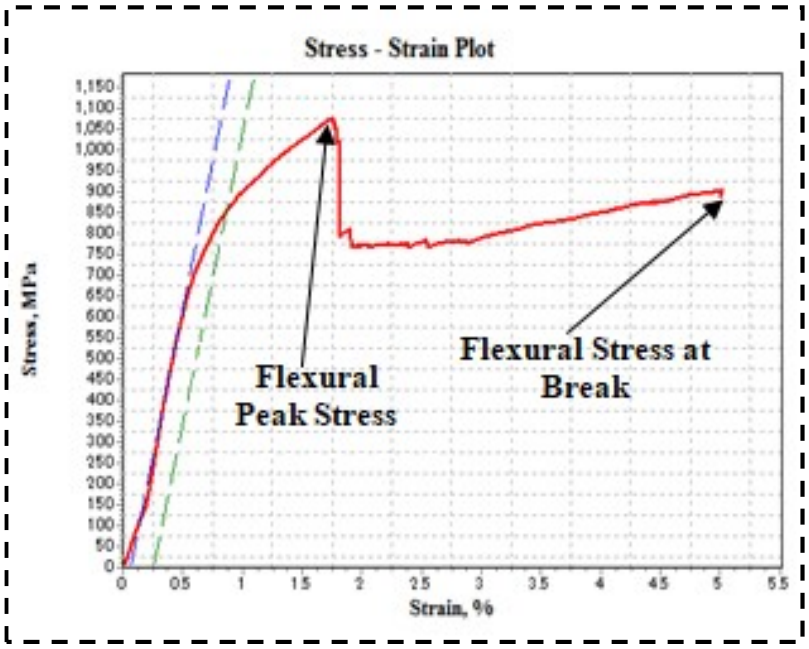

Figure 5.21: Stress-strain plot for un-doped carbide coating

The flexural peak stress value shows the capability to resist bending before yield. The average values of different mechanical properties obtained from flexural test were premeditated from stress-strain curve as depicted in Figure 5.21 and tabulated in Table 5.13.

Table 5.13: Flexural (3-point bend) test results of un-doped coated samples

Properties	**Average values (MPa)**
Flexural Peak Stress	1026.63
Offset Flexural Yield Stress	1.159
Flexural Stress at Break	743.87

5.7.3. Hardness Test:

The Vickers hardness test was carried out on un-doped carbide coated samples in accordance with ASTM-A270 standards with 300g load for 10 seconds of dwell time. The average hardness value of the carbide coated surface is 906.3 as shown in Table 5.14.

Table 5.14: Vickers hardness test values of un-doped coated samples

Powder	Hardness Value (HV0.3)			Average Value
Without rare earth oxide doped carbide coating (Experiment 1 (Cp-1000))	908.1	898.5	912.3	906.3

The presence of tungsten's hard carbide particles has resulted in an increased hardness value for the coating. The indentation marked on the coating has shown in Figure 5.22.

Figure 5.22: Indentation on un-doped coated sample

5.8. Tribological Characterization of Deposited Coating - Experiment 1 (Cp-1000):

To know the tribological behavior, the slurry erosion test has performed on without rare earth doped tungsten carbide coating at varied impingement angle.

5.8.1. Slurry Jet Erosive Behavior of Deposited Coating:

The slurry erosion testing was conducted in accordance with the ASTM standard (ASTM G-136) with a slurry/silt jet erosion test rig on coated samples. The impact of impingement angle on erosion rate is depicted in Figure 5.23.

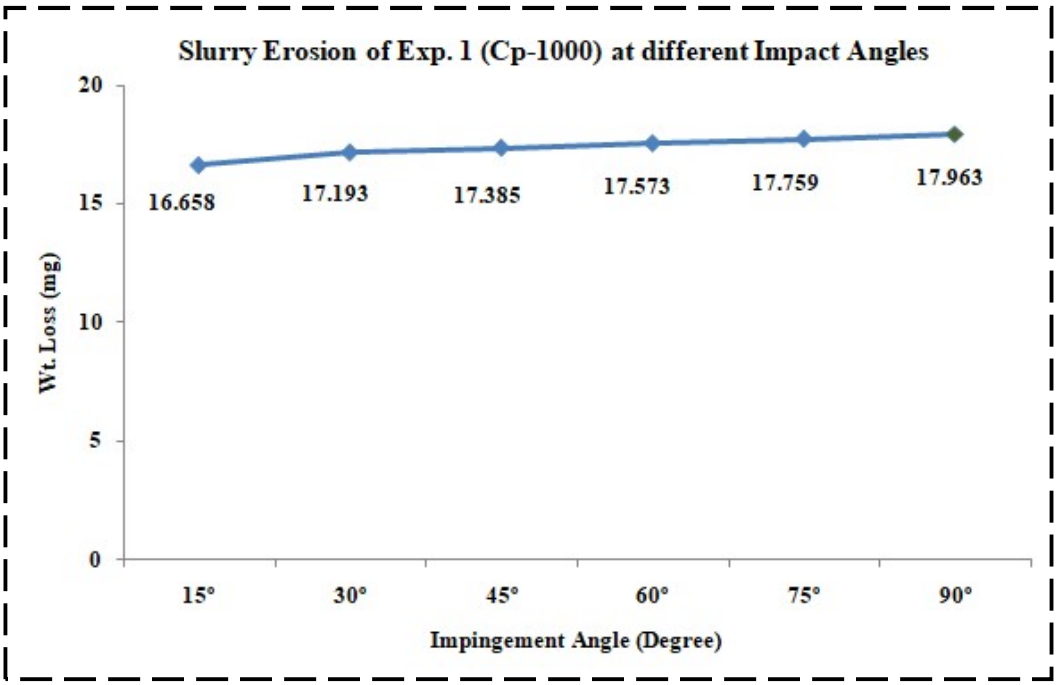

Figure 5.23: Plot of weight loss v/s impingement angle of experiment 1 (Cp-1000)

Similarly, the optimal parametric parameters including the impact velocity, erodent size, and duration as 30 m/sec, 300 µm, and 120 minutes respectively were considered for the test. Three experiments were conducted at a specific angle, and the average values of weight loss are presented in Figure 5.23. The loss of weight of coated sample was calculated at different impingement angles such as 15º, 30º, 45º, 60º, 75º and 90º. The weight loss of coated sample increases by increasing the impact angle and at angle 90º it was maximum i.e. 17.963 mg. The Figure 5.24 shows the micrographs of eroded surface at 500X magnification.

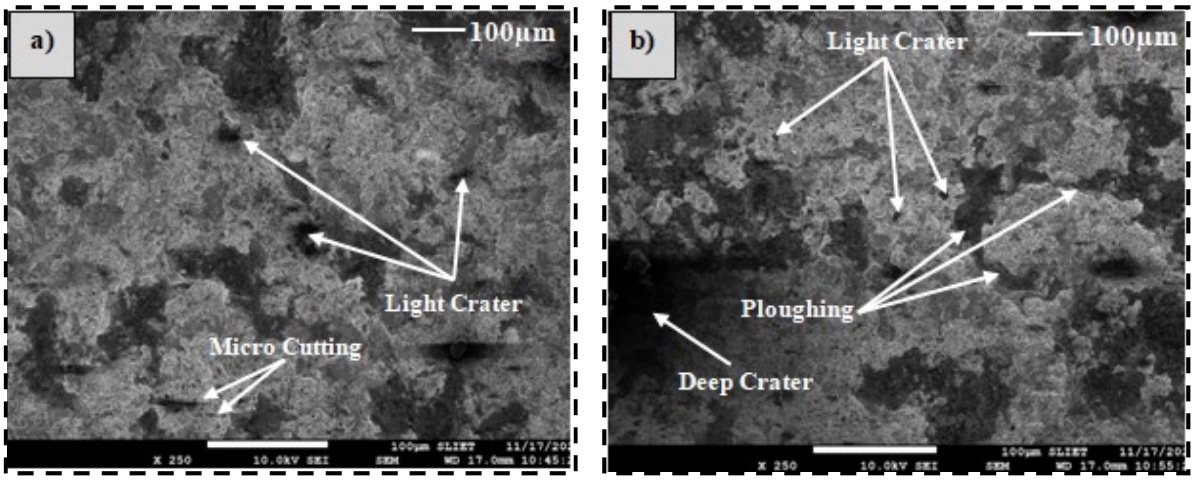

Figure 5.24: SEM micrographs of slurry jet eroded surfaces a) minimum erosion (at an angle 15º) and b) maximum erosion (at an angle 90º) of un-doped coated samples at 250X

Figures 5.24a and 5.24b show the micrographs of slurry jet eroded undoped tungsten carbide coated samples at an angle of 90 and 15 degree respectively. Through topographic analysis various types of wear mechanism such as micro-indentation, ploughing, micro-cutting and crater wear were observed in the eroded surfaces of coatings. The maximum and minimum weight loss has been observed at an angle 90 and 15 degree respectively.

Experiment 2 (CpLCE-2)

5.9. Surface Characterization of Deposited Coating - Experiment 2 (CpLCE-2):

In experiment 2, there was an addition of total 0.6 wt.% rare earth oxides such as (La_2O_3/ CeO_2/ Er_2O_3 – 0.2 wt.% each) in WC-10Co-4Cr powder as shown in Table 5.15.

Table 5.15: Composition of deposited coating for experiment 2 (CpLCE-2)

Experiment No.	Coating powder (WC-10Co-4Cr- wt.%)	Lanthanum oxide (La_2O_3 - wt.%)	Cerium oxide (CeO_2 - wt.%)	Erbium oxide (Er_2O_3 - wt.%)	Total rare earth oxides (wt.%)
(CpLCE-2) – Exp. 2.	99.4	0.2	0.2	0.2	0.6

The experiment 2 consists of tungsten carbide powder with the doping of rare earth oxides and denoted as CpLCE-2 indicates coating powder with mixture of rare earth oxides such as Lanthanum, Cerium, Erbium oxide with 0.2 wt.% each.

5.9.1. Energy Dispersive X-ray Spectroscopy (EDS):

The identification and mapping of various elements have done using EDS as shown in Figure 5.25.

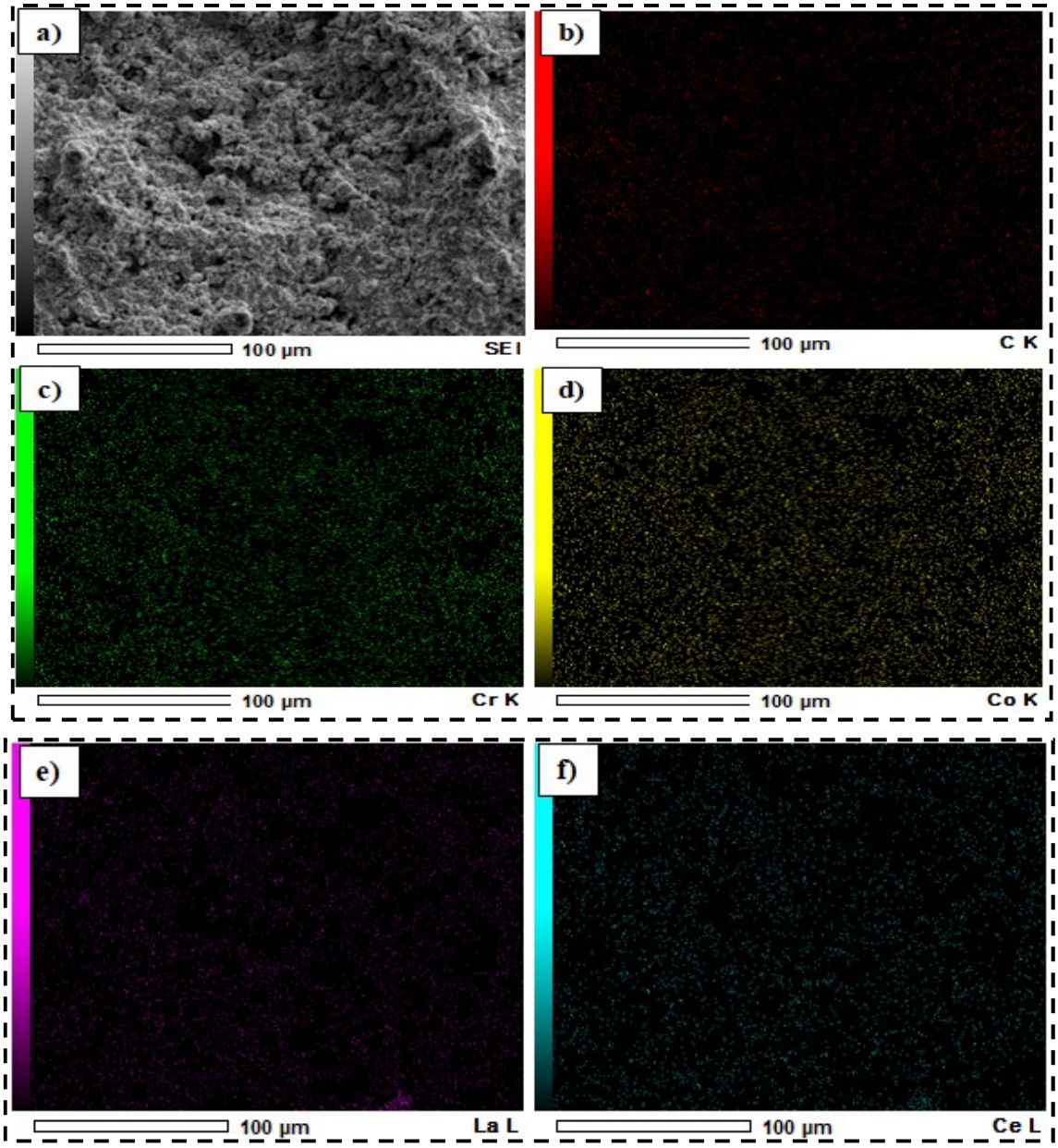

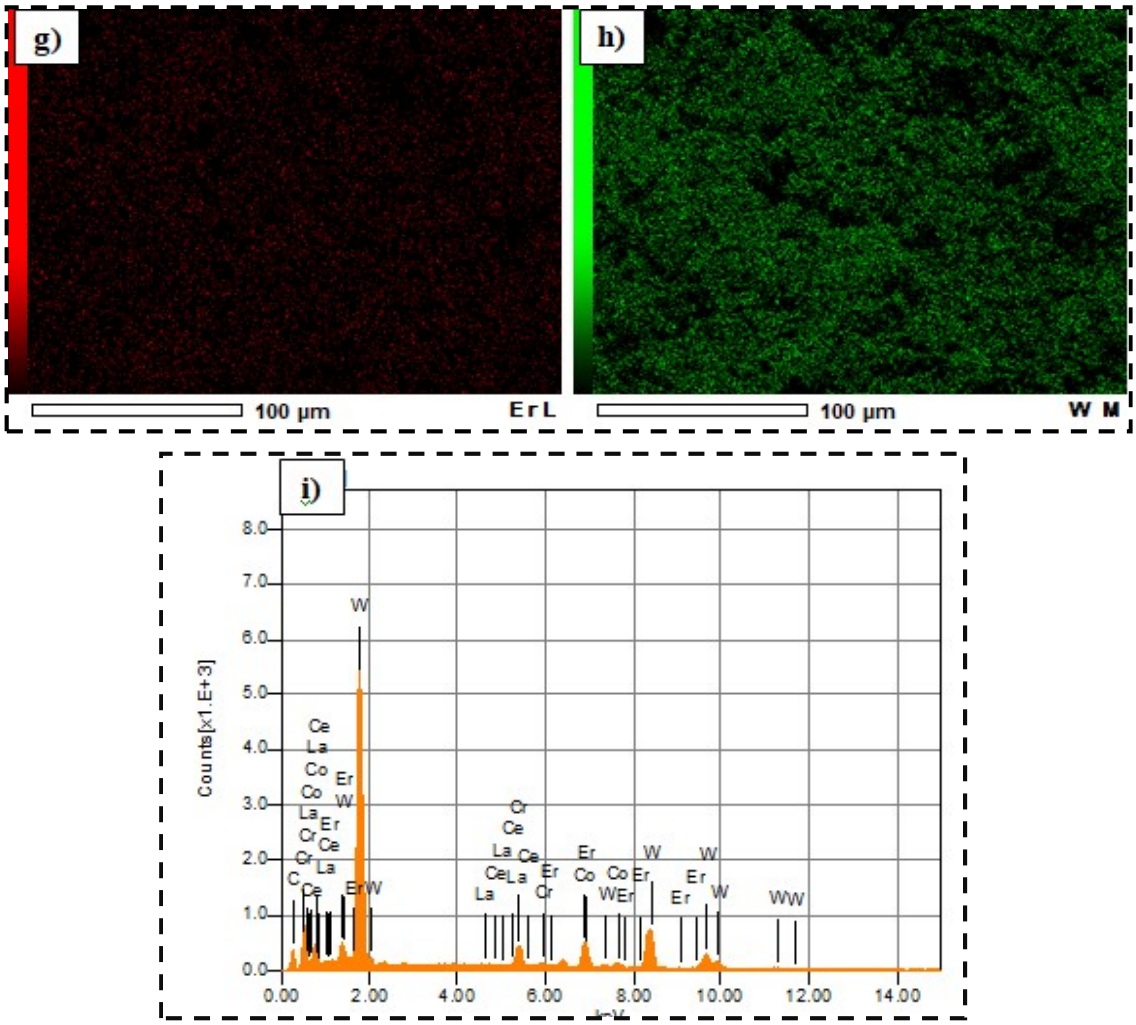

Figure 5.25: Identification of various elements using energy dispersive spectroscopy analysis a) mapped area, b) Carbon (C), c) Chromium (Cr), d) Cobalt (Co), e) Lanthanum (La), f) Cerium (Ce), g) Erbium (Er), h) Tungsten (W) and, i) specific intensity of peaks of various elements for experiment 2 (CpLCE-2)

The operational parameters of energy dispersive X-ray analysis (EDAX) have given in Table 5.16.

Table 5.16: Operational parameters

Acquisition Condition of EDS	
Volt (kV)	20.00
Live Time (sec.)	196.60
Real Time (sec.)	202.56
Dead Time (%)	2.00
Count Rate (CPS)	1774.00

The individual elements (like Carbon, Chromium, Cobalt, Lanthanum, Cerium, Erbium, and Tungsten) have been identified by different colors as shown in Figures 5.25b to 5.25g and collectively all the identified elements have illustrated in Figure 5.25i. Moreover Figure 5.25a shows the morphology of considered area for EDS. The used elements in powder such as Tungsten, Carbon, Cobalt, Chromium, Lanthanum, Cerium, and Erbium in the coating have been verified using EDS as well. The rare earth elements are uniformly distributed in a matrix of WC-Co-Cr as shown in Figures 5.25d to 5.25f.

5.9.2. X-ray Diffraction Analysis (XRD):

The various phases present on coatings surface has obtained using X-ray diffraction as shown in Figure 5.26.

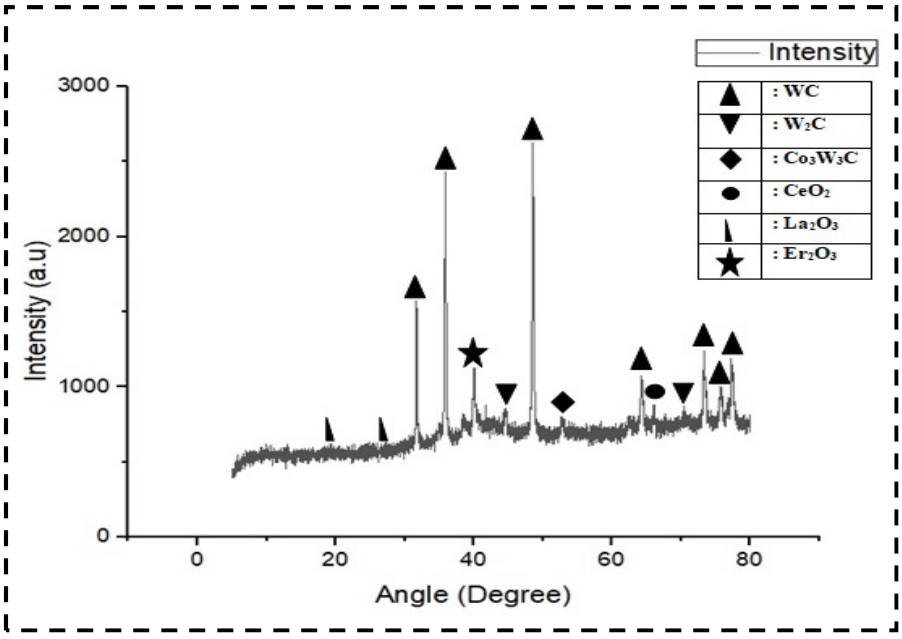

Figure 5.26: X-ray diffraction peaks of 0.6 wt.% rare earth oxides doped coating

The Figure 5.26 displays the X-ray diffraction (XRD) plots for the 0.6 wt.% rare earth oxides coated samples. It demonstrates the identification of various rare earth oxides, including different cerium (JCPDS 34-0394), lanthanum (JCPDS 05-0602), erbium (JCPDS 43-1005) oxides, as well as compounds of Co_3W_3C, W_2C and WC resulting from doping. It is important to note that the XRD analysis performed in this study aligns with the findings reported by other researchers in their respective works [157-160].The high-temperature

decarburization process leads to the conversion of tungsten carbide (WC) into tungsten semi-carbide (W_2C) as described by reactions (5.1) and (5.2).

5.9.3. Surface Morphology of Deposited Coating:

The image of 0.6 wt.% rare earth oxides doped coated sample captured at a magnification of 1000X using a scanning electron microscope.

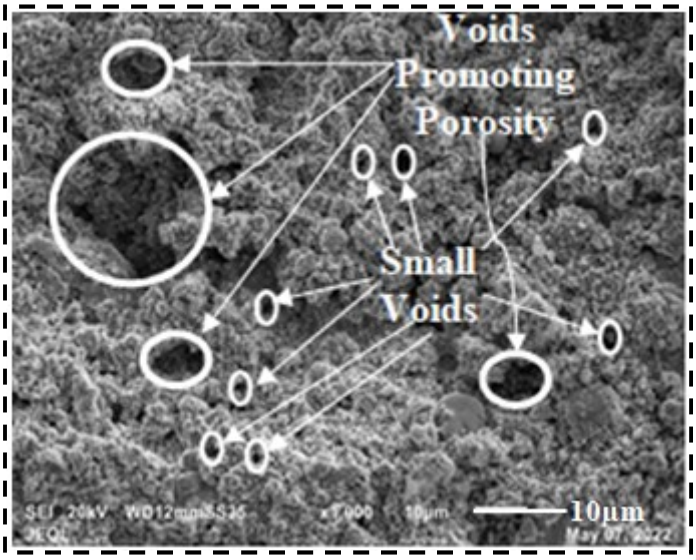

Figure 5.27: Micrographs of 0.6 wt.% rare earth (REOs) oxides doped coated sample at 1000X

The Figure 5.27 shows the micrograph of the of 0.6 wt.% rare earth oxides doped coated sample. Which shows many small voids and these voids promote the porosity.

5.9.4. Surface Roughness (SR) and Porosity Measurement:

The surface roughness of coated samples was measured using a surface roughness tester as per ASTM D7127 standard. The average roughness value of the coating was 7.02 µm as calculated in Table 5.17.

Table 5.17: Roughness values of coated sample for experiment 2 (CpLCE-2)

Rare earth (La_2O_3/ CeO_2/ Er_2O_3 – 0.2 wt.% each) oxide doped coating (Experiment 2 (CpLCE-2))	Roughness Value (µm)	Average Roughness (µm)
	7.1	
	7.16	7.02
	6.8	

The porosity test was conducted on a cross-section of the coating with standard ASTM E 2L09-01(2007, method A). The level of porosity was in the range of ≥1 to ≤ 2% in the 24 mm of coating length without RE carbide coatings. The presence of the porosity has already been revealed using SEM micrographs as shown in Figure 5.27. Hang et al. (2018) developed a coating using HVOF and considered doping of rare earth (CeO_2 -1 wt.%) in WC-12Co. They claimed the porosity level is 2.1% for nano WC-12Co and 1.6% for micro WC-12Co [88]. Sharma et al. (2008 and 2009) conducted a study on coating deposited using a flame spray process. They doped the NiCrBSi powder by rare earth-like ((CeO_2) with varying percentages as 0 %, 0.4 %, 0.8 %, 1.2 %, 1.6 %, and 2 % but (La_2O_3)- 0 %, 0.4 %, 0.8 %, 1.2 %, 1.6 %, and 2 %) respectively and claimed that the porosity level ranges from 5 to 8% [150, 151]. The current work showed a less porosity level which was better than most of the available investigations.

5.9.5. Coating Thickness and Contact Angle Measurement:

In order to gain further insights into the coated surface, porosity and thickness measurements were conducted on the coating deposited using the HP-HVOF process. The optical image (at 200X) of cross-section of the coating has depicted to know the thickness of the coating in Figure 5.28. The thickness of the coating was in the range of 282-300 µm.

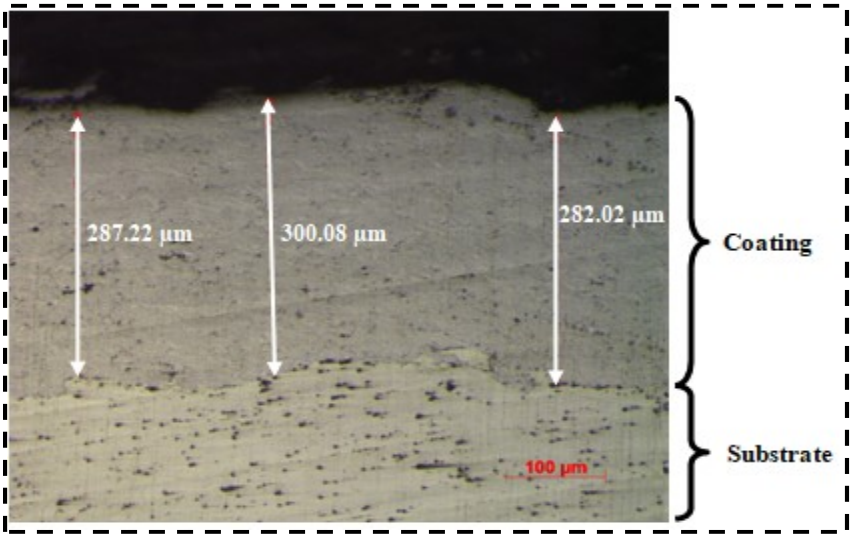

Figure 5.28: Microscopic image at 200X to measure the porosity level and thickness of the deposited coating

The coated sample showed an average contact angle value 134.4 degree as shown in Figure 5.29 The porosity provides surface roughness, which makes the surface hydrophobic.

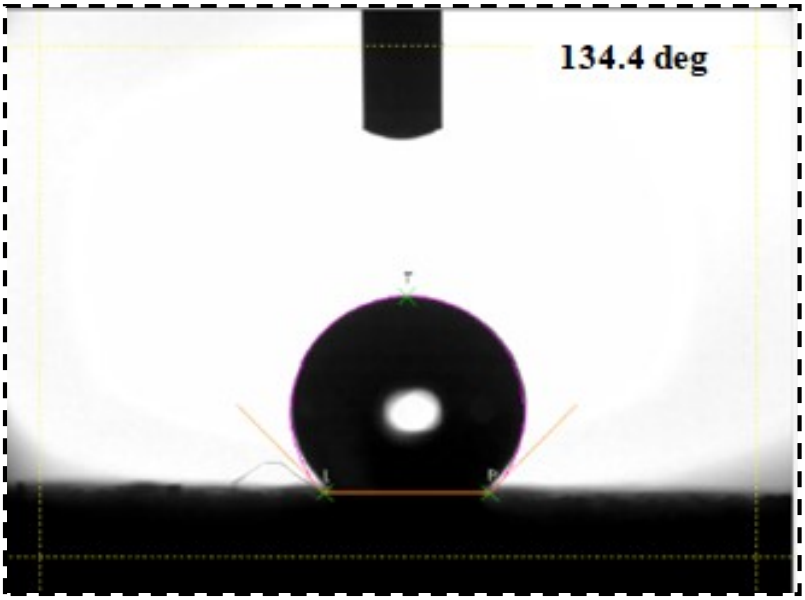

Figure 5.29: Contact angle of 0.6 wt.% rare earth oxides doped coating

The sessile drop technique was utilized to examine the wettability action of the coated samples in accordance with ASTM D7334-08. Surface roughness plays a vital function in assessing the wetting characteristics of a surface. The Wenzel and Cassie-Baxter state models were employed to explain the impact of surface roughness on wettability [161, 162]. As surface roughness increases, the surface tends to become more hydrophobic because of trapping of atmospheric air in the uneven areas [163, 164]. Once a water droplet is located on a hard surface, its behavior can vary, with the droplet either spreading across the surface or remaining confined to a specific area. This behavior depends on the interactions between the solid surface and the liquid droplet. The static water contact angle (WCA) is a commonly used metric to quantify the wettability behavior of a surface. A water contact angle measuring less than 90˚ indicates a hydrophilic surface, suggesting that the liquid spreads readily on the surface. Conversely, an angle greater than 90˚ suggests a hydrophobic surface, indicating that the liquid tends to bead up or remain confined rather than spread across the surface. Moreover, if the WCA of a surface is greater than 150˚, it

exhibits super-hydrophobic behavior. This is similar to the behavior observed in natural surfaces, such as lotus and colrabi leaves [165, 166]. The Table 5.18 shows static water contact angle values and average value in degree.

Table 5.18: Static water contact angle values for experiment 2 (CpLCE-2)

Experiment	Static Water Contact Angle (CA-Deg.)			Average CA (deg.)
Rare earth (La_2O_3/ CeO_2/ Er_2O_3 – 0.2 wt.% each) oxide doped coating (Experiment 2 (CpLCE-2))	133.2	135.3	134.7	134.4

5.10. Mechanical Characterization of Deposited Coating - Experiment 2 (CpLCE-2):

5.10.1. Tensile Test:

The specimen depicted in Figure 5.30 was fabricated in accordance with the ASTM-E8 standard. To ensure accuracy, three separate experiments were carried out, and the average values were determined.

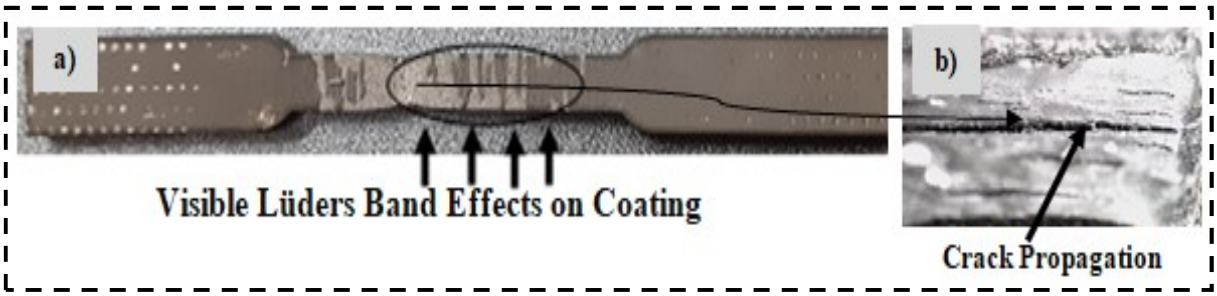

Figure 5.30: a) Fractured coated samples of tensile test with their b) fractography of fractured surface for experiment 2 (CpLCE-2))

The Figures 5.30a and 5.30b show the fractured coated samples and its fractography respectively. The presence of Lüders bands on the coating was observed in Figure 5.30a. The damaged coating exhibited multiple bands as a result of the Lüders band effect. It is worth noting that the substrate, which is inherently brittle, demonstrated enhanced ductility once the deploying of the coating. The coated sample fractography as shown in Figure 5.30b shows the large size crack propagation. The stress-strain diagram for the 0.6 wt.% rare earth (REOs) oxides doped coated sample was obtained from a universal tensile testing machine as shown in Figure 5.31.

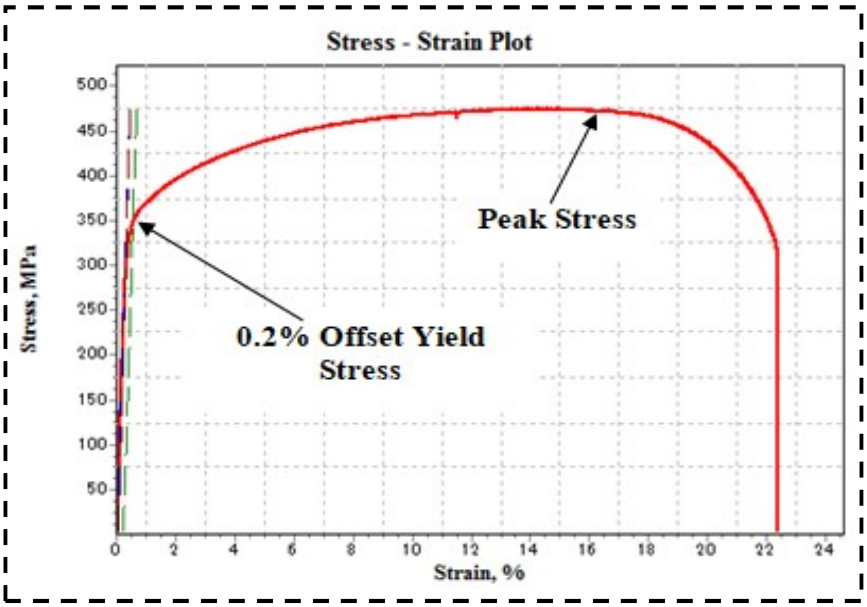

Figure 5.31: Stress-strain curve from the tensile test of 0.6 wt.% rare earth (REOs) oxides doped coated sample

The Table 5.19 showed that the various mechanical properties were obtained from the stress-strain curve.

Table 5.19: Tensile test results for experiment 2 (CpLCE-2)

Tensile Test Properties	**Coated sample**
Peak Stress (MPa)	475.32
0.2% Offset Yield Stress (MPa)	344.58
Yield Strain (%)	0.53
0.02% Offset Yield Stress (MPa)	264.65
Modulus (GPa)	109.66
Elongation at Break (Using Strain) (%)	22.37

5.10.2. Flexural Test:

In accordance with the ASTM-D790 standard, the specimen after test has shown in Figure 5.32, and a total of three experiments were carried out.

Figure 5.32: Sample of flexural test after bend test for experiment 2 (CpLCE-2)

The stress-strain curve as shown in Figure 5.33 was obtained from 3-point bend test.

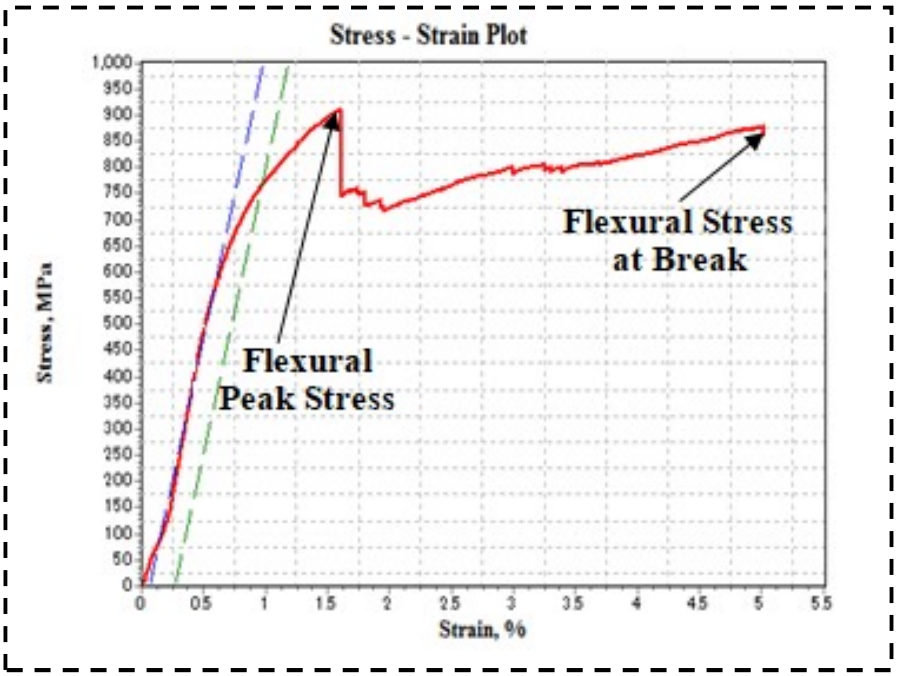

Figure 5.33: Stress-strain plot from the flexural/bend (3-point) test for experiment 2 (CpLCE-2)

The average values of various mechanical properties have been provided in the Table 5.20.

Table 5.20: Flexural (three-point bend) test results for experiment 2 (CpLCE-2)

Flexural Test Properties	Average values (MPa)
Flexural Peak Stress	908.73
Offset Flexural Yield Stress	0.95
Flexural Stress at Break	860.72

.

5.10.3. Hardness Test:

The Vickers (HV0.3) hardness test was conducted to determine the hardness values of coated samples followed by the ASTM-A270 standard. The test involved applying a 300g load with a dwell time of 10 seconds. The obtained indentations marked using indenter on coating has shown in Figure 5.34.

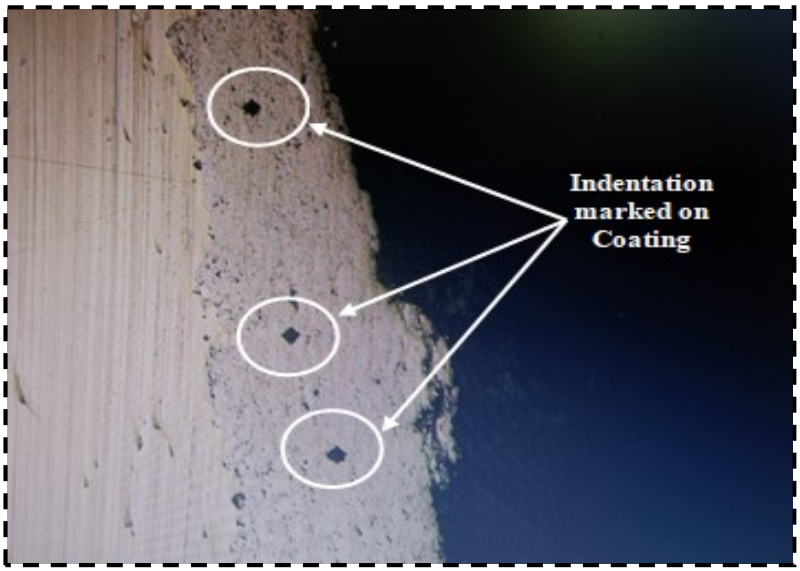

Figure 5.34: Indentation marked on coating

The average hardness value of the carbide coated surface is 906.3 as shown in Table 5.21. The presence of tungsten's hard carbide particles has resulted in an increased hardness value for the coating.

Table 5.21: Vickers hardness test values for experiment 2 (CpLCE-2)

Experiment	Hardness Value (HV0.3)			Average Value
Rare earth (La_2O_3/ CeO_2/ Er_2O_3 – 0.2 wt.% each) oxide doped coating (Experiment 2 (CpLCE-2))	799	792	802	797.67

5.11. Tribological Characterization of Deposited Coating - Experiment 2 (CpLCE-2):

To know the tribological behavior, the slurry erosion test has performed on 0.6 wt.% rare earth oxides such as (La_2O_3/ CeO_2/ Er_2O_3 – 0.2 wt.% each) doped tungsten carbide coating at varied impingement angle.

5.11.1. Slurry Jet Erosive Behavior of Deposited Coatings:

Slurry erosion testing was conducted in accordance with the ASTM standard (ASTM G-136) with a slurry/silt jet erosion test rig on a rare earth-doped coating (CpLCE-2). The impact of impingement angle on erosion rate is depicted in Figure 5.35.

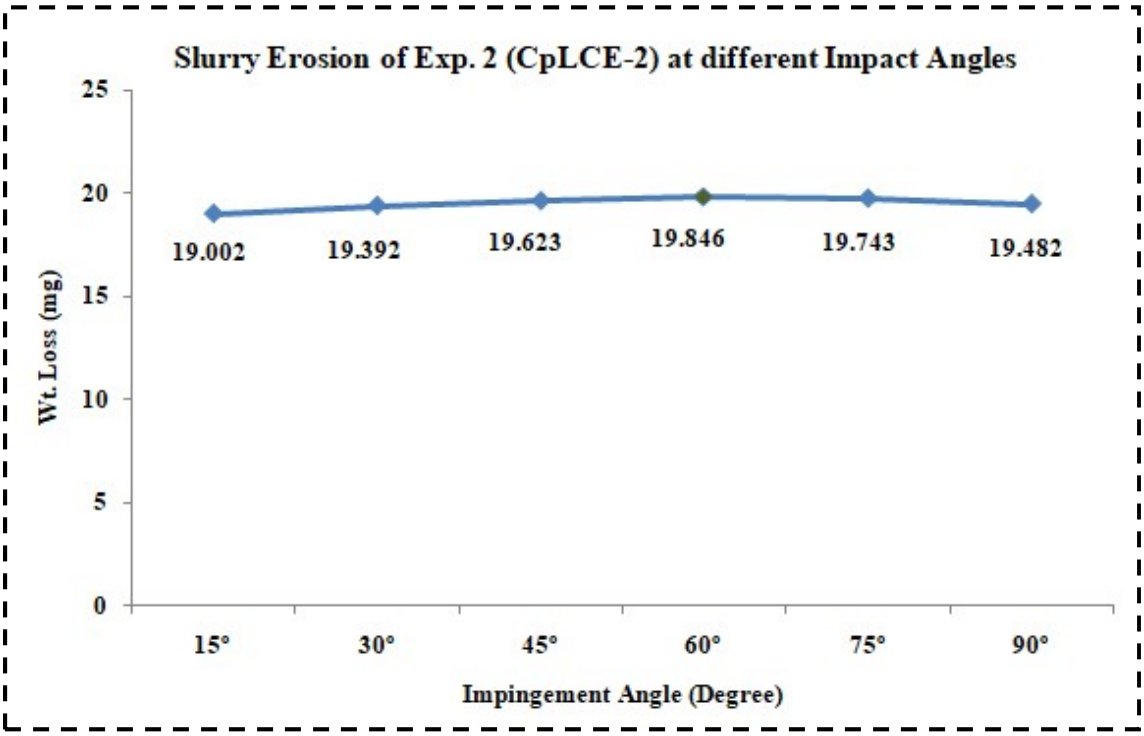

Figure 5.35: Plot of weight loss v/s impingement angle for experiment 2 (CpLCE-2)

In the same way, the optimal parametric factors including the impact velocity, erodent size and time duration as 30 m/sec, 300 µm and 120 minutes respectively were considered. Three experiments were conducted at a specific angle, and the average value of weight loss is presented in Figure 5.35. The loss of weight of coated sample was calculated at different impingement angles such as 15º, 30º, 45º, 60º, 75º and 90º. The weight loss of coated sample first increases with the increase in impact angle and maximum weight loss was observed at an angle of 60º i.e. 19.846 mg than weight loss decreases by increasing the impact angle and minimum weight loss was observed an at angle of 15º i.e. 19.002 mg. The Figure 5.36 shows the micrographs of eroded surface at 250X magnification.

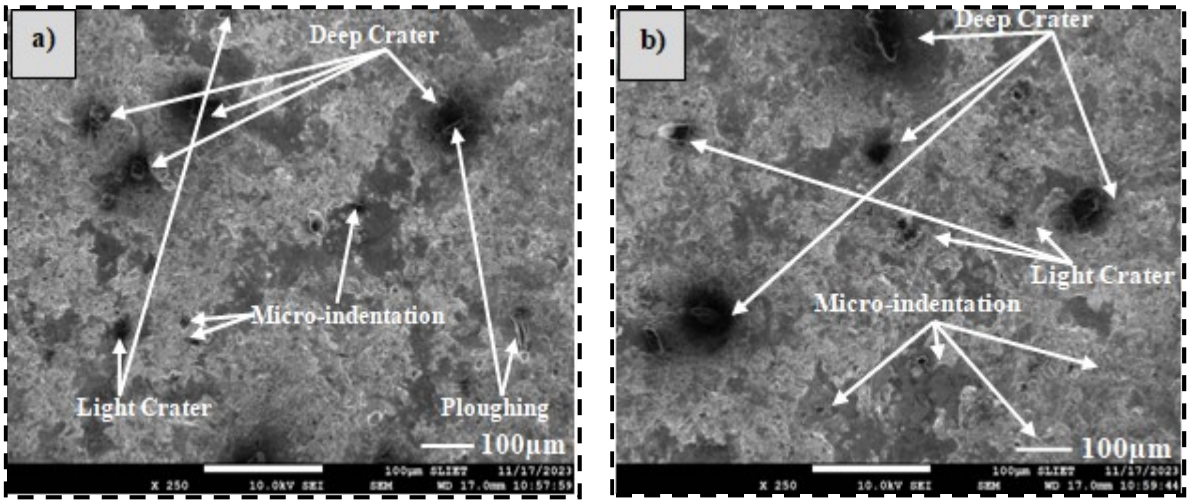

Figure 5.36: SEM micrographs of slurry jet eroded surfaces a) minimum erosion (at an angle 15º) and b) maximum erosion (at an angle 60º) for experiment 2 (CpLCE-2) at 250X

Figures 5.36a and 5.36b show the micrographs of slurry jet erosion of 0.6 wt.% rare earth oxides such as (La_2O_3/ CeO_2/ Er_2O_3 – 0.2 wt.% each) doped tungsten carbide coating. Through topographic analysis various types of wear mechanism such as micro-indentation, ploughing and crater wear were observed in the eroded surfaces of coatings. The maximum and minimum weight loss has been observed at an angle 60 and 15 degree respectively.

Experiment 3 (CpLCE-3)

5.12. Surface Characterization of Deposited Coating - Experiment 3 (CpLCE-3):

In experiment 3, there was an addition of total 0.9 wt.% rare earth oxides such as (La_2O_3/ CeO_2/ Er_2O_3 – 0.3 wt.% each) in WC-10Co-4Cr powder as shown in Table 5.22.

Table 5.22: Composition of deposited coating for experiment 3 (CpLCE-3)

Experiment No.	Coating powder (WC-10Co-4Cr-wt.%)	(La_2O_3 - wt.%)	(CeO_2 - wt.%)	(Er_2O_3 - wt.%)	Total rare earth oxides (wt.%)
(CpLCE-3) - Exp. 3.	99.1	0.3	0.3	0.3	0.9

The experiment 3 consists of tungsten carbide powder with the doping of rare earth oxides and denoted as CpLCE-3 indicates coating powder with mixture of rare earth oxides such as Lanthanum, Cerium, Erbium oxide with 0.3 wt.% each.

5.12.1. Energy Dispersive X-ray Spectroscopy (EDS):

The identification and mapping of various elements were done using EDS as shown in Figure 5.37.

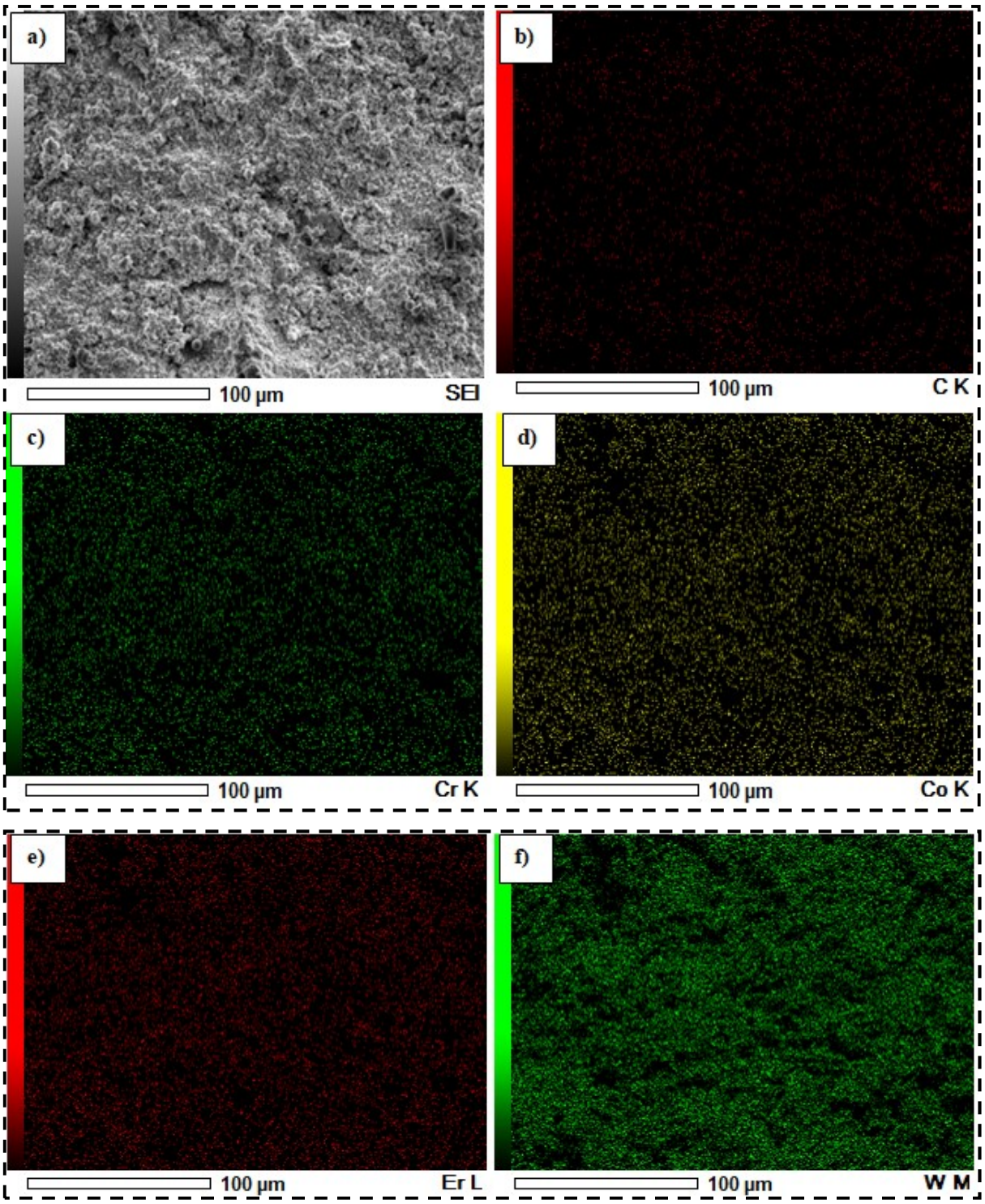

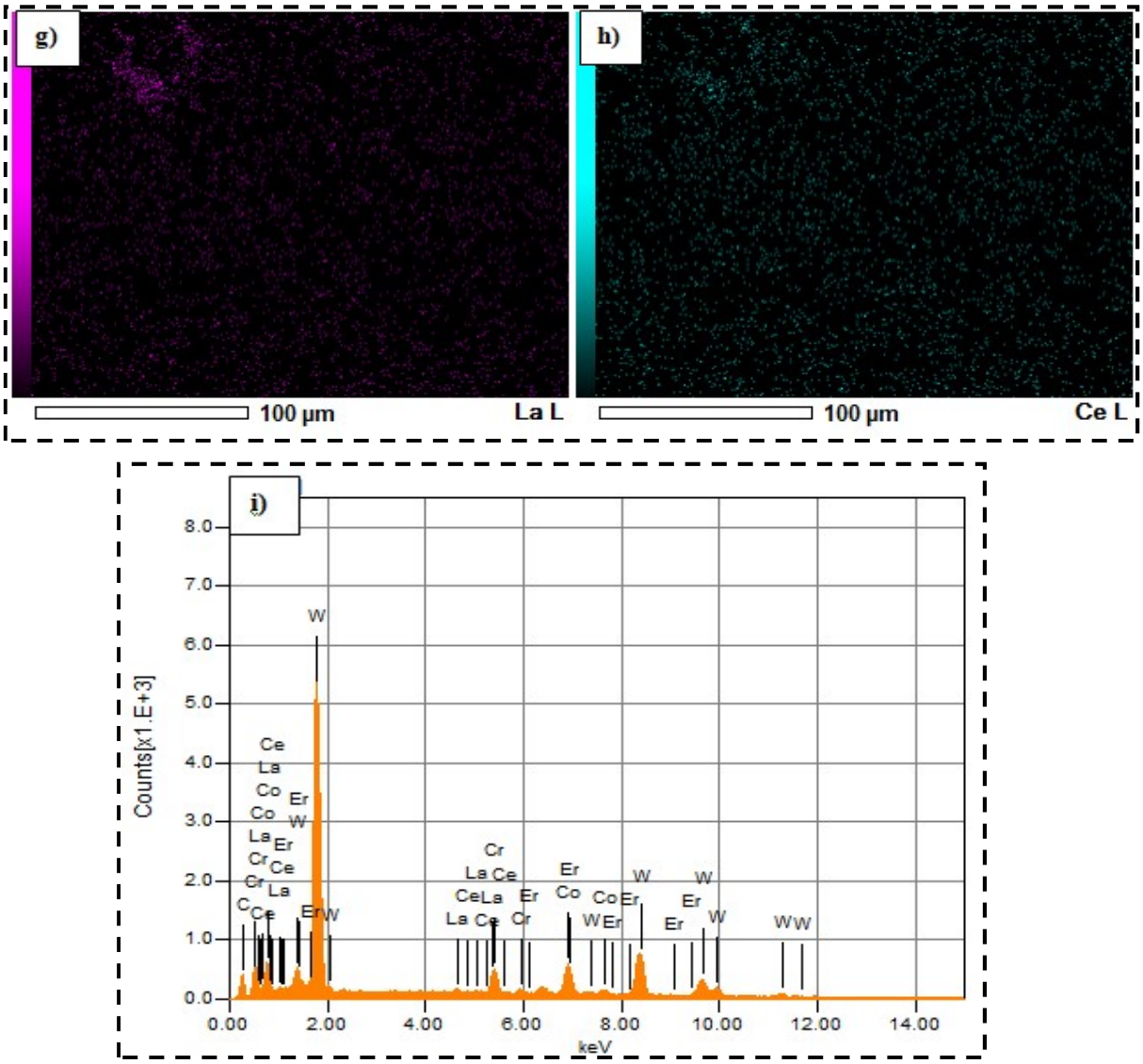

Figure 5.37: Identification of various elements using energy dispersive spectroscopy analysis a) mapped area, b) Carbon (C), c) Chromium (Cr), d) Cobalt (Co), e) Erbium (Er), f) Tungsten (W), g) Lanthanum (La), h) Cerium (Ce) and, i) EDS peaks of elements for experiment 3 (CpLCE-3)

The process parameters for the EDS test have depicted in Table 5.23. The Figure 5.37a shows the morphology of the coated surface. The detection of available elements (like Carbon, Chromium, Cobalt, Erbium, Tungsten, Lanthanum and Cerium) as shown in Figures 5.37b to 5.37h with different colors and intensity of peaks has been shown in Figure 5.37i.

Table 5.23: Process parameters of EDS

Acquisition condition of EDS	
Volt (kV)	20.00
Live time (sec)	196.60
Real time (sec)	202.65
Dead time (%)	4.00
Count rate (CPS)	1926.00

5.12.2. X-ray Diffraction Analysis (XRD):

The various phases present on coatings surface has obtained using X-ray diffraction as shown in Figure 5.38.

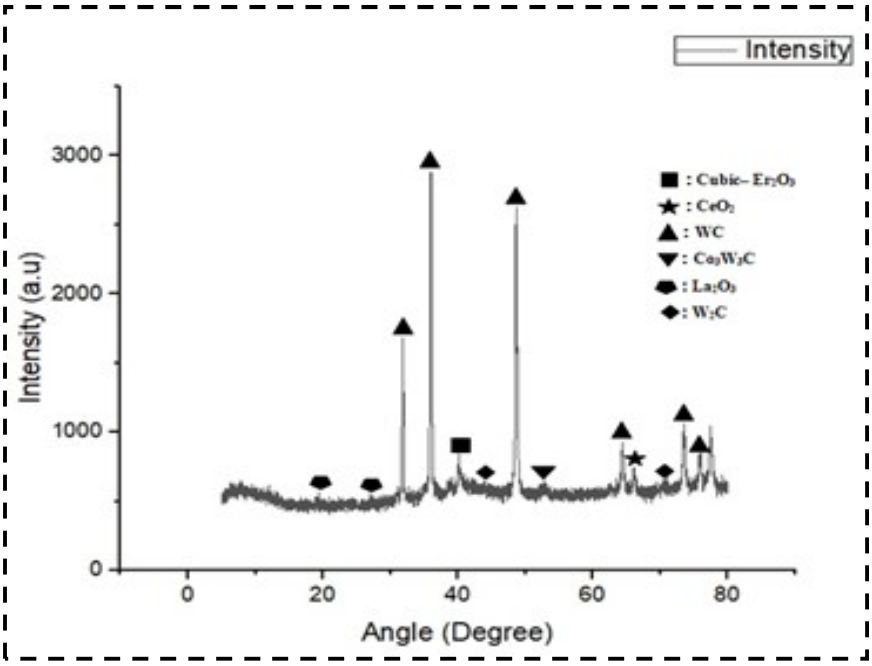

Figure 5.38: XRD analysis of rare earth (La_2O_3/ CeO_2/ Er_2O_3 – 0.3 wt.% each) doped coating

The Figure 5.38 displays the X-ray diffraction (XRD) plots for the rare earth oxides (La_2O_3/ CeO_2/ Er_2O_3 – 0.3 wt.% each) doped coated samples. It demonstrates the identification of various rare earth oxides, including different cerium, lanthanum, erbium oxides, as well as compounds of Co_3W_3C, W_2C and WC resulting from doping. The high-temperature decarburization process leads to the conversion of tungsten carbide (WC) into tungsten semi-carbide (W_2C) as described by reactions (5.1) and (5.2).

5.12.3. Surface Morphology of Deposited Coating:

The micrograph of a rare earth doped carbide coated surface using SEM at 1000X magnification has revealed in Figure 5.39.

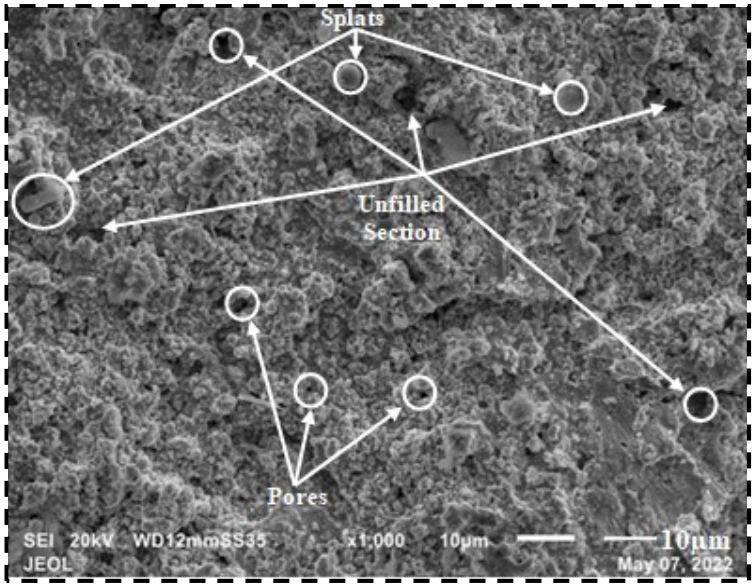

Figure 5.39: Surface morphology of rare earth (La_2O_3/ CeO_2/ Er_2O_3 – 0.3 wt.% each) doped carbide coating at 1000X

There were large numbers of splats and small pores available on the coated surface. The melting point of rare earth for example La_2O_3 (≈2300ºC)/ CeO_2 (≈2500ºC)/Er_2O_3 (≈2345 ºC), so these rare earth oxides are not completely melted but create heterogeneous nucleation sites [167]. The use of heterogeneous nucleation sites in the flame spraying method can help to control the microstructure simultaneously creating the obstacle in grain growth and improving the mechanical properties of the resulting coating or layer [150]. But in the HP-HVOF technique, the flame temperature reached up to 2630ºC, which melted even rare earth metal and created a uniform mixture in the coating. This is the biggest advantage of using the HP-HVOF process.

5.12.4. Surface Roughness (SR) and Porosity Measurement:

The surface roughness of coated samples was measured using a surface roughness tester as per ASTM D7127 standard. The average roughness value of the coating was 5.41 µm as calculated in Table 5.24.

Table 5.24: Roughness value of coated sample for experiment 3 (CpLCE-3)

	Roughness Value (µm)	Average Roughness (µm)
Rare earth (La_2O_3/ CeO_2/ Er_2O_3 – 0.3 wt.% each) oxide doped coating (Experiment 3 (CpLCE-3))	5.36	5.41
	5.49	
	5.38	

The porosity test was conducted on a cross-section of the coating with standard as ASTM E 2L09-01(2007, method A). The level of porosity was < 1% in the 24 mm of coating length RE doped carbide coatings. The porosity leads to a rough surface and the effect of surface roughness on wettability behavior, which has been analyzed using contact angle measurement.

5.12.5. Coating Thickness and Contact Angle Measurement:

The optical image (at 200X) of cross-section of the coating has depicted to know the thickness of the coating in Figure 5.40.

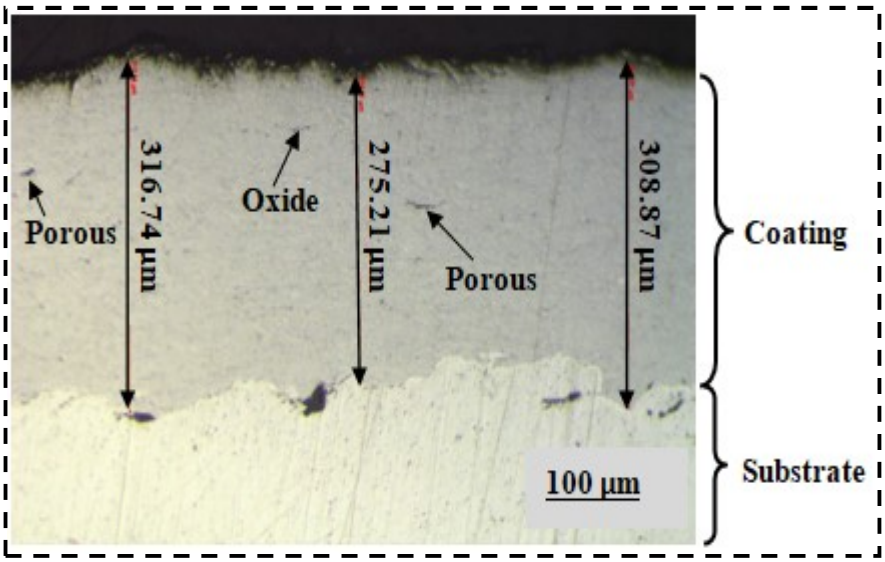

Figure 5.40: Microscopic image at 200X to measure the porosity level and thickness of coated sample

The thickness of the coated sample was in the range of 275-317 μm. The sessile drop technique is used to measure the wetting behavior of the surface as per ASTM D7334-08, which was analyzed using the static water contact angle measurement. The unevenness (roughness) of surface is the major parameter for explaining the wettability behavior. The Wenzel and Cassie Baxter state model is used to justify the effect of surface roughness on wettability [162, 168]. The air is trapped in the rough area due to the presence of R_{avg}, which imparts to the improvement in the hydrophobicity [163, 164].

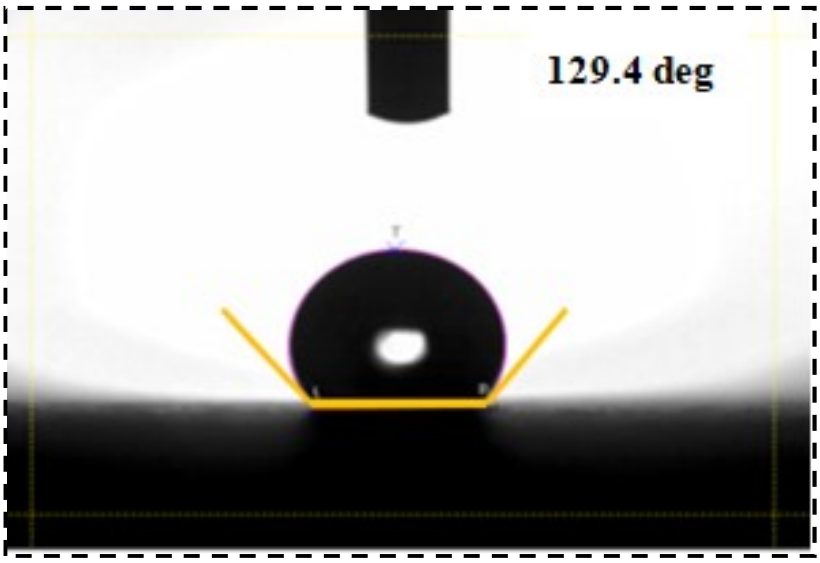

Figure 5.41: Contact angle of 0.9 wt.% rare earth oxides doped coating

The Table 5.25 shows the static water contact angle values and average value in degree. Based on the experimentation, it appears that the rare earth doped samples have an average contact angle of 129.4 degree, indicating a hydrophobic surface as shown in Figure 5.41. This means that droplets of water will tend to bead up and roll off the surface, rather than spreading out and wetting it.

Table 5.25: Static water contact angle values for experiment 3 (CpLCE-3)

Experiment	Contact Angle (CA-deg.)			Average CA (deg.)
Experiment 3 (CpLCE-3)	129.3	130.8	128.1	129.4

5.13. Mechanical Characterization of Deposited Coating - Experiment 3 (CpLCE-3):

5.13.1. Tensile Test:

The specimen depicted in Figure 5.42 was fabricated in accordance with the ASTM-E8 standard. To ensure accuracy, three separate experiments were carried out, and the average values were determined.

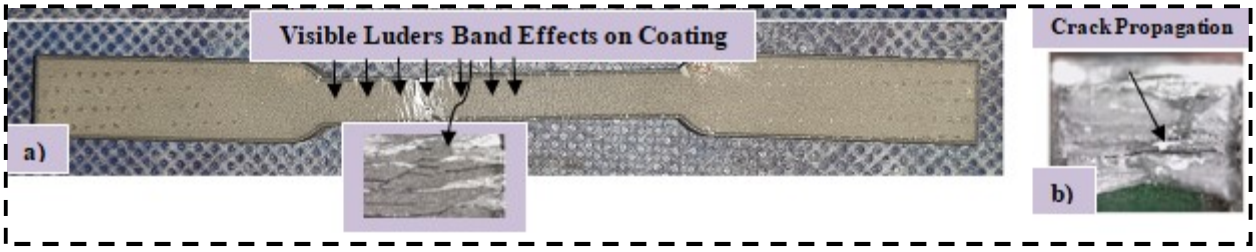

Figure 5.42: Fractured tensile test of 0.9 wt.% rare earth oxides doped sample with their fractography

The sample after the test has depicted in Figure 5.42a for coated samples. Due to crack propagation on the coated sample as shown in Figure 5.42a, there are stretcher-strain marks over the coated surface. The fractography analysis has been carried out using a digital microscope at 150X on coated sample as shown in Figure 5.42b. However, the study also indicates that a coating was applied to the sample using a high pressure high-velocity oxy-fuel (HP-HVOF) spraying method. This process involves intense heat, which may have played a role in reducing the number and size of cracks in the coated sample. The stress-strain curve for 0.9 wt.% rare earth doped coating has shown in Figure 5.43.

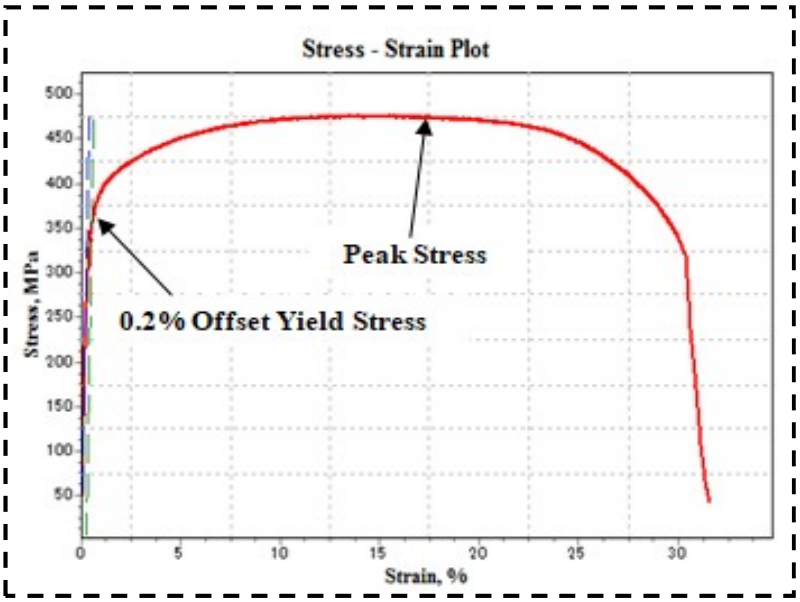

Figure 5.43: Stress-Strain plot for 0.9 wt.% rare earth doped coated sample

The different average values of mechanical properties were taken from the stress strain plot and depicted in Table 5.26. The peak stress value for rare earth doped coating (≈489 MPa) with elongation as 22.12 %.

Table 5.26: Tensile test results for experiment 3 (CpLCE-3)

Tensile Test Properties	Coated sample
Peak Stress (MPa)	489
0.2% Offset Yield Stress (MPa)	340
Yield Strain (%)	0.373
0.02% Offset Yield Stress (MPa)	261.89
Modulus (GPa)	201
Elongation at Break (Using Strain) (%)	22.12

5.13.2. Flexural Test:

The Figure 5.44 showed the coated sample after the bend test. The three-point bend test was conducted on the coated samples to know the flexural strength

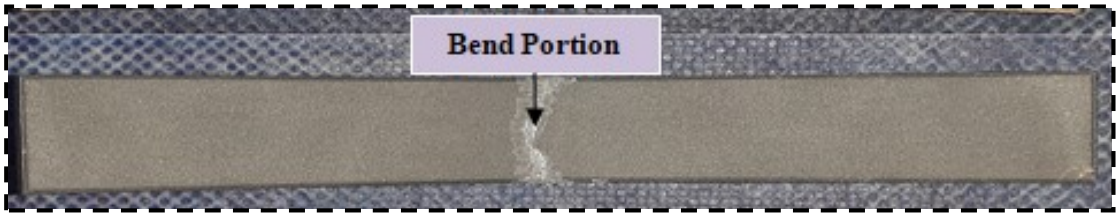

Figure 5.44: 0.9 wt.% rare earth doped coated sample after flexural (bend) test

The stress-strain curve as shown in Figure 5.45 was obtained from 3-point bend test.

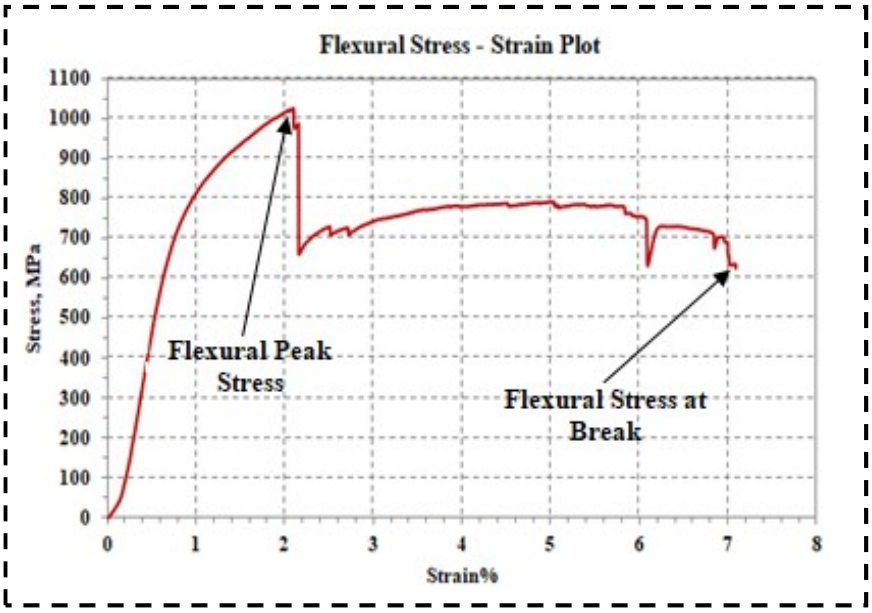

Figure 5.45: Stress-strain plot for 0.9 wt.% rare earth doped coated sample

The average values of various mechanical properties have provided in the Table 5.27 from stress-strain diagram.

Table 5.27: Flexural (three-point bend) test results for experiment 3 (CpLCE-3)

Flexural Test Properties	Coated Sample
Flexural Peak Stress (MPa)	1072
Offset Flexural Yield Stress (MPa)	1.124
Flexural Stress at Break (MPa)	885.27

5.13.3. Hardness Test:

The Vickers (HV0.3) hardness test was conducted to determine the hardness values of coated samples followed by the ASTM-A270 standard. The test involved applying a 300g load with a dwell time of 10 seconds. The average value of hardness was 1122.97 as shown in Table 5.28.

Table 5.28: Vickers hardness test values for experiment 3 (CpLCE-3)

Powder	Hardness Value (HV0.3)			Average Value
Rare earth (La_2O_3/ CeO_2/ Er_2O_3 – 0.3 wt.% each) oxide doped coating (Experiment 3 (CpLCE-3))	1116.87	1133.12	1118.92	1122.97

The indentation marked on the cross-section of coated sample has shown in Figure 5.46.

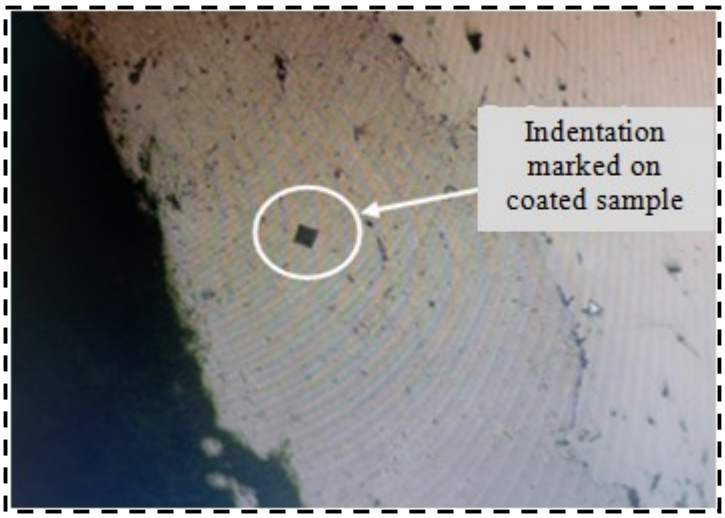

Figure 5.46: Indentation marked on coating

5.14. Tribological Characterization of Deposited Coating - Experiment 3 (CpLCE-3):

To know the tribological behavior, the slurry erosion test has performed on 0.9 wt.% rare earth oxides such as (La_2O_3/ CeO_2/ Er_2O_3 – 0.3 wt.% each) doped tungsten carbide coating at varied impingement angle.

5.14.1. Slurry Jet Erosive Behavior of Deposited Coatings:

The silt erosion test is done as per ASTM standard (ASTM G-136) using silt jet erosion test rig on rare earth doped coated samples (CpLCE-3).

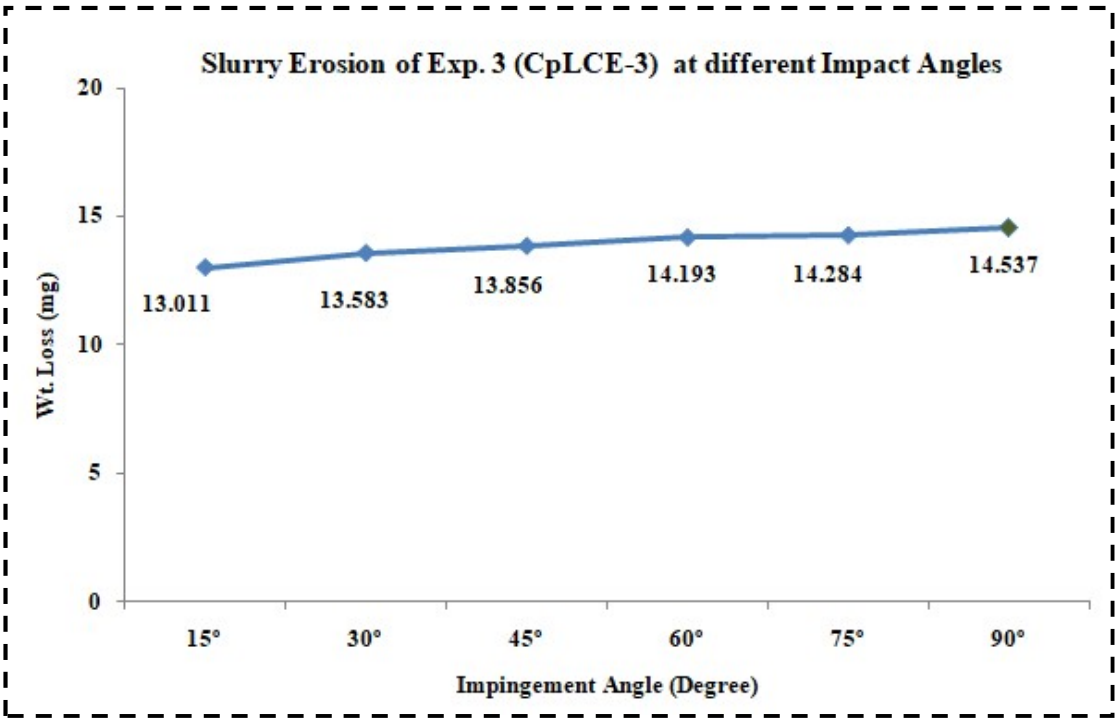

Figure 5.47: Plot of weight loss v/s impingement angle for experiment 3 (CpLCE-3)

The optimal parametric factors including the impact velocity, erodent size and time duration as 30 m/sec, 300 µm and 120 minutes respectively were considered for slurry erosion test. The impact of impingement angle on erosion rate is illustrated in Figure 5.47. Three experiments were conducted at a specific angle, and the average value is depicted in Figure 5.47. The loss of weight of coated sample was calculated at different impingement angles such as 15º, 30º, 45º, 60º, 75º and 90º. The weight loss of coated sample increases with the increase in impact angle and maximum weight loss was observed at an impact

angle 90º and minimum weight loss was observed an at angle 15º. The minimum and maximum weight loss was 13.011 and 14.537 mg respectively. The Figure 5.48 shows the micrographs of eroded surface at 500X magnification.

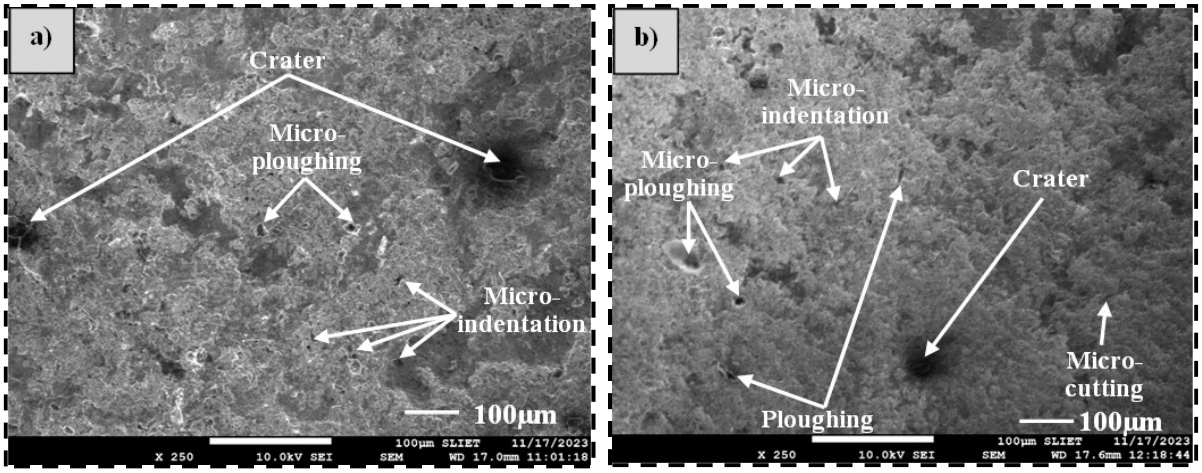

Figure 5.48: SEM micrographs of slurry jet eroded surfaces a) minimum erosion (at an angle 15º) and b) maximum erosion (at an angle 90º) for experiment 3 (CpLCE-3) at 250X

The Figures 5.48a and 5.48b show the micrographs of slurry jet erosion of 0.9 wt.% rare earth oxides such as (La_2O_3/ CeO_2/ Er_2O_3 – 0.3 wt.% each) doped tungsten carbide coating. Through topographic analysis various types of wear mehanism such as micro-indentation, micro-cutting ploughing and crater wear were observed in the eroded surfaces of coatings. The maximum and minimum weight loss has been observed at an angle of 90º and 15º respectively.

Experiment 4 (C_pLCE-4)

5.15. Surface Characterization of Deposited Coating - Experiment 4 (C_pLCE-4):

In experiment 4, there was an addition of total 1.2 wt.% rare earth oxides such as (La_2O_3/ CeO_2/ Er_2O_3 – 0.4 wt.% each) in WC-10Co-4Cr powder as shown in Table 5.29.

Table 5.29: Composition of deposited coating for experiment 4 (CpLCE-4)

Experiment No.	Coating powder (WC-10Co-4Cr-wt.%)	(La_2O_3 -wt.%)	(CeO_2 -wt.%)	(Er_2O_3 -wt.%)	Total rare earth oxides (wt.%)
(CpLCE-4) - Exp. 4.	98.8	0.4	0.4	0.4	1.2

The experiment 4 consists of tungsten carbide powder with the doping of rare earth oxides and denoted as C_pLCE-4 indicates coating powder with mixture of rare earth oxides such as Lanthanum, Cerium, Erbium oxide with 0.4 wt.% each.

5.15.1. Energy Dispersive X-ray Spectroscopy (EDS):

The identification and mapping of various elements were done using EDS as shown in Figure 5.49.

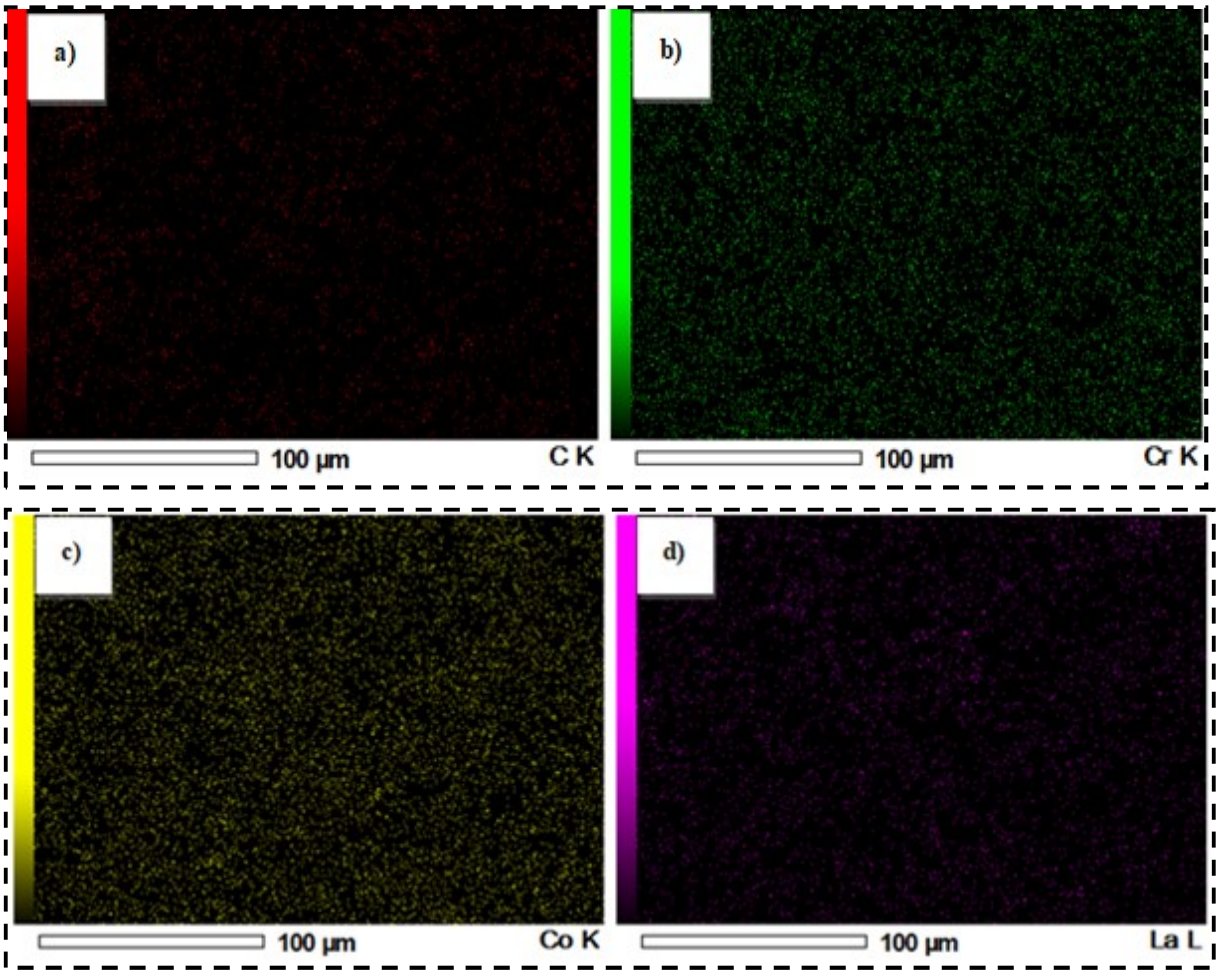

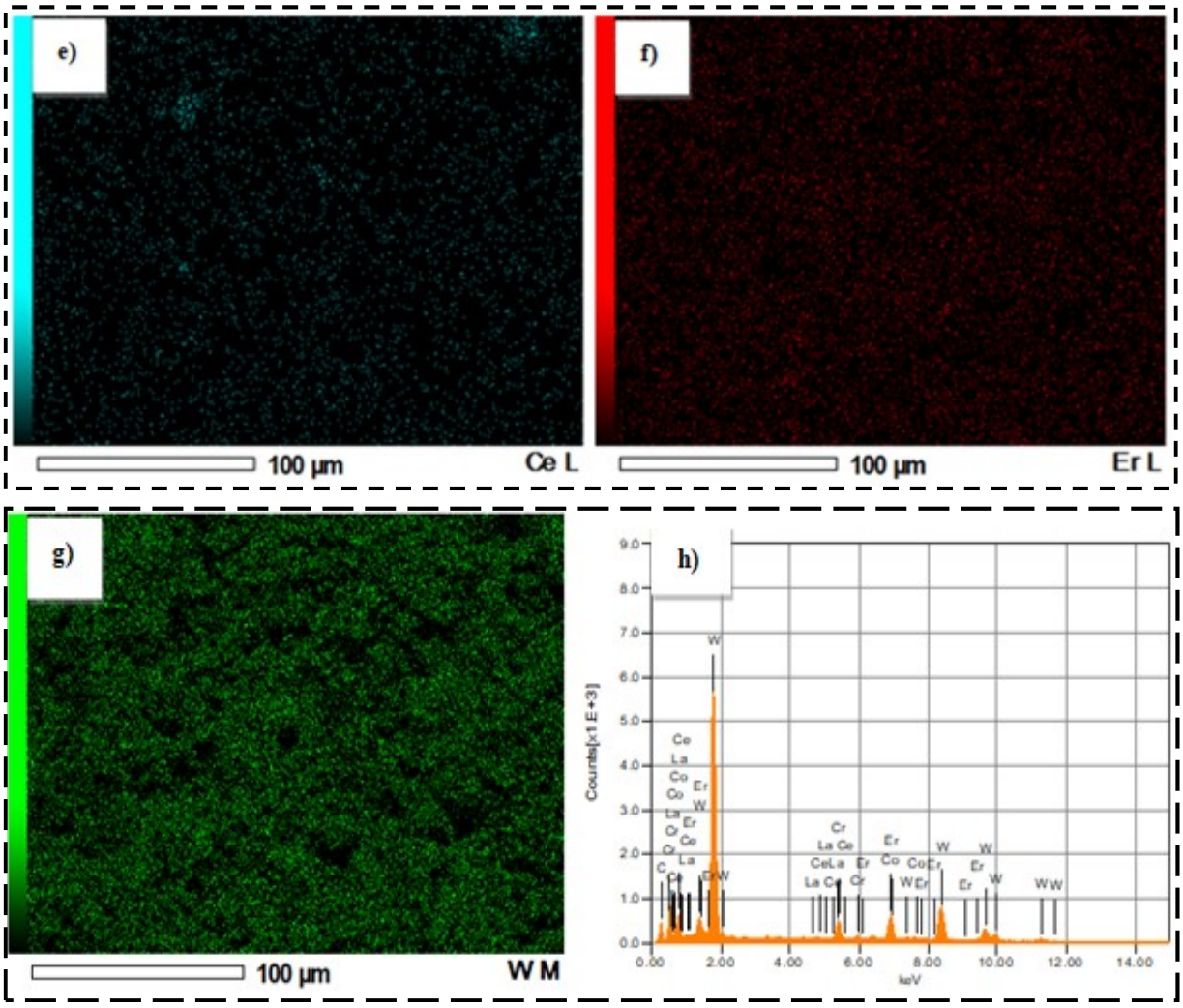

Figure 5.49: EDS area mapping showing presence of various elements; a) Carbon (C), b) Chromium (Cr), c) Cobalt (Co), d) Lanthanum (La), e) Cerium (Ce), f) Erbium (Er), g) Tungsten (W) and h) specific intensity of peaks of elements for experiment 4 (CpLCE-4)

The various process parameters of EDS are detailed in Table 5.30. The measurement lasted approximately 203.04 seconds, with the actual active time of the detector being approximately 196.60 seconds.

Table 5.30: Process parameters of EDS

Acquisition Condition of EDS	
Volt (kV)	20.00
Live Time (sec.)	196.60
Real Time (sec.)	203.04
Dead Time (%)	3.00
Count Rate (CPS)	1849.00

The detection of elements was carried out with energy dispersive X-ray (EDX) investigation as demonstrated in Figure 5.49h. Individual elements such as a Carbon, Chromium, Cobalt, Lanthanum, Cerium, Erbium, and Tungsten were identified and represented with distinct colors in Figures 5.49a to 5.49g. In Figure 1h, the EDX spectrum of the coating is depicted. Peaks in the spectrum correspond to X-rays emitted as electrons come back to the K-electron shell (for Carbon, Chromium, and Cobalt), to the L-electron shell for REOs as well as from the M-electron shell for tungsten. The peak location detection was achieved with Moseley's law.

5.15.2. X-ray Diffraction Analysis (XRD):

The various phases present on coatings surface has obtained using X-ray diffraction as shown in Figure 5.50.

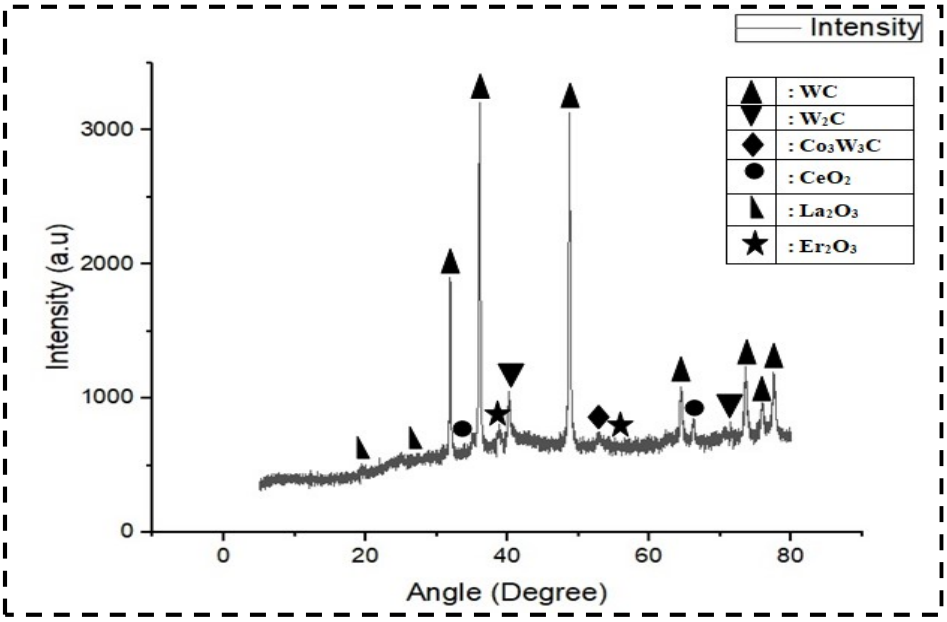

Figure 5.50: XRD analysis of rare earth (La_2O_3/ CeO_2/ Er_2O_3 – 0.4 wt.% each) doped coating

The Figure 5.50 displays the X-ray diffraction (XRD) plots for the rare earth oxides (La_2O_3/ CeO_2/ Er_2O_3 – 0.4 wt.% each) doped coated samples. It demonstrates the identification of various rare earth oxides, including different cerium, lanthanum, erbium oxides, as well as compounds of Co_3W_3C, W_2C and WC resulting from doping. The high-temperature decarburization process leads to the conversion of tungsten carbide (WC) into tungsten

semi-carbide (W_2C) as described by reactions (5.1) and (5.2).

5.15.3. Surface Morphology of Deposited Coating:

The micrograph of a rare earth doped carbide coated surface using SEM at 1000X magnification has revealed in Figure 5.51.

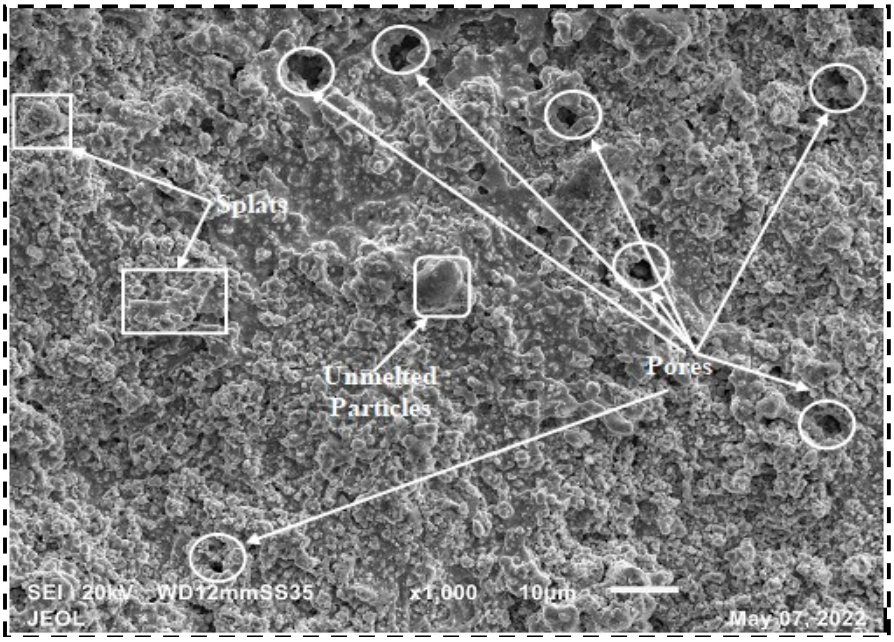

Figure 5.51: Surface morphology of rare earth (La_2O_3/ CeO_2/ Er_2O_3 – 0.4 wt.% each) doped carbide coating at 1000X

The images were captured with scanning electron microscope (SEM) at 1000X. The number of pores on the surface of coated samples is depicted in Figure 5.51. The surface of the coated sample exhibits numerous splats as well as unmelted particles.

5.15.4. Surface Roughness (SR) and Porosity Measurement:

Coated samples were evaluated for surface roughness using ASTM D7127. The average roughness was found to be 5.16 μm, as shown in Table 5.31.

Table 5.31: Roughness value of coated sample for experiment 4 (CpLCE-4)

Rare earth (La_2O_3/ CeO_2/ Er_2O_3 – 0.4 wt.% each) oxide doped coating (Experiment 4 (CpLCE-4))	Roughness Value (μm)	Average Roughness (μm)
	5.24	5.16
	5.06	
	5.18	

The porosity test was conducted on a cross-section of the coating with standard as ASTM E 2L09-01(2007, method A). The level of porosity was < 1% in the 24 mm of coating length RE doped carbide coatings. The porosity leads to a rough surface and the effect of surface roughness on wettability behavior, which has been analyzed using contact angle measurement.

5.15.5. Coating Thickness and Contact Angle Measurement:

The optical image (at 200X) of cross-section of the coating has depicted to know the thickness of the coating in Figure 5.52.The thickness of the coated sample was in the range of 296.88-305.35 µm.

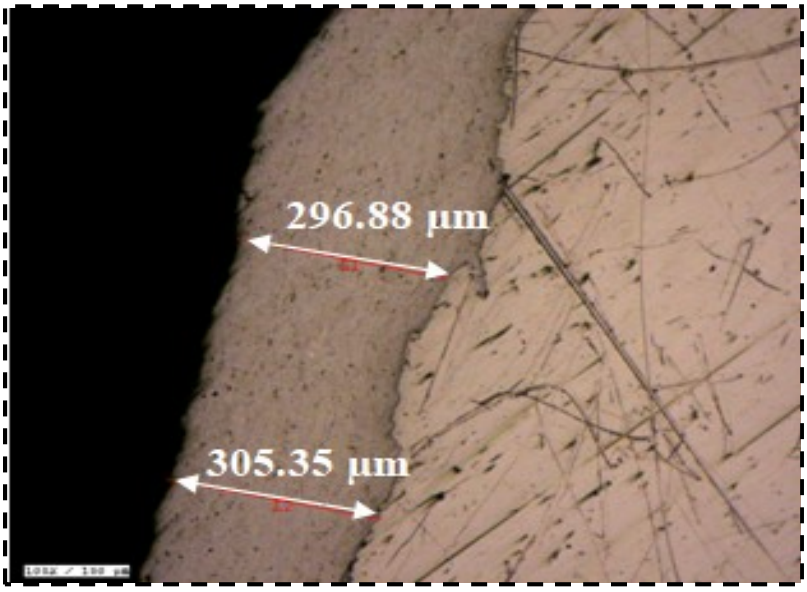

Figure 5.52: Microscopic image at 200X to measure the porosity level and thickness of coated sample

The wettability behavior of both the substrate and coated sample's surface was analyzed using the sessile droplet method, following the ASTM D7334-08 standard. Surface roughness is a key parameter influencing the wetting behavior of a surface, as explained by Wenzel and Cassie Baxter's state models. When a water droplet is positioned on a hard sample's surface, it can either spread across the surface or remain confined to a limited part, depending on the contacts amid the droplet and the hard shell. The average value of contact angle (CA) for coated sample was 129.9 degrees as shown in Figure 5.53, which

characterized the surface as hydrophobic. The Table 5.32 shows the static water contact angle values and average value in degree.

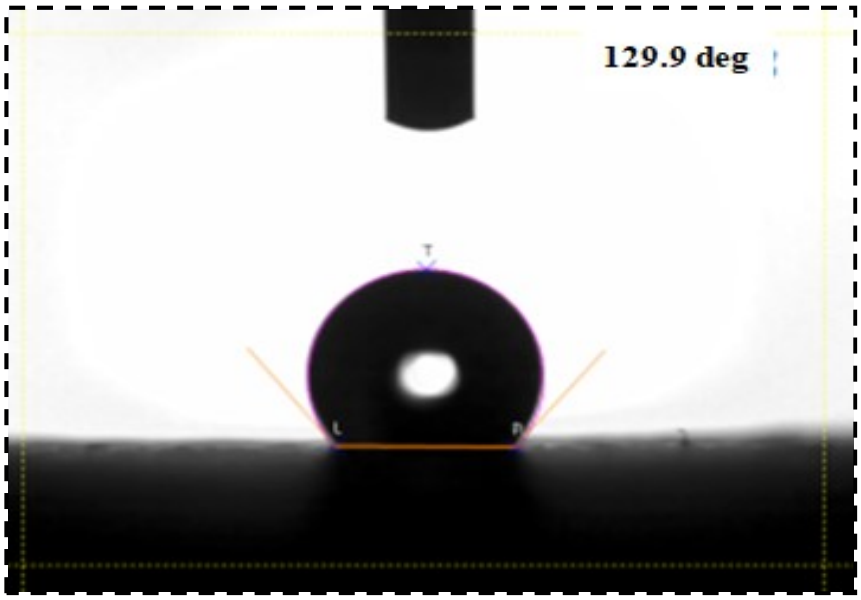

Figure 5.53: Static water contact angle of rare earth (La_2O_3/ CeO_2/ Er_2O_3 – 0.4 wt.% each) doped carbide coated sample

. Table 5.32: Static water contact angle values for experiment 4 (CpLCE-4)

Experiment No.	Contact Angle (CA-deg.)			Average CA (deg.)
Experiment 4 (CpLCE-4)	131.2	128.1	130.4	129.9

5.16. Mechanical Characterization of Deposited Coating - Experiment 4 (CpLCE-4):

5.16.1. Tensile Test:

The specimen was fabricated in accordance with the ASTM-E8 standard. To ensure accuracy, three separate experiments were carried out, and the average values were determined. The tensile test fractured sample after the test has depicted in Figure 5.54.

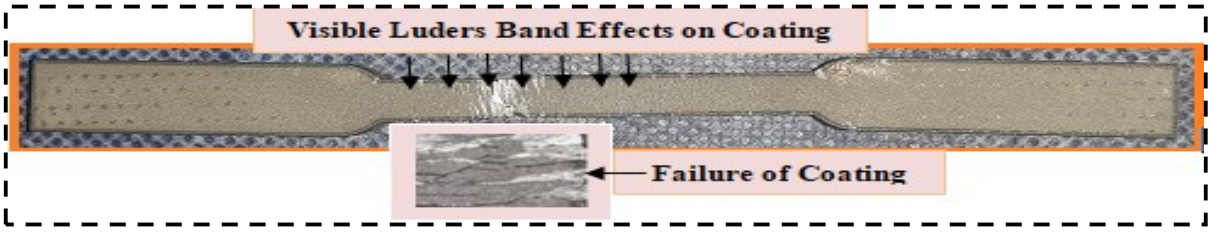

Figure 5.54: Fractured tensile test of 0.9 wt.% rare earth oxides doped sample

The stress-strain diagram as shown in Figure 5.55 for the coated sample was plotted from the universal tensile testing machine (UTM).

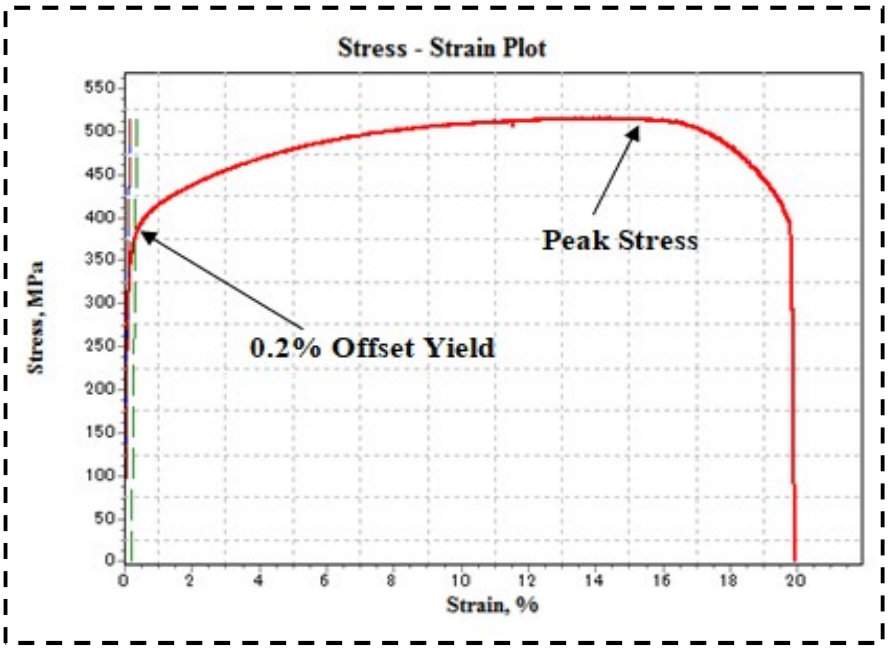

Figure 5.55: Stress-strain plot of rare earth (La_2O_3/ CeO_2/ Er_2O_3 – 0.4 wt.% each) doped carbide coated samples obtained from tension test

The values of various properties (mechanical) were derived from stress-strain plot, as presented in Table 5.33. The average peak stress value for rare earth doped coating (≈516 MPa) with elongation as 19.93 %.

. Table 5.33: Tensile test results for experiment 4 (CpLCE-4)

Properties	Average values
Peak Stress (MPa)	516.27
0.2% Offset Yield Stress (MPa)	374.95
Yield Strain (%)	0.31
0.02% Offset Yield Stress (MPa)	275.76
Modulus (GPa)	329.09
Elongation at Break (Using Strain) (%)	19.93

5.16.2. Flexural Test:

Three experiments were carried out, and the average values of all properties were compiled, as depicted in Table 5.34. The specimens were prepared according to the ASTM-D790 standard, as illustrated in Figure 5.56.

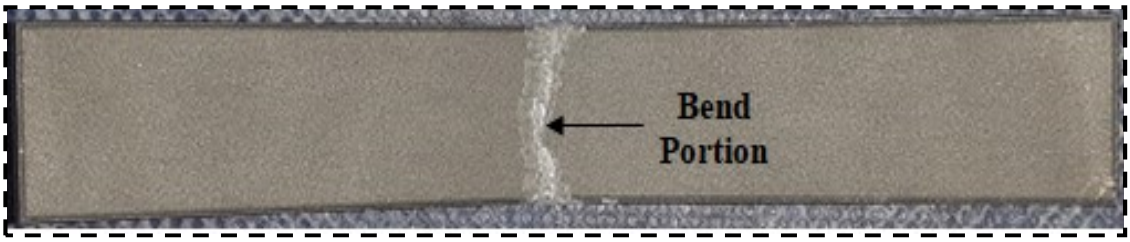

Figure 5.56: 1.2 wt.% rare earth doped coated sample after flexural (bend) test

The stress-strain curve has shown in Figure 5.57 for of rare earth (La_2O_3/ CeO_2/ Er_2O_3 – 0.4 wt.% each) doped carbide coated samples.

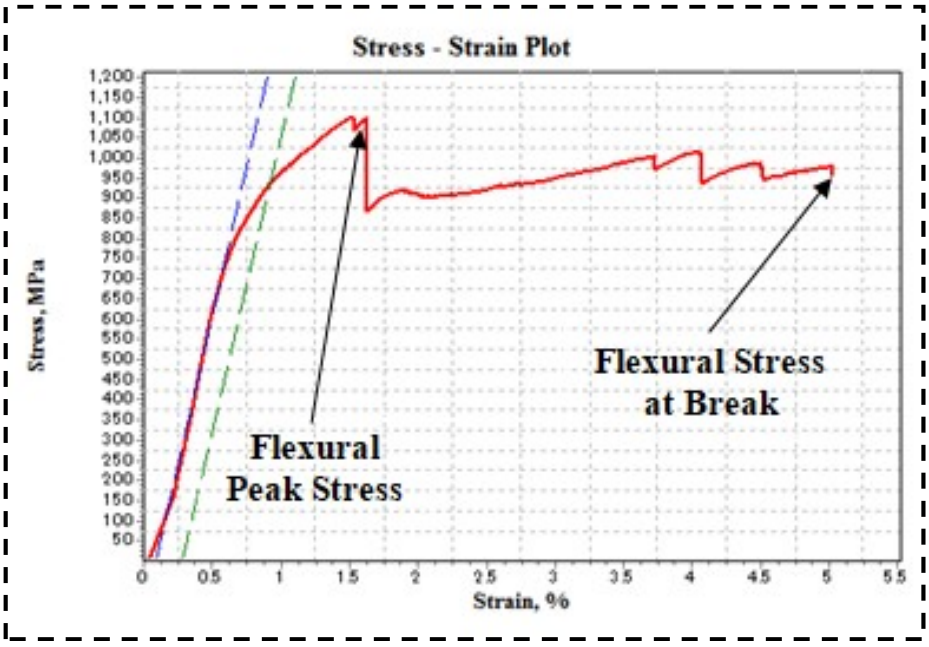

Figure 5.57: Stress-strain curve of rare earth (La_2O_3/ CeO_2/ Er_2O_3 – 0.4 wt.% each) doped carbide coated sample

The curve was generated from the bend test, and various values of properties were derived with stress-strain plots, as presented in Table 5.34.

Table 5.34: Flexural (3-point bend) test results for experiment 4 (CpLCE-4)

Properties	Average values (MPa)
Flexural Peak Stress	1101.17
Offset Flexural Yield Stress	1.16
Flexural Stress at Break	958.78

5.16.3. Hardness Test:

This test was conducted on rare earth ($La_2O_3/CeO_2/Er_2O_3$ – 0.4 wt.% each) doped carbide coated samples according to the ASTM-A270 standard. The test was performed under a load of 300g with a dwell time of 10 seconds. The average values of three readings were 931.1 as shown in Table 5.35.

Table 5.35: Vickers hardness test values for experiment 4 (CpLCE-4)

Powder	Hardness Value (HV0.3)			Average Value
Rare earth (La_2O_3/ CeO_2/ Er_2O_3 – 0.4 wt.% each) oxide doped coating (Experiment 4 (CpLCE-4))	926.5	935.1	931.7	931.1

Figure 5.58 displays the indentation marks on the surface of the coating. The inclusion of rare earth oxides in the WC-10Co-4Cr powder enhancement in the hardness values of the coated samples have observed. This increase in hardness can be attributed to the existence of hard WC particles, while the inclusion of REEs has reduced the porosity level, designates the increase in the density of the coated samples. In addition, the temperature of the coating powder is higher than the material's melting point, which causes matching oxides to form inside the coating. These oxides' existence implies that the covering possesses ceramic qualities.

Figure 5.58: Indentation marked on coating for experiment 4 (CpLCE-4)

5.17. Tribological Characterization of Deposited Coating - Experiment 4 (CpLCE-4):

To know the tribological behavior, the slurry erosion test has performed on 1.2 wt.% rare earth oxides such as (La_2O_3/ CeO_2/ Er_2O_3 – 0.4 wt.% each) doped tungsten carbide coating at varied impingement angle.

5.17.1. Slurry Jet Erosive Behavior of Deposited Coatings:

Slurry erosion testing was conducted on rare earth-doped coating (CpLCE-4) using slurry jet erosion tests rig, following the ASTM G-136 standard. The impact of impingement angle on erosion rate is illustrated in Figure 5.59.

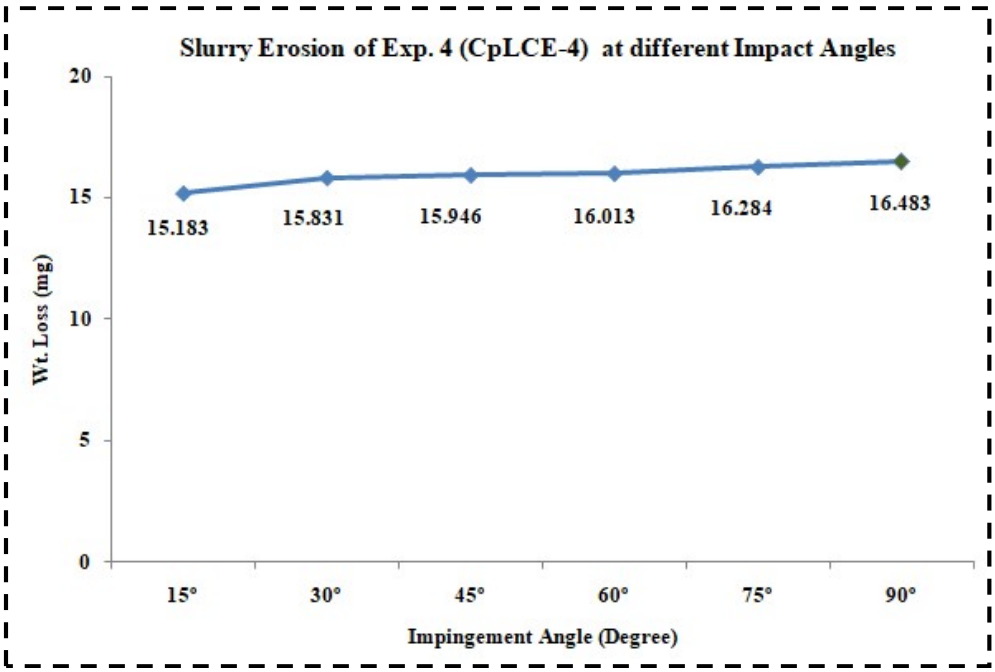

Figure 5.59: Plot of weight loss v/s impingement angle for experiment 4 (CpLCE-4)

The optimal parametric factors including the impact velocity, erodent size and time duration as 30 m/sec, 300 µm and 120 minutes respectively were considered. The tests were conducted at a specific angle, and the average value has been illustrated in Figure 5.58. Weight loss of coated samples was measured at various impingement angles (15º, 30º, 45º, 60º, 75º, and 90º). Weight loss increased with higher impact angles, peaking at 90º and lowest at 15º. The minimum and maximum weight losses were 16.483 mg and 15.183 mg, respectively. Figure 5.60 displays micrographs of the eroded surface at 500X magnification.

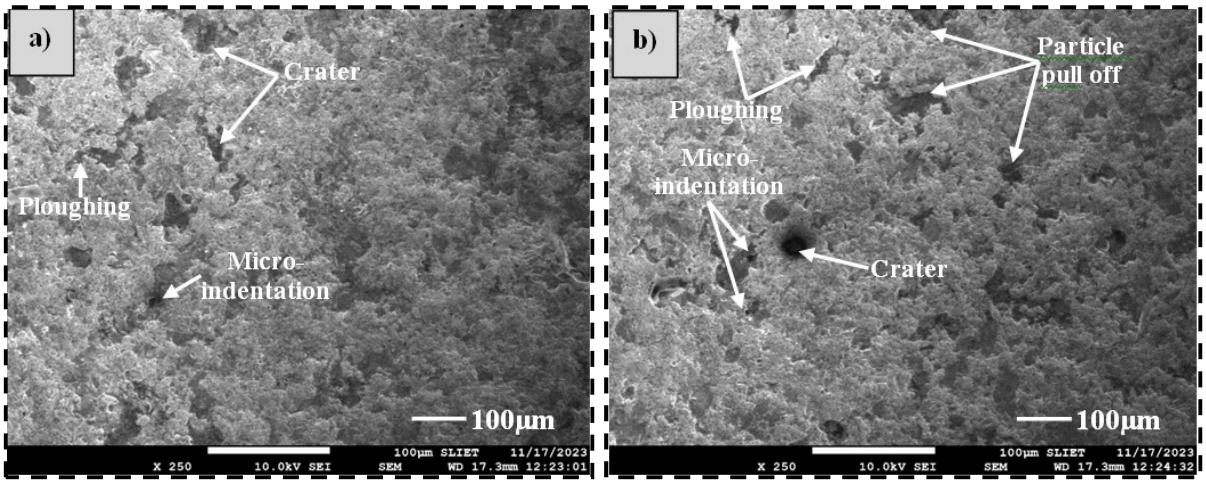

Figure 5.60: SEM micrographs of slurry jet eroded surfaces a) minimum erosion (at an angle 15º) and b) maximum erosion (at an angle 90º) for experiment 4 (CpLCE-4) at 250X

The Figures 5.60a and 5.60b show the micrographs of slurry jet erosion of 1.2 wt.% rare earth oxides such as (La_2O_3/ CeO_2/ Er_2O_3 – 0.4 wt.% each) doped tungsten carbide coating. Through topographic analysis various types of wear mechanism such as micro-indentation, ploughing and crater wear were observed in the eroded surfaces of coatings. The maximum and minimum weight loss has been observed at an angle of 90º and 15º respectively.

CHAPTER 6

Comparison of Results of Different Coated Samples

This chapter includes the comparison of results of all set of experimentation using surface, mechanical and surface characterization of the substrate, carbide coated samples (with and without rare earth oxides).

The analysis has been done on the substrate as well as different deployed coatings using HP-HVOF as shown in Table 6.1. There are five possible sets of experiments. The samples obtained from all set of experiments have analyzed using (surface, mechanical and tribological characterization).

Table 6.1: The substrate and different coatings with their compositions deployed using HP-HVOF

Experiment No.	Coating powder (WC-10Co-4Cr –wt.%)	Lanthanum oxide (La_2O_3 - wt.%)	Cerium oxide (CeO_2 - wt.%)	Erbium oxide (Er_2O_3 - wt.%)	Total rare earth oxides (wt.%)
The substrate	-	-	-	-	-
(Cp-1000) – Exp. 1.	100	-	-	-	0
(CpLCE-2) - Exp. 2.	99.4	0.2	0.2	0.2	0.6
(CpLCE-3) - Exp. 3.	99.1	0.3	0.3	0.3	0.9
(CpLCE-4) - Exp. 4.	98.8	0.4	0.4	0.4	1.2

The experiment consists of the following combinations of coatings as shown in Table 6.1.

(Cp-1000) - Experiment 1: Coating consists of (WC-10Co-4Cr) tungsten carbide powder.

(CpLCE-2) - Experiment 2: Coating consists mixture of WC-10Co-4Cr + 0.2 wt.% La_2O_3 + 0.2 wt.% CeO_2 + 0.2 wt.% Er_2O_3.

(CpLCE-3) - Experiment 3: Coating consists mixture of WC-10Co-4Cr + 0.3 wt.% La_2O_3 + 0.3 wt.% CeO_2 + 0.3 wt.% Er_2O_3.

Similarly **(CpLCE-4) - Experiment 4:** Coating consists mixture of WC-10Co-4Cr + 0.4 wt.% La_2O_3 + 0.4 wt.% CeO_2 + 0.4 wt.% Er_2O_3.

The specific rare earth oxides (La_2O_3, CeO_2, Er_2O_3) were selected based on their known ability to enhance coating properties such as mechanical properties, surface and erosion behavior. A concentration of 0.2, 0.3 and 0.4 wt.% each was chosen after preliminary studies, with the assistance of industry experts and the corpus of recent research [150, 151]. The comparative analyses of all the sets of experiments have done as follows:

6.1. Surface Behavior of Coated Samples:

The surface roughness of the substrate (SS410), coated carbide samples with rare earth oxides as 0, 0.6, 0.9 and 1.2 wt.% was measured using a surface roughness tester and the obtained average surface roughness values have shown in Figure 6.1.

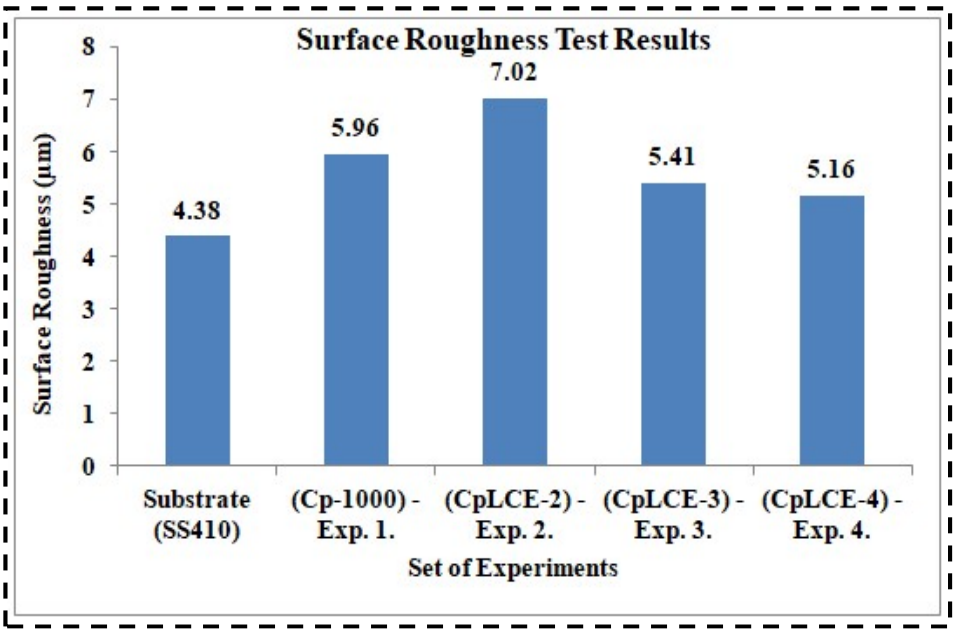

Figure 6.1: Surface roughness values of the HP-HVOF developed coatings

The roughness value of any surface describes the wettability behavior as well as aesthetic view of that surface. Moreover, the surface roughness describes the rough idea about the porosity level on the surface. The incorporation of rare earth oxides (0.6, 0.9, and 1.2% by weight) into the coating powder results in a reduction in the average surface roughness. The maximum and minimum value of surface roughness was obtained in (CpLCE-2) - Experiment 2 and (CpLCE-4) - Experiment 4 as 7.02 µm and 5.16 µm respectively. With the help of porosity test, it can be observed that the porosity level in case of (CpLCE-2) -

Experiment 2 was more as compare to the all other coated samples. The porosity value is less than 1 % for rare earth doped coatings but from microstructure, the porosity for un-doped coatings are little higher than rare earth-doped coatings. Due to the presence of porosity, the value of surface roughness is higher for un-doped coating. Moreover, the roughness of RE doped (0.6 wt.%) was observed to be highest due to insignificant quantity of which has been claimed by various literatures [48, 98, 99, 150, 151]. The above statement validation can be done with the help of SEM micrographs, which showed that the unfilled section for un-doped coating was more which leads to the higher roughness.

Table 6.2: Porosity level of the current experiment with other available literature

Coating Powders	Rare earth oxides	Process	Level of porosity	Reference
WC-10Co-4Cr	NA	HP-HVOF	≥1 to ≤ 2%	Current work
WC-10Co-4Cr	(La_2O_3+CeO_2+Er_2O_3)- 0.2, 0.3 and 0.4 wt%. each	HP-HVOF	< 1%	Current work
WC-12Co	Rare Earth (CeO_2-1%)	HVOF	1.6 %	[88]
Nano (WC-12Co)	NA		2.1 %	
NiCrBSi	(CeO_2)- 0, 0.4, 0.8, 1.2, 1.6, and 2 wt%.	Flame sprayed	6.2, 6.5, 5.2, 6.8, 7.9, and 7.3	[150]
NiCrBSi	(La_2O_3)- 0, 0.4, 0.8, 1.2, 1.6, and 2 wt%.	Flame sprayed	6.2, 7.1, 6.2, 5.8, 6.7, and 7.2	[151]

The Table 6.2 presents different values of porosity level obtained by various researchers through their experiments. The current experimented work has the lowest porosity level among other available literature. In general porosity leads to a rough surface and the effect of surface roughness on wettability behavior, which has been analyzed using contact angle measurement.

It is important to note that the relationship between surface roughness and hydrophobicity is complex, and other factors such as chemical composition, surface treatment, and temperature can also play significant roles. The wettability behavior of any surface is majorly dependent on the roughness of that surface. The effect of surface roughness on wettability behavior has been justified using Wenzel and Cassie Baxter's model as shown in Figures 6.2a and 6.2b respectively [177, 178]. Introducing the roughness on any surface increases the trapping of air in the roughened area, which enhances the hydrophobic behavior of the surface [179, 180].

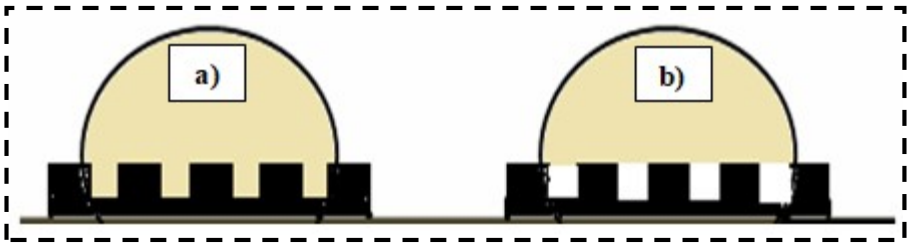

Figure 6.2: Possibilities of the interaction of drop with the pattern a) Wenzel and; b) Cassie state model [177, 178]

It is familiar that, the categorization of wettability behavior is based on the value of contact angle, if the contact angle of any surface is less than 90˚ then the surface is categorized as hydrophilic otherwise the surface is hydrophobic in nature [47, 65, 172]. As shown in Figure 6.3, all the HP-HVOF developed coatings have contact angle values more than 90º indicated that the all the coated samples are hydrophobic in nature except the substrate (hydrophilic).

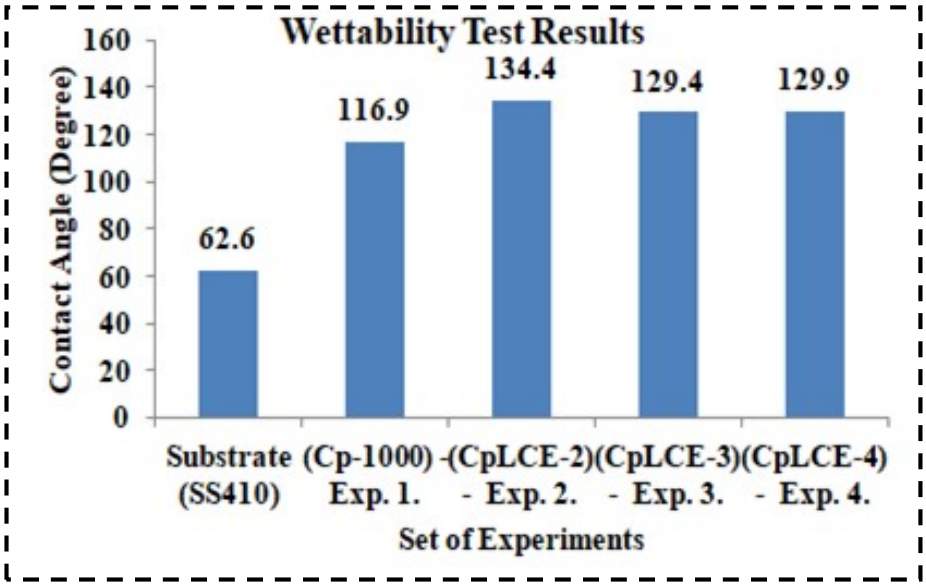

Figure 6.3: Contact angle values of the HP-HVOF developed coatings

The roughness value for the (CpLCE-2) - experiment 2 was the highest with a value for the water contact angle of 134.4º. Moreover, the surface roughness value for the substrate was less so obtained corresponding water contact angle was also minimum as 62.6º. The higher water contact angle observed in rare earth doped coatings might have been attributed to their smoother surface morphology, reduced surface energy, and enhanced hydrophobicity due to the presence of rare earth oxides.

6.2. Mechanical Behavior of Coated Samples:

The mechanical characterization such as tensile, flexural and hardness test of the substrate and coated samples have done and comparative results have discussed as follows:

6.2.1. Tensile Test Results of Coated Samples:

The samples were ready according to ASTM- E8 standard and the test was carried out using universal testing machine to obtain the different mechanical properties. The average values of peak stress of the different coatings have shown in Figure 6.4.

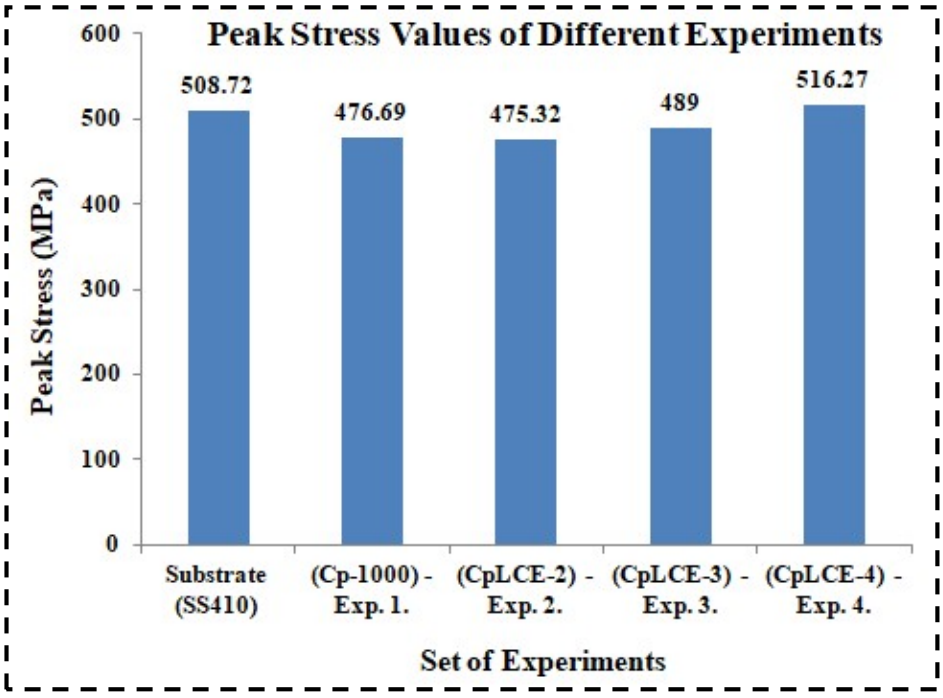

Figure 6.4: Peak stress values of the HP-HVOF developed coatings

In tensile testing, the peak stress corresponds to the maximum tensile strength of the material. Understanding the peak stress is essential for assessing the material's ability to withstand external forces without undergoing permanent deformation or failure. As shown in Figure 3, the peak stress value for the (CpLCE-4) - experiment 4 is the maximum and the all other coated samples show comparable peak stress value. After depositing coating on the substrate the peak stress has considerably enhanced as shown in Figure 6.4. This indicates that the coated samples can withstand more loads before undergoing permanent deformation. The average values of yield stress of different coatings have shown in Figure 6.5.

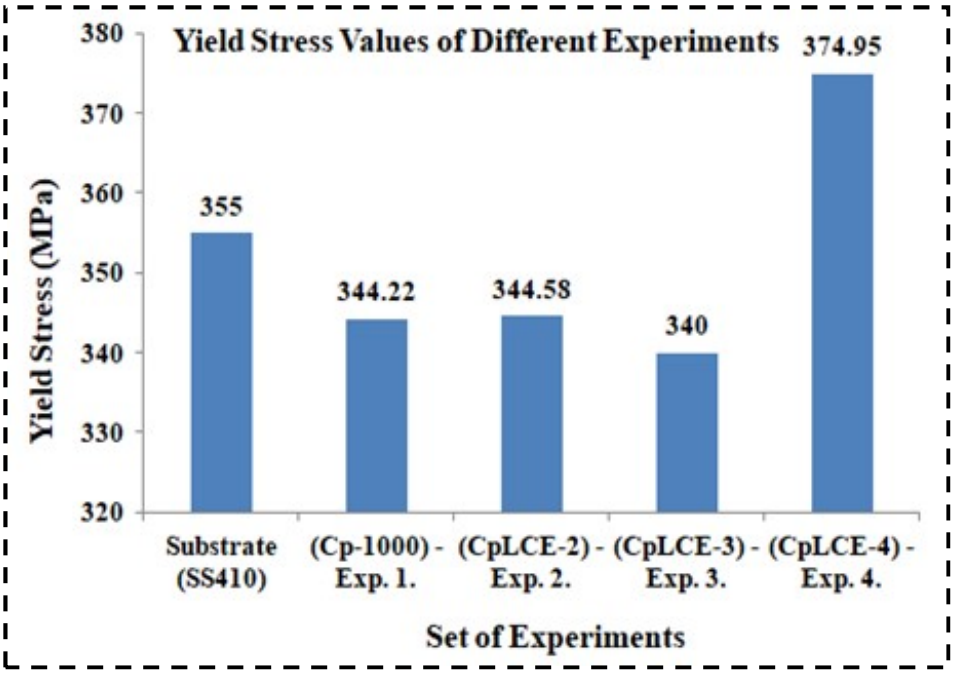

Figure 6.5: Yield stress values of the HP-HVOF developed coatings

The yield stress marks the transition from elastic to plastic deformation in a material. Prior to reaching the yield stress, a material undergoes elastic deformation, meaning it returns to its original shape once the applied stress is removed. After exceeding the yield stress, the material undergoes permanent, plastic deformation. The study of yield stress is integral to failure analysis. Knowing the yield stress of a material helps identify the point at which plastic deformation begins, contributing to a better understanding of the failure mechanisms. The yield stress value for the (CpLCE-4) - experiment 4 is the maximum and yield stresses for all other coated samples are comparable as shown in Figure 6.5. The modulus values of different coatings have shown in Figure 6.6.

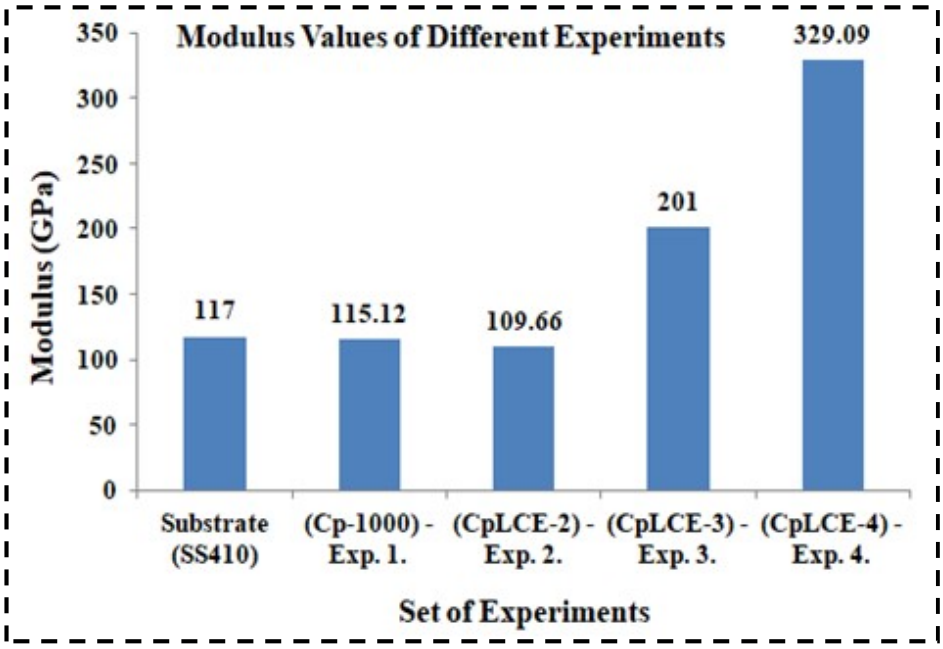

Figure 6.6: Modulus values of the HP-HVOF developed coatings

The term "modulus" typically refers to the modulus of elasticity, which is a material property describing the stiffness or rigidity of a material. Young's Modulus, generally designated by E, quantifies a material's resistance to elastic deformation when put through to axial or tensile loading. A higher Young's Modulus indicates a stiffer material, meaning it deforms less under a given load. The modulus value for the (CpLCE-4) - experiment 4 is the maximum. This indicates that the coating (CpLCE-4) - experiment 4 can with stand more elastic deformation as compared to all others experiments as shown in Figure 6.6. The average values of percentage elongation of different coatings have shown in Figure 6.7.

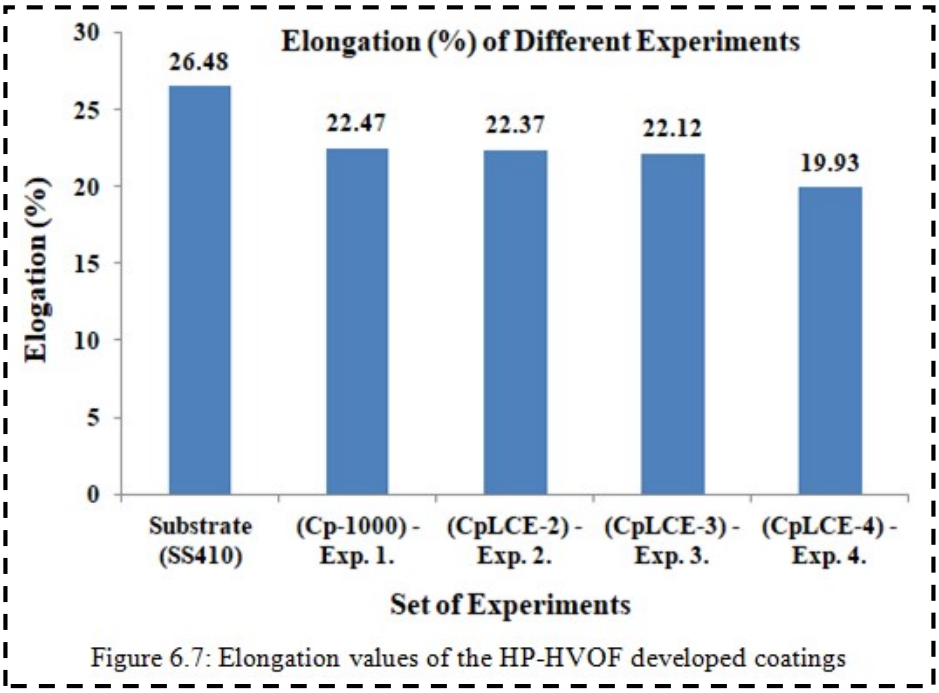

Figure 6.7: Elongation values of the HP-HVOF developed coatings

The percentage elongation is a key indicator of a material's ductility, which is the capability of a material to go through considerable plastic deformation before break. Materials with higher elongation can provide a margin of safety by allowing more deformation before failure. The percentage elongation value for the (CpLCE-4) - experiment 4 is the minimum as shown in Figure 6.7. This indicates that the (CpLCE-4) - experiment 4 coating shows less ductility as compared to other set of experiments. One of the coated as well as uncoated samples after tensile test has been considered for the detailed analysis using SEM as shown in Figure 6.8c.

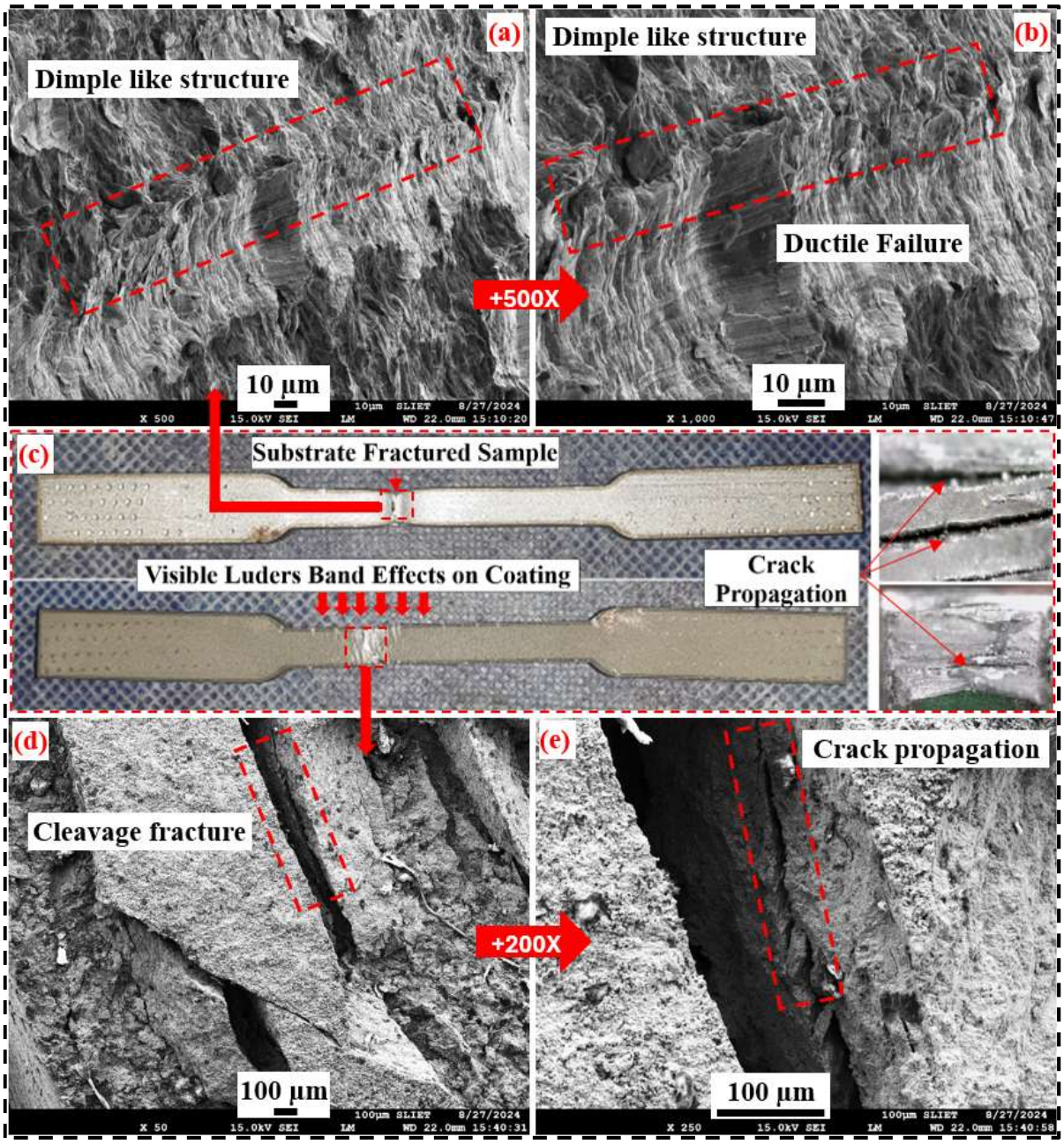

Figure 6.8: (a-b) SEM images showing fractured tensile samples of Substrate, (c) Actual image of after tensile test samples, and (d-e) SEM images showing fractured tensile samples of (0.9% doped) coating.

Due to crack propagation on the coated sample as shown in Figure 6.8(c), there are stretcher-strain marks over the coated surface, which was difficult to observe in the substrate sample. The fractography analysis on the same image reveals that the substrate

would likely experience a higher number and larger size of crack propagation compared to the coated sample. However, the study also indicates that a coating was applied to the sample using a high pressure high-velocity oxy-fuel (HP-HVOF) spraying process. This process involves intense heat, which may have played a role in reducing the number and size of cracks in the coated sample. This is supported by the information provided, which suggests that the coated sample had fewer and smaller cracks compared to the substrate.

Further, the SEM images of the after-failure tensile specimens have also been taken at higher magnifications, with an aim to provide valuable insights into the failure mechanisms of the coated and uncoated samples. For the uncoated SS410 substrate, the SEM images reveal dimple-like features and necking on the fractured surface (refer Figure 6.8 (a and b)). These dimples are indicative of micro void coalescence, a common mechanism in ductile materials where voids nucleate, grow, and eventually coalesce under tensile stress, leading to failure. The uniform distribution of these features suggests that the failure initiated and propagated within the substrate material, which is consistent with its relatively lower hardness and higher ductility.

In contrast, the SEM images of the coated sample (rare earth doped) showed a markedly different fracture surface (refer Figure 6.8 (d and e)). The images reveal a combination of brittle and ductile fracture features. The brittle regions are characterized by flat facets and typical of cleavage fracture, which likely originated from the hard coating. This suggests that the initial failure may have initiated within the hard WC phase, where localized stress concentrations led to crack initiation and propagation. The presence of such brittle features can be attributed to the high hardness and brittleness of the WC particles within the coating, which are prone to fracturing under tensile stress. However, the SEM images also show areas of ductile fracture in the coated sample, particularly near the interface with the substrate. These areas display micro void coalescence similar to that observed in the uncoated substrate, indicating that once the cracks propagated through the brittle coating, the failure mechanism transitioned to a more ductile mode as it reached the substrate. This transition from brittle to ductile failure could be due to the underlying substrate's ability to absorb more energy before fracturing, thereby delaying complete failure.

6.2.2. Flexural Test Results of Coated Samples:

A flexural test, also known as a bending test, is a material strength test in which a sample is subjected to bending under controlled conditions. This type of test is commonly used to determine the flexural strength, modulus of elasticity, and other mechanical properties of materials, especially brittle materials like ceramics and composites. The average values of flexural peaks stress of different coatings have shown in Figure 6.9.

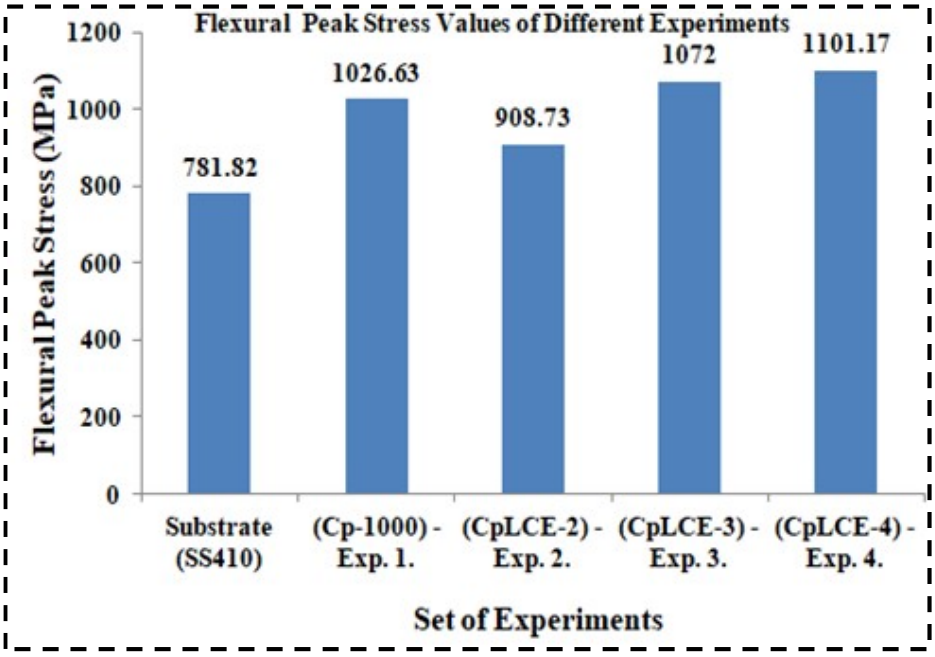

Figure 6.9: Flexural peak stress values of the HP-HVOF developed coatings

Understanding the flexural peak stress helps in predicting potential failure modes related to bending stresses. By designing HP-HVOF coatings with appropriate flexural strength, this can mitigate the risk of coating failure and prolong the service life of coated components. The flexural peak stress value for the (CpLCE-4) - experiment 4 was observed to the maximum i.e. 1101 MPa. The coating of (CpLCE-4) - experiment 4 can bear more bending load without failure as compare to all other coatings. As compare to the substrate the flexural peak stress value for coated samples were higher as shown in from Figure 6.9. The average values of offset flexural yield stress at break of the substrate and different coatings have shown in Figure 6.10.

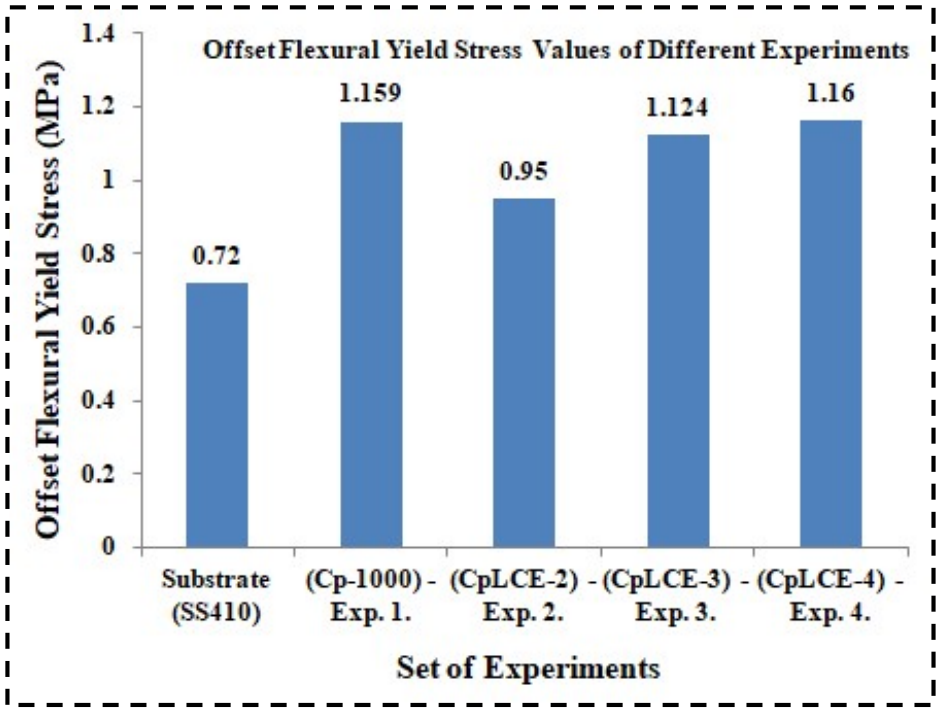

Figure 6.10: Flexural yield stress values of the HP-HVOF developed coatings

The flexural yield stress is a measure of the coating's ability to resist deformation and plastic flow under applied bending loads. A higher flexural yield stress indicates better structural integrity, which is crucial for coatings used in applications where the coated components may experience bending or flexural stresses. The flexural yield stress value for the (CpLCE-4) - experiment 4 and (CpLCE-1) - experiment 1 was observed to the maximum i.e.≈1.16 MPa. The coating of (CpLCE-1) - experiment 1 and (CpLCE-4) - experiment 4 can resist more deformation under bending load as compare to all other coatings. As compare to the substrate the flexural yield stress value for coated samples were higher as shown in from Figure 6.10. The average values of flexural stress at break of the substrate and different coatings have shown in Figure 6.11.

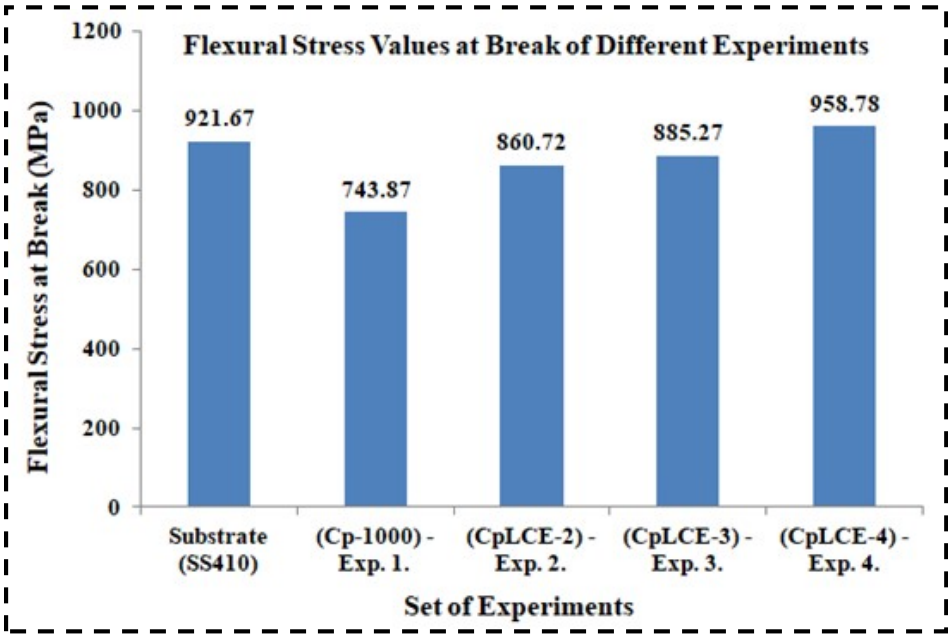

Figure 6.11: Flexural yield stress values of the HP-HVOF developed coatings

The flexural stress at break is an indicator of the coating's ductility, representing the maximum stress the coating can withstand before undergoing catastrophic failure or fracture. A higher flexural stress at break suggests better ductility, which can be desirable in applications where some level of deformation or elongation is expected before failure. The flexural stress value at break for the (CpLCE-4) - experiment 4 was observed to be maximum i.e.≈958.78 MPa. The coating of (CpLCE-4) - experiment 4 showed the lowest ductility and the substrate shows higher ductility than all set of coated samples as shown in from Figure 6.11. One of the bend coated as well as uncoated samples were considered for the detailed analysis using SEM as shown in Figure 6.12.

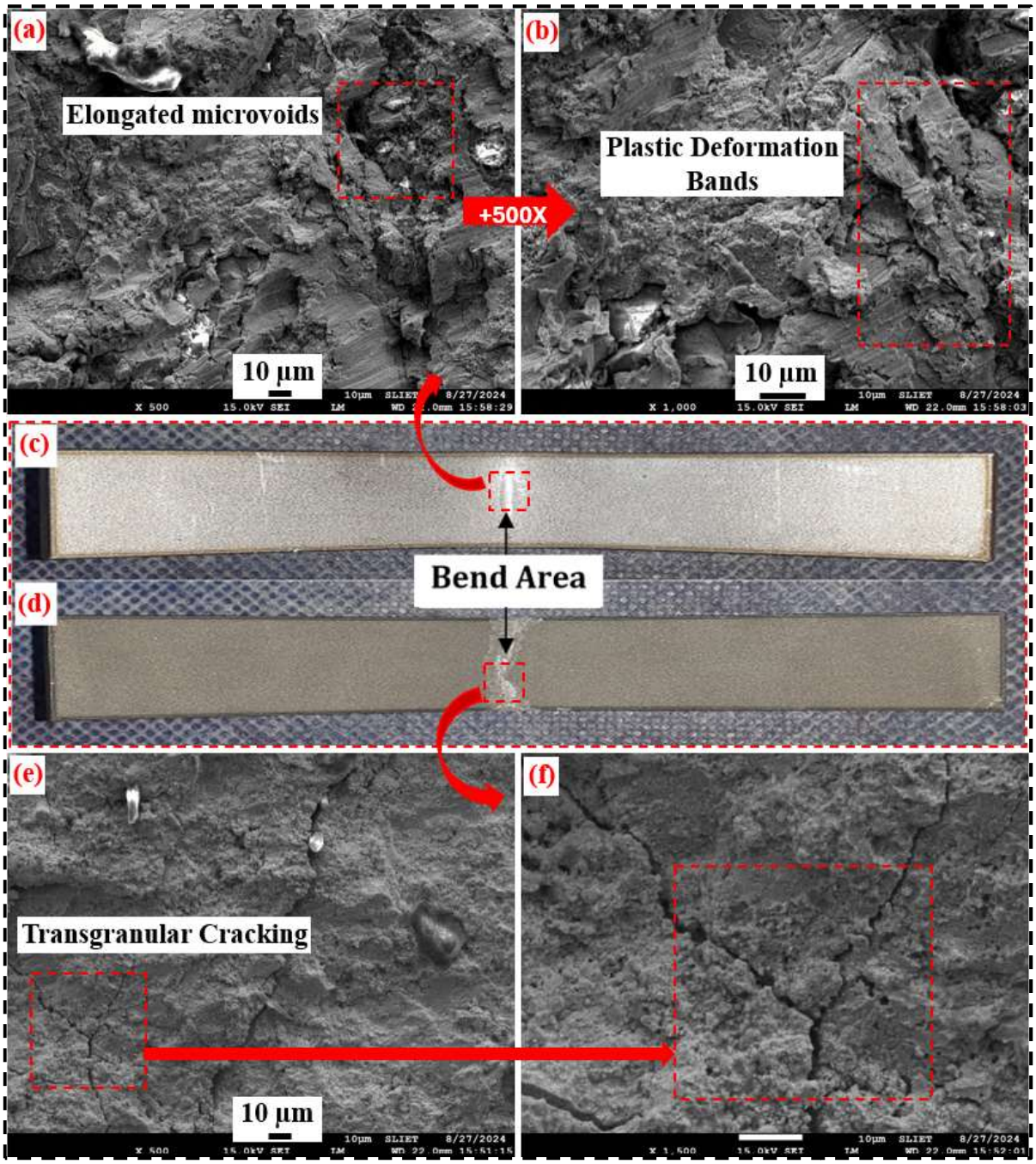

Figure 6.12: (a-b) SEM images showing fractured bend samples of Substrate, (c-d) Actual image of after bend test samples, and (e-f) SEM images showing fractured bend samples of (0.9% doped) coating.

Figures 6.12(c) and 6.12(d) showed the substrate and coated samples after the bend test. A 3-point bend test was conducted on the substrate and coated samples to know the flexural strength. The SEM images of the bend samples after flexural test, the specimens provide

critical insights into the failure mechanisms under bending stress for both the coated and uncoated samples. For the uncoated SS410 substrate, the SEM images reveal a predominantly ductile failure mode, characterized by the formation of elongated micro voids and plastic deformation bands (refer Figure 6.12 (a and b)). These features suggest that during bending, the material experienced significant plastic deformation, particularly in the tensile zone of the bent sample. The presence of slip lines and the relatively smooth fracture surface indicate that the material underwent extensive plastic flow before failure, which is typical of ductile metals like SS410.

In contrast, the coated sample with the RE-doped WC-10Co-4Cr coating exhibited a more complex failure behaviour. The SEM images show a clear distinction between the failure modes in the coating and the substrate. In the coating, the fracture surface reveals brittle characteristics, such as trans-granular cracking and the formation of cleavage planes (refer Figure 6.12 (e and f)). These features suggest that the hard coating fractured primarily through brittle mechanisms when subjected to bending stress. The brittle nature of the WC phase, combined with the high stiffness of the coating, likely led to the rapid propagation of cracks once initiated, resulting in a brittle fracture surface.

Interestingly, the SEM images also show evidence of delamination at the interface between the coating and the substrate. This delamination suggests that the differential mechanical properties of the coating and substrate, particularly their differing flexural rigidities, may have caused stress concentrations at the interface during bending. The rigid, brittle coating was less able to accommodate the plastic deformation experienced by the ductile substrate, leading to interfacial failure. This delamination could have been exacerbated by the inherent brittleness of the coating, which prevented it from deforming in unison with the substrate under bending stress. In the substrate beneath the coating, the SEM images reveal ductile fracture features similar to those observed in the uncoated sample.

The presence of micro voids and plastic flow lines suggests that, after the coating fractured, the substrate continued to bear the load, deforming plastically before eventual failure. The overall failure mechanism in the coated samples thus appear to be a combination of brittle fracture in the coating and ductile deformation in the substrate, with interfacial delamination playing a significant role in the failure process under bending.

6.2.3. Hardness Test Results of Coated Samples:

To know the hardness value of the substrate and coated samples, The Vickers hardness tests (HV0.3) has been conducted in accordance with ASTM-A270 standards with 300g load for 10 seconds of dwell time. The average values of Vickers hardness of different coatings have shown in Figure 6.13.

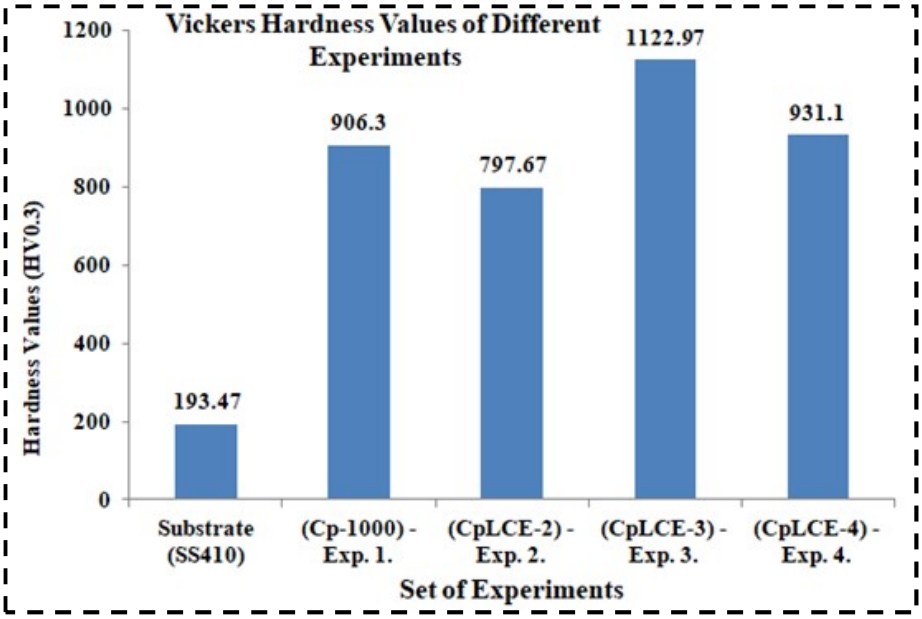

Figure 6.13: Hardness test values of the HP-HVOF developed coatings

The presence of tungsten's hard carbide particles has resulted in an increased hardness value for the coating. The Vickers hardness value of the un-doped rare earth oxides coating was 906.3. The addition of the mixture of rare earth oxides from 0.6, 0.9 and 1.2 wt.% the hardness value of the coating was observed as 797.67, 1122.97 and 931.1 respectively. The hardness value of coated sample was noticed to be maximum at 0.9 wt.% rare earth oxides doped coating in (CpLCE-3) - experiment 3 as shown in Figure 6.11.

As shown in Figure 6.13, the limited quantity (0.9wt.%) RE-doped coated sample exhibits a hardness value increase of approximately 480% compared to the substrate. The significant increase in hardness observed in rare earth doped coatings might have been attributed to the refinement of grain structure, solid solution strengthening, and the formation of hard inter-metallic phases induced by rare earth elements. The conclusion has been made from the value of hardness number that the rare earth doped cermet coating was

exceptionally harder than the substrate but the concentration of rare earth oxides would be in the range of (0.9-1.2 wt.%) after that there might be decrease in the hardness value.

Table 6.3: Hardness values of current work and other related work

Coating powder	**Rare earth (wt.%)**	**The load applied (gram)**	**Vickers hardness**	**References**
WC-Co-Cr (86-10-4)	0%	300	HV0.3: 906.3	Current work
WC-Co-Cr (86-10-4)	(La_2O_3+CeO_2+ Er_2O_3)-0.2, 0.3 and 0.4 wt%. each	300	HV0.3: 797.67, 1122.97 and 931.1 respectively	Current work
WC-Co-Cr (86-10-4)	0%	300	HV0.3: 983	[169]
Al_2O_3 and Al_2O_3-TiO_2	0%	300	HV0.3: 1117 and 1027 respectively	[170]
Cr_3C_2-NiCr	(La_2O_3)-1, 2, and 4 wt%.	200	HV0.2: 921, 932, 966 respectively.	[171]
	(CeO_2)-1, 2, and 4 wt%.		HV0.2: 905, 846, 957 respectively.	
	(La_2O_3+CeO_2)-2 wt%. each		HV0.2: 1063	
NiCrBSi	(CeO_2)- 0, 0.4, 0.8, 1.2, 1.6, and 2 wt%.	4996.6	HV5: 210, 215, 250, 238, 221, and 226 respectively.	[150]
NiCrBSi	(La_2O_3)- 0, 0.4, 0.8, 1.2, 1.6, and 2 wt%.	4996.6	HV5: ≈210, 220, 230, 256, 226 and 222 respectively.	[151]

Various investigators have conducted their research and achieved different hardness values as shown in Table 6.3, the conclusion made from Table 6.3; is that the hardness value of the experiment 3 is notably higher compared to that of other published works.

6.3. Slurry Erosion Behavior of Coated Samples:

The slurry erosion testing was conducted following the standard (ASTM G-136) by means of a silt erosion test. This testing examined both on the substrate (SS410) and coated samples.

Table 6.4: Weight loss (mg) due to slurry erosion at various impact angles (degree)

Impact angle (deg.) / Wt. loss (mg)	15º	30º	45º	60º	75º	90º
The substrate	20.273	20.964	21.647	21.491	21.228	21.102
(Cp-1000) – Exp. 1.	16.658	17.193	17.385	17.573	17.759	17.963
(CpLCE-2) – Exp. 2.	19.002	19.392	19.623	19.846	19.743	19.482
(CpLCE-3) – Exp. 3.	13.011	13.583	13.856	14.193	14.284	14.537
(CpLCE-4) – Exp. 4.	15.183	15.831	15.946	16.013	16.284	16.483

The Mass loss due to slurry erosion was calculated for substrate and coated samples at six different impingement angles such as 15°, 30°, 45°, 60°, 75° and 90° is presented in Table 6.4 and Figure 6.14. From the data it can be obtained that the mass loss trends at varying impact angles for different specimens: the substrate, a coating lacking rare earth (RE) doping, and a coating with (0.2, 0.3 and 0.4 wt.% each) RE doping. A comprehensive analysis incorporating scientific principles elucidates that the trend of mass loss across different impact angles is showing distinct erosion behaviours in the tested specimens. The substrate, exhibiting consistent mass loss increments with increasing impact angles, signifies inherent vulnerability to slurry erosion.

Conversely, the coating without RE doping displays a comparable pattern, albeit with slightly reduced mass loss values, suggesting a limited protective effect. However, the most striking observation emerges from the data pertaining to the (0.3 wt.% each)RE doped coating, which demonstrates a remarkable reduction in mass loss across all impact angles compared to the substrate and other coatings (refer Figure 6.14 and Table 6.4).

This substantial improvement in erosion resistance can be attributed to the enhanced material properties conferred by rare earth (0.3 and 0.4 wt.% each) doping. The elevated hardness of the RE doped coating, stemming from solid solution strengthening, grain refinement, and second phase strengthening, might have impeded material removal under erosive conditions.

Furthermore, the hydrophobic nature of the RE doped coating, facilitated by its refined microstructure and surface characteristics, acted as a deterrent against slurry penetration and adhesion, thereby minimizing erosive damage. The incorporation of rare earth (0.3 and 0.4 wt.% each) elements might have contributed to grain refinement within the coating structure, resulting in a denser and more resilient microstructure capable of withstanding abrasive impacts.

This refined structure, coupled with the inherent toughness imparted by RE doping, ensures the integrity of the coating is maintained even under severe erosive conditions. Further, it has been observed that in case of substrate, maximum mass loss is evident at 45° impingement angles, indicative of a propensity for deformation and material displacement under less forceful impacts. Conversely, as impingement angles increase, mass loss increases, likely due to increased energy transfer and more severe deformation. However, in the case of both the coated specimens, i.e., without rare earth (RE) doping and those with 0.3 wt.% each RE doping, the trend is almost same (refer Figure 6.14).

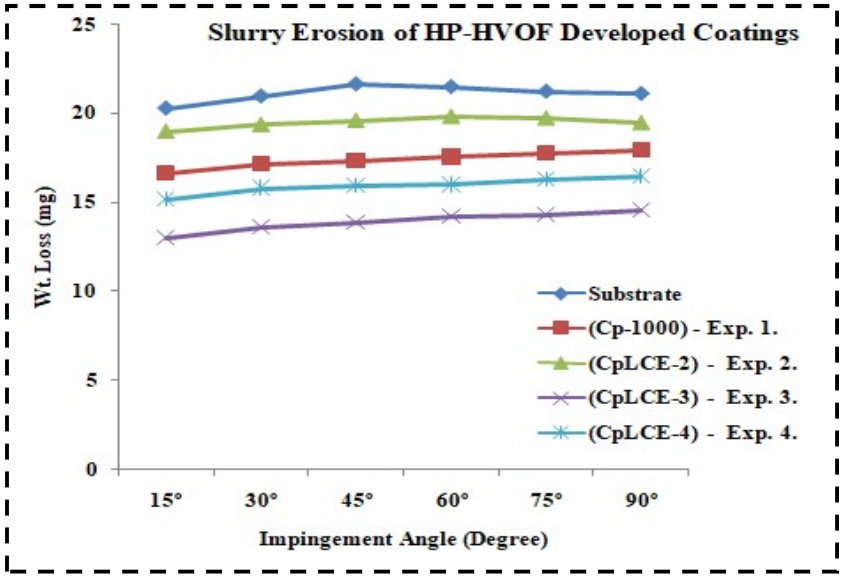

Figure 6.14: Plot of weight loss v/s impingement angle of the HP-HVOF developed coatings

Here, the erosion rate increases with rising impingement angles, reaching a maximum at 90°. This pattern suggests a tendency for brittle fracture and material fragmentation under more forceful impacts, leading to increased mass loss. The notably lower mass loss observed for the (0.3 wt.% each) RE doped coating compared to other experiments can be attributed to its higher hardness, which enhances resistance to deformation and material removal. This trend underscores the critical influence of material properties, such as ductility and hardness, on erosive behaviour and highlights the potential for tailored coatings to mitigate slurry erosion in industrial applications.

CHAPTER 7

Conclusions and Future Scope

Chapter 7: This chapter includes the conclusions of investigation regarding with and without rare earth doped tungsten carbide based composite coating including significant findings of all set of experiments followed by future scope of present work.

The research aims to develop and investigate rare earth-doped tungsten carbide composite coatings on martensitic stainless-steel substrates using thermal spraying techniques. The specific objectives include:

- The research successfully developed these coatings with precise control over the composition and microstructure, leading to enhanced mechanical and tribological properties.
- Comprehensive testing demonstrated that the rare earth-doped coatings exhibited significantly improved hardness, toughness, and wear resistance compared to conventional coatings, thus meeting these objectives.

The novelty of the research lies in the exploration of rare earth element doping in WC-Co-Cr coatings, which has been minimally studied. Additionally, the use of martensitic steel (SS 410) as a substrate for these coatings is another innovative aspect, as there is limited existing research on this combination. The research is justified by identified gaps in the existing literature, specifically the lack of comprehensive studies on HP-HVOF thermal spraying of rare earth-doped coatings and the limited work on SS 410 as a substrate material. The investigation into these areas is expected to contribute significantly to the fields of materials science and engineering, particularly in enhancing the durability and performance of coated materials across various industries, such as aerospace, automotive, and energy sectors. Also, this research is novel in several key aspects:

- *Innovative Material Combination:* The combination of rare earth elements with tungsten carbide-cobalt-chromium on a martensitic stainless steel substrate represents a novel material system that has not been explored in previous studies.

- *Advanced Coating Technique:* The use of HP-HVOF thermal spraying for applying these coatings introduced new possibilities for optimizing the microstructure and properties of the coatings, which had not been achieved with other techniques.
- *Industrial Application Focus:* The research directly addresses the needs of industries requiring high-performance coatings, bridging the gap between academic research and practical application.

7.1. Conclusions:

This investigation focuses on assessing the surface, mechanical and slurry erosion behavior of the substrate (SS410), along with the un-doped and rare earth oxides such as lanthanum oxide (La_2O_3)/ cerium oxide (CeO_2)/ erbium oxide (Er_2O_3) doped tungsten carbide coatings applied on the substrate (SS410) with 0, 0.2, 0.3 and 0.4 wt.% of each as (Cp-1000) - experiment 1, (CpLCE-2) - experiment 2, (CpLCE-3) - experiment 3 and (CpLCE-4) - experiment 4 respectively using the high-pressure high-velocity oxy fuel (HP-HVOF).

The conclusions drawn are based on a series of experiments on the substrate, (Cp-1000) - experiment 1, (CpLCE-2) - experiment 2, (CpLCE-3) - experiment 3 and (CpLCE-4) - experiment 4 with doping of varying amounts of rare earth oxide mixture in tungsten carbide (WC-10Co-4Cr) coating. The following conclusions have been made after detail study.

- This research has successfully developed and characterized rare earth (La_2O_3/CeO_2/Er_2O_3) doped tungsten carbide-cobalt-chromium (WC-Co-Cr) composite coatings (thickness: 275-327 µm) on martensitic stainless steel (SS410) substrates using high-pressure high-velocity oxy-fuel (HP-HVOF) thermal spraying technique. The study addressed key challenges in enhancing the mechanical and tribological properties of these coatings, which are critical for their application in environments requiring high durability and wear resistance.
- Energy dispersive X-ray analysis detected multiple elements within the coating, including Tungsten (W), Cobalt (Co), Chromium (Cr), Erbium (Er), Lanthanum (La), Cerium (Ce), among others.

- From the XRD pattern analysis indicates that the high-temperature conditions have led to the transformation of tungsten carbide through decarburization, resulting in the formation of tungsten semi-carbide (W_2C) and cobalt-tungsten bimetallic carbide (Co_3W_3C).
- The water contact angle for coating of (CpLCE-2) - experiment 2 was observed to be maximum i.e. 134.4º which shows that the surface has high hydrophobic nature as compared to others, due to its high roughness value (7.02 μm) and minimum for the un-doped coating as (Cp-1000) - experiment 1. Moreover, the substrate shows the hydrophilic behavior.
- The porosity level is less than 1% in all the experiments except (CpLCE-2) - experiment 2. This has the porosity level in the range of ≥1 to ≤ 2%.
- The incorporation of rare earth elements into the WC-Co-Cr coatings significantly improved the mechanical properties, such as hardness and adhesion strength, compared to conventional coatings. These enhancements can be attributed to the unique microstructural changes induced by the rare earth doping, which leads to grain refinement, which is resulted in the hydrophobic coatings as well as an increase in the mechanical properties.
- The tensile and flexural test results were considerably good for coating of (CpLCE-4) - experiment 4. Moreover, the hardness value of 0.9% rare earth oxides (La_2O_3/CeO_2/Er_2O_3-0.3% each) as (CpLCE-4) - experiment 4 was observed to be highest.
- The fractography analysis on the tensile image reveals that the substrate would likely experience a higher number and larger size of crack propagation compared to the coated sample but coated samples shows combination of brittle and ductile fracture features.
- Moreover, the fractography analysis on the flexural image reveals that the substrate would likely experience a predominantly ductile failure mode, characterized by the formation of elongated micro voids and plastic deformation bands but fracture surface of coated sample reveals brittle characteristics, such as trans-granular cracking and the formation of cleavage planes.

- The weight loss for coating of (CpLCE-3) - experiment 3 was observed to be least as compared to all experiments due to its high hardness value of coating i.e. HV(0.3) ≈ 1123 and minimum for 0.6% rare earth oxides (La_2O_3/CeO_2/Er_2O_3-0.2% each) as (CpLCE-2) - experiment 2 due to its low value of hardness. Moreover the weight loss was observed to be high for the substrate due to is very low hardness value. But hardness for all coated samples was high as compared to the substrate.
- The tribological analysis revealed that the rare earth-doped coatings exhibited superior wear resistance. This improvement is particularly significant for applications in harsh environments, where reduced wear and friction can extend the service life of components, thus reducing maintenance costs and downtime.
- This research provides a novel approach to improving the performance of thermal spray coatings by incorporating rare earth elements. The successful application of these coatings on SS410 substrates opens up new possibilities for their use in industries such as aerospace, automotive, and energy, where high-performance materials are essential.

7.2. Future Scope of Work:

In addition to the above experiments, many other available substrates, coating powders and rare earth oxides can be considered with varied proportions. These compositions can be optimized using various optimization tools. Moreover, various other thermal spraying techniques can be considered for coating deposition, and the various properties can be compared for various applications. Apart from the considered characterization, other tests can be conducted to learn more about the coatings for various applications.

7.2.1. New Areas of Focus

The revised research now concentrates on several innovative and critical areas that push the boundaries of current knowledge in coating technologies. These areas include:

- *Impact of Rare Earth Doping on Microstructure:* Exploring how the addition of rare earth elements alters the microstructure of WC-Co-Cr coatings, potentially leading to improved properties.
- *Performance in Harsh Environments:* Assessing how the doped coatings perform under

extreme conditions, such as high temperatures, corrosive environments, and high-stress mechanical loads.

- *Scalability and Industrial Applicability:* Investigating the feasibility of scaling up the coating process for industrial applications, ensuring that the coatings can be economically and efficiently produced for large-scale use.

7.2.2. Research Approach

The research will adopt a structured and multi-faceted approach to address these new focuses areas:

- *Microstructural Analysis:* Advanced characterization techniques, such as Scanning Electron Microscopy (SEM), Transmission Electron Microscopy (TEM), and X-ray Diffraction (XRD), will be utilized to examine the grain size, phase composition, and distribution of elements within the coatings. This analysis will reveal how rare earth elements influence the microstructure, potentially leading to enhanced hardness and toughness.
- *Mechanical and Tribological Testing:* The coatings will undergo rigorous testing, including microhardness tests, scratch adhesion tests, and wear resistance evaluations under various environmental conditions. The performance data will be compared against control samples (un-doped coatings) to quantify the improvements introduced by rare earth doping.
- *Environmental Performance Testing:* The doped coatings will be exposed to simulated high-temperature and corrosive environments to assess their durability and resistance to degradation. This testing will help determine the suitability of these coatings for use in industries such as aerospace and energy, where materials are often exposed to extreme conditions.
- *Scalability Assessment:* Pilot-scale production will be conducted using industrial-grade HP-HVOF thermal spray systems. This will include a detailed analysis of the process parameters to optimize coating quality at larger scales. Additionally, an economic feasibility study will be performed to evaluate the cost-effectiveness of producing these coatings on an industrial scale.

7.2.3. Expected Outcomes

The research is expected to yield the following significant outcomes:

- *Enhanced Understanding of Microstructure:* A comprehensive understanding of how rare earth doping influences the microstructure of WC-Co-Cr coatings, leading to improved mechanical and tribological properties. The findings will provide a basis for further research into other doping elements and their effects on coating performance.
- *Improved Coating Performance:* Demonstrated enhancements in hardness, wear resistance, and adhesion strength, confirming the potential of rare earth-doped coatings to outperform traditional coatings in harsh environments. These improvements could lead to longer-lasting, more durable materials for critical applications.
- *Feasibility of Large-Scale Production:* Validated methodologies for scaling up the production of rare earth-doped coatings, with proven industrial applicability. This outcome will include guidelines for optimizing the HP-HVOF process on an industrial scale, ensuring that the coatings can be produced efficiently and cost-effectively.
- *Industrial Application Potential:* A clear demonstration of the potential for these coatings to be adopted in high-stress industrial applications, such as aerospace components, energy sector equipment, and other environments where superior durability and performance are required.

These outcomes will significantly contribute to the field of materials science, offering new insights into coating technology and laying the groundwork for future innovations in the application of advanced materials.

REFERENCES:

[1]. Gummer, J. H. (2009). Combating Silt Erosion in Hydraulic Turbines-Some of the most attractive hydro sites are plagued by silt. While silt erosion of hydraulic turbines at these sites can be managed, further work is needed to better predict and control this erosion. Hydro review worldwide, 17(1), 28.

[2]. Mann, B. S. (2000). High-energy particle impact wear resistance of hard coatings and their application in hydroturbines. Wear, 237(1), 140-146.

[3]. Padhy, M. K., & Saini, R. P. (2012). Study of silt erosion mechanism in Pelton turbine buckets. Energy, 39(1), 286-293.

[4]. Mann, B. S., & Arya, V. (2001). Abrasive and erosive wear characteristics of plasma nitriding and HVOF coatings: their application in hydro turbines. Wear, 249(5-6), 354-360.

[5]. Goyal, D. K., Singh, H., Kumar, H., & Sahni, V. (2012). Slurry erosion behaviour of HVOF sprayed WC–10Co–4Cr and Al2O3+ 13TiO2 coatings on a turbine steel. Wear, 289, 46-57.

[6]. Thapa, B., Chaudhary, P., Dahlhaug, O. G., & Upadhyay, P. (2007, October). Study of combined effect of sand erosion and cavitation in hydraulic turbines. In International Conference on Small Hydropower-Hydro Sri Lanka (Vol. 22, p. 24).

[7]. Singh, R., Tiwari, S. A., & Mishra, S. K. (2012). Cavitation erosion in hydraulic turbine components and mitigation by coatings: current status and future needs. Journal of materials engineering and performance, 21, 1539-1551.

[8]. Singh, H., Kumar, M., & Singh, R. (2023). Microstructural and mechanical characterization of a cold-sprayed WC-12Co composite coating on stainless steel hydroturbine blades. Journal of Thermal Spray Technology, 32(4), 970-983.

[9]. Khalid Mohammed Ridha, W., Reza Kashyzadeh, K., & Ghorbani, S. (2023). Common failures in hydraulic Kaplan turbine blades and practical solutions. Materials, 16(9), 3303.

[10]. Kumar, M., Yadav, Y. K., & Singh, A. K. (2022). Mechanisms of slurry erosion in coatings of hydro-turbines. Materials Today: Proceedings.

[11]. Yang, Z., Jian, Y., Chen, Z., Qi, H., Huang, Z., Huang, G., & Xing, J. (2022). Microstructure, hardness and slurry erosion-wear behaviors of high-speed laser cladding Stellite 6 coatings prepared by the inside-beam powder feeding method. Journal of Materials Research and Technology, 19, 2596-2610.

[12]. Hong, S., Wu, Y., Wu, J., Zhang, Y., Zheng, Y., Li, J., & Lin, J. (2021). Microstructure and cavitation erosion behavior of HVOF sprayed ceramic-metal composite coatings for application in hydro-turbines. Renewable Energy, 164, 1089-1099.

[13]. Selvam Kevin, P., Tiwari, A., Seman, S., Beer Mohamed, S. A., & Jayaganthan, R. (2020). Erosion-corrosion protection due to Cr3C2-NiCr cermet coating on stainless steel. Coatings, 10(11), 1042.

[14]. Sharma, V., Kaur, M., & Bhandari, S. (2019). Micro and nano ceramic-metal composite coatings by thermal spray process to control slurry erosion in hydroturbine steel: an overview. Engineering Research Express, 1(1), 012001.

[15]. Ludwig, G. A., Malfatti, C. F., Schroeder, R. M., Ferrari, V. Z., & Muller, I. L. (2019). WC10Co4Cr coatings deposited by HVOF on martensitic stainless steel for use in hydraulic turbines: Resistance to corrosion and slurry erosion. Surface and Coatings Technology, 377, 124918.

[16]. Kumar, H., Chittosiya, C., & Shukla, V. N. (2018). HVOF sprayed WC based cermet coating for mitigation of cavitation, erosion & abrasion in hydro turbine blade. Materials Today: Proceedings, 5(2), 6413-6420.

[17]. Nath, G., & Kumar, S. (2018). Slurry erosion behaviour of pack boronized 13-4 martensitic stainless steel for hydro turbine blades. Materials Today: Proceedings, 5(9), 17380-17388.

[18]. Kumar, R. K., Kamaraj, M., & Seetharamu, S. (2017). A pragmatic approach and quantitative assessment of silt erosion characteristics of HVOF and HVAF processed WC-CoCr coatings and 16Cr5Ni steel for hydro turbine applications. Materials & Design, 132, 79-95.

[19]. Taillon, G., Pougoum, F., Lavigne, S., Ton-That, L., Schulz, R., Bousser, E., ... & Klemberg-Sapieha, J. E. (2016). Cavitation erosion mechanisms in stainless steels and in composite metal–ceramic HVOF coatings. Wear, 364, 201-210.

[20]. Singh, H., Goyal, K., & Goyal, D. K. (2014). Slurry erosion behaviour of plasma thermal sprayed (50%) WC-Co-Cr and Ni-Cr-B-Si coatings of different thickness on CA6NM turbine steel material. Manufacturing Science and Technology, 2(4), 81-92.

[21]. Chauhan, A. K., Goel, D. B., & Prakash, S. (2009). Solid particle erosion behaviour of 13Cr–4Ni and 21Cr–4Ni–N steels. Journal of Alloys and Compounds, 467(1-2), 459-464.

[22]. AF, P., & PR, R. (2002). Decomposition of austenite in austenitic stainless steels. ISIJ international, 42(4), 325-327.

[23]. Selokar, A., Goel, D. B., & Prakash, U. (2012). A comparative study of cavitation erosive behaviour of 23/8N nitronic steel and 13/4 martensitic stainless steel. Advanced Materials Research, 585, 554-558.

[24]. Ikegami, Y., & Nemoto, R. (1996). Effect of thermo-mechanical treatment on mechanical properties of high-nitrogen containing Cr-Mn-Ni austenitic stainless steels. Isij International, 36(7), 855-861.

[25]. Santa, J. F., Espitia, L. A., Blanco, J. A., Romo, S. A., & Toro, A. (2009). Slurry and cavitation erosion resistance of thermal spray coatings. Wear, 267(1-4), 160-167.

[26]. Slavin, T. P., & Nerz, J. (1991). Material characteristics and performance of WC-Co wear-resistant coatings. Thermal Spray Research and Applications, 159-165.

[27]. Wood, R. J. K., Mellor, B. G., & Binfield, M. L. (1997). Sand erosion performance of detonation gun applied tungsten carbide/cobalt-chromium coatings. Wear, 211(1), 70-83.

[28]. Hawthorne, H. M., Arsenault, B., Immarigeon, J. P., Legoux, J. G., & Parameswaran, V. R. (1999). Comparison of slurry and dry erosion behaviour of some HVOF thermal sprayed coatings. Wear, 225, 825-834.

[29]. Torkashvand, K., Joshi, S., & Gupta, M. (2022). Advances in thermally sprayed WC-based wear-resistant coatings: Co-free binders, processing routes and tribological behavior. Journal of Thermal Spray Technology, 31(3), 342-377.

[30]. Khare, R., & Prasad, V. (2021). Prediction of cavitation and its mitigation techniques in hydraulic turbines-A review. Ocean Engineering, 221, 108512.

[31]. Stokes, J. (2003). Production of coated and free-standing engineering components using the HVOF (High Velocity Oxy-Fuel) process (Doctoral dissertation, Dublin City University).

[32]. Fauchais, P. L., Heberlein, J. V., & Boulos, M. I. (2014). Thermal spray fundamentals: from powder to part. Springer Science & Business Media.

[33]. Pawlowski, L. (2008). The science and engineering of thermal spray coatings. John Wiley & Sons.

[34]. Herman, H., Sampath, S., & McCune, R. (2000). Thermal spray: current status and future trends. MRS bulletin, 25(7), 17-25.

[35]. Robert Jr, C. T. Praxair Surface Technologies, Inc.,(1994),"Thermal Spray Coating", J. Surface Engineering, 5, 497-509.

[36]. Al Fadhli, H. (2006). Analysis of the effect of bending, fatigue, erosion-corrosion and tensile stresses on HVOF coating of metallic surfaces (Doctoral dissertation, Dublin City University).

[37]. Marantz, D. R. (1974). The basic principles of electric-arc spraying.

[38]. Drzeniek, H., & Steffens, H. D. (1987). Cored tube wires for arc and flame spraying.(retroactive coverage). Thermal Spray: Advances in Coatings Technology, 33-40.

[39]. Souza, V. A. D., & Neville, A. (2007). Aspects of microstructure on the synergy and overall material loss of thermal spray coatings in erosion–corrosion environments. Wear, 263(1-6), 339-346.

[40]. Gao, J. G., Tang, Z. H., Wang, C. L., Guo, M. Q., & Cui, Y. J. (2015). Microstructure, mechanical and oxidation characteristics of detonation gun and HVOF sprayed MCrAlYX coatings. Transactions of Nonferrous Metals Society of China, 25(3), 817-823.

[41]. Al Harbi, N., & Stokes, J. (2015). Optimizing HVOF spray process parameters and post-heat treatment for Micro/Nano WC–12% Co, mixed with Inconel-625 Powders: A Critical Review.

[42]. Stokes, J. (2008). The theory and application of the HVOF thermal spray process.

[43]. Murtaza, Q. (2006). A critical investigation into the spray-drying of hydroxyapatite powder for thermal spray applications (Doctoral dissertation, Dublin City University).

[44]. Lee, K., Park, J., Ye, K., Jeon, C., Kim, S., Song, Y., ... & Lee, D. Y. (2006). Acoustic emission source analysis of vacuum plasma sprayed CoNiCrAlY coatings. JOURNAL-KOREAN PHYSICAL SOCIETY, 48(6), 1691.

[45]. Heimann, R. B. (2008). Plasma-spray coating: principles and applications. John Wiley & Sons.

[46]. Yin, S., Cavaliere, P., Aldwell, B., Jenkins, R., Liao, H., Li, W., & Lupoi, R. (2018). Cold spray additive manufacturing and repair: Fundamentals and applications. Additive manufacturing, 21, 628-650.

[47]. Hasan, S., & Stokes, J. (2011). Design of experiment analysis of the Sulzer Metco DJ high velocity oxy-fuel coating of hydroxyapatite for orthopedic applications. Journal of thermal spray technology, 20, 186-194.

[48]. Shelar, V. G., Davidson Jebaseelan, D., Karthikeyan, C. P., & Stokes, J. (2016). Finite Element Analysis of Particle Impact on Substrates Using HVOF Thermal Spray Coating. Applied Mechanics and Materials, 852, 446-451.

[49]. Vishnoi, M., Murtaza, Q., & Kumar, P. (2023). Characterization of erbium oxide doped HP-HVOF deposited carbide ceramic coating on martensitic steel. Proceedings of the Institution of Mechanical Engineers, Part C: Journal of Mechanical Engineering Science, 237(23), 5743-5754.

[50]. An Introduction to Thermal Spray V4 - Brochure | Environmental XPRT https://www.environmental-expert.com/downloads/an-introduction-to-thermal-spray-v4-brochure-445315 (accessed 2023 -01 -27).

[51]. Calabrese, L., Khaskhoussi, A., Patane, S., & Proverbio, E. (2019). Assessment of super-hydrophobic textured coatings on AA6082 aluminum alloy. Coatings, 9(6), 352.

[52]. Chen, S., Qian, G., & Yang, L. (2019). Precise control of surface texture on carbon film by ion etching through filter: optimization of texture size for improving tribological behavior. Surface and Coatings Technology, 362, 105-112.

[53]. Voyer, J., Zehetner, J., Klien, S., Ausserer, F., & Velkavrh, I. (2019). Production and tribological characterization of tailored laser-induced surface 3D microtextures. Lubricants, 7(8), 67.

[54]. Etsion, I. (2005). State of the art in laser surface texturing. J. Trib., 127(1), 248-253.

[55]. Arslan, A., Masjuki, H. H., Kalam, M. A., Varman, M., Mufti, R. A., Mosarof, M. H., ... & Quazi, M. M. (2016). Surface texture manufacturing techniques and tribological effect of surface texturing on cutting tool performance: a review. Critical Reviews in Solid State and Materials Sciences, 41(6), 447-481.

[56]. Yuan, S., Lin, N., Zou, J., Liu, Z., Wang, Z., Tian, L., ... & Wu, Y. (2019). Effect of laser surface texturing (LST) on tribological behavior of double glow plasma surface zirconizing coating on Ti6Al4V alloy. Surface and Coatings Technology, 368, 97-109.

[57]. Shimizu, T., Kan, H., Messaoudi, H., Vollertsen, F., & Yang, M. (2019). Impact of geometrical parameters of micro-textured DLC on tribological properties under dry sliding friction. Manufacturing Review, 6, 18.

[58]. Ghosh, G., Sidpara, A., & Bandyopadhyay, P. P. (2018, June). Characterization of nanofinished WC-Co coating using advanced 3D surface texture parameters. In International Manufacturing Science and Engineering Conference (Vol. 51388, p. V004T03A001). American Society of Mechanical Engineers.

[59]. Baino, F., Montealegre, M. A., Minguella-Canela, J., & Vitale-Brovarone, C. (2019). Laser surface texturing of alumina/zirconia composite ceramics for potential use in hip joint prosthesis. Coatings, 9(6), 369.

[60]. Zhou, W., Tang, J., & Shao, W. (2020). Modelling of surface texture and parameters matching considering the interaction of multiple rotation cycles in ultrasonic assisted grinding. International Journal of Mechanical Sciences, 166, 105246.

[61]. Lauwers, B., Bleicher, F., Ten Haaf, P., Vanparys, M., Bernreiter, J., Jacobs, T., & Loenders, J. (2010, October). Investigation of the process-material interaction in ultrasonic assisted grinding of ZrO2 based ceramic materials. In Proceedings of the 4th CIRP International Conference on High Performance Cutting (pp. 1-6).

[62]. Cakir, F. H., Gurgen, S., Sofuoglu, M. A., Celik, O. N., & Kushan, M. C. (2015). Finite element modeling of ultrasonic assisted turning of Ti6Al4V alloy. Procedia-Social and Behavioral Sciences, 195, 2839-2848.

[63]. Tawakoli, T., & Azarhoushang, B. (2008). Influence of ultrasonic vibrations on dry grinding of soft steel. International Journal of Machine Tools and Manufacture, 48(14), 1585-1591.

[64]. Ammosova, L., Mönkkönen, K., & Suvanto, M. (2020). Precise fabrication of microtextured stainless steel surfaces using metal injection moulding. Precision Engineering, 62, 89-94.

[65]. Jain, A., & Bajpai, V. (2019). Mechanical micro-texturing and characterization on Ti6Al4V for the improvement of surface properties. Surface and Coatings Technology, 380, 125087.

[66]. Pimenov, S. M., Jaeggi, B., Neuenschwander, B., Zavedeev, E. V., Zilova, O. S., & Shupegin, M. L. (2019). Femtosecond laser surface texturing of diamond-like nanocomposite films to improve tribological properties in lubricated sliding. Diamond and Related Materials, 93, 42-49.

[67]. López, A. J., Ramil, A., Pozo-Antonio, J. S., Rivas, T., & Pereira, D. (2019). Ultrafast laser surface texturing: a sustainable tool to modify wettability properties of marble. Sustainability, 11(15), 4079.

[68]. Zhang, H., & Marshall, C. L. (2019). Atomic layer deposition: catalytic preparation and modification technique for the next generation. Chinese Journal of Catalysis, 40(9), 1311-1323.

[69]. Li, J., Zhang, X., Wang, J., Li, H., Huang, J., & Xiong, D. (2019). Frictional properties of silver over-coated on surface textured tantalum interlayer at elevated temperatures. Surface and coatings technology, 365, 189-199.

[70]. Zhong, J., Qin, W., Wang, X., Medvedovski, E., Szpunar, J. A., & Guan, K. (2019). Mechanism of texture formation in iron boride coatings on low-carbon steel. Metallurgical and Materials Transactions A, 50, 58-62.

[71]. Barthwal, S., Lee, B., & Lim, S. H. (2019). Fabrication of robust and durable slippery anti-icing coating on textured superhydrophobic aluminum surfaces with infused silicone oil. Applied Surface Science, 496, 143677.

[72]. Niu, Y., Jiao, F., Zhao, B., & Gao, G. (2019). Investigation of cutting force in longitudinal-torsional ultrasonic-assisted milling of Ti-6Al-4V. Materials, 12(12), 1955.

[73]. Kurniawan, R., Kiswanto, G., & Ko, T. J. (2016). Micro-dimple pattern process and orthogonal cutting force analysis of elliptical vibration texturing. International Journal of Machine Tools and Manufacture, 106, 127-140.

[74]. Palumbo, F., Lo Porto, C., & Favia, P. (2019). Plasma nano-texturing of polymers for wettability control: Why, what and how. Coatings, 9(10), 640.

[75]. Kumar, M., Ranjan, V., & Tyagi, R. (2020). Effect of shape, density, and an array of dimples on the friction and wear performance of laser textured bearing steel under dry sliding. Journal of Materials Engineering and Performance, 29, 2827-2838.

[76]. Nikam, M. D., Shimpi, D., Bhole, K., & Mastud, S. A. (2019). Design and development of surface texture for tribological application. Key Engineering Materials, 803, 55-59.

[77]. Kasem, H., Stav, O., Grützmacher, P., & Gachot, C. (2018). Effect of low depth surface texturing on friction reduction in lubricated sliding contact. Lubricants, 6(3), 62.

[78]. Wang, S., Yan, F., & Chen, A. (2018). Tribological effects of laser surface texturing and residual stress. Industrial Lubrication and Tribology, 70(1), 126-132.

[79]. Liu, X. B., Kang, J. J., Yue, W., Fu, Z. Q., Zhu, L. N., She, D. S., ... & Wang, C. B. (2019). Performance evaluation of HVOF sprayed WC-10Co4Cr coatings under slurry erosion. Surface Engineering, 35(9), 816-825.

[80]. Krelling, A. P., Souza, M. M. D., Costa, C. E. D., & Milan, J. C. G. (2018). HVOF-sprayed coating over AISI 4140 steel for hard chromium replacement. Materials research, 21, e20180138.

[81]. Katranidis, V., Gu, S., Cox, D. C., Whiting, M. J., & Kamnis, S. (2018). FIB-SEM sectioning study of decarburization products in the microstructure of HVOF-sprayed WC-Co coatings. Journal of Thermal Spray Technology, 27, 898-908.

[82]. Mohanty, D., Kar, S., Paul, S., & Bandyopadhyay, P. P. (2018). Carbon nanotube reinforced HVOF sprayed WC-Co coating. Materials & Design, 156, 340-350.

[83]. Marques, A. S., de Costa, L. D. L., dos Santos, G. R., & da Silva Rocha, A. (2019). Wear study of hot forging punches coated with WC-CoCr and Cr3C2-NiCr through high-velocity oxygen fuel (HVOF) process. The International Journal of Advanced Manufacturing Technology, 100, 3-11.

[84]. Chen, C., Guo, Z., Li, S., Xiao, Y., Chai, B., & Liu, J. (2019). Microstructure and properties of WC-17Co cermets prepared using different processing routes. Ceramics International, 45(7), 9203-9210.

[85]. Singh, J., Kumar, S., & Mohapatra, S. K. (2019). Erosion wear performance of Ni-Cr-O and NiCrBSiFe-WC (Co) composite coatings deposited by HVOF technique. Industrial Lubrication and Tribology, 71(4), 610-619.

[86]. Behera, N., Medabalimi, S. R., & Ramesh, M. R. (2023). Elevated temperatures erosion wear behavior of HVOF sprayed WC-Co-Cr/Mo coatings on Ti6Al4V substrate. Surface and Coatings Technology, 470, 129809.

[87]. Bai, M., Kazi, H., Zhang, X., Liu, J., & Hussain, T. (2018). Robust hydrophobic surfaces from suspension HVOF thermal sprayed rare-earth oxide ceramics coatings. Scientific reports, 8(1), 6973.

[88]. Hang, Z. Q., Xi, N. Y., Liu, Y., Liu, Y., & Chen, H. (2018). High-temperature oxidation behavior of HVOF-sprayed rare earth-modified WC–12Co coating. Rare Metals, 1-8.

[89]. Mahesh, R. A., Jayaganthan, R., & Prakash, S. (2008). Characterisation of HVOF sprayed NiCrAlY–0˙ 4 wt-% CeO2 coatings on superalloys. Surface engineering, 24(5), 366-373.

[90]. Mahesh, R. A., Rao, G., Jayaganthan, R., & Prakash, S. (2010). Hot corrosion behaviour of HVOF sprayed NiCrAlY–0· 4 wt-% CeO2 coatings on superalloys in

aggressive environment at 900° C. Corrosion engineering, science and technology, 45(2), 142-149.

[91]. Kaushal, G., Kaur, N., Singh, H., & Prakash, S. (2013). Effect of zirconium addition in HVOF sprayed Ni–20Cr coating. Surface engineering, 29(1), 46-54.

[92]. Liu, Y., Gou, G., Wang, X., Jia, Q., Chen, H., & Tu, M. (2014). Effects of rare earth elements on the microstructure and mechanical properties of HVOF-sprayed WC-Co coatings. Journal of thermal spray technology, 23, 1225-1231.

[93]. Liu, Y., Hang, Z., Chen, H., Ceng, S., Gou, G., Wang, X., ... & Wu, X. (2016). Erosion–corrosion property of CeO 2-modified HVOF WC-Co coating. Journal of Thermal Spray Technology, 25, 815-822.

[94]. Liu, Y., Hang, Z., Yang, G., Fu, H., Xi, N., & Chen, H. (2018). Influence of rare earth on the high-temperature sliding wear behavior of WC-12Co coating prepared by HVOF spraying. Journal of Thermal Spray Technology, 27, 1143-1152.

[95]. Chen, S. F., Liu, S. Y., Wang, Y., Sun, X. G., Zou, Z. W., Li, X. W., & Wang, C. H. (2014). Microstructure and properties of HVOF-sprayed NiCrAlY coatings modified by rare earth. Journal of thermal spray technology, 23, 809-817.

[96]. Sharma, S. (2012). Erosive wear study of rare earth-modified HVOF-sprayed coatings using design of experiment. Journal of thermal spray technology, 21, 49-62.

[97]. Yin, B., Liu, G., Zhou, H., Chen, J., & Yan, F. (2010). Sliding wear behavior of HVOF-sprayed Cr 3 C 2–NiCr/CeO 2 composite coatings at elevated temperature up to 800 C. Tribology letters, 37, 463-475.

[98]. Vishnoi, M., Murtaza, Q., & Kumar, P. (2023). Mechanical and Surface Wettability Analysis of Rare Earth Modified Composite Coating Developed Using Metal Spraying. Arabian Journal for Science and Engineering, 1-12.

[99]. Vishnoi, M., Murtaza, Q., & Kumar, P. (2023). Mechanical and surface characterization of Er2O3/La2O3/CeO2 doped carbide coating developed using high velocity oxy fuel (HVOF). Physica Scripta, 98(11), 115618.

[100]. Dorfman, M. R. (2002). Thermal spray basics. Advanced Materials & Processes, 160(7), 47.

[101]. Mehta, J., Mittal, V. K., & Gupta, P. (2017). Role of thermal spray coatings on wear, erosion and corrosion behavior: a review. Journal of Applied Science and Engineering, 20(4), 445-452.

[102]. Espallargas, N. (2015). Introduction to thermal spray coatings. In Future Development of Thermal Spray Coatings (pp. 1-13). Woodhead Publishing.

[103]. Amin, S., & Panchal, H. (2016). A review on thermal spray coating processes. transfer, 2(4), 556-563.

[104]. Vardelle, A., Moreau, C., Akedo, J., Ashrafizadeh, H., Berndt, C. C., Berghaus, J. O., ... & Vuoristo, P. (2016). The 2016 thermal spray roadmap. Journal of thermal spray technology, 25, 1376-1440.

[105]. Ghadami, F., & Aghdam, A. S. R. (2019). Improvement of high velocity oxy-fuel spray coatings by thermal post-treatments: A critical review. Thin Solid Films, 678, 42-52.

[106]. Odhiambo, J. G., Li, W., Zhao, Y., & Li, C. (2019). Porosity and its significance in plasma-sprayed coatings. Coatings, 9(7), 460.

[107]. Anusha, K., Routara, B. C., & Guha, S. (2023). A Review on High-Velocity Oxy-Fuel (HVOF) Coating Technique. Journal of The Institution of Engineers (India): Series D, 104(2), 831-848.

[108]. Ning, W., Zhai, H., Xiao, R., He, D., Liang, G., Wu, Y., ... & Li, X. (2020). The corrosion resistance mechanism of Fe-based amorphous coatings synthesised by detonation gun spraying. Journal of Materials Engineering and Performance, 29, 3921-3929.

[109]. Li, W., Cao, C., & Yin, S. (2020). Solid-state cold spraying of Ti and its alloys: A literature review. Progress in Materials Science, 110, 100633.

[110]. Li, M., & Christofides, P. D. (2009). Modeling and control of high-velocity oxygen-fuel (HVOF) thermal spray: a tutorial review. Journal of thermal spray technology, 18, 753-768.

[111]. Sidhu, T. S., Prakash, S., & Agrawal, R. D. (2005). State of the art of HVOF coating investigations—A review. Marine Technology Society Journal, 39(2), 53-64.

[112]. Singh, V. P., Sil, A., & Jayaganthan, R. (2012). Tribological behaviour of nanostructured Al2O3 coatings. Surface engineering, 28(4), 277-284.

[113]. Li, C. J., Yang, G. J., & Li, C. X. (2013). Development of particle interface bonding in thermal spray coatings: a review. Journal of thermal spray technology, 22, 192-206.

[114]. Tucker, R. C. (2013). ASM handbook, volume 5A: thermal spray technology. ASM International, 57.

[115]. Hardwicke, C. U., & Lau, Y. C. (2013). Advances in thermal spray coatings for gas turbines and energy generation: a review. Journal of Thermal Spray Technology, 22(5), 564-576.

[116]. Talib, R. J., Saad, S., Toff, M. R. M., & Hashim, H. (2003). Thermal spray coating technology: A review. Solid State Sci Technol, 11(1), 109-117.

[117]. Ang, A. S. M., Sanpo, N., Sesso, M. L., Kim, S. Y., & Berndt, C. C. (2013). Thermal spray maps: Material genomics of processing technologies. Journal of thermal spray technology, 22, 1170-1183.

[118]. Ang, A. S. M., & Berndt, C. C. (2014). A review of testing methods for thermal spray coatings. International Materials Reviews, 59(4), 179-223.

[119]. Lanzutti, A., Lekka, M., Marin, E., & Fedrizzi, L. (2013). Tribological Behavior of Thermal Spray Coatings, Deposited by HVOF and APS techniques, and composite electrodeposits Ni/SiC at both room temperature and 300 C. Tribology in Industry, 35(2), 113.

[120]. Achanta, S., Drees, D., & Celis, J. P. (2011). Nanocoatings for tribological applications. In Nanocoatings and Ultra-thin Films (pp. 355-396). Woodhead Publishing.

[121]. Rico, A., Poza, P., & Rodríguez, J. (2013). High temperature tribological behavior of nanostructured and conventional plasma sprayed alumina-titania coatings. Vacuum, 88, 149-154.

[122]. Bolleddu, V., Racherla, V., & Bandyopadhyay, P. P. (2014). Microstructural and tribological characterization of air plasma sprayed nanostructured alumina–titania

coatings deposited with nitrogen and argon as primary plasma gases. Materials & Design, 59, 252-263.

[123]. Torrell, M., Dosta, S., Miguel, J. R., & Guilemany, J. M. (2010). Optimisation of HVOF thermal spray coatings for their implementation as MSWI superheater protectors. Corrosion engineering, science and technology, 45(1), 84-93.

[124]. Swain, B., Mallick, P., Bhuyan, S. K., Mohapatra, S. S., Mishra, S. C., & Behera, A. (2020). Mechanical properties of NiTi plasma spray coating. Journal of Thermal Spray Technology, 29(4), 741-755.

[125]. Kumar, R., & Kumar, S. (2018). Comparative parabolic rate constant and coating properties of nickel, cobalt, iron and metal oxide based coating: a review. I-manager's Journal on Material Science, 6(1), 45.

[126]. Kumar, R., Kumar, R., & Kumar, S. (2018). Erosion corrosion study of HVOF sprayed thermal sprayed coating on boiler tubes: a review. IJSMS, 1(3), 1-6.

[127]. Singh, L., Chawla, V., & Grewal, J. S. (2012). A review on detonation gun sprayed coatings. Journal of Minerals and Materials Characterization and Engineering, 11(03), 243.

[128]. Uusitalo, M. A., Vuoristo, P. M. J., & Mäntylä, T. A. (2002). High temperature corrosion of coatings and boiler steels in reducing chlorine-containing atmosphere. Surface and Coatings Technology, 161(2-3), 275-285.

[129]. Ahmaniemi, S., Vuoristo, P., & Mäntylä, T. (2004). Mechanical and elastic properties of modified thick thermal barrier coatings. Materials Science and Engineering: A, 366(1), 175-182.

[130]. Stokes, J., & Looney, L. (2001). HVOF system definition to maximise the thickness of formed components. Surface and Coatings Technology, 148(1), 18-24.

[131]. Tejero-Martin, D., Rezvani Rad, M., McDonald, A., & Hussain, T. (2019). Beyond traditional coatings: A review on thermal-sprayed functional and smart coatings. Journal of thermal spray technology, 28, 598-644.

[132]. Galedari, S. A., Mahdavi, A., Azarmi, F., Huang, Y., & McDonald, A. (2019). A comprehensive review of corrosion resistance of thermally-sprayed and thermally-

diffused protective coatings on steel structures. Journal of Thermal Spray Technology, 28, 645-677.

[133]. Singh, J. (2021). Application of thermal spray coatings for protection against erosion, abrasion, and corrosion in hydropower plants and offshore industry. In Thermal Spray Coatings (pp. 243-283). CRC Press.

[134]. Uczak de Goes, W., Somhorst, J., Markocsan, N., Gupta, M., & Illkova, K. (2019). Suspension plasma-sprayed thermal barrier coatings for light-duty diesel engines. Journal of Thermal Spray Technology, 28, 1674-1687.

[135]. Patel, P., Alidokht, S. A., Sharifi, N., Roy, A., Harrington, K., Stoyanov, P., ... & Moreau, C. (2022). Microstructural and tribological behavior of thermal spray CrMnFeCoNi high entropy alloy coatings. Journal of Thermal Spray Technology, 31(4), 1285-1301.

[136]. Swain, B., Mallick, P., Gupta, R. K., Mohapatra, S. S., Yasin, G., Nguyen, T. A., & Behera, A. (2021). Mechanical and tribological properties evaluation of plasma-sprayed shape memory alloy coating. Journal of Alloys and Compounds, 863, 158599.

[137]. Darweesh, S. Y., Ali, A. M., Khodair, Z. T., & Majeed, Z. N. (2019). The effect of some physical and mechanical properties of cermet coating on petroleum pipes prepared by thermal spray method. Journal of Failure Analysis and Prevention, 19, 1726-1738.

[138]. Pradeep, D. G., Venkatesh, C. V., & Nithin, H. S. (2022). Review on tribological and mechanical behavior in HVOF thermal-sprayed composite coatings. Journal of Bio-and Tribo-Corrosion, 8(1), 30.

[139]. Li, S., Yu, C., Deng, C., Liu, J., Tan, X., & Zeng, W. (2022). Optimized mechanical and tribological properties of thermally sprayed ceramic coatings by constructing crystalline–amorphous heterojunctions. Applied Surface Science, 604, 154552.

[140]. Schilder, B., Garling, A., Reimer, F., Hamann, M., Joos, R., Hüger, J., ... & Lampke, T. (2020). CFD enhanced thermal spray process for coating of cylinder bores of car engines. Journal of Thermal Spray Technology, 29, 546-559.

[141]. Gupta, N., Singh, S. K., & Pandey, S. M. (2021). Tribological characterisation of thermal sprayed CrC alloyed coating–A review. Advances in Materials and Processing Technologies, 7(4), 660-683.

[142]. Yang, C., Liu, J., Ren, Q., Liu, Y., Zhou, P., & Li, H. (2021). Development of novel thermal sprayed hydroxyapatite-rare earth (HA-Re) coatings for potential antimicrobial applications in orthopedics. Journal of Thermal Spray Technology, 30, 886-897.

[143]. Sivarajan, S., Joshi, A., Palani, K. C., Padmanabhan, R., & Stokes, J. T. (2022). Corrosion and wear protection of AISI 4140 carbon steel using a laser-modified high-velocity oxygen fuel thermal sprayed coatings. Journal of Electrochemical Science and Engineering, 12(5), 865-876.

[144]. Jagadeeshanayaka, N., Awasthi, S., Jambagi, S. C., & Srivastava, C. (2022). Bioactive surface modifications through thermally sprayed hydroxyapatite composite coatings: a review of selective reinforcements. Biomaterials Science, 10(10), 2484-2523.

[145]. Wang, Y., & Northwood, D. O. (2007). An investigation of the electrochemical properties of PVD TiN-coated SS410 in simulated PEM fuel cell environments. International Journal of Hydrogen Energy, 32(7), 895-902.

[146]. Yu, Y., Shironita, S., Souma, K., & Umeda, M. (2018). Effect of chromium content on the corrosion resistance of ferritic stainless steels in sulfuric acid solution. Heliyon, 4(11).

[147]. Kiragi, V. R., Patnaik, A., & Singh, T. (2019). Impact of high-velocity oxy-fuel sprayed TiAlN surface coating on mechanical and slurry erosion performance of aluminium alloys. Materialwissenschaft und Werkstofftechnik, 50(10), 1250-1261.

[148]. Kiragi, V. R., Patnaik, A., Singh, T., & Fekete, G. (2019). Parametric optimization of erosive wear response of TiAlN-coated aluminium alloy using Taguchi method. Journal of Materials Engineering and Performance, 28, 838-851.

[149]. Babu, A., Perumal, G., Arora, H. S., & Grewal, H. S. (2021). Enhanced slurry and cavitation erosion resistance of deep cryogenically treated thermal spray coatings for hydroturbine applications. Renewable Energy, 180, 1044-1055.

[150]. Sharma, S. P., Dwivedi, D. K., & Jain, P. K. (2008). Effect of CeO2 addition on the microstructure, hardness, and abrasive wear behaviour of flame-sprayed Ni-based coatings. Proceedings of the Institution of Mechanical Engineers, Part J: Journal of Engineering Tribology, 222(7), 925-933.

[151]. Sharma, S. P., Dwivedi, D. K., & Jain, P. K. (2009). Effect of La2O3 addition on the microstructure, hardness and abrasive wear behavior of flame sprayed Ni based coatings. Wear, 267(5-8), 853-859.

[152]. Koutsomichalis, A., Vardavoulias, M., & Vaxevanidis, N. (2017, February). HVOF sprayed WC-CoCr coatings on aluminum: tensile and tribological properties. In IOP conference series: materials science and engineering (Vol. 174, No. 1, p. 012062). IOP Publishing.

[153]. Al-Mutairi, S., Hashmi, M. S. J., Yilbas, B. S., & Stokes, J. (2015). Microstructural characterization of HVOF/plasma thermal spray of micro/nano WC–12% Co powders. Surface and Coatings Technology, 264, 175-186.

[154]. ASTM E2109-01. (2014). Standard Test Methods for Determining Area Percentage Porosity in Thermal Sprayed Coatings.

[155]. Vishnoi, M., Kumar, P., & Murtaza, Q. (2021). Surface texturing techniques to enhance tribological performance: A review. Surfaces and Interfaces, 27, 101463.

[156]. Liu, W., Luo, Y., Sun, L., Wu, R., Jiang, H., & Liu, Y. (2013). Fabrication of the superhydrophobic surface on aluminum alloy by anodizing and polymeric coating. Applied Surface Science, 264, 872-878.

[157]. Li, X., Wu, P., Qiu, H., Chen, S., & Song, B. (2012). Crystallization behavior and mechanical properties of erbium oxide coatings fabricated by pulsed magnetron sputtering. Thin Solid Films, 520(6), 2316-2320.

[158]. Wang, K. L., Zhang, Q. B., Sun, M. L., Wei, X. G., & Zhu, Y. M. (2001). Rare earth elements modification of laser-clad nickel-based alloy coatings. Applied surface science, 174(3-4), 191-200.

[159]. Jeyaprakash, N., Yang, C. H., Ramkumar, K. R., & Sui, G. Z. (2020). Comparison of microstructure, mechanical and wear behaviour of laser cladded stainless steel

410 substrate using stainless steel 420 and Colmonoy 5 particles. Journal of Iron and Steel Research International, 27, 1446-1455.

[160]. Zhang, Y., Yu, G., He, X., Ning, W., & Zheng, C. (2012). Numerical and experimental investigation of multilayer SS410 thin wall built by laser direct metal deposition. Journal of Materials Processing Technology, 212(1), 106-112.

[161]. Wenzel, R. N. (1936). Resistance of solid surfaces to wetting by water. Industrial & engineering chemistry, 28(8), 988-994.

[162]. Cassie, A. B. D., & Baxter, S. (1944). Wettability of porous surfaces. Transactions of the Faraday society, 40, 546-551.

[163]. De Foggi, C. C., Machado, A. L., Zamperini, C. A., Fernandes, D., Wady, A. F., & Vergani, C. E. (2016). Effect of surface roughness on the hydrophobicity of a denture-base acrylic resin and C andida albicans colonization. Journal of Investigative and Clinical Dentistry, 7(2), 141-148.

[164]. Kittu, A. T., Bulut, R., & Puckette, J. (2014). Effects of surface roughness on contact angle measurements on a limestone aggregate. In Recent developments in evaluation of pavements and paving materials (pp. 1-8).

[165]. Barthlott, W., & Neinhuis, C. (1997). Purity of the sacred lotus, or escape from contamination in biological surfaces. Planta, 202, 1-8.

[166]. Zhang, Y. (2007). The effect of surface roughness parameters on contact and wettability of solid surfaces. Iowa State University.

[167]. Vishnoi, M., Murtaza, Q., & Kumar, P. (2021). Effect of rare earth elements on coatings developed by thermal spraying processes (TSP)–a brief review. Materials Today: Proceedings, 44, 4053-4058.

[168]. Clark, H. M., & Hartwich, R. B. (2001). A re-examination of the ‘particle size effect’in slurry erosion. Wear, 248(1-2), 147-161.

[169]. Hong, S., Wu, Y. P., Gao, W. W., Wang, B., Guo, W. M., & Lin, J. R. (2014). Microstructural characterisation and microhardness distribution of HVOF sprayed WC–10Co–4Cr coating. Surface Engineering, 30(1), 53-58.

[170]. Matikainen, V., Niemi, K., Koivuluoto, H., & Vuoristo, P. (2014). Abrasion, erosion and cavitation erosion wear properties of thermally sprayed alumina based coatings. Coatings, 4(1), 18-36.

[171]. Zhang, Z., Lu, X., Han, B., & Luo, J. (2007). Rare earth effect on the microstructure and wear resistance of Ni-based coatings. Materials Science and Engineering: A, 454, 194-202.

RESEARCH PUBLICATIONS:

List of Papers Published in SCI/SCIE Indexed Journals:

[1]. Vishnoi, M., Kumar, P., & Murtaza, Q. (2021). Surface texturing techniques to enhance tribological performance: A review. Surfaces and Interfaces, 27, 101463.

[2]. Vishnoi, M., Murtaza, Q., & Kumar, P. (2023). Mechanical and Erosion Characterization of Untreated and Solution-Treated Nitrogen-Alloyed (23-8N) Austenitic Stainless Steel. Journal of Materials Engineering and Performance, 1-11.

[3]. Vishnoi, M., Murtaza, Q., & Kumar, P. (2023). Characterization of erbium oxide doped HP-HVOF deposited carbide ceramic coating on martensitic steel. Proceedings of the Institution of Mechanical Engineers, Part C: Journal of Mechanical Engineering Science, 09544062231164299.

[4]. Vishnoi, M., Murtaza, Q., & Kumar, P. (2023). Mechanical and Surface Wettability Analysis of Rare Earth Modified Composite Coating Developed Using Metal Spraying. Arabian Journal for Science and Engineering, 1-12.

[5]. Vishnoi, M., Murtaza, Q., & Kumar, P. (2023). Mechanical and surface characterization of $Er_2O_3/La_2O_3/CeO_2$ doped carbide coating developed using high velocity oxy fuel (HVOF). Physica Scripta, 98(11), 115618.

[6]. Vishnoi, M., Singh, V., Bansal, A., Murtaza, Q., & Kumar, P. (2024). Effect of laser ablation over cavitation, slurry erosion, and surface properties of 86WC-10Co-4Cr based ceramic coating developed using HP-HVOLF. Surface and Coatings Technology, 131230.

[7]. Vishnoi, M., Murtaza, Q., Kumar, P., Bansal, A., & Singh, V. (2024). Rare earth-doped ceramic coatings: Analysis of microstructure, mechanical properties, and slurry Erosion resistance using high pressure-high velocity oxy-liquid fuel deposition. International Journal of Refractory Metals and Hard Materials, 125, 106873.

[8]. Vishnoi, M., Murtaza, Q., & Kumar, P. (2024). Assessment of mechanical and slurry erosive behavior on laser textured stainless steel (SS410). Journal of Materials Engineering and Performance (Accepted).

Research Work Presented at Conferences:

[1]. Vishnoi, M., Kumar, P., & Murtaza, Q. (2020). A review on coating for hydro-turbine application by HVOF process. Advances in Materials Engineering and Manufacturing Processes: Select Proceedings of ICFTMM 2019, 79-103.

[2]. Vishnoi, M., Murtaza, Q., & Kumar, P. (2021). Effect of rare earth elements on coatings developed by thermal spraying processes (TSP)–a brief review. Materials Today: Proceedings, 44, 4053-4058.

Proof of Papers Published SCI/SCIE Indexed Journals

Surfaces and Interfaces 27 (2021) 101463

Contents lists available at ScienceDirect

Surfaces and Interfaces

journal homepage: www.sciencedirect.com/journal/surfaces-and-interfaces

Surface texturing techniques to enhance tribological performance: A review

Mohit Vishnoi *, Paras Kumar, Qasim Murtaza

Department of Mechanical Engineering, Delhi Technological University, Delhi 110042, India

ARTICLE INFO

Keywords:
Surface texturing
Friction
Wear
Corrosion resistance
Hydrophobicity

ABSTRACT

Texturing of the surface is a technique to form the surfaces of the desired pattern. It is extensively used to alter the mechanical and tribological properties, such as increased fatigue strength, corrosion, wear resistance, anti-biofouling hydrophobicity and load-carrying capacity. To get these benefits, many researchers have studied the importance of textured parameters on metals and non-metals and revealed that un-optimized parameters might deteriorate the properties of the materials. These texture parameters may be dimple shape, depth, diameter, and density. Even though laser surface texturing widely used method, this review article articulates detailed information about surface texturing methods available to fabricate, surface texture characterization, merits, demerits, and applications of textured surfaces on metals and non-metals to enhance tribological performance.

1. Introduction

Attributing to the rise in the need for materials in varied applications, recent decades witnessed a rise in the development of surface texturing techniques to augment material performance and characteristics. Surface texturing has become a vital area in material science pertaining to its ability to control exterior properties in specific applications, e.g., in self-cleaning of surfaces medicine, anti-biofouling [1]. Various researches articulated that enhancement in tribological performance was observed by carefully examining the effect of texturing on materials under different tribological environments such as adhesive wear, cavitation wear, and wear with lubrication. Encapsulating this need to enhance tribological characteristics such as wear and friction, extensive research has been conducted on material texturing techniques. To augment the mechanical properties of segments, surface texturing is readily employed. It was observed that surface texturing could not only improve tribological properties but, in addition, can improve the trapping of light in solar cells [2], improve biological implants [3,4] and help in obtaining super-hydrophobic coating [5–7]. The wettability of materials can be significantly improved using laser surface texturing [8]. Surface texturing helps improve lubrication coatings, which can give super-hydrophobic coatings [5].

Surface texturing entails surface alteration by Forming, micro grooving, micro dimples and microchannels. This is achieved by laser, micromachining, in addition to other related methods on the substrate surface. Surface texturing can be fabricated during the manufacturing of the material. This includes the fabrication of surface texturing using metal injection molding [1]. Various forms of surface texturing structures such as micro-dimple, micro-grooves [5], nano-dots [9], micro-pits, micro-pillars [1], and inverted pyramids [2] have been fabricated and analyzed. Researchers carried out researches on different sizes and geometries of textured surfaces for tribological applications. In addition, the effects of surface texturing parameters like the geometries [10], spacing [11], dimensions [12], shapes [13–15], width [16], distance [17], area fractions [18], and tuning of the depth [19] of the microstructures on the tribological properties have been studied [20]. Yet another aspect that expedited the study of surface texturing was its effect on friction wear and friction characteristics. The relative motion between the surfaces is the underlining phenomenon for friction varies with application. Reducing friction has been a primary concern for the enhanced longevity of mechanical components. However, high friction is required in some cases, such as in brakes and clutches of tyre road contact. Providing lubrication on moving parts is a common way of reducing friction [21,22].

The friction is the primary key which comes under tribology. Despite the presence of many techniques to alter friction, surface texturing has surfaced as a promising technique. Various techniques to fabricate surface texturing includes laser surface texturing, ball burnishing, chemical etching, two-photon lithography, atomic layer deposition, ultrasonic-assisted grinding, EDM and micro-milling, to name a few. Different texturing strategies are utilized in conjugation with one another, such as ion beam texturing, carving methods and laser texturing. One of the

* Corresponding author.
E-mail addresses: vishnoi.mohit06@gmail.com (M. Vishnoi), paraskumar@dtu.ac.in (P. Kumar), qasimmurtaza@dce.ac.in (Q. Murtaza).

https://doi.org/10.1016/j.surfin.2021.101463
Received 13 July 2021; Received in revised form 5 September 2021; Accepted 7 September 2021
Available online 16 September 2021

JMEPEG
https://doi.org/10.1007/s11665-023-07925-2

1059-9495/$19.00

TECHNICAL ARTICLE

Mechanical and Erosion Characterization of Untreated and Solution-Treated Nitrogen-Alloyed (23-8N) Austenitic Stainless Steel

Mohit Vishnoi, Qasim Murtaza, and Paras Kumar

Submitted: 31 May 2022 / Revised: 15 January 2023 / Accepted: 20 January 2023

The comparative study of as-rolled untreated and solution-treated 23-8N nitronic steel was studied. The results obtained from mechanical characterization revealed that the solution-treated nitronic steel specimens have shown higher toughness and ductility with marginal reduction in hardness as compared to as-rolled untreated nitronic steel specimens. The erosion behavior with surface characterizations of nitronic steel specimen has been evaluated by air jet and slurry jet erosion test rig at four different impingement angles (15°, 45°, 60°, and 90°) and (30°, 45°, 60°, and 90°), respectively. It is observed that the air jet and slurry jet erosion rate for untreated and solution-treated specimens, decreases as the impingement angle increases. The potentiodynamic polarization test in 3.5 wt.% NaCl aqueous solution has been conducted to evaluate the corrosion rate of specimens. The as-rolled solution-treated steel exhibits better corrosion resistance as compared to untreated steel. The surface characterization of eroded specimens was analyzed using scanning electron microscope and possible erosion mechanisms have been studied on untreated and solution-treated specimens.

Keywords air jet erosion, nitronic steel, potentiodynamic polarization, slurry jet erosion

1. Introduction

In the ever-increasing search for materials with high corrosion resistance with substantial tensile strength coupled with hardness, new materials are extensively being tested and experimented with. Austenitic steel is known for its good ductility and superior immunity to a wide range of varying temperatures, from cryogenic temperatures to high temperatures along with its non-magnetic nature (Ref 1). Above all, austenitic stainless steel is extensively utilized in applications subjected to high corrosion primarily, hydro-turbine blades where it is subjected to slurry erosion, and internal combustion engine, valves by virtue of their high corrosion resistance (Ref 2, 3). Though austenitic steel exhibits high corrosion resistance, its mechanical properties such as impact and tensile strength can be increased for better efficiency in hydro and internal combustion engines.

The nitrogen is added to improve the mechanical properties of austenitic steel. The incorporation of nitrogen in austenitic steel exhibited augmentation in wear resistance and strength, without significantly affect in ductility and toughness (Ref 4). This enhancement in mechanical properties, erosion, and corrosion resistance was attributed to nitrogen being an austenite stabilizer due to its superior solubility in austenite (Ref 5). In addition, alloying of nitrogen further decreases the need for incorporation of nickel in the alloy as nitrogen replaces the nickel in alloy formation. This reduction in the quantity of nickel mitigates nickel's harmful effects such as severe allergic reactions to the human system, frequently observed in biomedical applications. Nitrogen-alloyed steel is broadly categorized as nitronic steel, having nitrogen wt % less than 0.4%, and high nitrogen steel (HNS) having nitrogen wt.% more than 0.4% (Ref 6, 7). Among various grades of nitronic steel, 23-8N austenitic steel having $\sim$ 0.29 wt.% nitrogen has immerged as the focus of research in present times. 23-8N exhibited high corrosion and erosion resistance along with high mechanical tensile strength (Ref 8, 9).

To explore the effect of hardening on the mechanical characteristic of steel, various hardening processes namely solid solution hardening, phase transformation hardening, and precipitation hardening were researched (Ref 10-14). Among them, solution annealing (solution hardening) surfaced as a promising method for post heat treatment of 23-8N steel, prominent enhancement in mechanical properties was observed which was later explained based on the effective dissolution of carbides in austenite alloy (Ref 15). Solution treatment also enhanced work hardening (Ref 16). It is well established that work hardening plays a crucial role in determining the erosion resistance of a material. It was observed that as the work hardening coefficient increased in conjugation with ductility, there was a prominent enhancement in erosion resistance of nitronic steel (Ref 17). Similarly, treatment of 23-8N austenitic steel at higher temperature ranges $\sim$ 1200 °C showcased enhancement in mechanical properties pertaining to crack propagation and erosion.

Mohit Vishnoi, Qasim Murtaza, and **Paras Kumar**, Department of Mechanical Engineering, Delhi Technological University, Delhi 110042, India. Contact e-mails: vishnoi.mohit06@gmail.com, qasimmurtaza@dce.ac.in, and paraskumar@dtu.ac.in.

Journal of Materials Engineering and Performance

Published online: 14 February 2023

Original Article

Institution of MECHANICAL ENGINEERS

Journal of MECHANICAL ENGINEERING SCIENCE

Proc IMechE Part C:
J Mechanical Engineering Science
1–12

DOI: 10.1177/09544062231164299
journals.sagepub.com/home/pic
SAGE

Characterization of erbium oxide doped HP-HVOF deposited carbide ceramic coating on martensitic steel

Mohit Vishnoi[1,2], Qasim Murtaza[1] and Paras Kumar[1]

Abstract

Rare earth elements (REEs) are known as the "vitamin or nutrients" of metals. The addition of rare earth in a limited quantity can enhance the properties of materials. This article elucidates the effect of doping of rare earth oxide (0.9 wt.% Er_2O_3) on the mechanical and surface behavior of tungsten carbide (WC-10Co-4Cr) based coatings developed using high pressure high velocity oxygen fuel (HP-HVOF) thermal sprayed techniques on martensitic stainless steel (SS410). With the addition of rare earth oxides, the result shows that the hardness of the deposited coating (HV1261.17) is far higher than the substrate (HV193.47). The modulus of elasticity and flexural strength is enhanced for the coated sample as compared to the substrate. The porosity level of the coating is found to be less than 1% and the static water contact angle for coated surface (≈125.1°) shows the coated sample is hydrophobic in nature. The surface characterization was done using the scanning electron microscope attached with energy dispersive X-ray analysis which has identified the presence of various elements on the surface including rare earth. The surface of coated samples has various phases of rare earth oxides such as monoclinic and cubic rare earth oxides. Moreover, its compounds such as Co_3W_3C were confirmed by X-ray diffraction measurements. After comparing previous literature with current results can conclude that the addition of rare earth oxides (0.9 wt.% Er_2O_3) on carbide coatings enhanced the various properties of materials.

Keywords

Thermal spray coatings, rare earth, erbium oxide, SS410, wettability, HP-HVOF

Date received: 15 November 2022; accepted: 26 February 2023

Introduction

Ascribable to the fact that the world is rapidly heading toward technological advancements in every aspect, the demand for various kinds of material is on fleek of prominence. Pertaining to this, in recent years, numerous coating and texturing techniques and processes were being developed to ensure the best possible quality of material produced.

There are various sets of coating techniques (processes) to achieve the desired effects on the material surface's properties. Whether it is tribological performance enhancement such as reducing stress and friction, or it is erosion and corrosion performance enhancement, numerous techniques have been developed.[1] But there is always some sort of room for further making a process more efficient and productive. One such measure that was taken with different coating processes on numerous occasions was the involvement of Rare Earth Elements.

Rare earth elements like Cerium (Ce), Lanthanum (La), Erbium (Er), and Yttrium (Y) were widely used to enhance certain mechanical properties like elastic modulus, strength, and hardness. It also helped in reducing porosity and cracks and hence refining of overall microstructure. It improved tribological properties like erosion, corrosion, wear resistance, and the coating's grip (adhesion) on the substratum.[2]

Coating powder is mixed with these rare earth elements or their oxides during various coating processes which leads to the fabrication of coatings that are much better in quality as compared to those coated with standard coating powder and also much more economical.

[1]Department of Mechanical Engineering, Delhi Technological University, Delhi, India
[2]Department of Mechanical Engineering, JSS Academy of Technical Education, Noida, India

Corresponding author:
Mohit Vishnoi, Department of Mechanical Engineering, Delhi Technological University, Shahbad Daulatpur, Main Bawana Road, Delhi 110042, India.
Email: vishnoi.mohit06@gmail.com

Arabian Journal for Science and Engineering
https://doi.org/10.1007/s13369-023-08115-x

RESEARCH ARTICLE-MECHANICAL ENGINEERING

Mechanical and Surface Wettability Analysis of Rare Earth Modified Composite Coating Developed Using Metal Spraying

Mohit Vishnoi[1,2] · Qasim Murtaza[1] · Paras Kumar[1]

Received: 6 August 2022 / Accepted: 13 July 2023

Abstract
The high pressure—high velocity oxy fuel (HP-HVOF) process is a thermal spraying process (TSP) for developing the high melting point powder ceramic coating over the surface. The mixture of used rare earth, the erbium oxide is an untouched rare earth oxide in the field of metal spraying and the likes of metal spraying such as the HP-HVOF process is a recently industrial opted process; which is the modified form of the HVOF process. This paper articulates the effects of rare earth ($La_2O_3/CeO_2/Er_2O_3-0.4$ wt% each) addition on tungsten carbide coatings developed using high pressure-high velocity oxy fuel process on Martensitic steel having grade SS410. These effects have been analyzed using surface (like scanning electron microscope (SEM), porosity, surface roughness, wettability, and energy dispersive spectroscopy (EDS) test) and mechanical (such as tensile, flexural, and hardness test) characterization has been carried out on coated and uncoated samples. The porosity level of the coating was less than one percent, and the static water contact angle for coated sample (≈130°) was higher than the substrate (≈63°). This shows that fabricated coating is hydrophobic in nature. Moreover; the identification of doped elements has been done using EDS. The comparisons between the substrate and the coated samples have been done and the result shows that the coated sample possess enhanced surface and mechanical properties.

Keywords HP-HVOF · Wettability · Surface roughness · Porosity · Rare earth

1 Introduction

The elements (in limited quantities) which extraordinarily enhance the physical and chemical properties of metals by getting combined with them are called rare earth elements. Due to the high melting point, they are physically soft to the touch, appear silver in color, and get tarnished quickly in the air [1]. There is a total of seventeen elements that come under the group of rare earth elements (REEs) namely; lanthanum (La), cerium (Ce), praseodymium (Pr), neodymium (Nd), promethium (Pm), samarium (Sm), europium (Eu), gadolinium (Gd), terbium (Tb), dysprosium (Dy), holmium (Ho), erbium (Er), thulium (Tm), ytterbium (Yb), lutetium (Lu), which are fifteen lanthanides along with scandium (Sc) and yttrium (Y) [2]. Based on various physical and chemical properties, REEs are further classified into two sub-groups namely heavy rare earth elements (HREEs) which include Y, Tb, Dy, Ho, Er, Tm, Yb, and Lu, and light rare earth elements (LREEs) which include Sc, La, Ce, Pr, Nd, Pm, Sm, Eu, and Gd. The HREEs and LREEs are also known as the yttrium group and cerium group respectively [3]. Various elements such as hydrogen, oxygen, nitrogen, sulfur, and silicon interact with rare earth because of the large atomic radius and effective chemical activities and this plays a beneficial role in steel and its manufacturing [4]. REEs are useful in many surface engineering applications like surface modifications, surface chemical heat treatment, and electroplating [5]. Oxides of REEs find their application in diverse fields like chemical, metallurgy, and electronics engineering [6]. Clean and green energy comprises of wind turbines, Electric Vehicles, solar cells, etc. Terbium, dysprosium, neodymium, and yttrium are some of the rare elements which are advantageous for green energy science [7].

For industrial applications, the surface property of a material defines its performance. The surface alteration techniques

✉ Mohit Vishnoi
vishnoi.mohit06@gmail.com

Qasim Murtaza
qasimmurtaza@dce.ac.in

Paras Kumar
paraskumar@dtu.ac.in

[1] Department of Mechanical Engineering, Delhi Technological University, Delhi 110042, India

[2] Department of Mechanical Engineering, JSS Academy of Technical Education, Noida 201301, India

Published online: 25 July 2023

IOP Publishing Phys. Scr. 98 (2023) 115618 https://doi.org/10.1088/1402-4896/ad032f

Physica Scripta

PAPER

Mechanical and surface characterization of $Er_2O_3/La_2O_3/CeO_2$ doped carbide coating developed using high velocity oxy fuel (HVOF)

Mohit Vishnoi[1,2,*], **Qasim Murtaza**[1,*] and **Paras Kumar**[1]

[1] Department of Mechanical Engineering, Delhi Technological University, Delhi 110042, India
[2] Department of Mechanical Engineering, JSS Academy of Technical Education, Noida 201301, India
[*] Authors to whom any correspondence should be addressed.

E-mail: vishnoi.mohit06@gmail.com, qasimmurtaza@dce.ac.in and paraskumar@dtu.ac.in

Keywords: high velocity oxy fuel, rare earth, carbide coating, contact angle, energy dispersive spectroscopy

RECEIVED
29 July 2023

REVISED
25 August 2023

ACCEPTED FOR PUBLICATION
13 October 2023

PUBLISHED
25 October 2023

Abstract

This study is mainly focused on effect of rare earth oxides on a composite coating applied to martensitic steel (SS410) using the high velocity oxy fuel (HVOF) process. The composite coating consists of WC-10Co-4Cr doped with rare earth (erbium oxide/lanthanum oxide/cerium oxide; 0.2 wt%. each). The range of deposited coating thickness was 282–300 μm. Mechanical testing, including tensile, flexural, and hardness tests, along with surface characterization, such as examining morphology, porosity, elemental composition, and phase identification with wettability testing has been conducted on both the substrate and coated samples. The hardness of the coatings is increased by approximately four times to the substrate. The coated sample has porosity in the range of $\geqslant 1$ to $\leqslant 2\%$. The contact angle of the coated surface has enhanced ($\approx 134°$) than the substrate ($\approx 61°$), this indicates that the coated surface exhibits hydrophobicity.

1. Introduction

Rare earth elements, such as cerium (Ce), lanthanum (La), niobium (Nb), and zirconium (Zr), have found widespread application in various industries, particularly in the metallurgical field. These elements are utilized to enhance the properties of materials used in electronics, ceramics, lasers, machinery, and other related areas [1–3]. In addition, rare earth elements have been employed in surface engineering techniques, including chemical treatment, flame spraying, electric plating, laser alloying, and the development of antibacterial coatings for bone [4–7]. Due to its huge atomic radius and chemical activities, rare earth (RE) may react with many elements, including H, O, N, S, and Si, Moreover, they play a vital role in the production of steels [2]. They refine grains and stop grain development during heating as well as provide purifying properties that can get rid of undesirable contaminants. As a result, it was anticipated that rare earth-doped coating would have slower grain development [4]. Surface roughness and the degree of brittle fracture can both be efficiently reduced by rare earth [8]. Erbium oxide (Er_2O_3), a rare earth oxide, stands out due to its remarkable attributes, including a high dielectric constant, elevated bulk refractive index, and wide band gap. The thin films of Er_2O_3 have potential applications as up-conversion layers in optoelectronic devices [9]. Moreover, rare earth elements have proven to be effective in altering the surface characteristics of coatings applied using diverse techniques such as thermal spray, thermal spray welding (TSW), and laser-alloyed coatings [10]. Thermal spray methods such as flame, detonation guns and plasma sprayed are frequently used in power plants and other industrial fields to protect the surface against corrosion and wear [11]. The high-velocity oxygen fuel (HVOF) technique is a well-established method in thermal spraying. It is known for its high gas and particle velocities, which are typically three to four times the speed of sound (Mach 3 to 4). The combustion of fuels with oxygen produces both thermal and kinetic energy that is used to heat and accelerate feedstock powder in HVOF process. The Amorphous steel coatings, known for their exceptional resistance to wear, corrosion, and oxidation, are commonly produced using thermal spraying processes such as HVOF, Moreover, enhanced properties like hardness, density, and strength

Surface & Coatings Technology 492 (2024) 131230

Contents lists available at ScienceDirect

Surface & Coatings Technology

journal homepage: www.elsevier.com/locate/surfcoat

Effect of laser ablation over cavitation, slurry erosion, and surface properties of 86WC-10Co-4Cr based ceramic coating developed using HP-HVOLF

Mohit Vishnoi [a,b,*], Vikrant Singh [c], Anuj Bansal [c], Qasim Murtaza [a,**], Paras Kumar [a]

[a] Department of Mechanical Engineering, Delhi Technological University, Delhi 110042, India
[b] Department of Mechanical Engineering, JSS Academy of Technical Education, Noida 201301, India
[c] Sant Longowal Institute of Engineering and Technology, Longowal, Sangrur 148106, Punjab, India

ARTICLE INFO

Keywords:
HP-HVOLF
Laser ablation
WC-10Co-4Cr
SS410

ABSTRACT

The manuscript presents a detailed study on WC-10Co-4Cr powder coatings applied via HP-HVOLF and subjected to laser ablation. FESEM analysis showed strong metallurgical bonding between the coating and SS410 substrate (≈75 MPa), crucial for durability. Despite the presence of cavities and pits, the coating's overall thickness remains consistent post-ablation, affirming stability. EDS mapping confirmed uniform elemental distribution, with well-bonded transition zones. Vickers hardness increased in laser-ablated samples ($HV_{0.3}$ ≈ 1523) compared to unablated samples ($HV_{0.3}$ ≈ 1344). Slurry and cavitation erosion analyses demonstrated superior resistance in laser-ablated samples due to higher microhardness and elevated static contact angles. Contact angle measurements indicated hydrophobicity in both un-textured and textured samples, with textured surfaces showing increased hydrophobicity.

1. Introduction

Slurry erosion and cavitation erosion represent critical challenges in hydromachinery applications, where components are subjected to high-velocity fluid flows [1,2]. Slurry erosion occurs when solid particles suspended in a fluid impinge upon a material surface, leading to abrasive wear and material loss. This phenomenon is particularly prevalent in industries such as mining, where abrasive slurries are used in processes like ore transportation [3]. On the other hand, cavitation erosion results from the rapid formation and collapse of vapor bubbles on a material surface due to pressure fluctuations in the surrounding fluid [4]. This cyclic process induces localized stresses, causing surface pitting, fatigue, and ultimately, structural failure. In hydromachinery such as pumps, turbines, and propellers, where high-speed liquid flows are commonplace, both slurry and cavitation erosion pose significant challenges, compromising the efficiency, reliability, and lifespan of these critical components [5,6]. Hydromachinery components are commonly constructed from materials like SS410 steel due to their favorable mechanical properties and corrosion resistance [7,8]. However, even these robust materials are susceptible to erosion-induced deterioration over time. As a result, protective coatings have emerged as a viable strategy to enhance the erosion resistance and prolong the service life of hydromachinery components [9]. Among the various coating materials, thermal spray coatings comprising WC-10Co-4Cr have gained considerable attention for their exceptional hardness, wear resistance, and thermal stability [10–12]. The tungsten carbide (WC) phase provides hardness and abrasion resistance, while the cobalt (Co) and chromium (Cr) phases contribute to toughness and corrosion resistance, respectively. These coatings exhibit superior performance in erosive environments, making them an attractive choice for safeguarding hydromachinery components against slurry and cavitation erosion [7,13]. Within the realm of thermal spray coatings, different deposition techniques exist, each with its unique advantages and limitations [14]. Among these, High-Pressure High-Velocity Oxy-Fuel (HP-HVOLF) stands out as a promising method for applying WC-10Co-4Cr coatings. HP-HVOLF involves the combustion of oxygen and fuel gases in a high-pressure chamber, resulting in a supersonic jet of hot gases and molten particles directed towards the substrate [15,16]. This process facilitates

* Correspondence to: M. Vishnoi, Department of Mechanical Engineering, Delhi Technological University, Delhi 110042, India.
** Corresponding author.
E-mail addresses: vishnoi.mohit06@gmail.com (M. Vishnoi), anujbansal@sliet.ac.in (A. Bansal), qasimmurtaza@dce.ac.in (Q. Murtaza), paraskumar@dtu.ac.in (P. Kumar).

https://doi.org/10.1016/j.surfcoat.2024.131230
Received 26 May 2024; Received in revised form 6 August 2024; Accepted 7 August 2024
Available online 10 August 2024

International Journal of Refractory Metals and Hard Materials 125 (2024) 106873

Contents lists available at ScienceDirect

International Journal of Refractory Metals and Hard Materials

journal homepage: www.elsevier.com/locate/IJRMHM

Rare earth-doped ceramic coatings: Analysis of microstructure, mechanical properties, and slurry Erosion resistance using high pressure-high velocity oxy-liquid fuel deposition

Mohit Vishnoi [a,b,*], Qasim Murtaza [a,*], Paras Kumar [a], Anuj Bansal [c], Vikrant Singh [c]

[a] Department of Mechanical Engineering, Delhi Technological University, Delhi 110042, India
[b] Department of Mechanical Engineering, JSS Academy of Technical Education, Noida 201301, India
[c] Sant Longowal Institute of Engineering and Technology, Longowal, Sangrur 148106, Punjab, India

ARTICLE INFO

Keywords:
$La_2O_3/CeO_2/Er_2O_3$
WC-10Co-4Cr
SS410
Wettability
Slurry jet erosion

ABSTRACT

The high pressure-high velocity oxy liquid fuel (HP-HVOLF) is a current industry-adopted thermal spraying technique for developing high melting point powder coating over surfaces. In the current manuscript, the rare earth ($La_2O_3/CeO_2/Er_2O_3$–0.3 wt%. each) doped and without rare earth doped carbide (WC-10Co-4Cr) coatings have been deployed on stainless steel (SS410) via HP-HVOLF process. The comparison among the properties of the substrate, without rare earth coating and rare earth oxides doped coatings have been characterized by conducting mechanical, microstructural, and slurry jet erosion analysis. The results show that the hardness, modulus of elasticity, and flexural strength of the cermet coating are considerably higher for rare earth-doped coatings than those without rare earth-doped coatings and substrates (SS410). The EDX (energy dispersive X-ray spectroscopy) has recognized the occurrence of different elements on the surface together with rare earth. Moreover, its compounds such as Co_3W_3C and W_2C were inveterate using X-ray diffraction (XRD) measurements. The porosity level of the rare earth doped, and un-doped coatings are obtained to be less than 1 % and≥1 to ≤2 % respectively. Moreover, the rare earth-doped cermet coated surface shows hydrophobic behavior with a maximum water contact angle (WCA) of ≈129.4°. Furthermore, the slurry jet behavior of rare earth doped coating shows high wear resistance as compared to without RE doped coatings, indicating its potential for robust performance under erosive conditions.

1. Introduction

Rare earth (RE) element is also recognized as the "vitamins" of materials. By adding small amounts of rare earth elements to other materials, such as metals, ceramics, and glass, it is possible to improve their properties in many ways [1]. Due to the presence of different properties like large atomic radius and chemical properties, it can be reactive to different H, O, S, O, and Si which cover a majority of the composition of the steel [2]. They have the physical attributes of grain refinement properties; inhibit the growth of larger grains during heating and remove impurities. Therefore, in natural form, these metals can react with cold water to form hydroxides releasing hydrogen gas and they also tend to tarnish at a slow rate at room temperature. Oxides are formed when they react with steam. When it is heated to a temperature of about 400 °C and burns to produce a fierce colorful pyrotechnic flame [3]. Many researchers had claimed in their research that the corrosion, erosion resistance, and mechanical properties have been enhanced by the addition of rare earth elements in thermal sprayed composite coatings [4]. Many researchers conducted their experiment by considering the 1 % CeO_2 doped WC-12Co composite coating and claimed that there is an enhancement in the mechanical [5], tribological properties, reduction in porosity [6,7] and enhanced oxidation resistance [8]. The various rare earth elements' properties including their effect on coating behavior were reviewed thoroughly by various researchers [9]. There were comparisons of various cermets coating deployed using high velocity oxy fuel (HVOF) in their tabular-based review by considering the parameters such as coating powder, substrate, and characterization of different types of coatings. Moreover, the application of respective

* Corresponding authors at: Department of Mechanical Engineering, Delhi Technological University, Delhi 110042, India.
E-mail addresses: vishnoi.mohit06@gmail.com (M. Vishnoi), qasimmurtaza@dce.ac.in (Q. Murtaza), paraskumar@dtu.ac.in (P. Kumar), anujbansal@sliet.ac.in (A. Bansal), vikrantsingh520@gmail.com (V. Singh).

https://doi.org/10.1016/j.ijrmhm.2024.106873
Received 18 April 2024; Received in revised form 29 August 2024; Accepted 4 September 2024

Decision Letter (JMEP-24-04-36659.R1)

From: frazierwe@gmail.com

To: vishnoi.mohit06@gmail.com

CC:

Subject: Journal of Materials Engineering and Performance - Decision on Manuscript ID JMEP-24-04-36659.R1

Body: 14-Sep-2024

Dear Mr. VISHNOI:

It is a pleasure to accept your manuscript entitled "Assessment of mechanical and slurry erosive behavior on laser textured stainless steel (SS410)" in its current form for publication in the Journal of Materials Engineering and Performance. The comments of the reviewer(s) who reviewed your manuscript are included at the foot of this letter.

Please ensure that every author has completed the copyright transfer form. After all copyright transfer forms are complete, the manuscript files are transferred to Springer for typesetting and publication. In the weeks following file transfer, you may expect an e-mail message from do-not-reply@springernature.com with the subject line "Action required: Tasks to complete publication of your article in Journal of Materials Engineering and Performance." This message contains a link to a brief form that must be completed. You will receive page proofs of the article shortly after filling out Springer's form.

Thank you for your fine contribution. On behalf of the Editors of the Journal of Materials Engineering and Performance, we look forward to your continued contributions to the Journal.

Sincerely,
Dr. William E. Frazier
Editor-in-Chief, Journal of Materials Engineering and Performance
frazierwe@gmail.com

Assessment of mechanical and slurry erosive behavior on laser textured stainless steel (SS410)

Mohit Vishnoi[1,2]*, Qasim Murtaza[1]*, Paras Kumar[1]
[1]Department of Mechanical Engineering, Delhi Technological University, Delhi 110042, India
[2]Department of Mechanical Engineering, JSS Academy of Technical Education, Noida 201301, India
vishnoi.mohit06@gmail.com[1,2]*, qasimmurtaza@dce.ac.in[1], paraskumar@dtu.ac.in[1]
Corresponding authors: Mohit Vishnoi* and Qasim Murtaza*

Abstract:
In this paper, laser surface texturing (LST) has been used to create the circular and diamond shape texturing pattern on martensitic steel of grade SS410 to alter the various mechanical, surface, and tribological properties. The mechanical and surface characterizations have done on various shape textured surfaces on SS410. Moreover, the slurry jet erosion test has performed on textured surfaces using a slurry erosion test rig. The hardness value of the various textured shape surface is higher than the others because mechanism of material removal for pattern is melting and evaporation, after applying an intense heat sudden cooling takes place. This might be altering the microstructure and enhances the hardness of the textured steel. The hardness value was the highest for circular inward textured case (HV0.3≈206) among all texturing. The tensile and flexural yield strength has marginally increased after texturing. The value of percentage elongation has marginally decreased after texturing. The modulus values for all the textured samples have enhanced as compared to un-textured sample. Moreover, the modulus value of diamond-in textured samples are observed to be the highest i.e. ≈265GPa. The contact angles for all shapes of texturing patterns have greater values than un-textured samples. All the textured surfaces show the hydrophobic and un-textured surface as hydrophilic behavior. The outward textured surface has greater contact angle value (≈110º) as compared to others. The erosion resistance for the un-textured samples have lesser among all textured samples and the circular-in pattern has the highest erosion resistance. Because the erosion resistance is primarily depend on the hardness of the material. The ploughing, micro-cutting lips, crater, and carbide pull-out type of wear mechanism has been identified using a scanning electron microscope.

Keywords: Laser Surface Texturing, Mechanical Characterization, Wettability, SS410, Slurry Jet erosion.

Proof of Papers Published in Proceedings of the Conferences

Chapter 8
A Review on Coating for Hydro-turbine Application by HVOF Process

Mohit Vishnoi, Paras Kumar, and Qasim Murtaza

Abstract Erosive wear of hydro-turbine runner's blade is a complex aspect, which depends upon different factors like silt size, hardness, velocity of water and substrate material properties. The turbine runner's efficiency has been deteriorated with the increase in the erosive wear, and final failure of hydro-turbine runners occurs. In many of the literatures, researchers have conducted different experiments to investigate the effect of these factors on erosive wear, but the size of samples has been considered in various types of test apparatus to affect the flow conditions in the turbine, but actual flow conditions and the fact of erosive wear are too complex to replicate. The literature presents the concern associated with materials and fabrication process of deployed coatings by HVOF approach used for the stability of hydro-turbine runner. The primitive mechanisms of annihilation techniques resulting in the hydro-turbine runner's blade were given in article. The primitive approaches of thermal spraying were described, which grant the deployment of coatings with the chemical composition, phase structure and properties convenient for the improvement of functional performance. There are some recently used and possible target materials, and coating materials were presented in this article. The advantages and disadvantages of the approach of HVOF were discussed. The primitive groups of coatings with a considerable resistance to corrosion and slurry erosion wear produced by thermal spraying (HVOF) method, which can be used in the hydro-electric power plant industry, were described, and also studies undertaken in this field by several investigators have been discussed broadly.

Keywords HVOF (high-velocity oxy fuel) · Silt erosion · Erosion wear

M. Vishnoi (✉) · P. Kumar · Q. Murtaza
Department of Mechanical Engineering, Delhi Technological University, Delhi 110042, India
e-mail: vishnoi.mohit06@gmail.com

P. Kumar
e-mail: paraskumar@dtu.ac.in

Q. Murtaza
e-mail: qasimmurtaza@dce.ac.in

I. Singh et al. (eds.), *Advances in Materials Engineering and Manufacturing Processes*,
Lecture Notes on Multidisciplinary Industrial Engineering,
https://doi.org/10.1007/978-981-15-4331-9_8

Materials Today: Proceedings 44 (2021) 4053–4058

Contents lists available at ScienceDirect

Materials Today: Proceedings

journal homepage: www.elsevier.com/locate/matpr

Effect of rare earth elements on coatings developed by thermal spraying processes (TSP) – A brief review

Mohit Vishnoi *, Qasim Murtaza, Paras Kumar

Department of Mechanical Engineering, Delhi Technological University, Delhi 110042, India

ARTICLE INFO

Article history:
Received 7 October 2020
Received in revised form 11 October 2020
Accepted 16 October 2020
Available online 17 December 2020

Keywords:
Rare earth element
Thermal spraying process
High velocity oxy fuel (HVOF)
Surface engineering
Turbine blades

ABSTRACT

A coating is deployed on the substrate by different deposition techniques to elevate the substrate's surface properties, such as chemical, mechanical, and tribological. The elevation in the properties of the substrate depends on elements used in coating powder. In this work, the effect and significance of rare earth elements on the substrate has been presented. The objective of the work is coating by different thermal spraying methods. From the literature survey on TSP, there is a significant increase in corrosion resistance than other material properties. The tribological properties of substrate material were analysed with and without the rare earth material in coating powder by various researcher's work. It is found that very less or little researchers have explored rare earth material as a coating material. There are different areas in which these coatings are used for various applications like the turbine's blade, aero-engines, miniaturized electronics, display panels, and others. By using RE metals mechanical, physical, tribological, and thermal shock resistance of the substrate material increased considerably.

Selection and peer-review under responsibility of the scientific committee of the International Conference on Advances in Materials Processing & Manufacturing Applications.

1. Introduction

Rare earth (RE) is known as the "nutrient" of metals, which implies that a limited quantity of RE can extraordinarily elevate material properties. Rare earth (RE) oxides have been utilized effectively in numerous fields, like metallurgical, chemical, and electronics engineering [1]. Due to the large atomic radius and chemical activities, RE can undoubtedly respond to various elements. Such as H, O, N, S, Si, and they show a significant part in steels and their manufacturing [2]. These days, the rare earth elements are used in surface modifications and also engaged in surface chemical heat treatment, electroplating, and comparative techniques [3]. In recent studies, RE was effectively used to change the surface properties of coatings deployed by thermal spray process, thermal spray welding, and the laser-alloyed coatings, but contemplated the impact of RE elements on the corrosion resistance, wear, and microstructure of modified surfaces [4]. The articles on surface alteration techniques show an increasing attraction in understanding the rapid solidification, particle re-melting and precipitation, interface transformation, interface moving effect, counter flow pattern, alloying reaction, and the relationship between properties surface-modified layers and microstructures [5–6].

Wang et al. (1992) had accurately applied CeO_2 to alter the surface properties of coatings deployed by thermal spray, thermal spray weld, and laser-alloyed weld with the investigation on the effect of RE elements on the microstructure, wear, and corrosion behaviour of the altered coatings [7].

In some cases, coating powder could not meet the requirement of improving the properties economically. To overcome the problem, generally the addition of rare earth metal in coating powder fulfils the requirements. There are various rare earth elements such as cerium (Ce), Yttrium (Y), Lanthanum (La), Niobium (Nb), Zirconium (Zr).

Sharma et al. (2012) were investigated the behaviour of abrasive wear on Ni-Cr-Fe-Si-B alloy coatings deployed over carbon steel. The flame spraying process deployed the coating of Ni-Cr-Fe-Si-B. The assessment of microstructure, porosity, and hardness of the coatings were carried out.

Generally, iron, Nickel, cobalt-based alloys are known as hard facing alloys. The wear resistance combined with oxidation, hot corrosion resistance is required in the field (pumps, mill rolls, piston extruders, and glass mould industry) on Nickel-based alloy

* Corresponding author.
E-mail address: vishnoi.mohit06@gmail.com (M. Vishnoi).

https://doi.org/10.1016/j.matpr.2020.10.439
2214-7853/
Selection and peer-review under responsibility of the scientific committee of the International Conference on Advances in Materials Processing & Manufacturing Applications.

DELHI TECHNOLOGICAL UNIVERSITY
(Formerly Delhi College of Engineering)
Shahbad Daulatpur, Main Bawana Road, Delhi-42

PLAGIARISM VERIFICATION

Title of the Thesis _____**"Tribological and Mechanical Behavior of Rare Earth Doped Composite Coating by Thermal Spraying"**_____

Total Pages _____ Name of Scholar _____**Mohit Vishnoi**_____

Supervisor (s)

(1) ____**Prof. Qasim Murtaza**_____

(2) ____**Dr. Paras Kumar**_____

Department _____**Mechanical Engineering**_____

This is to report that the above thesis was scanned for similarity detection. Process and outcome is given below:

Software used: __**Turnitin**__ Similarity Index: __**12% after excluding self citations**__

Total Word Count: __**31454**__

Date: **21/10/2024**

Candidate's Signature **Signature of Supervisor(s)**

PLAGIARISM REPORT

PAPER NAME	AUTHOR
3. Thesis for Plag.pdf	q m

WORD COUNT	CHARACTER COUNT
31454 Words	171618 Characters
PAGE COUNT	**FILE SIZE**
156 Pages	4.9MB
SUBMISSION DATE	**REPORT DATE**
Sep 5, 2024 1:11 AM PDT	Sep 5, 2024 1:12 AM PDT

12% Overall Similarity

The combined total of all matches, including overlapping sources, for each database.

- 2% Internet database
- 10% Publications database
- Crossref database
- Crossref Posted Content database
- 2% Submitted Works database

Excluded from Similarity Report

- Bibliographic material
- Small Matches (Less then 10 words)

BRIEF PROFILE

I, **Mohit Vishnoi**, completed **B. Tech** in Mechanical Engineering from **Uttar Pradesh Technical University, Lucknow, India**, and **M.Tech** (honors) in Materials Science and Engineering from **National Institute of Technology, Tiruchirappalli (Tamil Nadu, India).** Currently I am working as an **Assistant Professor** in the Department of Mechanical Engineering at JSS Academy of Technical Education, Noida since 1-Aug-2013. I have enrolled **Ph.D**. in Department of Mechanical Engineering at **Delhi Technological University, Delhi-42, (India)** under the supervision of **Prof. Qasim Murtaza and Dr. Paras Kumar**. I have published **16 SCI/SCIE, 3 ESCI** and **15 Scopus** papers in the reputed journals. I have been awarded for **Commendable Research Award** (Cash value of **Rs. 50,000/- and 1, 00,000/-** along with the certificate of merit) for his excellence in Research on March 3, 2022 and September 5, 2024 respectively, at **Delhi Technological University, Delhi.** Moreover, I have received **Best Young Researcher Award** for the outstanding excellence and remarkable achievements in the field of Research and publications on January 15, 2024, at **Coimbatore.**